Crystalline Transition Metal-Based Sensors for the Optical Detection of Oxygen

A DISSERTATION
SUBMITTED TO THE FACULTY OF THE GRADUATE SCHOOL
OF THE UNIVERSITY OF MINNESOTA BY

Lindsay Marie Hinkle

IN PARTIAL FULFILLMENT OF THE REQUIREMENTS
FOR THE DEGREE OF
DOCTOR OF PHILOSOPHY

Professor Kent R. Mann

September 2012

Acknowledgements

First, I must thank my advisor, Kent Mann, for his guidance throughout this process. He encouraged me to go into lab and just…try. I spent many an hour with Kent talking about experiments, sighting down K_{SV} plots, and determining what the data were saying (remember - it's *always* data were, never data was). I learned to let the data speak to me rather than the other way around. Along the way, Kent shared with me some great stories about science and life that I will never forget. I am also grateful that Kent allowed me to explore any teaching opportunity that came my way. Through these positions, I gained valuable experience leading a classroom.

I have shared the Mann Group office with many people along this journey. Kari McGee's persistence, encouragement, and friendship helped me challenge myself and grow both as a person and a chemist throughout graduate school. Raghu Chitta taught me how to "think like a scientist" and the value of passion and investment. I learned so much just by standing next to him in lab and watching him work. His synthetic skills far surpass my own, but he was more than willing to share his knowledge with the rest of us. Conor Smith showed me that a little time spent tinkering is often time well spent. His LabVIEW prowess made much of this thesis possible. Lisa Smith opened up her classroom and allowed me to watch. We often discussed how she implements new teaching strategies, making me a better instructor. Jon Bohnsack's ability to play the devil's advocate taught me how to develop strong arguments and to be confident in my conclusions. I'm also grateful that Jon was also willing to lend a hand, especially in a pinch. Kyle Schwartz demonstrated that coupling scientific patience with determination gets results. He often took on the Holy Grail of a project and made progress toward the end goal. This last year would have been much different without his friendship. The guidance and camaraderie of the Mann Group has been invaluable, and for that I am incredibly grateful.

Daron Jansen and Ted Pappenfus entrusted me with endless supplies of (mostly) X-ray quality crystals, allowing me to develop as a crystallographer. Many thanks are also due to Victor G. Young Jr. and Doyle Britton for encouraging me during difficult structure solutions and helping me when refinements would not converge. I also want to thank Daron for listening to me ramble. Your mentorship is invaluable and I hope we can continue to collaborate in the future.

I would not be the instructor that I am without the help of Michelle Driessen. Michelle's drive to try new teaching methods for the benefits of the *students* inspires me. Despite the obstacles, she always pushes through, because the best interest of the students is at stake. She works for the students, changing what does not work for something that does—a philosophy I have adopted. I am incredibly grateful for her open door policy, which I honestly abused. Thank you, Michelle, for your guidance and friendship.

Letitia Yao and Elodie Marlier's love for pan fried noodles and duck led to many lunch dates that helped me more than they know. Thank you, Melissa Maurer-Jones, for being a listening ear or a shoulder to cry on at the drop of a hat. I'm lucky that I can call you all friends.

Karla McCain, my undergraduate advisor from Austin College, believed in me from day one. She knew I could reach my goals, even when I doubted myself. She continues to encourage me and, most importantly, push me to be the best chemist and teacher I can be. I hope to show my students as much care and concern as Karla shows for her students, past and present.

Finally, I could not have achieved this goal without my family. They encouraged me to follow my dreams, and supported me even when those dreams took me 1,000 miles from home. For their unconditional love, grace, and unwavering support, I am eternally grateful. Last and most certainly not least, Bob, thank you for holding me together when things got tough. You helped me realize that I can and will accomplish great things. Your love, patience, and encouragement from every corner of the country are priceless gifts. Thank you for being there through it all.

Thanks, y'all!

Dedication

For my grandfather, Rodney Hinkle.
I hope we've made you proud.

Abstract

Oxygen is essential to life, motivating the development of optical oxygen sensors. Current sensing methods rely on either electrochemical measurements or an optical response from solutions or polymer based materials. These techniques often suffer from support degradation, oxygen consumption, and response plots that are difficult to interpret. A promising alternative to current optical sensing technologies are porous crystalline solids, as these solids provide a consistent emission site along with the necessary open space to facilitate diffusion of molecular oxygen through the material.

This thesis explores neutral, mono-, di-, and tricationic coordination complexes for use as solid-state devices to detect oxygen. This series of transition metal complexes was synthesized, and the packing motifs studied by single crystal X-ray diffraction. After investigating the crystalline packing, photophysical properties, and sensitivity of emission toward oxygen, it was determined that the mono- and dicationic complexes are the most promising materials based on their sensitivity and long term stability.

In Chapter 1, a brief introduction to oxygen sensing and the goals of this project are given. In Chapter 2, the synthesis and characterization of a series of neutral zinc(II) compounds are reported. One specific compound, $Zn(terpy\text{-}*)Br_2$ (where terpy-* = 4,4′,4″-tri-*tert*-butyl-2,2′:6′,2″-terpyridine) showed promise for detecting small oxygen concentrations. However, stability testing determined the compound was not stable toward LED illumination and oxygen exposure.

In Chapter 3, a monocationic family of compounds based on the $[Cu(P\text{^}P)(N\text{^}N)]^+$ core (where P^P is a bidentate phosphine and N^N is a bidentate amine) was explored. After the sensing ability of the compounds was determined, their stability was rigorously

tested. The studies demonstrate that compounds with $tfpb^-$ (where $tfpb^-$ = *tetrakis*[*bis*-3,5-trifluoromethyl(phenylborate)]) counterions were typically more stable and more sensitive to changes in oxygen than their BF_4^- and $pfpb^-$ ($pfpb^-$ = *tetrakis*-(pentafluorophenyl)borate) counterparts. Additionally, a mechanism for the degradation of these sensors is proposed.

In Chapter 4, a zinc(II) dicationic polypyridine complex was tested and compared to a previously reported and analogous ruthenium(II) compound. Based on the knowledge that similarly shaped molecules tend to pack in a similar way, it was hypothesized that crystalline materials of both the Ru(II) and Zn(II) compounds would pack similarly and therefore sense oxygen in a similar manner. Even though the compounds crystallize in a similar manner and the trends in oxygen sensitivity are the same, the K_{SV} parameters were not as similar as was predicted. The difference in sensing ability is due to a different quenching mechanism in the Ru(II) and Zn(II) complexes. Nonetheless, the Zn(II) family of compounds is a reliable and inexpensive solid-state oxygen sensing material.

Finally in Chapter 5, tricationic, 4′-tolyl-2,2′:6′,2″-terpyridine (tol-terpy) iridium(III) compounds were synthesized and tested for oxygen sensitivity. While none of these materials were sensitive toward changes in oxygen concentration, three new crystal structures of iridium(III) *bis*-tol-terpy compounds have been reported along with the structure of one neutral mono-tol-terpy complex. These four structures represent a significant contribution to the crystallographic database as only seven structures of this class of compound had been reported before this work.

Table of Contents

List of Tables

List of Figures

Chapter 4

List of Abbreviations and Symbols

ϕ	axis of rotation for the crystal during X-ray crystal structure determination
ϕ	quantum yield
(r_l+r_{O2})	sum of encounter radii for lumiphore and molecular oxygen
^{19}F NMR	fluorine nuclear magnetic resonance spectroscopy
^{1}H NMR	proton nuclear magnetic resonance spectroscopy
^{1}MLCT	singlet metal to ligand charge transfer state
$^{1}O_2$	singlet excited state oxygen
2θ	axis of rotation for the detector platform during X-ray crystal structure determination
^{3}MLCT	triplet metal to ligand charge transfer state
$^{3}O_2$	triplet ground state oxygen
A	complex in its ground state
Å	angstrom
A*	complex in its excited state
a.u.	arbitrary unit
a_1 and a_2	contribution of the given process to the overall lifetime
a_3	correctional constant for the lifetime measurements
atm	atmosphere
bath	4,7-diphenyl-1,10-phenanthroline
bcp	2,9-dimethly-4,7-diphenyl-1,10-phenanthroline
bpy	2,2′-bipyridine
CCD	charge coupled device
CCDC	Cambridge Crystallographic Data Center
cm	centimeter
CSD	Cambridge Structural Database
d	doublet
dd	doublet of doublets
d-d	d to d transition
deg	degree
dimephen	4,7-dimethyl-1,10-phenanthroline
dmp	2,9-dimethyl-1,10-phenanthroline
DMSO	dimethylsulfoxide
DMSO-d_6	deuterated dimethylsulfoxide
D_{O2}	molecular oxygen diffusion constant
dpbpy	4,4'-diphenyl-2,2'-bipyridine
ET	energy transfer
f	fractional contribution to unquenched emission
f	statistical factor incorporating probability of oxygen reaching emissive site
g	gram
G.S.	ground state

GOF	goodness of fit
H	proton
hr	hour
HRESIMS	high resolution electron spray ionization mass spectrometry
Hz	hertz
hν	light
I	emission under a given concentration of oxygen
I	light intensity at a given time
I	reduced source light
I_0	emission under nitrogen
I_0	incident light intensity
I_{emit}	emitted light
ISC	intersystem crossing
J	proton coupling constant
K	Kelvin
k_1, k_2	rate constants for the individual processes that contribute to the lifetime
k_{nr}	non-radiative decay rate constant
k_q	quenching rate constant
k_r	radiative decay rate constant
K_{SV}	Stern-Volmer quenching constant
L	liter
LECs	light-emitting electrochemical cells
LED	light emitting diode
m	multiplet
m/z	mass to charge ratio
M^+	monocationic complex
mg	milligram
MHz	megahertz
min	minutes
mL	milliliter
MLCT	metal to ligand charge transfer
mm	millimeter
mmol	millimole
MoKα	K_α line of molybdenum radiation
mol	moles
ms	millisecond
N^N	bidentate amine
N_a	Avogadro's number
NIST	national institute of standards and technology
nm	nanometer
NMR	nuclear magnetic resonance
no-d ^{1}H NMR	no deuterium proton resonance nuclear resonance spectroscopy

ns	nanosecond
ºC	degrees Celsius
OLED	organic light emitting diode
P	pressure
P^P	bidentate phosphine
$pfpb^-$	*tetrakis*-(pentafluorophenyl)borate
pH	scale used to measure acidity
phen	1,10-phenanthroline
PMT	photon multiplier tube
p_{O2}	partial pressure of molecular oxygen
POP	bis[2-(diphenylphosphino)phenyl]ether
ppm	parts per million
ppm	parts per million (or mg/L)
psi	pounds per square inch
q	quartet
Q	quencher
Q*	excited state quencher
r.m.s.	root mean square
s	seconds
s	singlet
S_{O2}	solubility of molecular oxygen
sol'n	solution
t	time
t	triplet
terpy	2,2':6',2"-terpyridine
terpy-*	4,4′,4″-tri-*tert*-butyl-2,2′:6′,2″-terpyridine
$tfpb^-$	*tetrakis*[*bis*-3,5-trifluoromethyl(phenylborate)]
tol-terpy	4′-tolyl-2,2′:6′,2″-terpyridine
V	volt
V	volume
xantphos	4,5-bis(diphenylphosphino)-9,9-dimethylxanthene
Z	number of formula units per unit cell
δ	chemical shift in ppm
θ	measure of data completeness
λ	wavelength
μ	absorption coefficient
μs	microsecond
π to π*	excited state transition of a ligand
τ	excited state lifetime under given concentration of oxygen
τ_0	excited state lifetime under nitrogen
ω	axis of rotation for the goniometer platform during X-ray crystal structure determination

Chapter One

An Introduction to Oxygen Sensing

The detection of gases has been at the forefront of public interest, especially with the increased global demand for fossil fuels. For example, the burning of fossil fuels releases a cocktail of chemicals into the air that can damage the environment. Nitrogen oxide and sulfur gases released during this process react with water in the atmosphere to produce acid rain. When this acid rain reaches oceans and other water sources, the changing pH greatly affects the respiration of plants, decreasing the available oxygen concentration, which in turn affects wildlife.[1,2] There are several other problems associated with low oxygen concentrations in these environments, making the detection of oxygen gas in both water and air increasingly important.

Electrochemical Sensors

Currently, two classes of oxygen sensors are used extensively: electrochemical and optical. The most commonly used electrochemical sensors are based on the amperometric Clark cell which measures the change in current at the reduction potential of oxygen.[3] The Clark electrode was developed to measure blood oxygen levels *in vivo* by measuring changes in current due to the reduction of oxygen at a specific voltage. While the first generation of the electrode was able to detect oxygen, it was susceptible to poisoning by a variety of contaminants such as red blood cells, CO_2, or H_2S present in the analyte solutions.[4-8]

Current Clark-type electrodes consist of a platinum disk surrounded by a thin film of potassium chloride and a silver chloride anode supported within the polyethylene membrane.[6] The membrane allows more reliable and accurate measurements of oxygen to be made as both electrodes are in the same electrochemical cell and eliminates the

possibility of electrode poisoning.[6] Response times for Clark-type electrodes are on the order of seconds, but most still require minimal stirring of the analyte solution and are influenced by temperature changes, electrical interference, and electrolyte loss.[3,5-7,9]

While great steps have been taken to improve electrochemical oxygen sensing technology, disadvantages remain.[10] These devices inherently consume oxygen near the electrode surface in order to make measurements, altering the concentration of oxygen in the sampling environment.[3,4,11] Partial pressures can be measured instead, but this value changes with temperature, complicating the determination of the oxygen concentration within a specific sample.[5-7] Additionally, the instrumentation to support these electrodes are bulky, difficult to miniaturize, and susceptible to electrical interference.[3,4,12] Further technical problems are associated with electrolyte solutions leaking or evaporating, decreasing apparatus longevity.[3,10] As a result, new optical technologies have been developed to eliminate many of the problems associated with electrochemical measurements while still allowing the reproducible and sensitive detection of oxygen.

Optical Sensors

Optical sensors are promising candidates for replacing electrochemical sensors, particularly in areas where miniaturization is required. Such devices can make sensitive and reproducible measurements that do not suffer from electrical interference or electrolyte loss as they rely solely on the ability of oxygen to quench emission from triplet states.[3] Excitation of a complex in its ground state (A) by light generates an excited triplet state (A^*) through intersystem crossing from the singlet excited state. Normally, the excited state relaxes to the ground state through either non-radiative

processes or the emission of light (Equation 1). When a quencher (Q), such as oxygen, is introduced into the system, it provides an additional non-radiative relaxation pathway (Equation 2 and Figure 1). As a result of the energy transfer, the complex returns to the ground state and the quencher is now in the excited state, Q^* (Equation 2). In the case of oxygen, the singlet excited state relaxes to the ground state through an undetected radiative process. Consequently, the emission of the complex decreases with increases in oxygen concentration.

$$A \xrightarrow{h\nu} A^* \longrightarrow A + h\nu \qquad \textbf{(1)}$$

$$A \xrightarrow{h\nu} A^* + Q \longrightarrow A + Q^* \qquad \textbf{(2)}$$

The relationship between luminescence intensity (or excited state lifetime) and the concentration of quencher is described by the Stern-Volmer equation as shown in Equation 3. The emission intensity of the complex in the presence and in the absence of the quencher are represented by I and I_0, respectively. Lifetime measurements made in the presence (τ) or absence (τ_0) of quencher can be substituted for the corresponding intensity value. The Stern-Volmer quenching constant is represented by K_{SV}. This constant is derived from the rate constants for quenching (k_q), radiative (k_r) and non-radiative (k_{nr}) decay processes as shown in Equation 4.[13]

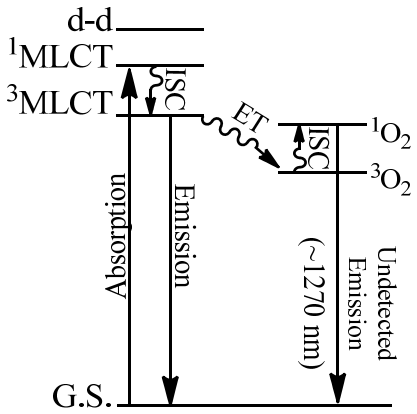

Figure 1. Energy transfer processes involved in the spectroscopic detection of oxygen.

$$\frac{I_0}{I} = \frac{\tau_0}{\tau} = 1 + K_{SV}[O_2] \quad \textbf{(3)}$$

$$K_{SV} = \frac{k_q}{k_r + k_{nr}} \quad \textbf{(4)}$$

This simple relationship allows quantification of oxygen concentration due to the direct relationship between it and the amount of emission quenching.[3, 8,14] The Stern-Volmer equation has been modified to explain the quenching dynamics of a rigid lumiphore and is given below in Equation 5.[15]

$$\frac{I_0}{I} = 1 + \tau_0 f N_A 4\pi D_{O_2}(r_L + r_{O_2}) S_{O_2} p_{O_2} \quad \textbf{(5)}$$

In this equation, the modifiable variables are defined as follows:

τ_o	Lumiphore lifetime in absence of quencher
D_{O_2}	Molecular oxygen diffusion constant
$(r_L + r_{O_2})$	Sum of the encounter radii for the lumiphore and molecular oxygen
S_{O_2}	Solubility of molecular oxygen
p_{O_2}	Partial pressure of molecular oxygen

and the constants are given as:

f	Statistical factor incorporating probability of oxygen reaching an emissive site
N_A	Avogadro's number

Alteration of any modifiable variable can greatly improve the sensing ability of a complex. Optical sensors based on these straightforward principles are an attractive alternative due to the elimination of prior difficulties with electrochemical detection.

Optical sensors have been developed using organic and inorganic components.[3,4,8,16-19] Ruthenium(II) complexes with three polypyridine ligands are most commonly used in optical devices. Photostable dyes like $[Ru(bath)_3]^{2+}$ (bath = 4,7-diphenyl-1,10-phenanthroline), $[Ru(phen)_3]^{2+}$ (phen = 1,10-phenanthroline), $[Ru(bpy)_3]^{2+}$ (bpy = 2,2′-bipyridine) are used for their long excited state lifetimes, high quantum yields, and have well characterized excited states.[3,4,8,16-18] In addition to these properties, complexes based on ruthenium(II) have significant Stokes shifts and can be excited by light from the visible region of the spectrum.[17] The excitation of the complex with visible light promotes a metal centered d electron to a ligand π^* orbital in a process known as metal-to-ligand charge transfer (MLCT).[17] MLCT is responsible for intensely colored complexes and is also a favorable electronic transition, increasing the likelihood of emission from the resulting excited state.[20]

Another class of transition metal complexes used for optical sensors is based on metalloporphyrins. Sensing devices with platinum and palladium porphyrins have been used extensively due to their long lived excited states and tendency to phosphoresce.[3,21-24] For most Pd and Pt metalloporphyrin systems, lifetimes are on the order of hundreds of microseconds and the excitation is largely a π to π^* transition based in the porphyrin.[17,21,24] The porphyrin can be modified to achieve the desired luminescent properties. Pt and Pd porphyrin modified with ketone functionalities have been embedded into polystyrene to produce oxygen sensing films. The films are stable to photooxidation and have lifetimes of approximately 450 μs but quantum yields less than 0.01.[24] The addition of fluorinated substituents on the porphyrin red shifts the emission, but the lifetime and quantum yield decrease by at least a factor of ten.[24,25] Platinum

octaethylporphyrin complexes sense low concentrations (less than 10 ppm) of dissolved oxygen, but curved Stern-Volmer plots indicate two components are responsible for quenching.[23] Metalloporphryin complexes are advantageous due to their intense luminescence, but are not optimal due to the curved Stern-Volmer plots and temperature sensitivity.[21-24] Encapsulation of these materials within a polymer matrix can improve the ruggedness of the sensor, but generating a uniform film is difficult.

In polymer device fabrication, the polymer absorbs a solution of the metal complex and the solution evaporated. The resulting doped material is used to make a film. If temperatures used to generate the films are too high, the transition metal complexes cluster within the film, leading to uneven doping. The emission of these materials changes over the surface of the film, leading to inconsistent oxygen sensitivity.[3,22,23] The thickness of the film can also vary from one device to another with thinner areas showing faster response times.[3,21,22] Different responses have also been observed due to the polymer chosen for the device. Silicon rubber appears to be the encapsulation material of choice as it has a high oxygen permeability, is hydrophobic, and experiences minimal dye leaching.[3] Siloxanes are also popular due to their low glass transition temperature, benign response to many physiological processes, and high permeability to oxygen.[17]

Stern-Volmer plots of oxygen quenching by polymer-based devices have characteristic downward curvatures, indicating multiple sites are responsible for emission quenching.[3,17] Analysis of this type of data is complex and time consuming. Eliminating one component can be difficult, especially if its presence is the result of encapsulation.

Unfortunately, the time consuming data interpretation makes application of such devices into commonplace technologies impractical.

Metal complexes suspended in an oxygen permeable polymer may offer decreased decomposition of the metal complex, but the presence of multiple quenching sites remains problematic.[3,17,26] Ideally, an optical sensing device would rely on equivalent emission sites that react reversibly in the presence of oxygen, providing a more simplistic model for data interpretation. An optical sensor using an emissive crystalline material may potentially be a significant improvement based on the simplistic relationship between concentration of oxygen and quenching of emission.

Moving Toward Solid-State Crystalline Optical Sensing

Recent work of the Mann group has focused on the development of crystalline materials for use in a variety of sensing applications.[27-31] Several of these crystalline materials detect oxygen while overcoming the problems associated with previous sensing methods including the presence of multiple emission sites, complicated instrumental operation, slow response times, and the inability to miniaturize instrumentation as mentioned above.[28-32] Crystalline optical sensing materials ideally contain one emissive site with a long excited state lifetime, are chemically inert toward the analyte, and contain void space in the form of channels. Based on previous research, all of the aforementioned problems may be overcome through the use of luminescent transition metal complexes made from zinc(II), copper(I), and iridium(III).[3,14,27-34]

The examples of emissive zinc(II) complexes are numerous. Since zinc is a biologically relevant element, there exist many spectrofluorimetric sensors for the zinc

ion.[34-38] In these sensors, chelation of the organic material by the zinc ion results in strong luminescence.[38] There has also been much interest in using zinc(II) complexes in fluorescence-based organic light emitting diodes (OLEDs), specifically to produce blue emitters.[39,40] This blue color is the result of the emission from the ligand-based π to π^* transitions. The metal contributes little to the emission as zinc(II) is d^{10}.[34] As a result, the emission of these devices can be tuned by simply modifying the ligand.[41-43] Zinc(II) complexes have other luminescent applications such as fluorescent labels for various proteins and as sensors for phosphates, explosives, and nerve gas mimics.[34,36,44-48]

Terpy (terpy = 2,2':6',2"-terpyridine) complexes of zinc(II) are emissive and their photophysical properties suggest that they can be used in the solid-state to sense oxygen.[36,44-47,49] Using terpy, a series of neutral compounds was generated and the sensing ability of such complexes was explored as a part of this work. The molecules are composed of $Zn(terpy)Br_2$-like molecules. The decision to use halogen atoms as the two anionic ligands was made with the intent to red shift the emission of the neutral compound based on the heavy atom effect.[50]

It is known that molecules with similar shapes tend to crystallize in similar fashions.[27] Based on this observation, a dicationic series of zinc(II) polypyridine compounds analogous to a previously studied set of ruthenium(II) compounds was synthesized.[27,28,32] These ruthenium compounds were found to crystallize with significant amounts of void space in the desired form of channels that would allow oxygen to diffuse into the crystal lattice.[32] It was proposed that the less expensive zinc based compounds would pack similarly. If the structures were similar, the sensitivity

toward oxygen could be as well.[32] The similarities between the crystal structures and photophysical properties of two specific compounds were examined.

Copper complexes are another inexpensive alternative to ruthenium- and platinum-based emissive complexes. They have been used in OLEDs to achieve efficient green emission and as polymer-supported oxygen sensors.[34,51-55] However, an interesting relationship between the structure of these copper(I) complexes and their photophysical properties hinders luminescence efficiency. McMillin has found that a square planar distortion in the tetrahedral geometry about the metal center occurs when copper(I) complexes reach their excited state.[56-60] As a result, an additional non-radiative pathway competes with any photophysical pathways that return the complex to the ground state. When sterically bulky substituents are added in the 2 and 9 position of 1-10 phenanthroline, this distortion is hindered and the photophysical properties are significantly improved.[34,52,57,61,62] The more rigid the complex can be made, the more efficient the emission.

Additionally, complexes of copper(I) and 2,9-substituted phenanthroline ligands have been found to exhibit long-lived excited-state luminescence, making them ideal candidates for oxygen sensing applications.[55] Our group recently published several investigations of these copper(I)-phenanthroline complexes and found that they are efficient oxygen sensors.[29-31] Some of these compounds were found to sense oxygen with K_{SV}'s greater than 90![31] However, the stability of these complexes was not systematically investigated. Herein, the stability of several oxygen sensing copper(I)-phenanthroline based complexes is presented.

Iridium(III) complexes have been investigated for their use in several optical applications due to their long excited state lifetimes and high quantum yields.[63-67] Applications in OLEDs and light-emitting electrochemical cells (LECs) have received the most attention due to the increased efficiency of such devices caused by the mixing of the singlet and triplet iridium excited state.[63,68-73] Terpy complexes with iridium have been used in many applications from emissive devices to optical sensors.[74-84] For example, terpy complexes with a pendant, non-bonding, pyridine ring at the 4′ position have been used as optical pH sensors based on the ability of this free pyridine ring to be protonated.[80] Similar complexes have proven to be effective optical chloride sensors due to the interaction of the chloride ion with pendant pyridyl substituents.[79] Terpy derivatives of ruthenium tend to have short lived MLCT states making them weak emitters, but when these ligands are bound to iridium intense phosphorescence is observed with lifetimes on the order of microseconds, due to the strong mixing of the singlet and triplet excited states of iridium.[83,85]

Solution-based luminescence measurements of iridium(III) tridentate polypyridine complexes suggest solid-state crystalline forms may also exhibit several of these favorable luminescence characteristics. The additional advantage of *bis*-terpyridine Ir(III) compounds is that the neutral nature of the ligand and the charge of the metal center necessitates three counterions. It is hypothesized that when the emissive metal complex is paired with three highly fluorinated anions, the amount of void space generated in the crystal lattice will be significant enough to assist in oxygen diffusion, resulting in a better oxygen sensor. The synthesis of these materials has been attempted and the obtained compounds were tested for sensitivity toward oxygen.

References

1. Chestnut, L. G.; Mills, D. M. *J. Environ. Manage.* **2005**, *77*, 252.

2. Grubert, J. P. *J. Environ. Eng. Sci.* **2003**, *2*, 99.

3. Mills, A. *Platinum Met. Rev.* **1997**, *41*, 115.

4. Choi, M. M. F.; Xiao, D. *Anal. Chim. Acta* **2000**, *403*, 57.

5. Clark, L. C., Jr.; Wold, R.; Granger, D.; Taylor, Z. *J. Appl. Physiol.* **1953**, *6*, 189.

6. Severinghaus, J. W.; Astrup, P. B. *J. Clin. Monit.* **1986**, *2*, 174.

7. Severinghaus, J. W.; Astrup, P. B. *J. Clin. Monit.* **1986**, *2*, 125.

8. Trettnak, W.; Gruber, W.; Reininger, F.; Klimant, I. *Sens. Actuators, B* **1995**, *B29*, 219.

9. Skoog, D. A. W., Donald M.; Holler, F. John; Crouch, Stanley R. *Fundamentals of Analytical Chemistry*; 8th ed.; Brooks/Cole-Thompson Learning: Belmont, CA, 2004.

10. Yan, H.; Lu, J. *Sens. Actuators* **1989**, *19*, 33.

11. Preidel, W.; Rao, J. R.; Mund, K.; Schunck, O.; David, E. *Sens. Actuators, B* **1995**, *B28*, 71.

12. Mortimer, A. G.; Reed, G. P. *Sens. Actuators, B* **1995**, *B24*, 328.

13. Turro, N. J. *Modern Molecular Photochemistry*; University Science Books: Sausalito, CA, 1991.

14. Demas, J. N.; Harris, E. W.; McBride, R. P. *J. Am. Chem. Soc.* **1977**, *99*, 3547.

15. Douglas, P.; Eaton, K. *Sens. Actuators, B* **2002**, *B82*, 200.

16. Mills, A. *Chem. Soc. Rev.* **2005**, *34*, 1003.

17. Demas, J. N.; DeGraff, B. A.; Coleman, P. B. *Anal. Chem.* **1999**, *71*, 793A.

18. McFarland, S. A.; Lee, F. S.; Cheng, K. A. W. Y.; Cozens, F. L.; Schepp, N. P. *J. Am. Chem. Soc.* **2005**, *127*, 7065.

19. Ramasamy, S. M.; Hurtubise, R. J. *Talanta* **1998**, *47*, 971.

20. Miessler, G. L.; Tarr, D. A. *Inorganic Chemistry*; 3rd ed.; Pearson Prentice Hall: Upper Saddle River, New Jersey, 2004.

21. DiMarco, G.; Lanza, M. *Sens. Actuators, B* **2000**, *B63*, 42.

22. Amao, Y.; Asai, K.; Okura, I. *J. Porphyrins Phthalocyanines* **2000**, *4*, 292.

23. Gillanders, R. N.; Tedford, M. C.; Crilly, P. J.; Bailey, R. T. *Anal. Chim. Acta* **2004**, *502*, 1.

24. Papkovsky, D. B.; Ponomarev, G. V.; Trettnak, W.; O'Leary, P. *Anal. Chem.* **1995**, *67*, 4112.

25. Atwater, B. W. *Journal of Fluorescence* **1992**, *2*, 237.

26. Meier, B.; Werner, T.; Klimant, I.; Wolfbeis, O. S. *Sens. Actuators, B* **1995**, *29*, 240.

27. McGee, K. A.; Mann, K. R. *J. Am. Chem. Soc.* **2009**, *131*, 1896.

28. McGee, K. A.; Marquardt, B. J.; Mann, K. R. *Inorg. Chem.* **2008**, *47*, 9143.

29. Smith, C. S.; Branham, C. W.; Marquardt, B. J.; Mann, K. R. *J. Am. Chem. Soc.* **2010**, *132*, 14079.

30. Smith, C. S.; Mann, K. R. *Chem. Mater.* **2009**, *21*, 5042.

31. Smith, C. S.; Mann, K. R. *J. Am. Chem. Soc.* **2012**, *134*, 8786.

32. McGee, K. A.; Veltkamp, D. J.; Marquardt, B. J.; Mann, K. R. *J. Am. Chem. Soc.* **2007**, *129*, 15092.

33. Demas, J. N.; DeGraff, B. A. *J. Chem. Educ.* **1997**, *74*, 690.

34. Barbieri, A.; Accorsi, G.; Armaroli, N. *Chem. Commun.* **2008**, 2185.

35. Walesa-Chorab, M.; Stefankiewicz, A. R.; Ciesielski, D.; Hnatejko, Z.; Kubicki, M.; Klak, J.; Korabik, M. J.; Patroniak, V. *Polyhedron* **2011**, *30*, 730.

36. Ma, Z.; Cao, Y.; Li, Q.; Guedes da Silva, M. F. C.; Frausto da Silva, J. J. R.; Pombeiro, A. J. L. *J. Inorg. Biochem.* **2010**, *104*, 704.

37. Righetto, S.; Rondena, S.; Locatelli, D.; Roberto, D.; Tessore, F.; Ugo, R.; Quici, S.; Roma, S.; Korystov, D.; Srdanov, V. I. *J. Mater. Chem* **2006**, *16*, 1439.

38. Mikata, Y.; Yamashita, A.; Kawamura, A.; Konno, H.; Miyamoto, Y.; Tamotsu, S. *Dalton Trans.* **2009**, 3800.

39. Li, X.; Zhu, D.; Gao, W.; Zhang, Y.; Mu, Y. *J. Chem. Res.* **2006**, 371.

40. Liu, Q.-D.; Wang, R.; Wang, S. *Dalton Trans.* **2004**, 2073.

41. Chen, S.-C.; Yu, R.-M.; Zhao, Z.-G.; Chen, S.-M.; Zhang, Q.-S.; Wu, X.-Y.; Wang, F.; Lu, C.-Z. *Cryst. Growth Des.* **2010**, *10*, 1155.

42. Gomes, C. S. B.; Gomes, P. T.; Duarte, M. T.; Di Paolo, R. E.; MacÌ§anita, A. n. L.; Calhorda, M. J. *Inorg. Chem.* **2009**, *48*, 11176.

43. Kuo, K.-L.; Huang, C.-C.; Lin, Y.-C. *Dalton Trans.* **2008**, 3889.

44. Zhou, X.; Jin, X.; Li, D.; Wu, X. *Chem. Commun.* **2011**, *47*, 3921.

45. Liang, L. J.; Zhao, X. J.; Huang, C. Z. *Analyst* **2012**, *137*, 953.

46. Wild, A.; Winter, A.; Hager, M. D.; Schubert, U. S. *Chem. Commun.* **2012**, *48*, 964.

47. Winter, A.; Friebe, C.; Chiper, M.; Schubert, U. S.; Presselt, M.; Dietzek, B.; Schmitt, M.; Popp, J. *Chem. Phys. Chem.* **2009**, *10*, 787.

48. Galardon, E.; Tomas, A.; Roussel, P.; Artaud, I. *Dalton Trans.* **2009**, 9126.

49. Priimov, G. U.; Moore, P.; Helm, L.; Merbach, A. E. *Inorg. Reac. Mech.* **2001**, *3*, 1.

50. Benniston, A. C.; Harriman, A.; Lawrie, D. J.; Mayeux, A. *Phys. Chem. Chem. Phys,* **2004**, *6*, 51.

51. Cuttell, D. G.; Kuang, S.-M.; Fanwick, P. E.; McMillin, D. R.; Walton, R. A. *J. Am. Chem. Soc.* **2002**, *124*, 6.

52. Miller, M. T.; Karpishin, T. B. *Sens. Actuators, B* **1999**, *61*, 222.

53. Shi, L.; Li, B. *Eur. J. Inorg. Chem.* **2009**, *2009*, 2294.

54. Shi, L.; Li, B.; Yue, S.; Fan, D. *Sens. Actuators, B* **2009**, *137*, 386.

55. Zhang, Q.; Zhou, Q.; Cheng, Y.; Wang, L.; Ma, D.; Jing, X.; Wang, F. *Adv. Mater.* **2004**, *16*, 432.

56. Everly, R. M.; Ziessel, R.; Suffert, J.; McMillin, D. R. *Inorg. Chem.* **1991**, *30*, 559.

57. Cuttell, D. G.; Kuang, S.-M.; Fanwick, P. E.; McMillin, D. R.; Walton, R. A. *J. Am. Chem. Soc.* **2001**, *124*, 6.

58. Palmer, C. E. A.; McMillin, D. R. *Inorg. Chem.* **1987**, *26*, 3837.

59. Ichinaga, A. K.; Kirchhoff, J. R.; McMillin, D. R.; Dietrich-Buchecker, C. O.; Marnot, P. A.; Sauvage, J. P. *Inorg. Chem.* **1987**, *26*, 4290.

60. Rader, R. A.; McMillin, D. R.; Buckner, M. T.; Matthews, T. G.; Casadonte, D. J.; Lengel, R. K.; Whittaker, S. B.; Darmon, L. M.; Lytle, F. E. *J. Am. Chem. Soc.* **1981**, *103*, 5906.

61. McMillin, D. R.; McNett, K. M. *Chem. Rev.* **1998**, *98*, 1201.

62. Cunningham, C. T.; Moore, J. J.; Cunningham, K. L. H.; Fanwick, P. E.; McMillin, D. R. *Inorg. Chem.* **2000**, *39*, 3638.

63. McGee, K. A.; Mann, K. R. *Inorg. Chem.* **2007**, *46*, 7800.

64. DeRosa, M. C.; Hodgson, D. J.; Enright, G. D.; Dawson, B.; Evans, C. E. B.; Crutchley, R. J. *J. Am. Chem. Soc.* **2004**, *126*, 7619.

65. Gao, R.; Ho, D. G.; Hernandez, B.; Selke, M.; Murphy, D.; Djurovich, P. I.; Thompson, M. E. *J. Am. Chem. Soc.* **2002**, *124*, 14828.

66. Tamayo, A. B.; Alleyne, B. D.; Djurovich, P. I.; Lamansky, S.; Tsyba, I.; Ho, N. N.; Bau, R.; Thompson, M. E. *J. Am. Chem. Soc.* **2003**, *125*, 7377.

67. Neve, F.; Crispini, A.; Campagna, S.; Serroni, S. *Inorg. Chem.* **1999**, *38*, 2250.

68. Chin, C. S.; Eum, M.-S.; Kim, S. y.; Kim, C.; Kang, S. K. *Eur. J. Inorg. Chem.* **2007**, 372.

69. Chou, P.-T.; Chi, Y. *Chem.--Eur. J.* **2007**, *13*, 380.

70. Lamansky, S.; Djurovich, P.; Murphy, D.; Abdel-Razzaq, F.; Lee, H.-E.; Adachi, C.; Burrows, P. E.; Forrest, S. R.; Thompson, M. E. *J. Am. Chem. Soc.* **2001**, *123*, 4304.

71. Okada, S.; Okinaka, K.; Iwawaki, H.; Furugori, M.; Hashimoto, M.; Mukaide, T.; Kamatani, J.; Igawa, S.; Tsuboyama, A.; Takiguchi, T.; Ueno, K. *Dalton Trans.* **2005**, 1583.

72. Ragni, R.; Plummer, E. A.; Brunner, K.; Hofstraat, J. W.; Babudri, F.; Farinola, G. M.; Naso, F.; De Cola, L. *J. Mater. Chem.* **2006**, *16*, 1161.

73. Su, H.-C.; Chen, H.-F.; Fang, F.-C.; Liu, C.-C.; Wu, C.-C.; Wong, K.-T.; Liu, Y.-H.; Peng, S.-M. *J. Am. Chem. Soc.* **2008**, *130*, 3413.

74. Ayala, N. P.; Flynn, C. M., Jr.; Sacksteder, L.; Demas, J. N.; DeGraff, B. A. *J. Am. Chem. Soc.* **1990**, *112*, 3837.

75. Baranoff, E.; Dixon, I. M.; Collin, J.-P.; Sauvage, J.-P.; Ventura, B.; Flamigni, L. *Inorg. Chem.* **2004**, *43*, 3057.

76. Bolink, H. J.; Coronado, E.; Costa, R. D.; Lardies, N.; Orti, E. *Inorg. Chem.* **2008**, *47*, 9149.

77. Flamigni, L.; Collin, J.-P.; Sauvage, J.-P. *Acc. Chem. Res.* **2008**, *41*, 857.

78. Flamigni, L.; Ventura, B.; Barigelletti, F.; Baranoff, E.; Collin, J.-P.; Sauvage, J.-P. *Eur. J. Inorg. Chem.* **2005**, 1312.

79. Goodall, W.; Williams, J. A. G. *Dalton* **2000**, 2893.

80. Licini, M.; Williams, J. A. G. *Chem. Commun.* **1999**, 1943.

81. Natrajan, L. S.; Toulmin, A.; Chew, A.; Magennis, S. W. *Dalton Trans.* **2010**, *39*, 10837.

82. Williams, J. A. G.; Wilkinson Andrew, J.; Whittle Victoria, L. *Dalton Trans.* **2008**, 2081.

83. Yoshikawa, N.; Matsumura-Inoue, T.; Kanehisa, N.; Kai, Y.; Takashima, H.; Tsukahara, K. *Anal. Sci.* **2004**, *20*, 1639.

84. Yoshikawa, N.; Yamabe, S.; Kanehisa, N.; Kai, Y.; Takashima, H.; Tsukahara, K. *Eur. J. Inorg. Chem.* **2007**, 1911.

85. Yoshikawa, N.; Matsumura-Inoue, T. *Anal. Sci.* **2003**, *19*, 761.

Chapter Two

Sensing of Oxygen Using a Family of Zn(terpy)Br_2 Based Complexes

Overview

A series of $Zn(terpy)Br_2$ (terpy = 2,2':6',2''-terpyridine) based compounds was synthesized in an attempt to generate an inexpensive and emissive solid-state oxygen sensor. The structures of two compounds were determined through single crystal X-ray diffraction and the structure of the third was available from previous reports. The structures were examined and void space within the lattice analyzed. One of the three compounds, $Zn(terpy\text{-}*)Br_2$ (terpy-* = 4,4',4''-(tri-*tert*-butyl)-2,2':6',2''-terpyridine), showed initial promise for use in oxygen sensing applications due to the highly sensitive response of the compound to small changes in oxygen concentration. However, issues with sample purity and emission stability revealed the compound is not an inadequate means of oxygen detection.

Introduction

The field of oxygen sensing has reached a critical stage where the development of materials must also focus on the cost of the material. One of the most inexpensive metals that could be utilized in this application is zinc.[1,2] Currently, 2,2':6',2''-terpyridine (terpy) based zinc(II) complexes are used in photoluminescent devices, emissive metallopolymers, and luminescent sensors.[3-10] Based on their emissive characteristics, this class of zinc(II) terpy complexes could constitute a new class of oxygen sensors using an earth abundant metal center.

Due to the d^{10} nature of the metal center, the zinc(II) ion rarely participates in any low energy charge transfer processes. Therefore, zinc complexes tend to exhibit ligand centered emission that is fluorescent, but not phosphorescent.[11] Any changes in the

emission spectrum must be the result of the ligand. In this study, terpy derivatives will be used due to the ease of modifying the 4' position of the ligand which consequently alters the electronic and photophysical properties of resulting compounds.[7,12]

When developing solid-state oxygen sensors, our group aims to incorporate bulky components to generate void space within the crystal lattice. Void space is of the utmost importance as it allows oxygen to diffuse through the crystalline lattice. In the past, we have utilized propeller-shaped cations, tetrahedral anions, and various ligand substituents to generate the required void space. Since terpy ligands are easily modified, three different terpy ligands were chosen for this study, each with varying amounts of steric bulk. The compound made with terpy is expected to pack efficiently as there are no substituents on the ligand. The second compound will be made with *p*-tolyl-terpyridine. This larger tolyl group on the 4' position of the terpy may be able to π-stack with the tolyl group of a second molecule. Such directional interactions may help to dictate the void space within the lattice. A third and much more bulky ligand, terpy-* (where terpy-* = 4,4',4"-(tri-*tert*-butyl)-2,2':6',2"-terpyridine) will also be used. The *tert*-butyl groups are appended to each ring of the terpy ligand and should create space within the crystalline lattice due to their steric bulk. Compounds that showed initial sensitivity toward oxygen, were further tested for long term stability and characterized photophysically.

Experimental

General Considerations for Synthesis. Zinc(II) bromide was purchased from Fisher Scientific. The ligands 2,2':6',2''-terpyridine (terpy), 4'-(*p*-tolyl)-2,2':6',2''-terpyridine (tol-terpy), and 4,4',4''-(tri-*tert*-butyl)-2,2':6',2''-terpyridine (terpy-*) were purchased from Sigma-Aldrich and used as received. All solvents were used as received without further purification.

A 300 MHz Varian Unity NMR spectrometer was utilized to obtain ^{1}H NMR spectra. Chemical shifts are reported in units of ppm using an external reference to the residual proton resonance in deuterated solvents.

Zn(terpy)Br_2 (1)

To a solution of 0.0564 g (0.250 mmol) of $ZnBr_2$ in 5 mL of absolute ethanol was added a hot solution of ethanol (15 mL) and 0.0579 g (0.250 mmol) of 2,2':6',2''-terpyridine. Upon addition of the ligand, a yellow precipitate formed. The resulting solid was collect by vacuum filtration and washed with cold ethanol. The light yellow solid was then dried under vacuum (0.0788 g, 68 % yield). ^{1}H NMR (DMSO-d_6) δ 8.92 (m, 2 H), 8.84 (d, 2 H, J = 8.4 Hz), 8.77 (d, 2 H, J = 6.9 Hz), 8.60 (m, 1 H), 8.37 (m, 2 H), 7.92 (m, 2 H)

Zn(tol-terpy)Br_2 (2)

To a solution of 0.0488 g (0.217 mmol) of $ZnBr_2$ in 5 mL of absolute ethanol was added a hot solution of ethanol (15 mL) and 0.0955 g (0.295 mmol) of 4'-(*p*-tolyl)-2,2':6',2"-terpyridine. Upon addition of the ligand, a precipitate formed. The resulting solid was collected by vacuum filtration and washed with cold ethanol. The light yellow solid was then dried under vacuum (0.0525 g, 44 % yield). Crystals suitable for single crystal X-ray diffraction were grown from the slow evaporation of a dichloromethane solution. ^{1}H NMR (DMSO-d_6) δ 9.11 (s, 2 H), 9.00 (d, 2 H, *J* = 3.9 Hz), 8.90 (m, 2 H), 8.37 (t, 2 H, *J* = 7.5 Hz), 8.22 (d, 2 H, *J* = 7.5 Hz), 7.92 (m, 2 H), 7.49 (d, 2 H, *J* = 7.2 Hz), 2.46 (s, 9 H).

Zn(terpy-*)Br_2 (3)

To a solution of 0.2588 g (1.149 mmol) of $ZnBr_2$ in 10 mL of absolute ethanol was added a hot solution of ethanol (40 mL) and 0.5325 g (1.326 mmol) of 4,4',4"-(tri-*tert*-butyl)-2,2':6',2"-terpyridine. Upon addition of the ligand, a precipitate formed. The resulting solid was collect by vacuum filtration and washed with cold ethanol. The light yellow solid was then dried under vacuum (0.4819 g, 67 % yield). Crystals suitable for single crystal X-ray diffraction were grown from the slow evaporation of a dichloromethane solution. ^{1}H NMR (DMSO-d_6) δ 9.06 (d, 2 H, *J* = 5.1 Hz) 8.18 (s, 2 H), 8.08 (s, 2 H), 7.67 (dd, 2 H, *J* = 5.1, 1.2 Hz), 1.56 (s, 9H), 1.45 (s, 18 H)

X-ray Crystallography

The metrics for the crystal structure of $Zn(terpy)Br_2$ were available in *.cif format from the CCDC database.[13]

All data for the structure determinations of **2** and **3** were collected at the X-ray Crystallographic Laboratory (Department of Chemistry, University of Minnesota). Single crystals were attached to glass fibers and mounted on a Bruker APEX II Platform CCD for data collection at 173 K using graphite monochromated MoKα radiation (λ = 0.71073 Å).[14] An initial set of cell constants was calculated from reflections harvested from three sets of 12 frames oriented such that orthogonal wedges of reciprocal space were surveyed. Final cell constants were calculated from a minimum set of 7945 strong reflections from the actual data collection. Data were collected to the extent of at least 1.5 hemispheres at a resolution of 0.77 Å using φ-scans. Three major sections of frames were collected with 0.50 º steps in ω at 3 different ϕ settings and a detector position of -28 º in 2θ. For all structures, the intensity data were corrected for absorption and decay using SADABS.[15,16] Space groups were determined based on systematic absences and intensity statistics and the structures were determined using a direct-methods solution. Several full-matrix least-squares/difference Fourier cycles were performed to locate remaining non-hydrogen atoms. All calculations were performed using the SHELXTL-V6.12 suite of programs on Pentium computers.[17,18] Additional crystallographic information can be found in Table 1.

Packing analysis parameters were measured using PLATON/VOID.[19] with pictorial representations of the solvent channels generated with edited *.res files in Mercury.[20] The detection of solvent accessible voids by PLATON/VOID is done in the

following way: The unit cell is filled with the atoms from the structural model and each specific atom is assigned its respective van der Waals radius. A grid search generates a list of grid points with a minimum distance of 1.2 Å from the nearest van der Waals surface. This list of grid points is then used to produce a new list of grid points that makes up the solvent accessible areas. For the sets of grid points, the center of gravity and volume of the void are calculated. The overall solvent accessible volume is calculated along with the volume and center of gravity of individual 'voids'. PLATON/CAVPLOT was then used to create the edited *.res files that were used to generate the packing diagrams that include red spheres as representations of the solvent accessible void space.

Table 1. Crystallographic Data and Refinement Parameters.

Compound	**2**	**3**
empirical formula	$C_{22}H_{17}Br_2N_3Zn$	$C_{27}H_{35}Br_2N_3Zn$
crystal color, morphology	colorless, block	colorless, block
crystal system	Monoclinic	Hexagonal
space group	$P2_1/c$	$P3_221$
crystallization solvent	dichloromethane	dichloromethane
a, Å	8.1828(6)	12.4200(8)
b, Å	14.9028(10)	12.4200(8)
c, Å	16.6440(11)	15.9692(10)
α, deg	90	90
β, deg	97.6170(10)	90
γ, deg	90	120
volume (V), Å^3	2011.8(2)	2133.3(2)
Z	4	3
formula weight, g mol^{-1}	548.58	626.77
density (calculated), g cm^{-3}	1.811	1.464
temperature, K	173(2)	173(2)
absorption coefficient (μ), mm^{-1}	5.206	3.692
F(000)	1080	954
θ range, deg1.16 to 26.37	2.47 to 27.48	2.28 to 27.48
index ranges	$-10 \le h \le 10$	$-12 \le h \le 16$
	$-19 \le k \le 19$	$-16 \le k \le 13$
	$-21 \le l \le 21$	$-20 \le l \le 20$
reflections collected	22683	13272
independent reflections	4601 [R_{int} = 0.0232]	3261 [R_{int} = 0.0239]
weighting factors,[a] a, b	0.0301, 0.6950	0.0470, 0.0000
max, min transmission	0.4224, 0.1805	0.2597, 0.2597
data/restraints/parameters	4601/0/254	3261/0/172
R_1, wR_2 [$I > 2\sigma(I)$]	0.0189, 0.0494	0.0292, 0.0727
R_1, wR_2 (all data)	0.0236, 0.0512	0.0343, 0.0749
GOF	1.016	1.045
largest diff. peak, hole eÅ^{-3}	0.374, -0.401	0.644, -0.314

[a] $w = [\sigma^2(F_o^2) + (aP)^2 + (bP)]^{-1}$, where $P = (F_o^2 + 2F_c^2)/3$.

Preliminary Oxygen Sensing

The samples for preliminary testing were prepared by placing a small amount of the material into a depression in a ¼'' diameter aluminum rod. The sample was then placed into a swage cross-tube fitting apparatus designed to allow gas to flow over the sample and allow front face illumination as shown in Figure 1. An LED (light emitting diode) which was filtered through an interference filter was used as the excitation source and light brought to the sample by the center leg of a "six around one" bifurcated fiber optic probe. Resulting emission was collected through the six fiber channel and sent to an Ocean Optics USB-2000 spectrometer. The air, nitrogen, or oxygen gas was brought to the sample cross from a compressed gas cylinder and the flow was adjusted manually using needle valves. Spectra were collected manually through the Ocean Optics interface and data were analyzed with Microsoft Excel.

Controlled Oxygen Sensing

The same sample holder and fiber optic set up described for the preliminary testing was also used for these experiments (again, shown in Figure 1). However, in this instrumental set up, the spectrometer, mass flow controllers, temperature, and pressure monitors were interfaced to a computer to allow control of the unattended data acquisition via a custom LabVIEW program.[21-24]

The emission data collected were analyzed with a spreadsheet written in Microsoft Excel. Data from three cycles of spectra obtained at approximately 0.0, 0.003, 0.005, 0.008, 0.010, 0.013, 0.015, 0.017, 0.020, 0.022, 0.024, 0.027, 0.037, 0.047, 0.056, 0.065, 0.072, 0.079 0.10, 0.21, 0.25, 0.40, 0.50, 0.65, 0.80, 0.90 and 1.0 mole fraction

of oxygen in nitrogen were used for the Stern-Volmer plots. The acquisitions were performed at room temperature, or 21.8 ± 1 °C. Exact gas mole fractions were calculated by referencing the feedback voltage of the mass flow controllers to a calibration previously performed.[23] The emission intensity was integrated across the entire peak and divided by the integrated LED intensity (or in the case of weakly emitting samples, the second order diffraction from the grating) for each spectrum to give I_0 (intensity under N_2) and I (intensity at a given O_2 mixture). I_0/I was plotted versus oxygen mole fraction in nitrogen to yield a Stern-Volmer plot. A linear regression model was used to calculate the slope or K_{SV} parameter.

It should be noted that the K_{SV}*'s* reported here are expressed in units of mole fraction and have not been corrected for the atmospheric pressure in Minneapolis, MN of 0.97 atm. In order to compare these K_{SV} numbers to those reported previously, the K_{SV} in mole fraction needs to be corrected by dividing the current value by 0.97 atm to give the K_{SV} in units of atm^{-1}.

Stability Studies

The automated set up was used to collect data for stability investigations. In these experiments, the program exposed the sample to the following conditions. First, two Stern-Volmer runs were performed where the sample was exposed to approximately 0.0, 0.10, 0.21, 0.25, 0.40, 0.50, 0.65, 0.80, 0.90 and 1.0 mole fraction of O_2 in N_2. Next, the sample was exposed to nitrogen for approximately 8 hours, with a spectrum collected every 10 minutes. Then, the sample was exposed to oxygen for approximately 8 hours, again with a spectrum collected every ten minutes. Finally, two more Stern-Volmer runs

were performed. The LED remained on for the entire data collection. The spectra collected with LABVIEW were then analyzed using Microsoft Excel.

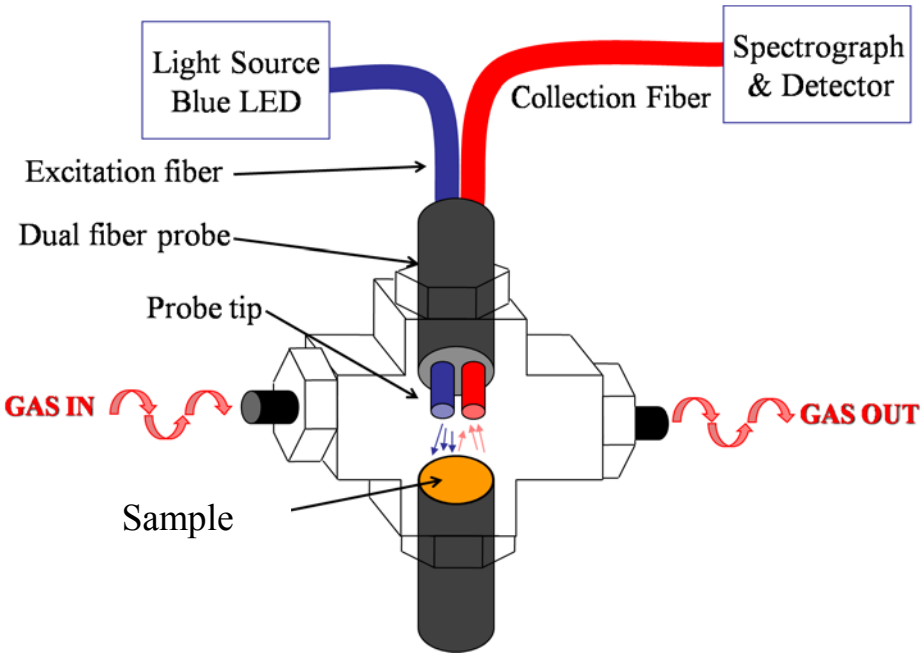

Figure 1. A schematic diagram of the sample holder used for all sensing measurements.

Results and Discussion

X-ray Crystallography

The *.cif file for the structure of **1** was available from the Cambridge Structural Database. The molecule lies on a twofold axis making half of the molecule unique. The available data were used to perform the PLATON/VOID calculation. No solvent accessible voids were found within the structure. The π-stacking of the terpy ligand along the *c** axis coupled with the distorted trigonal bipyramidal molecular geometry allows efficient packing in a head to tail fashion. A diagram of the packing is shown in Figure 2. The bond lengths about the metal center were within normal ranges with the zinc to bromine atom distance equal to 2.4179(2) Å and the distance from the zinc to the nitrogen atoms of the terpy are 2.1861(14) and 2.106(2) Å for the outer and central nitrogen atoms respectively.

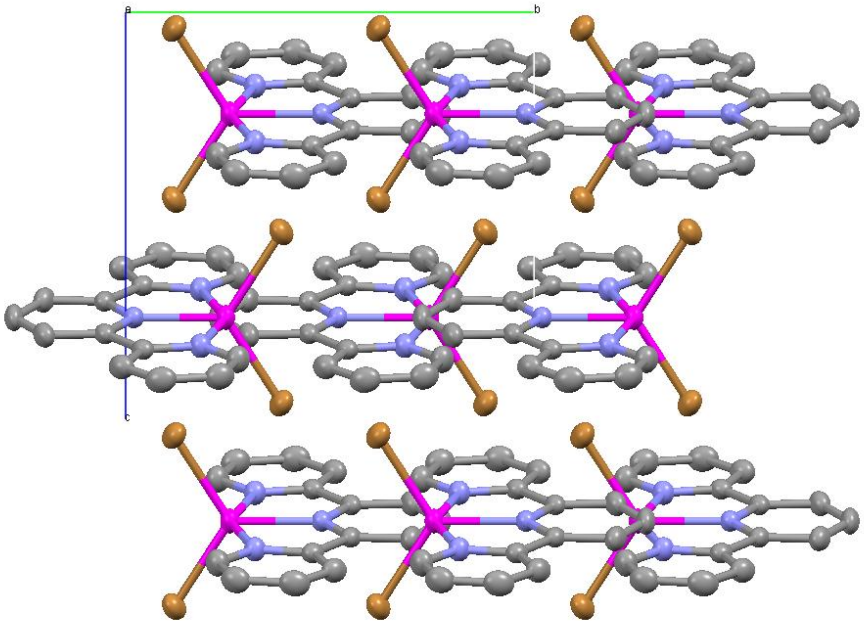

Figure 2. Packing diagram of **1** as viewed down the *a* axis. Hydrogen atoms have been removed for clarity.

The structure of **2** was determined using X-ray quality crystals grown from the slow evaporation of a dichloromethane solution (Figure 3). The compound crystallizes in the monoclinic space group $P2_1/c$ with no disorder. After the structure was refined to convergence, PLATON/VOID was performed on the data. Approximately 29.1 $Å^3$ (1.4 %) of void space was found in the unit cell. This void space takes the form of isolated pockets throughout the crystal. These isolated pockets are shown in Figures 4-6 as red spheres. The bond lengths about the metal center were within normal ranges with the zinc to bromine atom distance equal to 2.3890(3) and 2.4040(3) Å and the distance from the zinc to the outer ring nitrogen atoms of the tol-terpy equal to 2.2036(14) and 2.2186(14) Å. The distance from the zinc to the nitrogen atom of the central ring is significantly shorter at 2.0981(14) Å.

We were hopeful that the tolyl portion of the tol-terpy ligand would aid in the creation of void space though π-stacking interactions. However, these interactions are not present in the structure. It is possible that changing the crystallization solvent may direct the compound to π-stack, but issues with solubility in the desired solvents preclude this route.

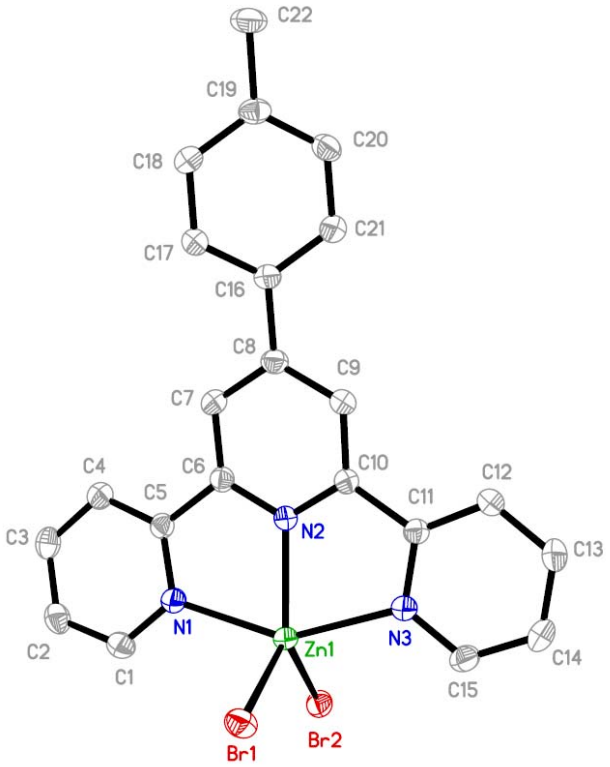

Figure 3. Labeled thermal ellipsoid plot of **2** with hydrogen atoms removed for clarity. Thermal ellipsoids are drawn at 50 % probability.

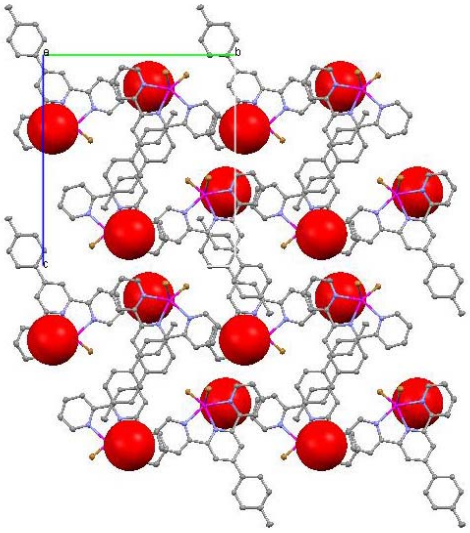

Figure 4. Void space representation of **2** as viewed down the *a* axis. The voids are isolated pockets throughout the structure and are represented as red spheres.

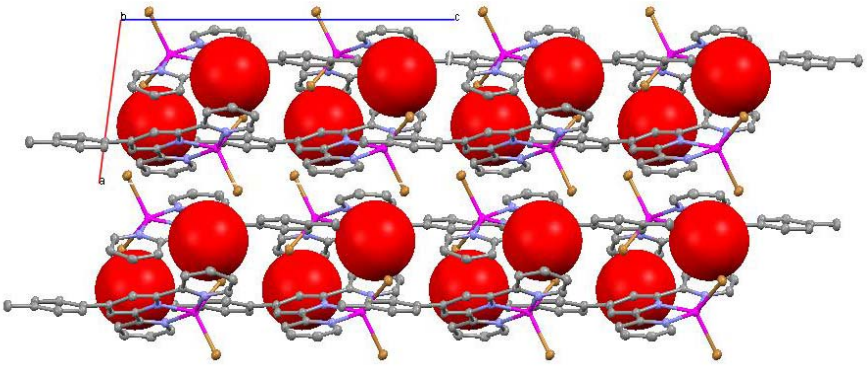

Figure 5. Void space representation of **2** as viewed down the *b* axis. The voids are isolated pockets throughout the structure and are represented as red spheres.

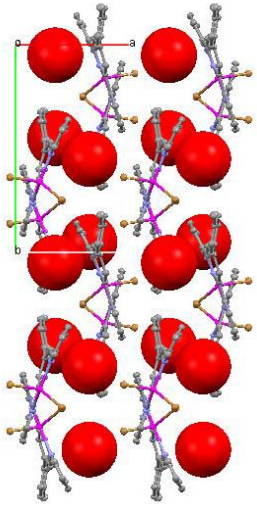

Figure 6. Void space representation of **2** as viewed down the *c* axis. The voids are isolated pockets throughout the structure and are represented as red spheres.

The structure of **3** was determined from X-ray quality crystals grown from the slow evaporation of a dichloromethane solution. The compound crystallizes in the hexagonal space group of $P3_221$ (Figure 7). Half of the molecule is unique as Zn1 N2 C8 C13 sit on a twofold axis located at (x, 0, 1/6). The methyl group of the central pyridine ring is disordered over this special position and is modeled as such with equal occupancies. After the structure was refined and converged, PLATON/VOID was performed on the data and 71.8 $Å^3$ (3.4 %) of void space was found within the structure.

Similar to the structure of **2**, the void space in the crystal structure of **3** takes the form of isolated pockets (Figures 8-10). Again, all bond distances fall within the normal range based on a CCDC search. The bond lengths about the metal center are within normal ranges with the distance from the zinc to the bromine atom equal to 2.3943(4) Å and the distance from the zinc to the nitrogen atoms of the terpy-* are 2.152(2) and 2.099(3) Å for the outer and central nitrogen atoms respectively.

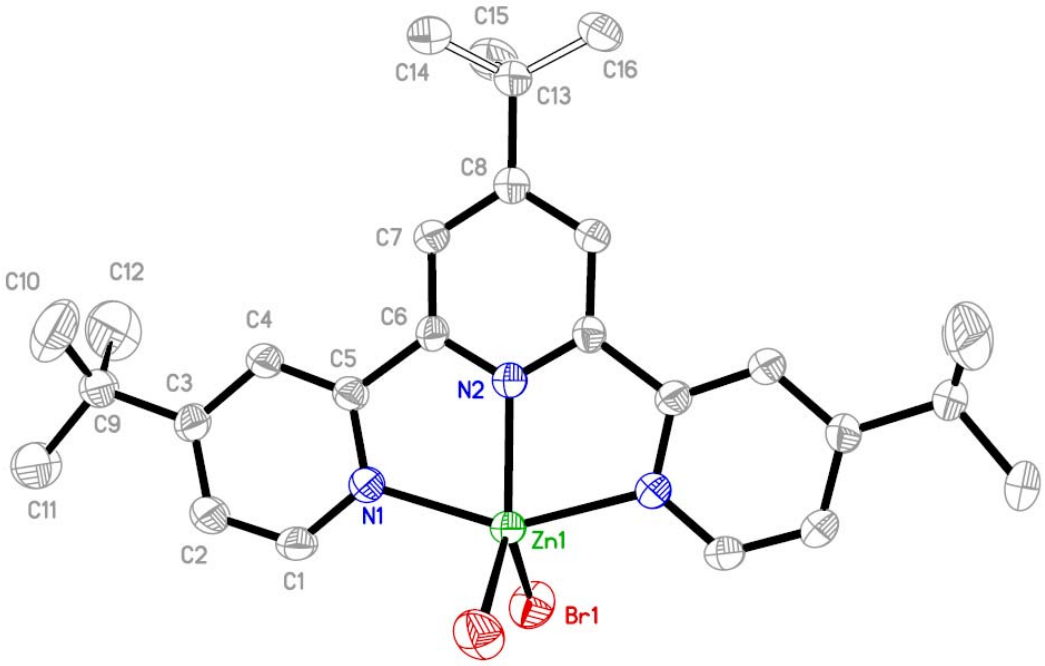

Figure 7. The structure of **3** is shown with hydrogen atoms removed for clarity and thermal ellipsoids drawn at 50 % probability. Only the unique atoms are labeled as the rest are symmetry generated.

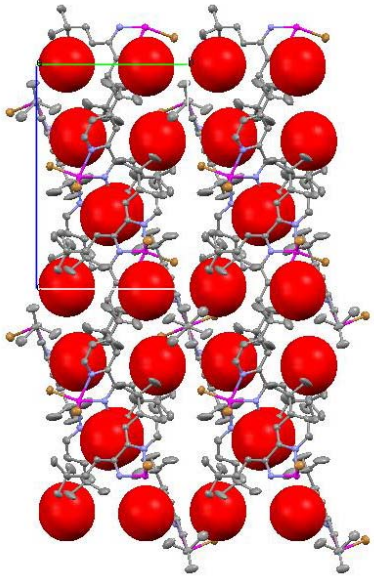

Figure 8. Void plot of **3** as viewed down the *a* axis. The voids are isolated pockets throughout the structure and are represented as red spheres.

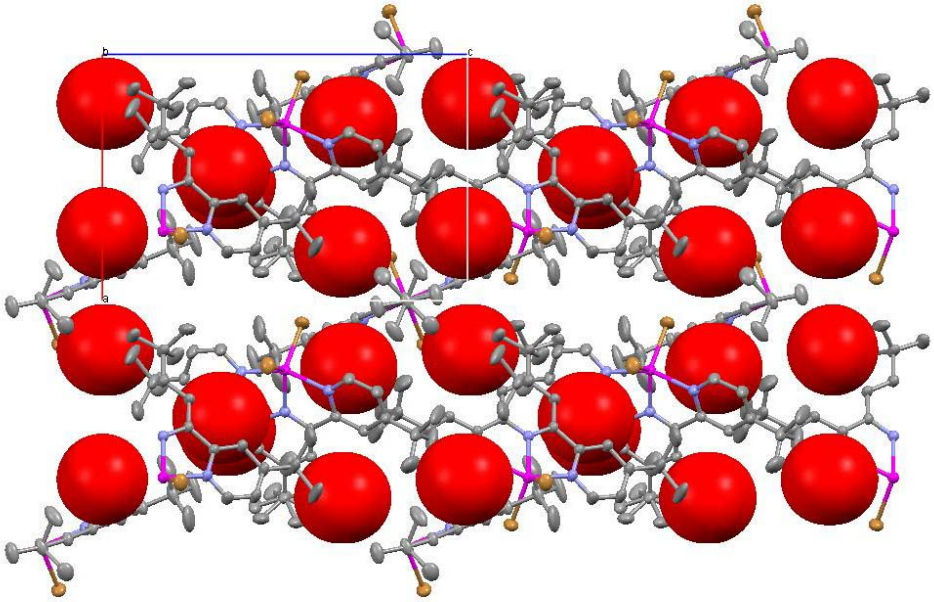

Figure 9. Void plot of **3** as viewed down the *b* axis. The voids are isolated pockets throughout the structure and are represented as red spheres.

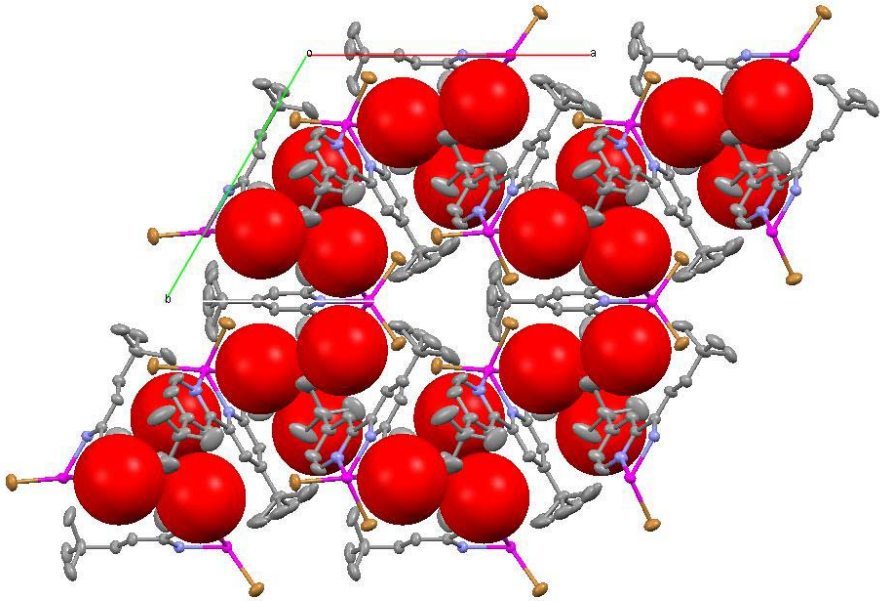

Figure 10. Void plot of **3** as viewed down the *c* axis. The voids are isolated pockets throughout the structure and are represented as red spheres.

Oxygen Sensing Measurements

Initially the reaction powder of **1** was manually exposed to alternating cycles of nitrogen, air, and oxygen. Emission spectra were obtained under each of the three conditions using a 405 nm LED excitation source. The compound is weakly emissive and does not exhibit any sensitivity toward oxygen as the spectra remained unchanged during the switching of the gasses (Figure 11). The compound also proved to be stable to continued exposure to the LED light source. During continued exposure of the sample to the LED, the emission intensity did not significantly change with time (Figure 12). No further testing of this compound with the more controlled concentrations of oxygen was performed.

The crystal structure of $Zn(terpy)Br_2$ is consistent with the lack of oxygen sensitivity as there is no void space within the material for oxygen to diffuse. Thus, the oxygen cannot interact with the excited state of the material and no luminescence quenching is observed.

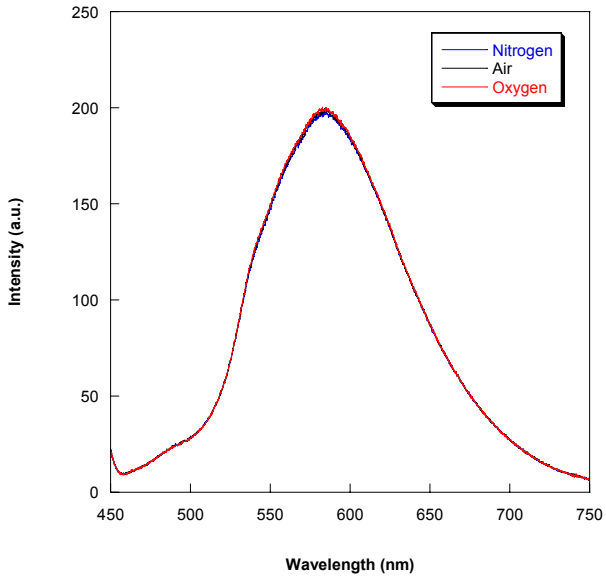

Figure 11. Emission profile of **1** when exposed to nitrogen, air, and oxygen. No change in intensity is observed, but the compound was found to be stable to continuous LED illumination.

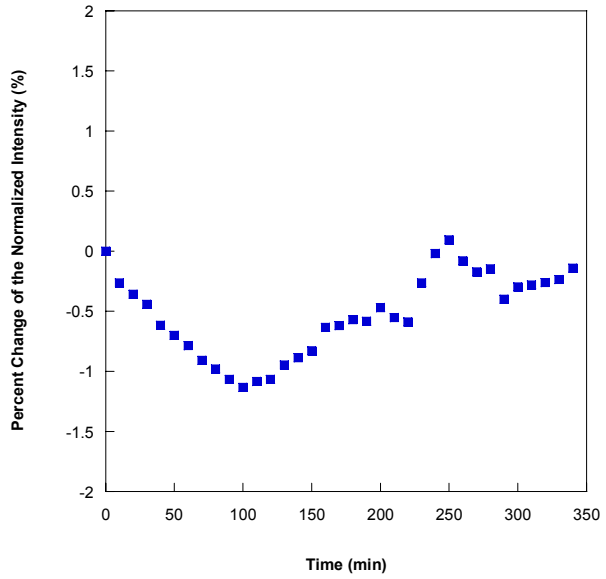

Figure 12. The compound **1** was tested for stability while being exposed to nitrogen gas and constant illumination from a 405 nm LED light source. The emission intensity does not change significantly with time, revealing that this compound is photophysically stable.

Emission spectra of crystals of **2** grown from dichloromethane were obtained under nitrogen and oxygen using a 350 nm LED excitation source. Much like **1**, **2** is weakly emissive. Initial exposure to oxygen caused little change in emission intensity. Upon switching back to nitrogen, the emission intensity did not return to the original intensity obtained under nitrogen. At this point, the sample was allowed to sit under nitrogen and a spectrum collected every five minutes. During this time, the emission intensity decreased roughly 4 % (Figure 13).

The compound is not reliably sensitive to oxygen as the emission intensity does not return after oxygen exposure. Additionally the instability of the compound to LED illumination indicates the material is a poor candidate for oxygen sensing devices.

While the instability of the compound is surprising, the lack of oxygen sensitivity is not. The crystal structure of **2** reveals little void space. The void space that is present in the material is also found in pockets meaning that any oxygen that can diffuse into the pocket cannot easily continue through the crystal and interact with any additional excited metal complexes.

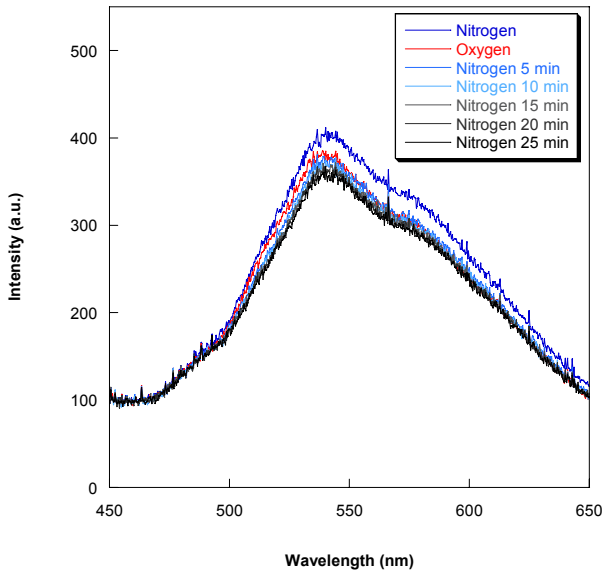

Figure 13. Emission profile of **2** under both nitrogen and oxygen. With time, the emission slowly degrades.

Crystals of **3** grown from dichloromethane were initially tested using a 10 point Stern-Volmer plot on the automated set up using a 365 nm LED excitation source. A large jump in the sensitivity was found between nitrogen and approximately 0.09 mole fraction of oxygen in nitrogen. This large increase was followed by relatively no change in the response with exposure to higher oxygen concentrations. A second experiment was then performed to determine the nature of the large increase in sensitivity. This study generated much smaller concentrations of oxygen to determine the K_{SV} of the material within this range.

The results (Figure 14) indicate the material is highly sensitive to the initial changes in oxygen concentration. Due to the curvature of the response, the Stern-Volmer data were fit to a model which uses two K_{SV} parameters. This model has been previously reported and will briefly be described.[21] Curved Stern-Volmer plots can be fit to a two-site model according to Equation 1 where I_0 is the integrated emission intensity with no quencher present, I is the integrated emission intensity with a given concentration of oxygen present, f is the fractional contribution to the unquenched emission where $f_1 + f_2 = 1$. The different Stern-Volmer quenching constants are given as K_{SV1} and K_{SV2} and $[O_2]$ is the concentration of oxygen under which I was determined.

$$\frac{I_0}{I} = \frac{1}{\frac{f_1}{1+K_{SV1}[O_2]} + \frac{f_2}{1+K_{SV2}[O_2]}} \qquad \textbf{(1)}$$

The data collected during the sensing experiments were fit to this two-site model using Microsoft Excel to give the resulting K_{SV1}, K_{SV2}, f_1, and f_2 parameters.

From this model, K_{SV1} of **3** in this region is approximately 300! This large K_{SV1} parameter explains more than 70 % of the data and a smaller K_{SV2} of less than 1 explains

the remaining fraction of the change in emission. However, there should be only one component responsible for the emission in these materials based on their crystalline nature. At this point, a non-sensing ligand impurity was suspected and attempts were made to purify the material.

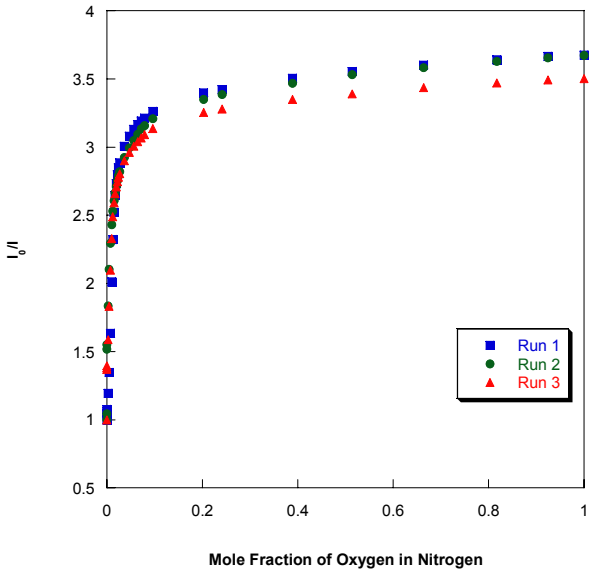

Figure 14. Stern-Volmer plots for **3** acquired to investigate the sensing behavior of the material in the low oxygen concentration range.

Identifying and Removing the Impurity

Suspecting the impurity was free ligand, the emission spectrum of terpy-* was acquired under nitrogen with the same 365 nm LED source. The emission of **3** is similar to the emission profile of the free terpy-* ligand but red-shifted approximately 40 nm (Figure 15). The ligand emission is expected to be similar to the emission of the complex as the electronic transition responsible for the emission of the compound is the same π to π^* ligand-based transition. The red shift is attributed to the heavy atom effect caused by the ligation of the terpy-* to the $ZnBr_2$ core.[25] The emission from **3** has a shoulder in the region of the free ligand emission, although this terpy-* impurity was not readily noticed in the ^1H NMR of the material. A terpy-* impurity was also not observed in the diffraction pattern or found to be an additional component during the determination and refinement of the single crystal structure.

Samples of the free ligand were then tested for oxygen sensitivity and the material showed no sensitivity toward oxygen. The spectrum of **3** obtained at 20 % oxygen was subtracted from the spectrum of **3** obtained under pure nitrogen. The result was a spectrum which appears to have no component of free ligand emission as the baseline practically returns to zero over the wavelength range for the free ligand emission (Figure 16). These results suggest that the emission of the ligand is present in both of these emission spectra. The ligand again is shown to not sense and can be identified as the second component found with the two-site model.

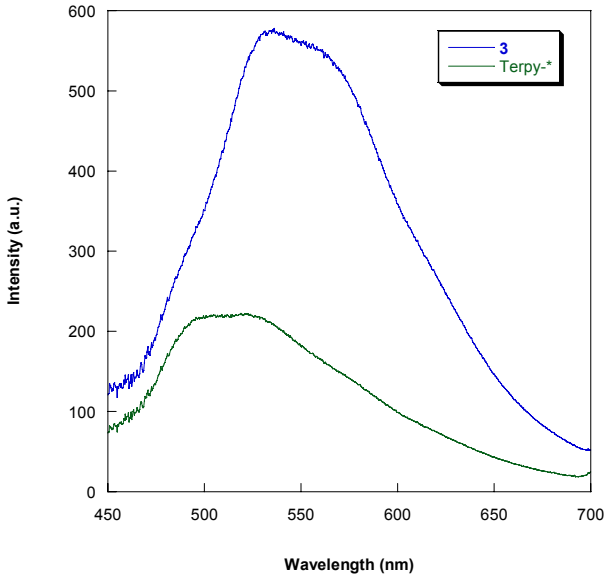

Figure 15. The emission profile of **3** (blue) under nitrogen in comparison of the emission of the free ligand terpy-* (green). The two emission profiles are shifted from one another approximately 40 nm.

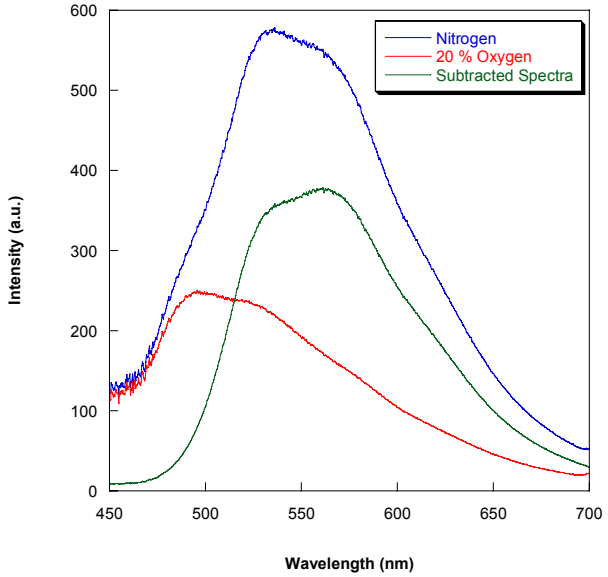

Figure 16. The spectra of **3** under both nitrogen and a concentration of oxygen similar to that found in air are shown. The oxygen spectrum was then subtracted from the nitrogen spectrum to gain insight to the emission profile of the sensing material.

Several attempts to eliminate the free ligand impurity were made. Thinking that the impurity may simply be a ligand coating on the crystals, the crystals were crushed to increase the surface area of the crystals and decrease the proportion of impurity to compound. The testing of these crushed crystals did not improve the sensing ability (Table 2). A large scale synthesis of the complex was carried out hoping to decrease the amount of excess ligand present in the synthesis. Crystals of this material were grown from dichloromethane, were crushed and tested, but again, the spectroscopic purity was not improved. Then, crystals of **3** grown from dichloromethane were washed with hexanes to remove any ligand coating. These crystals were allowed to dry, then were crushed and tested for oxygen sensitivity. While the spectra show slightly less emission from the terpy-* impurity, it was not removed completely. As can be seen in Table 2, the washing of the crystals did improve the K_{SV1} parameter, but the second component still remained in a significant proportion.

An alternative explanation for the ligand impurity could be that any exposed surface decomposes in the humid atmosphere of the lab. The compound **3** would decompose into $ZnBr_2 \bullet x\ H_2O$ and free terpy-*. The terpy-* would then emit along with **3** while the $ZnBr_2 \bullet x\ H_2O$ species would not. This newly formed film is not detected during X-ray crystallographic studies due to its proposed amorphous nature, but would still contribute to the sensing response of the material.

A third explanation for the free ligand impurity could be attributed to the labile nature of the Zn atom. As the material sits in solution, the coordination environment about the metal center may be in flux. Some of the ligand may be bound to the metal

center as **3** while the rest has dissociated to form $ZnBr_2$ and free terpy-* There appears to be few options to systematically remove any impurity from the material.

Table 2. Two-site Modeling Parameters for Various Samples of **3**.

	Unwashed Whole Crystals of **3**	Powder of Free Terpy-*	Unwashed Crushed Crystals of **3**	Washed and Crushed Crystals of **3**
K_{SV1}	266.5	266.49	259.65	505
f01	73%	2%	69%	83%
K_{SV2}	0.007	0.0398	0.132	0.067
f02	27%	98%	31%	17%

Stability Testing

Crystals of the **3** were tested for stability toward both oxygen and LED exposure. From these studies, it was determined that while the emission intensity of the complex under both nitrogen and oxygen did increase over the course of the 8 hour exposure, the sensitivity slowly decreased. Under nitrogen, the emission intensity increased approximately 75 % and while the emission intensity increased 21 % under oxygen (Figure 17). Based on the increase of emission under these two conditions, it was expected that the sensitivity of the compound after the gas exposures would have remained the same or improved from the sensitivity before the gas exposures.

However, the data collected indicate that the compound became less sensitive to oxygen after the gas exposures (Figure 17b). Despite the increase in the intensity of emission, the sensitivity of the compound degrades. Based on these results and the problems with ensuring sample purity, **3** is not a viable compound for use in solid state oxygen sensing devices.

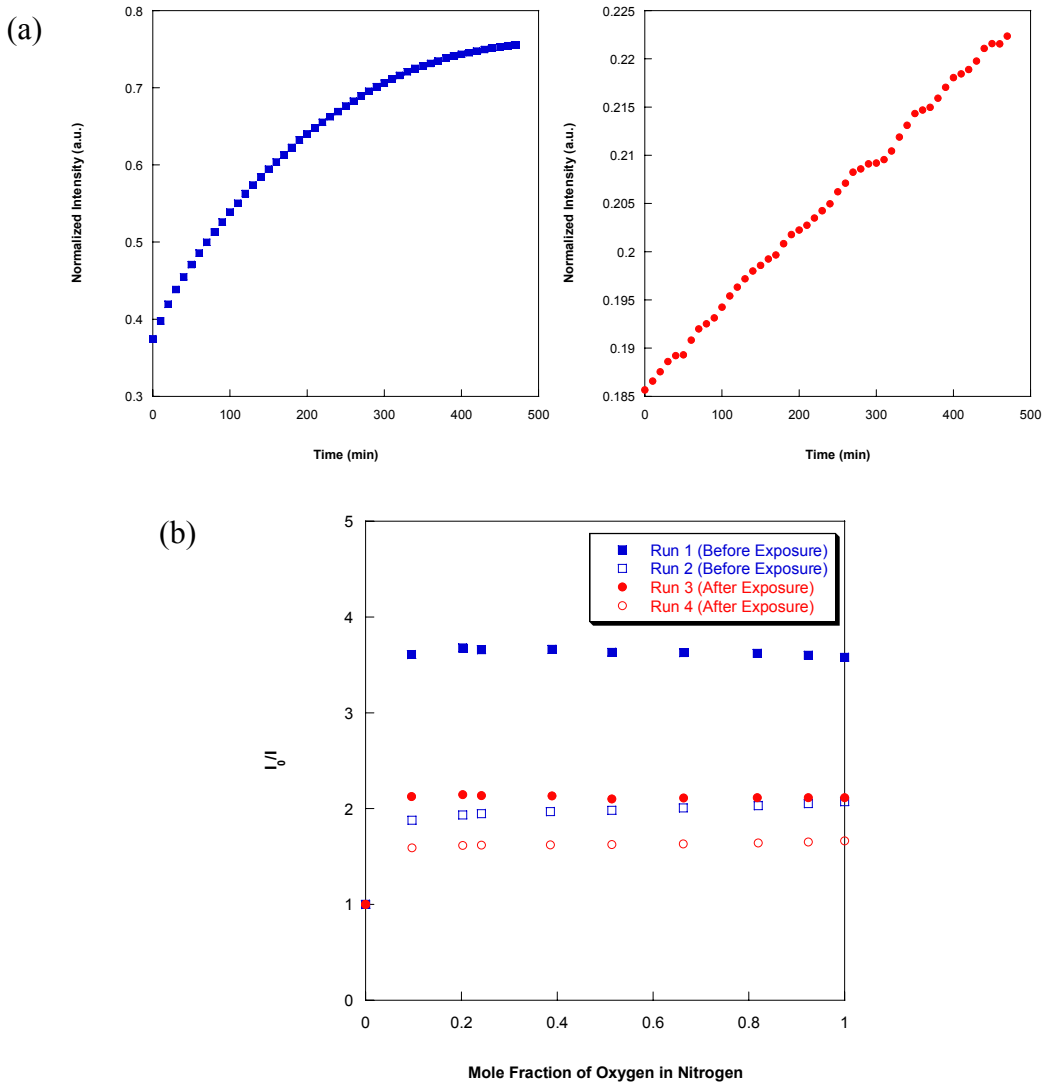

Figure 17. The normalized intensity of emission of **3** under both nitrogen (■) and oxygen (●) are shown in A. Two consecutive K_{SV} experiments were performed before (■/□) and after (●/○) the gas exposures and are shown in B.

Conclusions

When these compounds were initially proposed, we thought that not only would zinc be a cheaper alternative to platinum systems but also that the bulky groups that could be appended to the terpy core would generate the necessary space for oxygen to flow. The result would be an inexpensive, efficient oxygen sensor. A family of terpy compounds was successfully synthesized, but only one compound (**3**) showed any sensitivity toward oxygen.

While this compound is easy to synthesize, several problems keep it from being used in oxygen sensing devices. The first is the instability of the compound to LED illumination. Maintaining the purity of the compound is also of concern. The lability of the metal center will always pose a problem unless a different ligand set is chosen. A more practical obstacle includes the need for a 365 nm LED excitation source, which is more expensive than the longer wavelength options available.

If a ligand with more heavy-atom character could be synthesized and used, it is possible that the excitation wavelength and emission wavelength would shift to the red, making the spectroscopy more practical. This ligand could be achieved through the addition of various halogen atom substituents. A chromophoric or highly colored ligand could also be used to shift the absorption into the visible range of the spectrum. However, changing the metal center might be more appropriate as it could decrease the likelihood of ligand dissociation, potentially increase the purity, and simplify the data interpretation by eliminating the need for a two site model. Two potential metal centers are five coordinate ruthenium(II) and iridium(III) as these would adopt the same

coordination geometry as these zinc(II) compounds.[26] Changing to these metals would lead to an increased cost as these heavier metals are not as earth abundant.

Neutral complexes by their very nature do not require counterions, eliminating one potential avenue for creating void space. As a result, only the ligand set can be modified to generate void space within the crystalline lattice and hopefully improve the sensing ability of the material. However, changing the ligand set might significantly alter the photophysical properties of the complex. The difficulty in manipulating the void space within the crystal structures and the lack of photophysical stability make this class of compound impractical for use as luminescent solid-state oxygen sensors.

References

1. Matthey, J., *Platinum Today*, http://www.platinum.matthey.com/pgm-prices/ (accessed June 2012).

2. Media, B., *Daily Metal Prices & Market News*, www.metalmarkets.org.uk, (accessed June 2012).

3. Liang, L. J.; Zhao, X. J.; Huang, C. Z. *Analyst* **2012**, *137*, 953.

4. Walesa-Chorab, M.; Stefankiewicz, A. R.; Ciesielski, D.; Hnatejko, Z.; Kubicki, M.; Klak, J.; Korabik, M. J.; Patroniak, V. *Polyhedron* **2011**, *30*, 730.

5. Wild, A.; Winter, A.; Hager, M. D.; Schubert, U. S. *Chem. Commun.* **2012**, *48*, 964.

6. Zhou, X.; Jin, X.; Li, D.; Wu, X. *Chem. Commun.* **2011**, *47*, 3921.

7. Hwang, S.-H.; Wang, P.; Moorefield, C. N.; Jung, J.-C.; Kim, J.-Y.; Lee, S.-W.; Newkome, G. R. *Macromol. Rapid Comm.* **2006**, *27*, 1809.

8. Ma, Z.; Cao, Y.; Li, Q.; Guedes da Silva, M. F. t. C.; FraÃºsto da Silva, J. o. J. R.; Pombeiro, A. J. L. *J. Inorg. Biochem.* **2010**, *104*, 704.

9. Righetto, S.; Rondena, S.; Locatelli, D.; Roberto, D.; Tessore, F.; Ugo, R.; Quici, S.; Roma, S.; Korystov, D.; Srdanov, V. I. *J. Mater. Chem* **2006**, *16*, 1439.

10. Winter, A.; Friebe, C.; Chiper, M.; Schubert, U. S.; Presselt, M.; Dietzek, B.; Schmitt, M.; Popp, J. *Chem. Phys. Chem.* **2009**, *10*, 787.

11. Barbieri, A.; Accorsi, G.; Armaroli, N. *Chem. Commun.* **2008**, 2185.

12. Winter, A.; Friebe, C.; Hager, M. D.; Schubert, U. S. *Macromol. Rapid Comm.* **2008**, *29*, 1679.

13. Zhao, Q.-L.; Li, G.-P. *Acta Cryst. E* **2009**, *65*, m693.

14. Bruker, **2008**, *APEX II*, Madison, Wisconsin, USA.

15. Blessing, R. H. *Acta Cryst. A* **1995**, *A51*, 33.

16. Sheldrick, G. M., **2008**, *SADABS*, University of Gottingen, Germany.

17. Bruker, **2003**, *SMART and SAINT*, Madison, Wisconsin, USA.

18. Sheldrick, G. M. *Acta Cryst. A* **2008**, *A64*, 112.

19. Spek, A. L., **2005**, *PLATON, A Multipurpose Crystallographic Tool*, Utrecht University, Utrecht, The Netherlands.

20. Bruno, I. J.; Cole, J. C.; Edgington, P. R.; Kessler, M.; Macrae, C. F.; McCabe, P.; Pearson, J.; Taylor, R. *Acta Cryst. B* **2002**, *B58*, 389.

21. McGee, K. A.; Mann, K. R. *J. Am. Chem. Soc.* **2009**, *131*, 1896.

22. McGee, K. A.; Veltkamp, D. J.; Marquardt, B. J.; Mann, K. R. *J. Am. Chem. Soc.* **2007**, *129*, 15092.

23. Smith, C. S.; Branham, C. W.; Marquardt, B. J.; Mann, K. R. *J. Am. Chem. Soc.* **2010**, *132*, 14079.

24. Smith, C. S.; Mann, K. R. *Chem. Mater.* **2009**, *21*, 5042.

25. Benniston, A. C.; Harriman, A.; Lawrie, D. J.; Mayeux, A. *Phys. Chem. Chem. Phys,* **2004**, *6*, 51.

26. Cotton, F. A.; Wilkinson, G. S.; Murillo, C. A.; Bochmann, M. *Advanced Inorganic Chemistry*; 6th ed.; Interscience Publishers: New York, 1972.

Chapter Three

Oxygen Sensing with Copper Phosphine/Phen Derivatives

Overview

Much of the work in the area of detecting molecular oxygen (O_2) through luminescence quenching has focused on the use of emissive transition metal complexes embedded into host matrices. These support materials often complicate the sensing response and can lead to an increased likelihood of device degradation. We have characterized, by several photophysical methods and X-ray crystallography, a series of luminescent, microcrystalline copper(I) complexes capable of detecting O_2 without the use of a host matrix. The stability of the best O_2 sensor was studied by exposing the sample to different intensities and wavelengths of excitation light, concentrations of oxygen, and irradiation times. Changes in both emission intensity and sensitivity toward oxygen were used to monitor sensor stability. These changes are interpreted and a photodegradation model proposed.

Introduction

Much of the work in the area of detecting oxygen through luminescence quenching uses emissive transition metal complexes embedded into different support materials.[1-11] These support materials often complicate the sensing response, increase the likelihood of device degradation, and limit reproducibility.

To investigate the effects of the support, our group has focused on the development of luminescent crystalline materials for the detection of oxygen.[12-18] These porous materials allow oxygen to penetrate the lattice, eliminating the need for a support material. The crystallographically imposed site symmetry also insures the production of identical sensing sites, simplifying sensor response. The ability to reproduce the sensing

behavior also increases since each crystalline sample will be uniform in the solid-state and respond to oxygen in the same manner.

Recently, we have shown complexes of the form $[Cu(P\hat{}P)(N\hat{}N)]^+$ (where P^P is a diphosphine and N^N is a phenanthroline derivative) with significant ligand variations could be used in oxygen sensing materials.[16] These complexes use copper as an earth abundant alternative to metals such as platinum and ruthenium, but still generate complexes with the desired photophysical properties. Previously, some of these complexes were found to have K_{SV}'s greater than 3 atm^{-1} and solid-state quantum yields greater than 60 %.[16] Notably, those compounds with substituents in the 2 and 9 positions of the phenanthroline ligand possessed the longest excited state lifetime and higher sensitivity toward oxygen.[16] It is thought that these substitutions restrict the ability of the complex to distort from a pseudo-tetrahedral ground state to a pseudo-square planar excited state, resulting in a longer emission lifetime.[19-22]

As an extension of these results and to further investigate this class of compounds, we have synthesized and tested several new copper(I) complexes that contain 1,10-phenanthroline (phen), 4,7-diphenyl-1,10-phenanthroline (bath) and 2,9-dimethyl-4,7-diphenyl-1,10-phenanthroline (bcp) as the phenanthroline derivative and either *bis*[2-(diphenylphosphino)phenyl]ether (POP) or 4,5-*bis*(diphenylphosphino)-9,9-dimethylxanthene (xantphos) as the diphosphine derivative.

There has been little systematic study of the rate and cause of luminescent device degradation. The degradation of several porphyrin-based platinum complexes has been reported. In each case the compounds were supported in a host matrix and suffered degradation ranging from as little as 0.5 % per day to 100 % degradation over 7.5

hours.[2,23,24] Our group has previously found crystalline copper(I) complexes suffer degradation ranging from 15 % per day to 77 % degradation per day.[16]

It should be mentioned that while the degradation of these sensing materials has been reported, the conditions explored are not consistent. Thus, it is often difficult to compare the results of such studies. Some rates of degradation are measured by observing the change in luminescence intensity under air while others study the degradation under various concentrations of oxygen. Determining exactly what property is degrading can be complicated. More often than not, the property degrading is luminescence intensity. It is important to also study the degradation of the sensing ability of the compound as this property helps determine the viability of the compound for use in oxygen sensing devices. It is possible that the emission intensity can degrade and the sensing ability of the compound remain consistent. This type of degradation would still allow the compound to be used as an oxygen sensor since the sensitivity of the decreased emission does not suffer.

This paper reports a systematic study of the degradation of [Cu(POP)(phen)]tfpb (tfpb = *tetrakis*-[*bis*-3,5-trifluoromethyl(phenylborate)]) sensing stability toward both LED (light emitting diode) irradiation and oxygen exposures. Results indicate that the degradation of emission only occurs when the complex is simultaneously exposed to LED irradiation and oxygen. Based on the observations made, a mechanism for the degradation kinetics is proposed.

Experimental

General Considerations for Synthesis. $Cu(BF_4)_2 \cdot X\ H_2O$, 4,7-diphenyl-1,10-phenanthroline (bath) and 2,9-dimethyl-4,7-diphenyl-1,10-phenanthroline (bcp), *bis*[2-(diphenylphosphino)phenyl]ether (POP), and 4,5-*bis*(diphenylphosphino)-9,9-dimethylxanthene (xantphos) were purchased from Aldrich Chemical Co. and used as received. Potassium *tetrakis*-(pentafluorophenyl)borate (Kpfpb) was purchased from Boulder Scientific Company. Sodium *tetrakis*-[*bis*-3,5-trifluoromethyl(phenylborate)] (Na(tfpb)) was available from a previous study.[25] The solvents (acetonitrile, dichloromethane, diethyl ether, hexanes, methanol, and toluene) were obtained from commercial sources and used without further purification. $[Cu(CH_3CN)_4]BF_4$ was synthesized according to literature procedure.[26]

A 300 MHz Varian Unity NMR spectrometer was utilized to obtain ^1H and ^{19}F NMR spectra. Chemical shifts are reported in units of ppm using an external reference to the residual proton resonance in deuterated methanol for ^1H NMR spectra and the internal $CFCl_3$ reference for the ^{19}F NMR. High-resolution electrospray ionization mass spectrometry (HRESIMS) was performed on a Bruker BioTOF II mass spectrometer.

Synthesis and Characterization. The $[Cu(POP)(phen)]BF_4$ used in this study was synthesized as previously reported by adding a solution of phen to a solution of $[Cu(CH_3CN)_4]BF_4$ and POP in CH_2Cl_2 followed by precipitation of the salt with diethyl ether.[27] The new BF_4^- salts containing the POP and xantphos ligands were made by analogous routes; metatheses to the $tfpb^-$ and $pfpb^-$ salts were carried out by a literature procedure.[16]

[Cu(POP)(phen)]BF_4 (1a)

$[Cu(CH_3CN)_4]BF_4$ (0.0178 g, 0.0566 mmol) and POP (0.0310 g, 0.0576 mmol) were dissolved in 6 mL of CH_2Cl_2 and stirred for 1 hour. Phen (0.0109 g, 0.0605 mmol) was dissolved in 1 mL of CH_2Cl_2 and the resulting solution was added drop-wise to the Cu solution. A yellow color was observed and the solution stirred for an additional hour. The solution volume was reduced using rotary evaporation and a yellow solid precipitated with diethyl ether. The solid was collected via vacuum filtration and then dried under vacuum, yielding 0.0322 g (64 %) of **1a**. ^{1}H NMR (CD_3OD): δ 8.88 (d, 2 H, *J* = 4.8 Hz), 8.61 (d, 2 H, *J* = 7.8 Hz), 8.12 (s, 2 H), 7.73 (dd, 2 H, *J* = 4.8, 8.1 Hz), 7.38 (m, 2 H), 7.28 (m, 4 H), 7.14 (m, 10 H), 7.04 (m, 10 H), 6.78 (m, 2 H) ^{19}F NMR ($CDCl_3$): δ -153.48 HRESIMS (M^+). Calc. for ($CuC_{48}H_{36}N_2OP_2$) *m/z* 781.1599. Found *m/z* 781.1603.

[Cu(POP)(phen)]pfpb (1b)

1a (0.0196 g, 0.0226 mmol) was dissolved in 1 mL of methanol. In a separate vial, K(pfpb) (0.0248 g, 0.0345 mmol) was also dissolved in 1 mL of methanol. Addition of the K(pfpb) solution to the solution of **1a** resulted in a bright yellow solution that on addition of distilled water yielded a bright yellow solid that was collected via vacuum filtration. The solid was dried under vacuum yielding 0.0293 g (87 %) of **1b**. ^{1}H NMR (CD_3OD): δ 8.88 (d, 2 H, *J* = 6.38 Hz), 8.61 (d, 2 H, *J* = 8.4), 8.12 (s, 2 H), 7.73 (dd, 2 H, *J* = 4.8, 8.4 Hz), 7.38 (m, 2 H), 7.28 (m, 4 H), 7.14 (m, 10 H), 7.04 (m, 10 H), 6.78 (m, 2 H) ^{19}F NMR ($CDCl_3$): δ -133.12, -163.78, -167.48

HRESIMS (M^+). Calc. for ($CuC_{48}H_{36}N_2OP_2$) *m/z* 781.1599. Found *m/z* 781.1618. X-ray quality crystals were grown through the slow evaporation of a MeOH and H_2O solution.

[Cu(POP)(phen)]tfpb (1c)

1a (0.0308 g, 0.0354 mmol) was dissolved in 2 mL of methanol. In a separate vial, Na(tfpb) (0.0458 g, 0.0517 mmol) was also dissolved in 2 mL of methanol. Addition of the Na(tfpb) solution to the solution of **1a** resulted in a yellow solution. A bright orange-yellow solid was precipitated with distilled water and collected via vacuum filtration. The solid was dried under vacuum, yielding 0.0433 g (76 %) of **1c**. ^{1}H NMR (CD_3OD): δ 8.88 (d, 2 H, *J* = 4.5 Hz), 8.61 (d, 2 H, *J* = 8.1 Hz), 8.12 (s, 2 H), 7.73 (dd, 2 H, *J* = 4.8, 7.8 Hz), 7.59 (m, 12 H), 7.38 (m, 2 H), 7.28 (m, 4 H), 7.15 (m, 10 H), 7.04 (m, 10 H), 6.78 (m, 2 H) ^{19}F NMR (CD_3OD): δ -64.85 HRESIMS (M^+). Calc. for ($CuC_{48}H_{36}N_2OP_2$) *m/z* 781.1599. Found *m/z* 781.1585. X-ray quality crystals were grown through the slow evaporation of an acetonitrile solution.

The same procedures used to produce **1a-1c** were followed for the synthesis of **2a-5c**. Only the quantities of ligands and anions used, product yields, and spectroscopic analysis are given. In the cases where solvent systems deviated, full procedures are given.

[Cu(xantphos)(bath)]BF_4 (2a)

$[Cu(CH_3CN)_4]BF_4$ (0.0524 g, 0.167 mmol), xantphos (0.0956g, 0.165 mmol), and bath (0.0542 g, 0.163 mmol) were combined using the same procedure for **1a**. Solvent was removed via rotary evaporation and the resulting solid redissolved in 10 mL methanol. Addition of distilled water resulted in precipitation of a bright yellow solid that was filtered via vacuum filtration and dried under vacuum, yielding 0.110 g (63 %) of **2a**. ^1H NMR (CD_3OD): δ 8.64 (d, 2 H, *J* = 5.1 Hz), 8.05 (s, 2 H), 7.84 (dd, 2 H, *J* = 1.2, 7.8 Hz), 7.71 (d, 2 H, *J* = 4.8 Hz), 7.60 (m, 8 H), 7.27 (q, 4 H, *J* = 7.7, 7.5 Hz), 7.12 (t, 10 H, *J* = 7.5 Hz), 7.03 (m, 10 H), 6.71 (m, 2 H), 1.79 (s, 6 H) ^{19}F NMR (CD_3OD): δ -155.47 HRESIMS (M^+). Calc. for ($CuC_{63}H_{48}N_2OP_2$) *m/z* 973.2538. Found *m/z* 973.2620.

[Cu(xantphos)(bath)]pfpb (2b)

The same procedure used to synthesized **1b** was used to generate **2b**. **2a** (0.0350 g, 0.0330 mmol) and K(pfpb) (0.0361 g, 0.0503 mmol) were used. A bright yellow solid was collected yielding 0.0482 g (88 %) of **2b**. ^1H NMR (CD_3OD): δ 8.64 (d, 2 H, *J* = 5.1 Hz), 8.05 (s, 2 H), 7.84 (dd, 2 H, *J* = 1.5, 7.8 Hz), 7.71 (d, 2 H, *J* = 5.1 Hz), 7.58 (m, 8 H), 7.27 (q, 4 H, *J* = 7.6, 7.5), 7.12 (t, 10 H, *J* = 7.5 Hz), 7.03 (m, 10 H), 6.71 (m, 2 H), 1.80 (s, 6 H) ^{19}F NMR (CD_3OD): δ -134.42, -166.34, -170.22 HRESIMS (M^+). Calc. for ($CuC_{63}H_{48}N_2OP_2$) *m/z* 973.2538. Found *m/z* 973.2589. X-ray quality crystals were grown through the slow evaporation of a MeOH and H_2O solution.

[Cu(xantphos)(bath)]tfpb (2c)

The same procedure used to synthesize **1c** was used to generate **2c**. **2a** (0.0348 g, 0.0328 mmol) and Na(tfpb) (0.0432 g, 0.0487 mmol) were used. A bright yellow solid was collected, yielding 0.0156 g (26 %) of **2c**. ^{1}H NMR (CD_3OD): δ 8.64 (d, 2 H, *J* = 5.1 Hz), 8.05 (s, 2 H), 7.84 (d, 2 H, *J* = 6.6 Hz), 7.71 (d, 2 H, J = 5.1 Hz), 7.60 (m, 20 H), 7.27 (q, 4 H, *J* = 7.6, 7.2), 7.12 (t, 10 H, *J* = 7.9 Hz), 7.03 (m, 10 H), 6.72 (m, 2 H), 1.80 (s, 6 H) ^{19}F NMR (CD_3OD): δ -64.85 HRESIMS (M^+). Calc. for ($CuC_{63}H_{48}N_2OP_2$) *m/z* 973.2538. Found *m/z* 973.2646.

[Cu(POP)(bath)]BF_4 (3a)

The same procedure used to synthesize **1a** was used to generate **3a**. $[Cu(CH_3CN)_4]BF_4$ (0.0537 g, 0.171 mmol), POP (0.0925 g, 0.172 mmol), and bath (0.0576 g, 0.173 mmol) were used. After precipitation, a bright yellow solid was collected, yielding 0.1479 g (85 %) of **3a**. ^{1}H NMR (CD_3OD): δ 8.92 (d, 2 H, *J* = 5.1 Hz), 8.04 (s, 2 H), 7.68 (d, 2 H, *J* = 5.1 Hz), 7.60 (m, 10 H), 7.39 (t, 2 H, *J* = 7.7 Hz), 7.34 (t, 4 H, *J* = 7.2 Hz), 7.19 (t, 10 H, *J* = 7.3 Hz), 7.10 (m, 10 H), 6.85 (m, 2 H) ^{19}F NMR (CD_3OD): δ -155.49 HRESIMS (M^+). Calc. for ($CuC_{60}H_{44}N_2OP_2$) *m/z* 933.2225. Found *m/z* 933.2286.

[Cu(POP)(bath)]pfpb (3b)

The same procedure used to synthesized **1b** was used to generate **3b**. **3a** (0.0449 g, 0.0440 mmol) and K(pfpb) (0.0467 g, 0.0650 mmol) were used. A bright yellow solid was collected yielding 0.0432 g (63 %) of **3b**. ^{1}H NMR (CD_3OD): δ 8.92 (d, 2 H, *J* = 5.1 Hz), 8.04 (s, 2 H), 7.68 (d, 2 H, *J* = 5.1 Hz), 7.59 (m, 10 H), 7.39 (t, 2 H, *J* =7.8 Hz), 7.31 (t, 4 H, *J* = 7.5 Hz), 7.18 (t, 10 H, *J* = 7.5 Hz), 7.10 (m, 10 H), 6.85 (m, 2 H) ^{19}F NMR (CD_3OD): δ -134.42, -166.33. -170.21 HRESIMS (M^+). Calc. for ($CuC_{60}H_{44}N_2OP_2$) *m/z* 933.2225. Found *m/z* 933.2268.

[Cu(POP)(bath)]tfpb (3c)

The same procedure used to synthesized **1c** was used to generate **3c**. **3a** (0.0443 g, 0.0434 mmol) and Na(tfpb) (0.0578 g, 0.0652 mmol) were used. A bright yellow solid was collected, yielding 0.0463 g (59 %) of **3c**. ^{1}H NMR (CD_3OD): δ 8.92 (d, 2 H, *J* = 4.8 Hz), 8.04 (s, 2 H), 7.68 (d, 2 H, *J* = 4.8 Hz), 7.60 (m, 22 H), 7.38 (t, 2 H, *J* = 7.8 Hz), 7.31 (t, 4 H, *J* = 7.2 Hz), 7.19 (t, 10 H, *J* = 7.3 Hz), 7.08 (m, 10 H), 6.85 (m, 2 H) ^{19}F NMR (CD_3OD): δ -64.85 HRESIMS (M^+). Calc. for ($CuC_{60}H_{44}N_2OP_2$) *m/z* 933.2225. Found *m/z* 933.2261.

The following compounds were not fully characterized because the preliminary testing revealed them to be poor oxygen sensors. Synthetic procedures and *preliminary* NMR data are reported.

[Cu(POP)(bcp)]BF_4 (4a)

The same procedure used to synthesize **1a** was used to generate **4a**. $[Cu(CH_3CN)_4]BF_4$ (0.0362 g, 0.115 mmol), POP (0.0616 g, 0.114 mmol), and bcp (0.0423 g, 0.117 mmol) were used. Solvent was removed via rotary evaporation and the resulting solid redissolved in 2 mL of methanol. Addition of distilled water resulted in precipitation of a bright yellow solid that was filtered via vacuum filtration and dried under vacuum, yielding 0.0771 g (44 %) of **4a**. ^{1}H NMR (CD_3OD): δ 8.10 (s), 7.90 (s), 7.86 (s), 7.69 (m), 7.64 (s), 7.57 (m), 7.43 (t), 7.34 (m), 7.10 (m), 2.61 (s), 2.56 (s) ^{19}F NMR (CD_3OD): δ -155.475

[Cu(POP)(bcp)]pfpb (4b)

The same procedure used to synthesized **1b** was used to generate **4b**. **4a** (0.0238 g, 0.0227 mmol) and K(pfpb) (0.0233 g, 0.0324 mmol) were used. An orange solid was collected, yielding 0.0297 g (81 %) of **4b**. ^{1}H NMR (CD_3OD): δ 8.10 (s), 7.90 (s), 7.86 (s), 7.68 (m), 7.64 (s), 7.59 (m), 7.26 (m), 7.10 (m), 7.10 (m), 2.61 (s), 2.56 (s) ^{19}F NMR (CD_3OD): δ -134.438, -166.328, -170.211

[Cu(POP)(bcp)]tfpb (4c)

The same procedure used to synthesized **1c** was used to generate **4c**. **4a** (0.0233 g, 0.0222 mmol) and Na(tfpb) (0.0283 g, 0.0319 mmol) were used. An orange solid was collected, yielding 0.0223 g (71 %) of **4c**. ^{1}H NMR (CD_3OD): δ 8.10 (s), 7.90 (s), 7.86 (s), 7.68 (m), 7.64 (s), 7.59 (m), 7.43 (t), 7.34 (m), 7.28 (t), 7.10 (m), 2.61 (s), 2.56 (s) ^{19}F NMR (CD_3OD): δ -64.849

[Cu(xantphos)(bcp)]BF_4 (5a)

The same procedure used to synthesized **1a** was used to generate **5a**. $[Cu(CH_3CN)_4]BF_4$ (0.0511 g, 0.162 mmol), xantphos (0.0930 g, 0.161 mmol), and bcp (0.0585 g, 0.162 mmol) were used. An orange solid was collected, yielding 0.0579 g (33 %) of **5a**. ^{1}H NMR (CD_3OD): δ 8.10 (s), 7.90 (s), 7.81 (s), 7.78 (d), 7.64 (m), 7.56 (m), 7.29 (m), 7.13 (m), 7.02 (m), 2.61 (s), 2.39 (s), 1.76 (s) ^{19}F NMR (CD_3OD): δ -155.486

[Cu(xantphos)(bcp)]pfpb (5b)

The same procedure used to synthesized **1b** was used to generate **5b**. **5a** (0.0175 g, 0.0161 mmol) and K(pfpb) (0.0175 g, 0.0244 mmol) were used. An orange solid was collected, yielding 0.0086 g (31 %) of **5b**. ^{1}H NMR (CD_3OD): δ 8.10 (s), 7.90 (s), 7.81 (s), 7.78 (d), 7.68 (m), 7.59 (m), 7.30 (m), 7.13 (m), 7.02 (m), 2.61 (s), 2.39 (s), 1.76 (s) ^{19}F NMR (CD_3OD): δ -134.444, -166.333, -170.214

[Cu(xantphos)(bcp)]tfpb (5c)

The same procedure used to synthesized **1c** was used to generate **5c**. **5a** (0.0173 g, 0.0159 mmol) and Na(tfpb) (0.0210 g, 0.0237 mmol) were used. An orange solid was collected, yielding 0.0123 g (41 %) of **5c**. ^{1}H NMR (CD_3OD): δ 8.10 (s), 7.90 (s), 7.81 (s), 7.78 (d), 7.68 (m), 7.58 (m), 7.29 (m), 7.13 (m), 7.03 (m), 2.61 (s), 2.39 (s), 1.76 (s) ^{19}F NMR (CD_3OD): δ -64.849

X-ray Crystallography

All data for the structure determinations of **1b**, **1c**, and **2b**, were collected at the X-ray Crystallographic Laboratory (Department of Chemistry, University of Minnesota). Crystals were grown by the slow evaporation of saturated acetonitrile solutions or a solution of water and methanol. Single crystals were attached to glass fibers and mounted on a Bruker APEX II Platform CCD for data collection at 173 K (**1b** and **2b**) or 123 K (**1c**) using graphite monochromated MoKα radiation (λ = 0.71073 Å).[28] An initial set of cell constants was calculated from reflections harvested from three sets of 12 frames oriented such that orthogonal wedges of reciprocal space were surveyed. Final cell constants were calculated from a minimum set of 2000 strong reflections from the actual data collection. Data were collected to the extent of at least 1.5 hemispheres at a resolution of at least 0.84 Å using φ-scans. Three major sections of frames were collected with 0.50 º steps in ω at 3 different ϕ settings and a detector position of -28 º in 2θ. For all structures, the intensity data were corrected for absorption and decay using SADABS.[29,30] Space groups were determined based on systematic absences and intensity statistics. The structures were determined using a direct-methods solution. Several full-

matrix least-squares/difference Fourier cycles were performed to locate remaining non-hydrogen atoms. All calculations were performed using the SHELXTL-V6.12.[31] suite of programs on Pentium computers. Additional crystallographic information can be found in Table 1.

Packing analysis parameters were measured using PLATON/VOID with pictorial representations of the solvent channels done with edited *.res files in Mercury.[32-34] The detection of solvent accessible voids by PLATON/VOID is done in the following way: The unit cell is filled with the atoms from the structural model and each specific atom is assigned its respective van der Waals radius. A grid search generates a list of grid points with a minimum distance of 1.2 Å from the nearest van der Waals surface. This list of grid points is then used to produce a new list of grid points that makes up the solvent accessible areas. For the sets of grid points, the center of gravity and volume of the void are calculated. The overall solvent accessible volume is calculated along with the volume and center of gravity of individual 'voids'.

Table 1. Crystallographic Data and Refinement Parameters.

Compound	**1b**	**1c**	**2b**
empirical formula	C_{72} H_{36} B Cu F_{20} N_2 O P_2	C_{80} H_{48} B Cu F_{24} N_2 O P_2	C_{87} H_{48} B Cu F_{20} N_2 O P_2
crystal color, morphology	yellow, plate	yellow, block	yellow, hexagonal
crystal system	Monoclinic	Monoclinic	Monoclinic
space group	$P2_1$/c	$P2_1$/n	$P2_1$/n
crystallization solvent	MeOH/H_2O	Acetonitrile	MeOH/H_2O
a, Å	12.7386(13)	12.6158(7)	17.2221(9)
b, Å	30.699(3)	15.2683(9)	19.2715(10)
c, Å	15.8151(17)	37.034(2)	23.8846(13)
α, deg	90	90	90
β, deg	97.2480(10)	93.2500(10)	111.0230(10)
γ, deg	90	90	90
volume (V), Å^3	6129.3(11)	57122.1(7)	7399.5(7)
Z	4	4	4
formula weight, g mol^{-1}	1461.32	1645.49	1653.56
density (calculated), g cm^{-3}	1.584	1.535	1.484
temperature, K	173(2)	123(2)	173(2)
absorption coefficient (μ), mm^{-1}	0.519	0.464	0.440
F(000)	2936	3320	3344
θ range, deg	1.46 to 27.42	2.10 to 27.40	1.65 to 25.11
index ranges	$-16 \le h \le 11$	$-16 \le h \le 16$	$-20 \le h \le 20$
	$-39 \le k \le 36$	$-19 \le k \le 19$	$-22 \le k \le 22$
	$-19 \le l \le 20$	$-47 \le l \le 44$	$-28 \le l \le 27$
reflections collected	34814	67560	49019
independent reflections	13697 [R_{int} = 0.0454]	16135 [R_{int} = 0.0308]	13178 [R_{int} = 0.0517]
weighting factors,[a] *a, b*	0.0479, 0.9355	0.0579, 11.6108	0.0335, 4.0593
max, min transmission	0.9846, 0.7812	0.8011, 0.8011	0.9657, 0.8793
data/restraints/parameters	13697/0/892	16135/0/986	13178/0/1029
R_1, wR_2 [$I > 2\sigma(I)$]	0.0451, 0.0953	0.0499, 0.1231	0.0393, 0.0795
R_1, wR_2 (all data)	0.0838, 0.1105	0.0650, 0.1325	0.0715, 0.0956
GOF	1.004	1.020	1.001
largest diff. peak, hole eÅ^{-3}	0.523, -0.372	1.050, -1.080	0.311, -0.372

[a] $w = [\ \sigma^2(F_o^2) + (aP)^2 + (bP)]^{-1}$, where $P = (F_o^2 + 2F_c^2)/3$.

O_2 Sensing Instrumentation and Procedure

The instrumentation used for these measurements has been described in detail previously.[13,15-18] A brief summary of the apparatus is given here.

The samples for oxygen sensing were prepared by placing a small amount of crushed crystals or reaction powder into a depression of a ¼'' diameter aluminum rod. The prepared sample was then placed into a swage cross-tube fitting apparatus designed to allow gas to flow over the sample and for front face illumination (Figure 1). A 405 nm LED filtered through an interference filter was used as the excitation source and was brought to the sample through the center fiber of a "six around one" bifurcated fiber optic probe. The emission was collected through the six fiber channel and sent to an Ocean Optics USB-2000 spectrometer. The spectrometer, mass flow controllers, temperature, and pressure monitors were interfaced to a computer to allow unattended data acquisition via a custom LabVIEW program. [13,15-17]

The emission data collected were analyzed with a spreadsheet written in Microsoft Excel. Data from six cycles of spectra obtained at approximately 0.0, 0.10, 0.21, 0.25, 0.40, 0.50, 0.65, 0.80, 0.90 and 1.0 mole fraction of oxygen in nitrogen were used for the Stern-Volmer plots. The acquisitions were performed at room temperature or 21.8 ± 1 °C. Exact gas mole fractions were calculated by referencing the feedback voltage of the mass flow controllers to a calibration previously performed.[16] The emission intensity was integrated across the entire peak and divided by the integrated LED intensity for each spectrum to give I_0 (intensity under N_2) and I (intensity at a given O_2 mixture). I_0/I was plotted versus oxygen mole fraction in nitrogen to yield a Stern-Volmer plot. A linear regression model was used to calculate the slope or K_{SV} parameter.

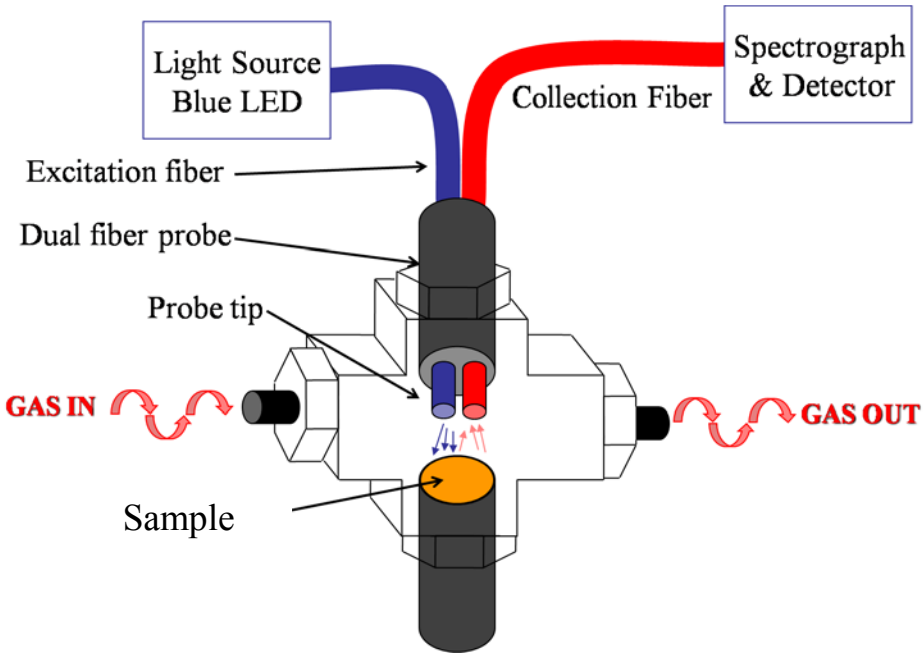

Figure 1. Diagram of the swage cross-tube fitting apparatus used for sensing and lifetime measurements.

It should be noted that the K_{SV}'s reported here are expressed in units of mole fraction and have not been corrected for the atmospheric pressure in Minneapolis, Minnesota of 0.97 atm. In order to compare these K_{SV} numbers to those reported previously, the K_{SV} in mole fraction needs to be corrected by dividing the current value by 0.97 atm to give the K_{SV} in units of atm^{-1}.

Lifetime Measurements

Lifetime measurements of sensing compounds are made using the same method reported previously.[15,16] A brief summary of the apparatus is given.

A similar swage cross-tube fitting apparatus used for the sensing measurements was used for lifetime measurements. The sample, light, and gas ports were oriented in the same fashion. The atmosphere within the cell is controlled with mass flow controllers and a computer program. The sample is illuminated by light from a pulsed LED that is sent to the sample through one leg of the fiber optic probe. Emitted light is filtered and then returns through the other leg of the fiber optic probe to a Hamamatzu R928 PMT run at 1250 V using the last 5 dynodes. The signal from the PMT is amplified and read by an oscilloscope that has been triggered by a logic pulse produced by the LED. At least 30 transients are averaged, with each consisting of the average of at least 20 traces using a custom LabVIEW program. Further fitting is done with Solver in Excel. For monoexponential lifetimes, the slopes of the resulting plots of ln(emission intensity) vs. t are used to calculate the lifetime of the sample.[15] For those lifetimes that were found to be biexponential the resulting plot of ln(emission intensity) vs. t were fit to a biexponential of the form shown in Equation 1.

$$I = a_1 \exp(-k_1 t) + a_2 \exp(-k_2 t) + a_3 \quad \textbf{(1)}$$

where I is equal to the light intensity at some time t. The values of a_1, a_2 are related to the fractional contribution of that process to the overall lifetime. The sum of these two values must equal 1. The term a_3 is a correction constant. The rate constants for the individual processes are given by k_1 and k_2. The biexponential lifetimes components are obtained by dividing 1 by either k_1 or k_2.

Quantum Yield Measurements

Quantum yield measurements are made through a modification of Wrighton's method as described previously.[13,15,16,35] Diffuse reflectance is captured from a "perfectly" scattering surface to give a quantity proportional to the incident light intensity (I_0, units of photons/wavenumber). The emission of the sample (I_{emit}, the emitted light) and the remaining scattered intensity from the light source (I, the reduced source intensity) are then taken and corrected. The measurements obtained from the scatterer and the sample can then be used with Equation 2 to calculate the solid-state emission quantum yield (ϕ).[15]

$$\phi = \frac{I_{emit}}{I_0 - I} \quad \textbf{(2)}$$

A bifurcated (six around one) fiber optic probe with an angle tip is used to bring light to and from the sample. A calibrated Ocean Optics CCD (charge-coupled device) spectrophotometer is used to capture the light intensities. A Fluorilon scattering target is used instead of the MgO scatterer used by Wrighton as Fluorilon is the NIST standard of fused powdered Teflon with a scattering coefficient greater than 99 % across the spectral

region.[36] The diffuse reflectance of the Fluorilon is collected and the sample is rubbed into the pores of the Fluorilon target and spectra again collected. The unabsorbed excitation beam and emitted light from the sample embedded target are collected and calculations carried out in Excel. Reproducible results are obtained by controlling the atmosphere at the surface of the scattering sample by blowing dry gas across the surface. These gases are controlled by two mass flow controllers, one for dry nitrogen and the other for dry oxygen, that also allow for mixing of the two gases in a variety of proportions if desired.[15]

Stability Studies

Bulk stability studies were conducted using the same apparatus used to collect the oxygen sensing measurements. Several different configuration files were used to change the amount of time a sample was exposed to pure nitrogen and oxygen gases. Configuration file "A" exposes the sample to two cycles of approximately 0.0, 0.10, 0.21, 0.25, 0.40, 0.50, 0.65, 0.80, 0.90 and 1.0 mole fraction of oxygen in nitrogen to collect two Stern-Volmer plots, beginning with the nitrogen exposure. Each gas exposure is approximately 5 minutes. Next, the sample is exposed to 8 hours of pure nitrogen with spectra collected every 10 minutes followed by an 8 hour exposure to pure oxygen, again with spectra collected every 10 minutes. The data collection finishes by collecting the necessary spectra for two Stern-Volmer plots as mentioned before. From these data, the percent change of emission intensity under nitrogen and oxygen were calculated. The percent change in the average K_{SV} before and after the gas exposures was also obtained.

In order to study the stability of the sample with regards to oxygen exposure, configuration file "B" was used. The sample is exposed to 1 hour of nitrogen (with a spectrum collected every 10 minutes), followed by exposure to oxygen with spectrum collected every 10 minutes (the time of oxygen exposure was varied). Finally, the sample is exposed to 1 hour of nitrogen (again, with a spectrum collected every 10 minutes). A two point K_{SV} was determined from the pure nitrogen and pure oxygen data at the beginning and end of the study. The percent change in the emission under oxygen was calculated and used with the time of exposure to oxygen used to calculate the percentage of sample decomposition per hour.

In order to study the stability of the sample when the surface of the sensing material was undisturbed and then refreshed, the following configuration file was used. For the undisturbed sample, configuration file "C" collected a spectrum every 10 minutes for an hour while the sample was under nitrogen and then the appropriate spectra at various concentrations of oxygen were collected for 4 Stern-Volmer runs. This process was repeated 5 times concluding with an hour long exposure to nitrogen (with a spectrum collected every 10 minutes). This entire data collection process was repeated 3 times without moving the sample in the setup. The sample was then removed and the microcrystalline material in the depression stirred. The sample was placed back into the setup and the data collection repeated. The sample was removed for a second time, stirred, and replaced for one final data collection.

For the stirred sample, configuration file "D" collected a spectrum every 10 minutes for an hour while the sample was under nitrogen and then the appropriate spectra at various concentrations of oxygen to collect 4 Stern-Volmer runs. The sample

was then removed from the setup, the microcrystalline material in the depression stirred, and the sample was replaced in the setup. The data collection was repeated. The entire process was repeated a total of 15 times.

For the studies where the LED power was modified, configuration file "B" was used. The sample was exposed to 12 hours of oxygen. The percent of normalized emission signal decrease under oxygen was determined and plotted against the intensity of the 405 nm LED peak, which was used to monitor the intensity of the light incident on the sample. After each run, the voltage of the LED was changed either up or down within the range of 3.1 to 4.6 V, and the data collection started again. The process was repeated with a 365 nm LED and **1c** to determine if the wavelength of the LED affected the rate of decomposition.

Stability studies conducted on the Quantum Yield Setup

In order to determine if changes in absorption and emission occurred during degradation, a sample of [Cu(POP)(phen)]tfpb was pressed into the perfect scatterer and placed on the quantum yield setup described above. The sample was exposed to oxygen for approximately 6 hours and a spectrum was collected every 10 minutes. The integrated intensity of the LED and the sample emission were plotted versus time to determine if changes in sample absorption and/or emission were occurring during exposure to oxygen.

Low Temperature Emission Studies

In order to monitor emission changes upon cooling of the sample, a small amount of powdered **1c** was attached to the end of a bifurcated fiber optic cable. A 405 nm LED light source was brought down one leg of the fiber and the emitted light returned to an Ocean Optics USB-2000 spectrometer through the second leg of the fiber optic. A thermocouple was attached to the fiber optic cable at the point where the sample was held to gain an accurate measure of the temperature of the sample environment. The fiber optic cable and thermocouple were then slowly inserted into a 50 L dewar of liquid helium containing approximately 15 L of liquid helium. The process was repeated by using a 4 L dewar containing approximately 2 L of liquid nitrogen. Spectra were collected at various temperatures and then analyzed using Microsoft Excel.

Results and Discussion

Oxygen Sensing

All the compounds reported here (in various forms) were tested for sensitivity toward oxygen. Table 2 contains the K_{SV} parameters for all materials synthesized and tested. Examination of the data in Table 2, shows that in general compounds with the $tfpb^-$ anion sense oxygen well while compounds with the $pfpb^-$ anion do not. Interestingly, the $tfpb^-$ containing compounds with the bath (bath = 4,7-diphenyl-1,10-phenanthroline) derivatives possessing a methyl substituent in the 2 and 9 positions do not sense oxygen. This result was not expected as these compounds should have higher quantum yields and lifetimes due to the restriction of the Cu(I) excited state geometry.

Their excited state should be more likely to be quenched by oxygen and as a result be better oxygen sensors.

One compound, **1c** sensed oxygen with a relatively high K_{SV} and the response plot of this material was linear. Based on these results, compound **1c** was chosen for further study. The emission profile of **1c** is shown in Figure 2. The K_{SV} for independent samples of the reaction powder microcrystalline form of **1c** has been collected multiple times. The average of K_{SV} over all of these experiments is 3.40(9).

Table 2. The Average Stern-Volmer Sensing Constant (K_{SV}) Determined with Six Concentration Runs.

Compound	K_{SV}
1a [Cu(POP)(phen)]BF_4	0.41(1)
1b [Cu(POP)(phen)]pfpb	0.022(1)
1c [Cu(POP)(phen)]tfpb	3.54(3)
2a [Cu(xantphos)(bath)]BF_4	3.12(5)
2b [Cu(xantphos)(bath)]pfpb	0.230(9)
2c [Cu(xantphos)(bath)]tfpb *	3.91(4)
3a [Cu(POP)(bath)]BF_4	1.04(2)
3b [Cu(POP)(bath)]pfpb	1.40(2)
3c [Cu(POP)(bath)]tfpb	3.03(8)
4a [Cu(POP)(bcp)BF_4	0.0†
4b [Cu(POP)(bcp)]pfpb	0.0†
4c [Cu(POP)(bcp)]tfpb	0.64(4)
5a [Cu(xantphos)(bcp)]BF_4	0.0†
5b [Cu(xantphos)(bcp)]pfpb	0.0†
5c [Cu(xantphos)(bcp)]tfpb	0.0†

*Response plot of this material is curved. The value reported is for the linear fit.
†The sensing ability of these compounds is near the detection limit of our instrumentation.

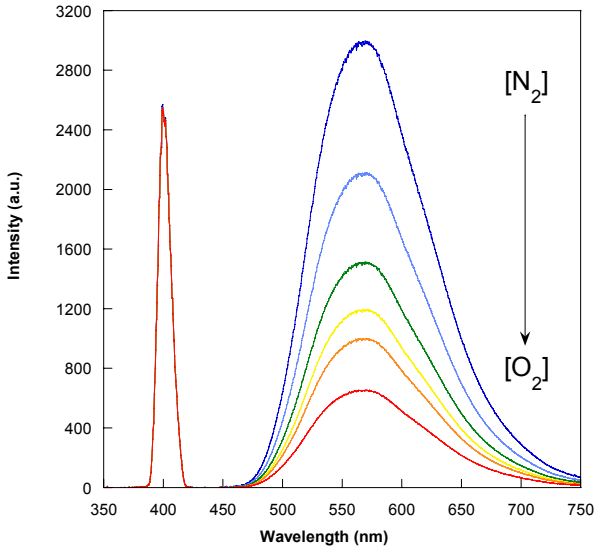

Figure 2. Emission profile of **1c** with the LED shown centered at 405 nm. This emission profile is reversible as decreasing the concentration of oxygen increases the emission observed from the complex.

X-ray Structure Determination and Characterization.

The structural connectivity and packing diagrams of **1b** are shown in Figures 3-6. This compound crystallizes without any molecules of solvation. All bond distances and angles are within normal ranges and there is no disorder to model in the structure. No solvent accessible void space was found within this structure. The lack of void space within the crystal lattice correlates with a lack of oxygen sensitivity as these crystals had a K_{SV} of 0.018(2).

The structure of **1c** was also determined and the structural and packing diagrams are shown in Figures 7-10. The structure contains no co-crystallized solvent. There are two disordered $-CF_3$ groups on the $tfpb^-$ anion. These were modeled over two positions with occupancy percentages of 86:14 and 89:11 for the two $-CF_3$ groups. All bond lengths and angles are within normal ranges. Analysis of the void space with PLATON/VOID indicated a solvent accessible volume of 1.4 % of the total volume or 98.7 $Å^3$. Representations of the void space are shown in Figure 11 and 12. Interestingly, when viewed down the *c* axis it appears as though channels of void space snake through the material. However, rotation of the structure reveals that the two disordered $-CF_3$ groups are responsible for the channel's disruption (Figure 12). It is possible that these $-CF_3$ groups can act as turnstiles to allow oxygen to pass through the structure as has been proposed before.[16] These crystals were tested and found to not significantly sense oxygen as the K_{SV} was determined to be 0.028(2).

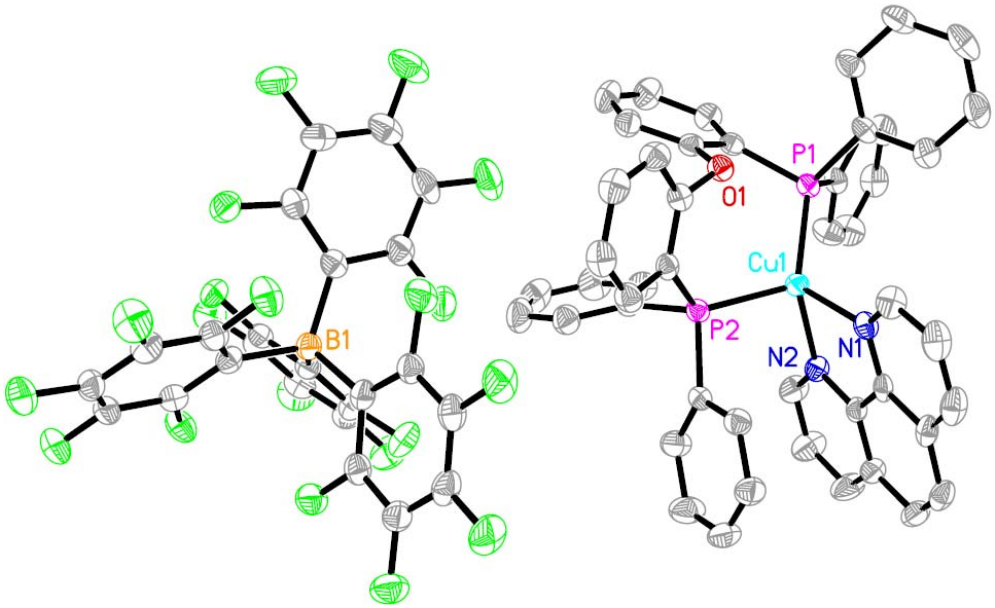

Figure 3. Thermal ellipsoid diagram of **1b**. All thermal ellipsoids are drawn at 50 % probability and hydrogen atoms have been removed for clarity.

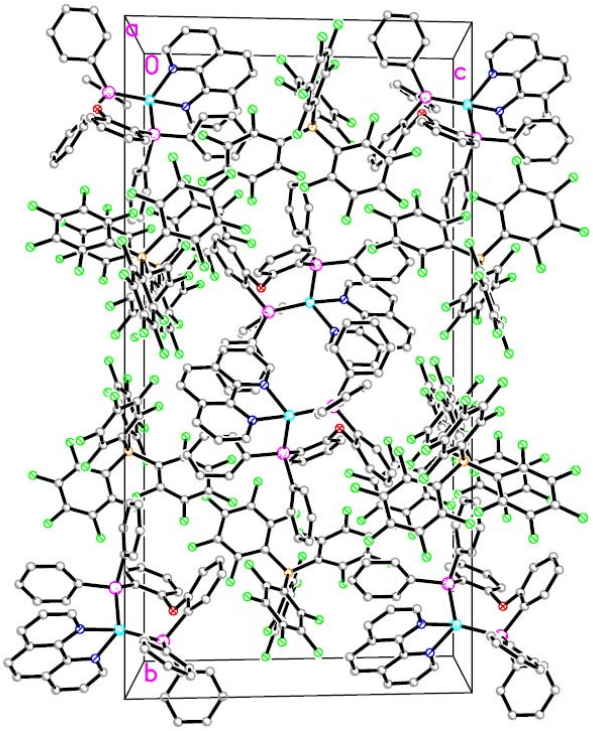

Figure 4. View of the packing of **1b** down the *a* axis with hydrogen atoms removed for clarity.

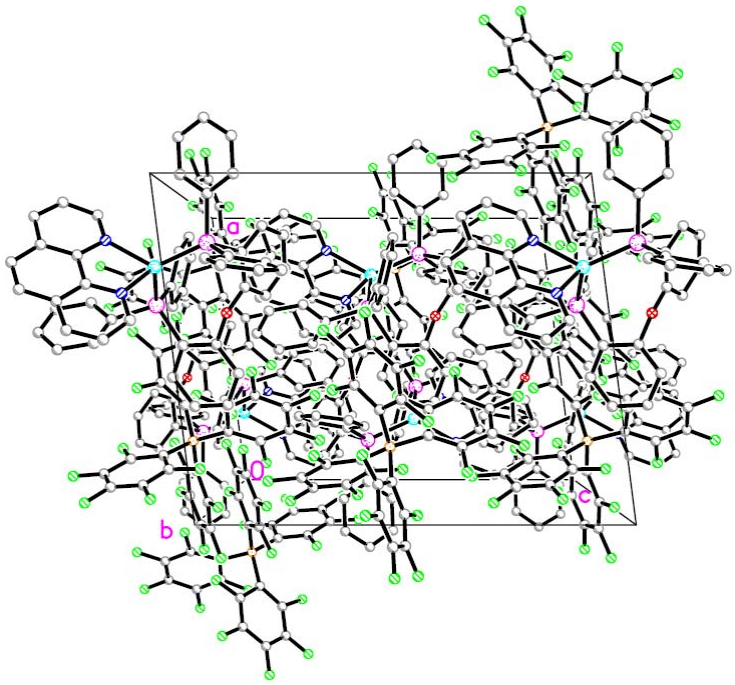

Figure 5. View of the packing of **1b** down the *b* axis with hydrogen atoms removed for clarity.

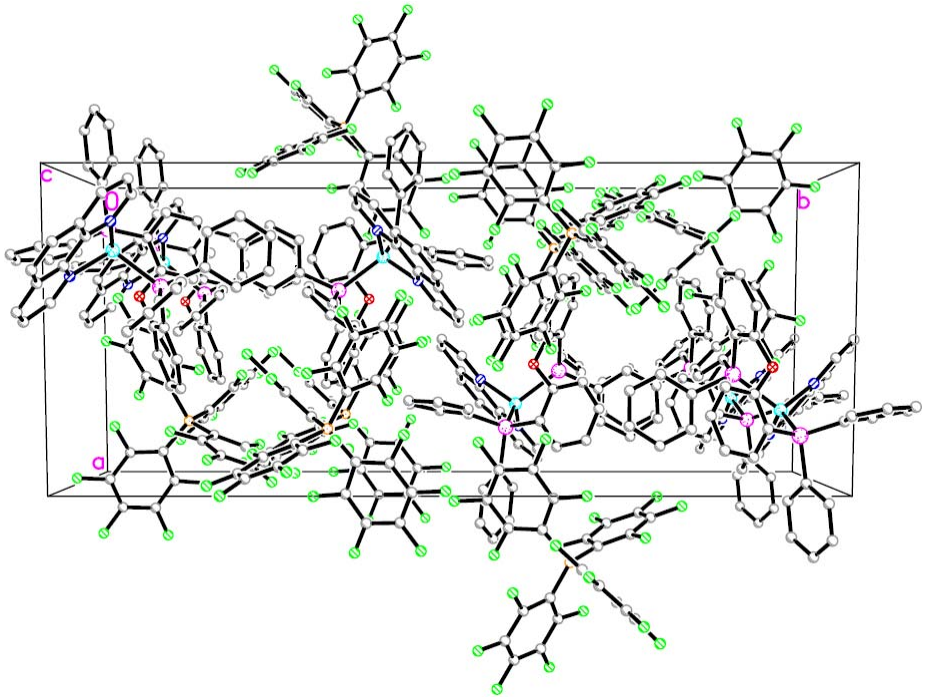

Figure 6. View of the packing of **1b** down the *c* axis with hydrogen atoms removed for clarity.

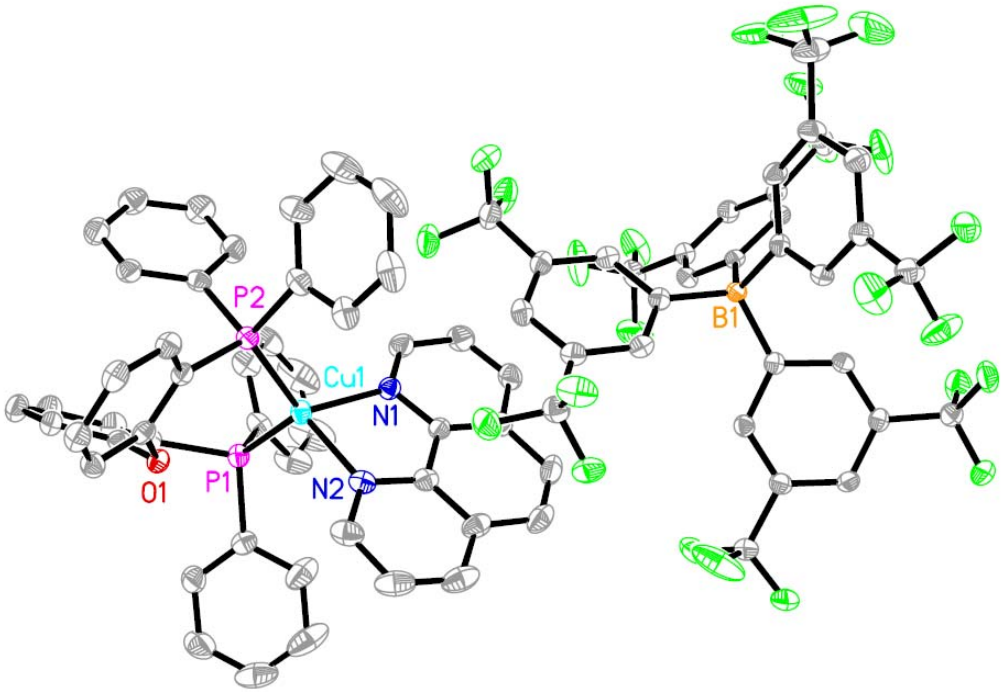

Figure 7. Thermal ellipsoid diagram of **1c**. All thermal ellipsoids are drawn at 50 % probability with hydrogen atoms and disorder modeling of $-CF_3$ groups removed for clarity.

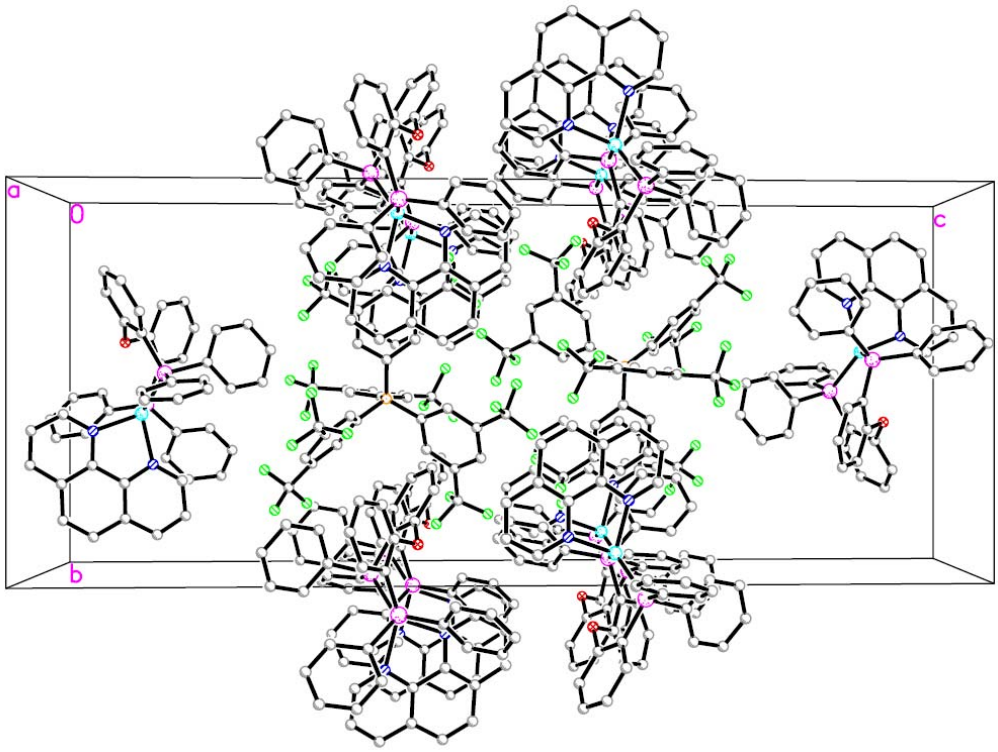

Figure 8. View of the packing of **1c** down the *a* axis with hydrogen atoms and modeled disorder removed for clarity.

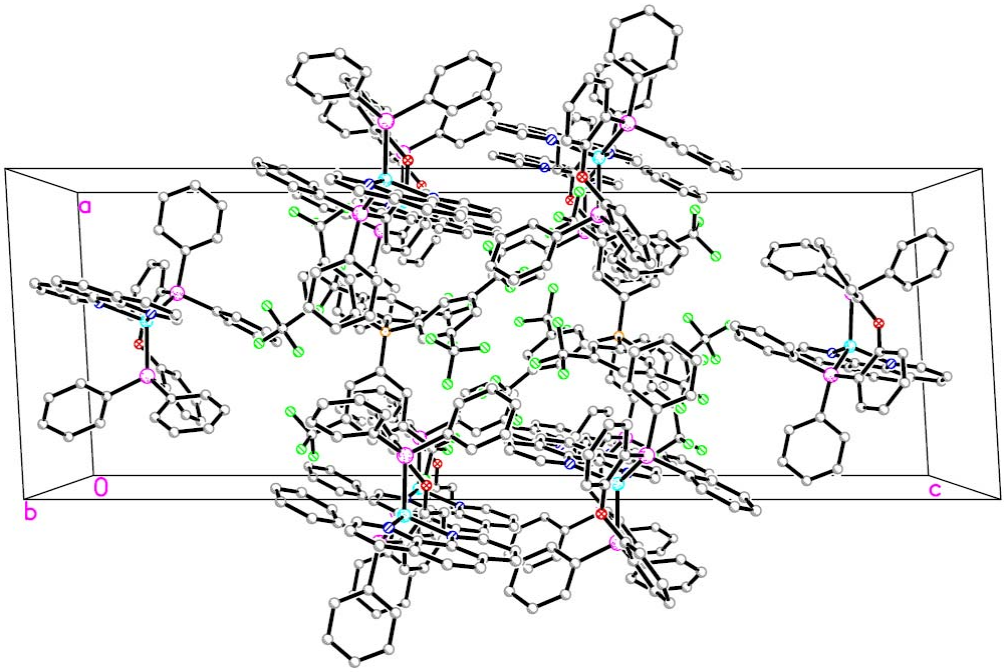

Figure 9. View of the packing of **1c** down the *b* axis with hydrogen atoms and modeled disorder removed for clarity.

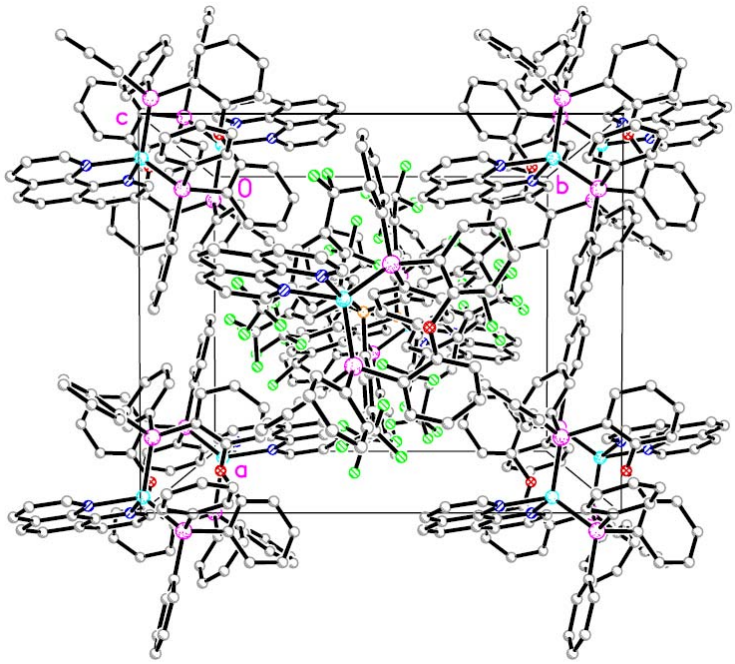

Figure 10. View of the packing of **1c** down the *c* axis with hydrogen atoms and modeled disorder removed for clarity.

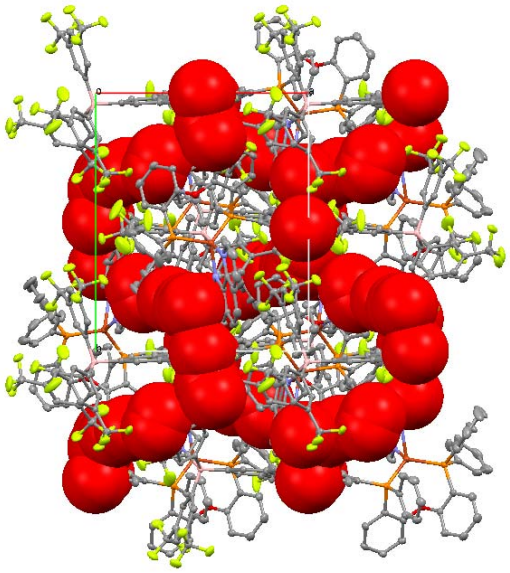

Figure 11. View of **1c** down the *c* axis. It appears that there are channels of void space that snake through the structure. Further examination of these channels shows that the two disordered $-CF_3$ groups of the $tfpb^-$ anion disrupt the channels. The rotational disorder of these components suggest that oxygen could flow through this channel with the $-CF_3$ groups serving as a "molecular turnstile". The channel would then be completed and oxygen could move freely.

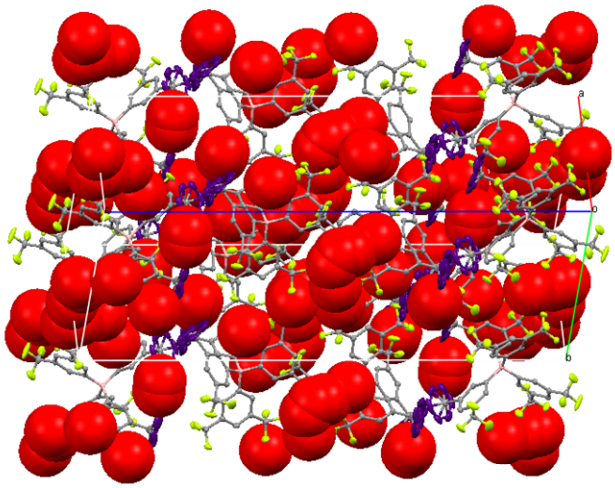

Figure 12. A view of the channel rotated 90 ° from the previous figure. The disordered $-CF_3$ groups are shown in purple. It can be seen that it is these disordered groups block the connection of the channel.

The crystals used for this structure determination were grown from acetonitrile while the microcrystalline material used in all of the studies presented herein was obtained from a methanol and water mixture. Therefore, comparison of the void space in this structure to the sensing ability of the microcrystalline compound cannot be made. Numerous attempts to grow crystals of **1c** from a solvent mixture of methanol and water have been made, but have not yielded X-ray quality crystals. Based on the small amount of void space present in the acetonitrile structure and the significant sensing ability of the methanol and water microcrystalline material, it is hypothesized that the methanol and water crystals have a larger amount of void space present in the lattice. As a result, crystals grown from methanol and water could be difficult to obtain since the lattice may not be able to support the amount of void space proposed.

The structure of **2b** was determined and the structure contains no molecules of solvation (Figures 13-16). All bond lengths and angles fall within normal ranges. Analysis of the void space with PLATON/VOID reveals 335.3 $Å^3$ of void space present in the structure accounting for 4.5 % of the total cell volume. Representations of the void space are shown in Figure 17. It appears that there is a channel running parallel to the *a* axis, but rotation of the structure shows that these channels are not connected and are more accurately described as large pockets of void space within the structure. Based on previous study, the large amount of void space might support a large K_{SV} value; however, the channels are blocked by a component that cannot rotate or otherwise move out of the way like the $–CF_3$ group blocking the channels in the structure of **1c**.[15,16] The lack of void space in the appropriate configuration helps to explain why this compound does not sense oxygen well as the K_{SV} determined for the compound was 0.259(4).

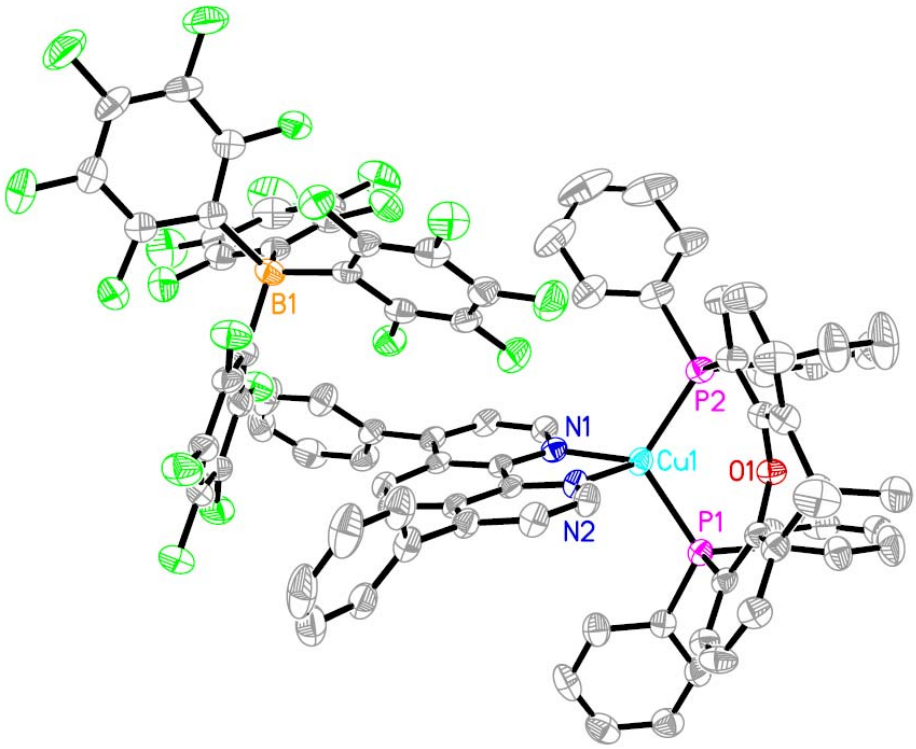

Figure 13. Thermal ellipsoid diagram of **2b**. All thermal ellipsoids are drawn at 50 % probability and hydrogen atoms removed for clarity.

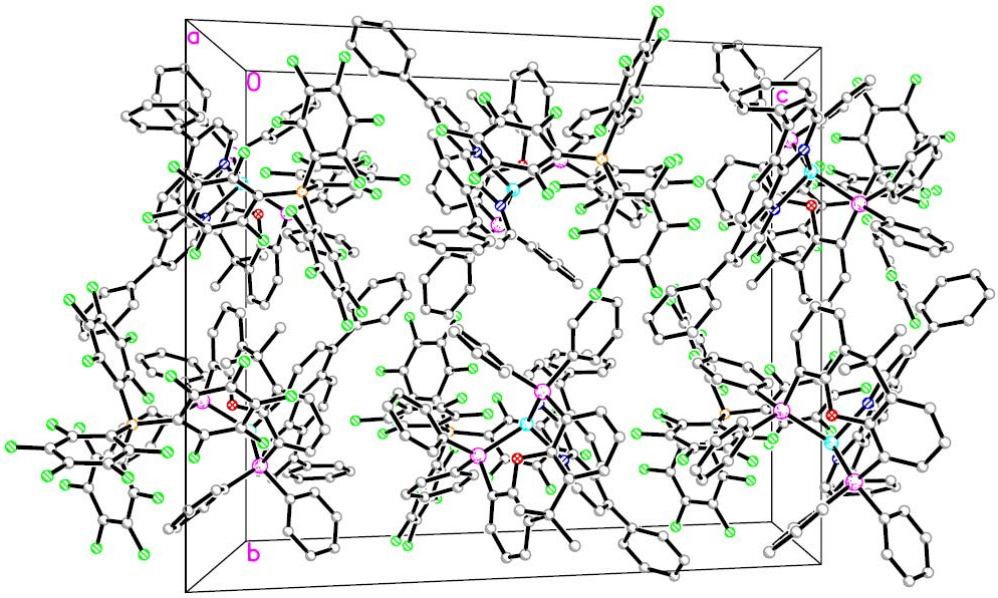

Figure 14. View of the packing of **2b** down the *a* axis with hydrogen atoms removed for clarity.

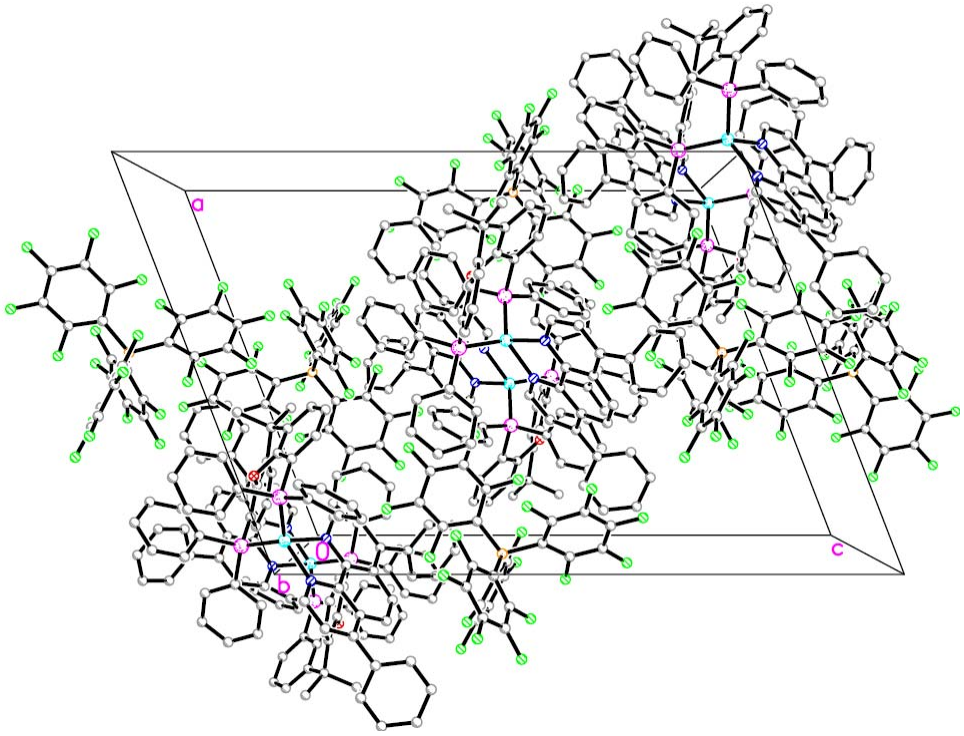

Figure 15. View of the packing of **2b** down the *b* axis with hydrogen atoms removed for clarity.

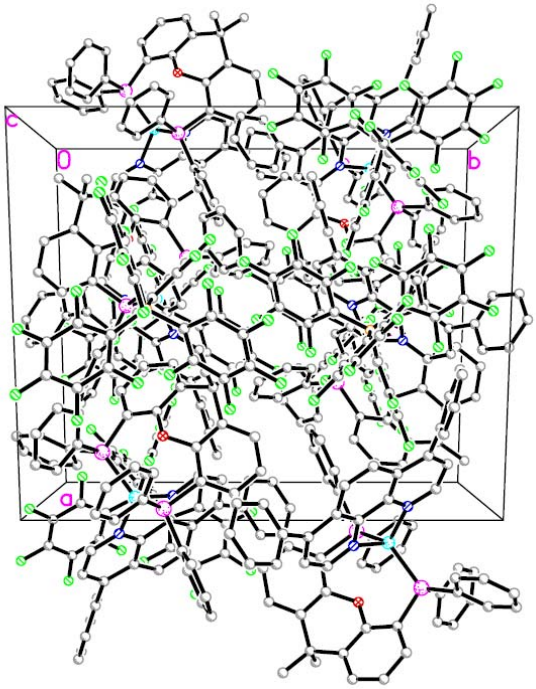

Figure 16. View of the packing of **2b** down the *c* axis with hydrogen atoms removed for clarity.

(a)

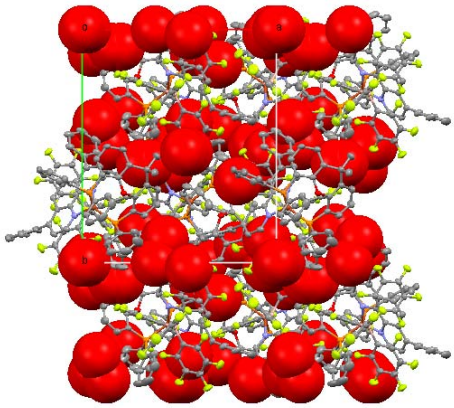

(b)

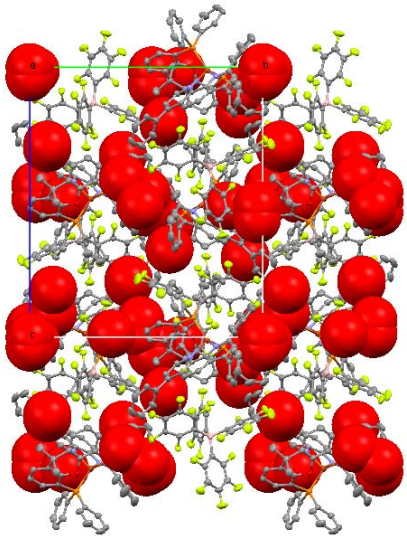

Figure 17. View of the void space in the structure of **2b**. The top view (a) shows the structure as viewed down the *c* axis. It appears in this view that the voids are connected as channels. However, rotation of the structure 90 ° (b) so that it is viewed down the *a* axis shows that the voids are not connected.

Lifetime Determination

The lifetimes of all sensing compounds were determined and data are summarized in Table 3. In general, materials with a $pfpb^-$ anion have longer lifetimes when compared to those with BF_4^- or $tfpb^-$ anions. However, the lifetimes of compounds with the $tfpb^-$ anion are the most sensitive toward oxygen in their respective family of compounds. The nature of the phen ligand does not appreciably affect the lifetime of the compound. Compounds that contain xantphos have longer lifetimes than analogous compounds made with POP. The K_{SV} calculated for **1c** using the lifetime data is in agreement with the K_{SV} determined through emission intensity, suggesting no static quenching is responsible for the sensing mechanism of the compound.

Quantum Yields

The quantum yields of all sensing compounds were determined and the results are summarized in Table 3. In general, compounds with xantphos have higher quantum yields than analogous compounds made with POP due to the more restricted nature of the xantphos ligand. Compounds with bath as the N^N ligand generally have higher quantum yields than analogous compounds made with phen. When comparing anions, $pfpb^-$ compounds have higher quantum yields than those with the $tfpb^-$ anion.

When compared to previously reported $[Cu(P\text{^}P)(N\text{^}N)]^+$ compounds, those reported here have a smaller quantum yield.[16] The lower quantum yield values are attributed to the absence of the methyl substituents at the 2 and 9 positions. The unsubstituted phen compounds are able to undergo excited state distortion to allow faster non-radiative decay.[20] The absence of the 2,9-dimethyl substituents decreases the

quantum yield significantly as the compound [Cu(POP)(dmp)]tfpb (where dmp = 2,9-dimethyl-1,10-phenanthroline) has a quantum yield 10 times greater than that of **1c**. However, the decrease in the magnitude of the quantum yield does not appear to significantly affect the sensing ability of the compound as the K_{SV} of **1c** is 3.40(9) compared to 3.49(2) for [Cu(POP)(dmp)]tfpb.[16]

Table 3. Combined Photophysical Data.

Compound	K_{SV}*(emission)*	τ(N_2) μs	τ(Air) μs	τ(O_2) μs	K_{SV}(τ)	ϕ (N_2)	ϕ (O_2)
1a‡	0.41(1)	7.06	6.32	5.55	0.272	0.138	0.13
1b	0.022(1)	24.4	24.3	23.9	0.0201	0.41	0.412
1c‡	3.54(3)	6.59	3.53	1.54	3.28	0.082	0.046
2a‡	3.12(5)	14.2	9.75	4.63	2.08	0.11	0.073
2b	0.230(9)	11.0	10.7	9.45	0.167	0.215	0.16
2c*‡	3.91(4)	7.3	3.79	1.85	2.95	0.091	0.046
3a‡	1.04(2)	8.57	7.34	4.52	0.896	0.268	0.12
3b‡	1.40(2)	5.92	4.40	2.58	1.29	0.116	0.055
3c‡	3.03(8)	6.13	3.47	1.75	2.50	0.113	0.026
4a	0.0	*NM*	*NM*	*NM*	*NM*	*NM*	*NM*
4b	0.0	*NM*	*NM*	*NM*	*NM*	*NM*	*NM*
4c	0.64(4)	*NM*	*NM*	*NM*	*NM*	*NM*	*NM*
5a	0.0	*NM*	*NM*	*NM*	*NM*	*NM*	*NM*
5b	0.0	*NM*	*NM*	*NM*	*NM*	*NM*	*NM*
5c	0.0	*NM*	*NM*	*NM*	*NM*	*NM*	*NM*

* Curved emission Stern-Volmer plot

‡ Lifetime was biexponential; Weighted average of the two exponentials is reported

NM = Not Measured

Degradation Studies

All compounds were tested for degradation under oxygen and LED irradiation. Results of these studies for **1a-c** are shown in Figure 18. Compounds found to sense oxygen tend to show degradation under nitrogen, oxygen, and consequently, the K_{SV} sensing parameter decreases slightly. Degradation under nitrogen or oxygen was minimal for compounds that are not oxygen sensors. This lack of degradation is most likely the result of gases' inability to reach the core of the material as these compounds also lack significant amounts of void space in their crystalline forms. Since the gases cannot interact with a large portion of the metal excited states, degradation is not observed.

There is little evidence in this study that points to one particular P^P or N^N derivative as being necessary for stability and/or sensitivity. Previously, the inclusion of methyl groups at the 2 and 9 positions of the phen significantly improved the photophysical properties while moderately improving the K_{SV}.[17,20] In this work, compounds made with 2,9 substituents did not sense oxygen while analogs without the substituents did sense. This result points to the fact that while the 2,9 substituent can improve the photophysics, the restriction they can provide might not be necessary for the development of the best Cu(I) based oxygen sensor. The photophysical properties studied here suggest that using xantphos over POP increases the lifetime and quantum yield, but again there is no systematic effect on sensing ability or stability.

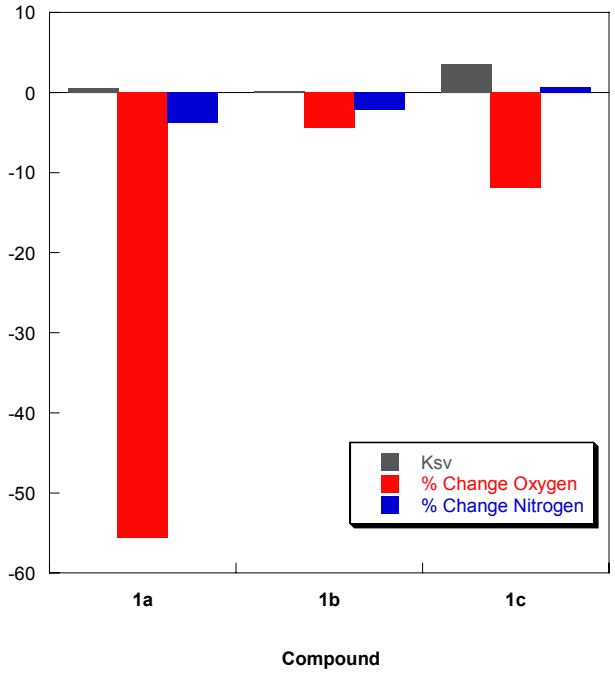

Figure 18. Stability of the $[Cu(POP)(phen)]^+$ family of compounds. The degradation under nitrogen and oxygen is shown as a percent change in the luminescence intensity over 8 hours. The average K_{SV} is also shown.

In general, the compounds with the $tfpb^-$ anion are the most sensitive toward changes in oxygen and sense with the most stable K_{SV}. This sensitivity trend is also seen in the lifetime measurements as the K_{SV}'s determined for these compounds through this technique are the largest within their respective families. These $tfpb^-$ compounds see little degradation under nitrogen and modest degradation under oxygen.

When the BF_4^- anion is used, there appears to be no trend in the photophysical properties of the resulting compounds. In general, the photophysical and sensing behaviors of BF_4^- salts are unpredictable perhaps as a result of the more hydroscopic nature of these salts. If the compounds pick up water from the air, their stability and sensing behavior could be more erratic since the composition of the material is changing. There could also be an effect due to the relative size of the BF_4^- anion compared to the size of the Cu(I) cation. Since the size of the two components is largely different, the crystalline lattice may have difficulty forming without the presence of solvent molecules. The inclusion of solvent molecules can cause rapid degradation to occur as the flow of gas removes these solvent molecules and collapses the lattice. The structure of **1a** is available from the crystallographic database and is a solvate including molecules of both CH_3CN and Et_2O.[37]

The $pfpb^-$ compounds do not appear to be valuable oxygen sensors as they do not show any sensitivity to oxygen. This lack of sensitivity is most likely the result of insufficient void space within the crystal lattice of these compounds. Thus, oxygen cannot flow through the material and reach the excited metal complex to quench the emission. These compounds also degrade under both nitrogen and oxygen.

*Further Study with **1c** and Excitation Wavelength*

Configuration file "B" was used with a sample of **1c** along with a 365 nm LED as the light source. Comparison of these data with the data collected using a 405 nm LED reveals that the wavelength of the source light has an effect on the rate of degradation. The 365 nm LED caused the intensity of emission under oxygen to change faster (0.57 % per hour) when compared to the change in emission intensity under oxygen with the 405 nm LED source (0.22 % per hour). This result is likely due to the combination of the higher energy of the 365 nm LED light source and the smaller penetration depth of this light into the sample. Therefore, the surface of the sample sees a more intense light source, causing the faster degradation of the material.

*Degradation of **1c** with Varied 405 nm LED power*

The degradation of **1c** under oxygen with varied LED power was investigated. Oxygen gas was chosen as there does not appear to be a significant degradation of the compound under nitrogen. The results of this study indicate that the degradation of the sample is much faster with a more intense LED source (Figure 19). This increased degradation is again due to the fact that the surface of the sample is seeing a more intense light source during the course of the study.

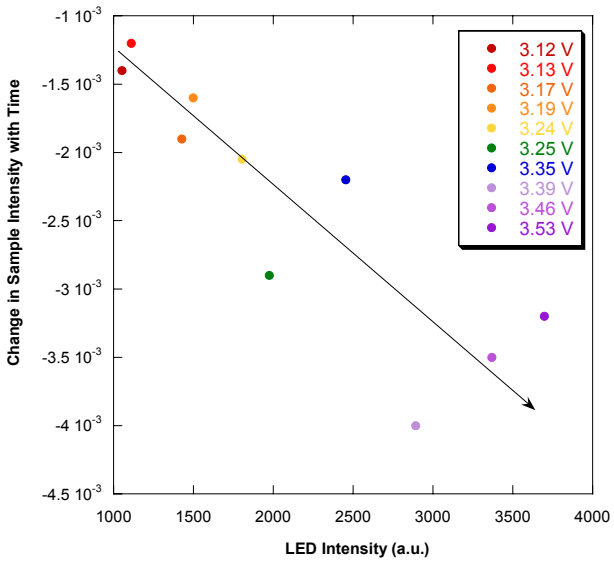

Figure 19. Rate of emission decomposition for [Cu(POP)(phen)]tfpb as a function of LED intensity. The variation in the last few points is most likely due to the changing temperature of the lab during these data collections, which spanned several days.

Stability Studies on the Quantum Yield Setup

A quantum yield stability study was conducted to determine if the LED intensity or the absorbance of the sample change significantly over the course of a data collection. All studies were conducted with **1c** reaction powder embedded into the pores of a Teflon block. The data collected using a clean Teflon block and LED illumination indicate that there is no inherent significant change in the LED intensity with time (Figure 20). When the sample of **1c** was embedded into the pores of the Teflon block, the emission of the sample did not change with irradiation under nitrogen (Figure 21). The LED also shows no change in intensity during the sample runs indicating that the absorption of the material does not change.

When a sample of **1c** embedded in the Teflon block is exposed to LED illumination and oxygen, the intensity of the emission decreases over time as can be seen in Figure 22. This result is consistent with the degradation observed during the stability studies as both oxygen and LED illumination were required for intensity degradation. The LED intensity does not change during the course of the exposure indicating that the decomposition product does not absorb the LED light in a manner much different from that of **1c**.

A second compound, **2c**, was also tested in this manner since stability testing revealed the K_{SV} appeared to change more drastically than that of **1c** with time. To deduce whether the mechanism of degradation was consistent, regardless of the ligand set, **2c** was tested on the quantum yield setup. This compound shows a slight increase in the LED spectrum with time indicating that the absorbance of the material decreases

(Figure 23). The sample emission intensity also decreases during the time of the study, consistent with the results obtained with **1c**.

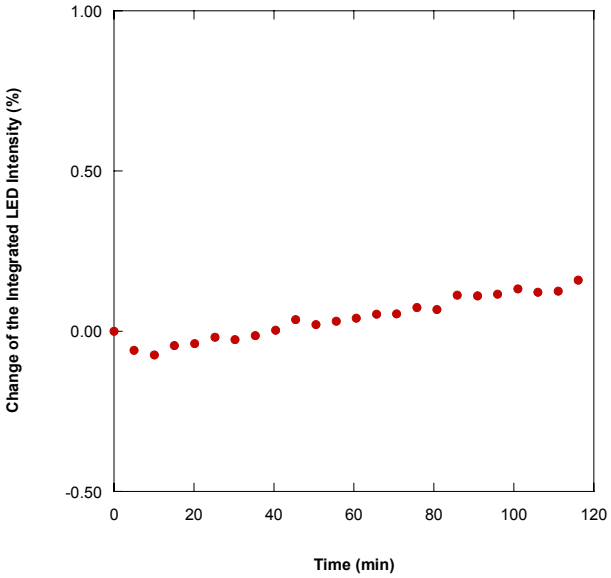

Figure 20. The percent change of the integrated LED intensity is shown. The LED intensity changes less than 0.25 % over the course of two hours.

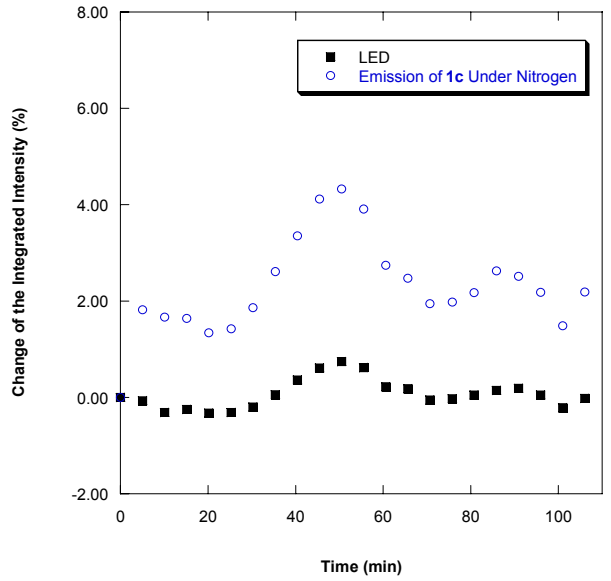

Figure 21. The percent change of the integrated emission intensity of the LED and **1c** under nitrogen are shown. The increase in emission intensity observed for both the LED and **1c** at approximately 50 minutes is due to a change in temperature of the laboratory.

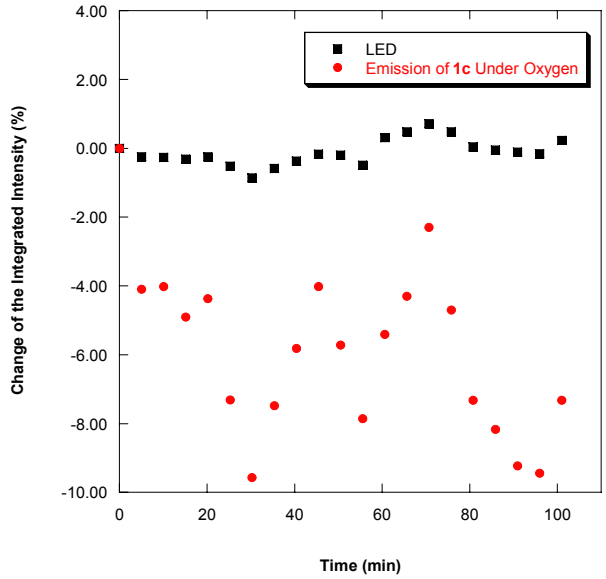

Figure 22. Data collected during the exposure of **1c** to oxygen indicate the decrease in emission intensity coupled with no change in the absorbance of the material. The change in the LED emission is generally less than 0.75 % while the change in the sample emission decreases approximately 9 % over a period of 100 minutes.

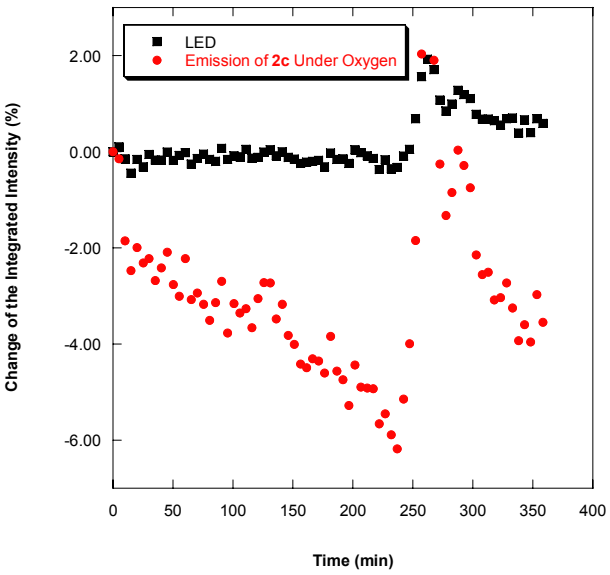

Figure 23. The behavior of **2c** under oxygen is shown. The increase in the LED intensity is approximately 1 %, indicating a slight change in the absorption of the material. The emission intensity of the sample decreases approximately 4 % over the 6 hour time period.

Studying the Long Term Intensity Decay Under Oxygen

Several long term oxygen exposure studies were conducted with oxygen exposure times ranging from 6 hours to 140 hours with spectra collected every 10 minutes. A graph of the data from the 140 hour exposure is shown in Figure 24. The emission decay rate is 4.3 % per day or 0.18 % per hour and the sample does not reach a point where the degradation of the intensity levels off. The initial quick increase in the degradation is due to the LED warming up after it is initially turned on. A similar change in emission intensity is observed when the sample is under nitrogen.

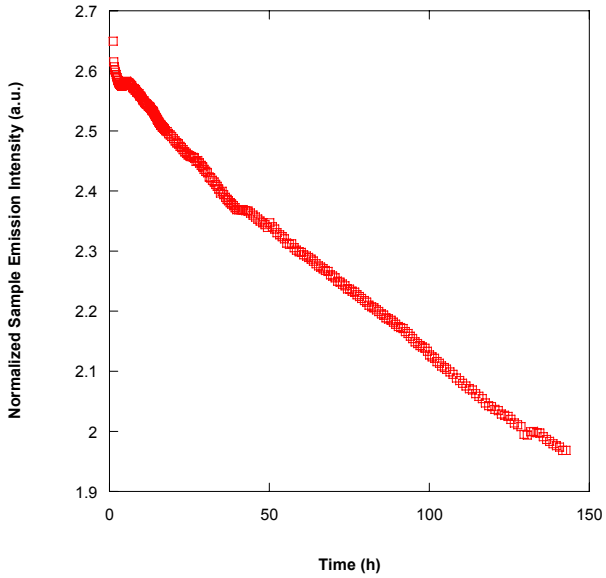

Figure 24. Sample intensity versus time of a sample of **1c** under oxygen. The emission intensity of the sample decays 0.18 % per hour, consistent with the previous observations.

Studying the Effect of Stirring on Sensor Longevity

In order to determine if refreshing the surface of the sample was an effective means of prolonging the life of the sensing material, a sample of **1c** was prepared and tested using configuration file "C" multiple times in order to allow the sensing behavior of the compound to degrade (Figure 25). After this period of time, the sample was stirred on the sample rod and retested, again using configuration file "C". The first observed K_{SV} was 3.23(7). After about 3 days of study, the K_{sv} settles to a value of 3.13(2). After the sample was stirred, the first set of 4 Stern-Volmer runs returns a K_{SV} of 3.23(7) but then this value decreases back down to the 3.13(2) over the remainder of the data collection. The sample was stirred a second time and the data collection started again. Again, the first set of Stern-Volmer runs gives a K_{SV} of 3.21(3). At the conclusion of the experiment, a K_{SV} of 3.14(2) is obtained. These results indicate that the sensitivity of the sample can be restored temporarily after an initial degradation of the compound. However, the rate of degradation remains the same and the sensitivity of the compound continues to decrease.

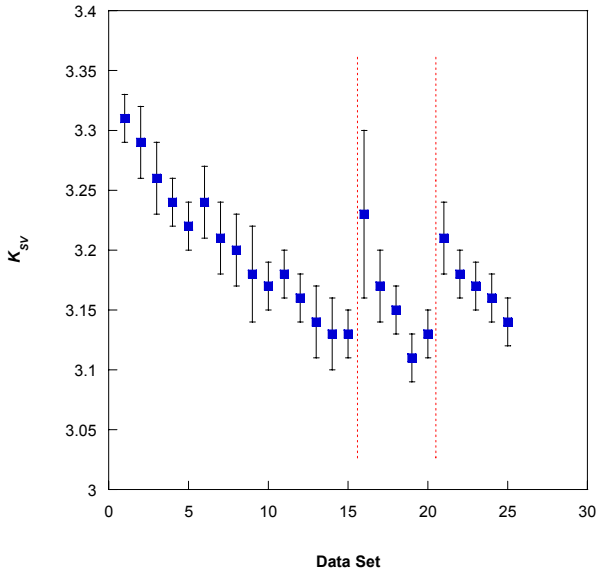

Figure 25. The change of the K_{SV} parameter of **1c** is shown. Fifteen data sets were collected without moving the sample to allow the sensitivity of the material to decrease. Then, the sample was removed from the setup, the surface of the sample refreshed through stirring at the two times indicated by red, dashed lines. Stirring the surface temporarily improves the sensitivity of the material.

To determine if the life of the sample could be extended, a new sample of **1c** was prepared and the surface refreshed through stirring the material after each data collection. During this study, data were collected for only one set of 4 Stern-Volmer runs. After each set, the sample was removed from the setup, stirred, and returned without changing any of the collection parameters. The results indicate that over the same experimental time period (15 data collections) a sample with a refreshed surface exhibits no change in the K_{SV} parameter (Figure 26). A comparison of the two samples is shown in Figure 27 and illustrates the difference in the rate of sample degradation when the surface is refreshed.

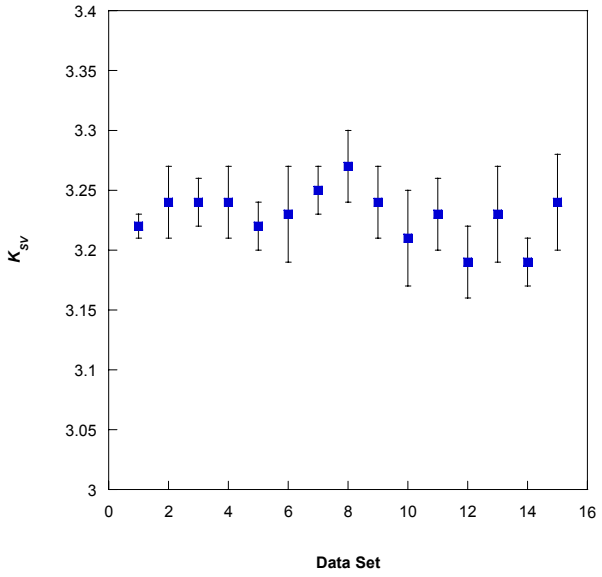

Figure 26. During this study, the surface of the **1c** sensing material was refreshed after each data collection through stirring. The data suggest that refreshing the surface mitigates the decrease of the K_{SV} parameter, prolonging the life of the sensing material.

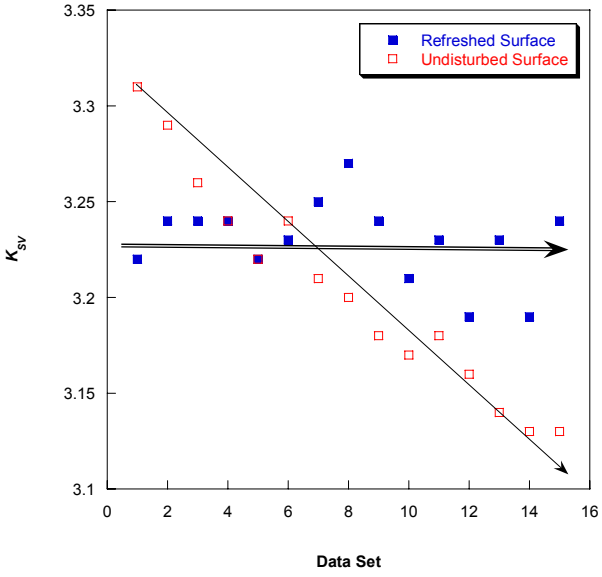

Figure 27. Two different samples of **1c** were prepared and the effects of surface refreshing on the K_{SV} parameter were examined. The refreshing of the surface lessens degradation of the sensing ability.

Low Temperature Emission Study

A microcrystalline sample of **1c** was submerged into liquid helium and liquid nitrogen and a representative selection of the spectra are shown in Figure 28. The initial emission intensity at room temperature is shown in black and the emission maximum occurs at approximately 565 nm. As the sample is cooled, the red spectrum is observed. The emission intensity has decreased and begun to red shift as a result in the shift of the emission from the ^{1}MLCT state to emission from the ^{3}MLCT and/or $^{3}\pi$-π* states.[18] Further cooling results in an increase in emission intensity and a complete shift in the emission maximum to approximately 575 nm, as is seen in the green spectrum. Finally, when the lowest temperature is reached, the emission intensity is almost 2 times the initial room temperature emission intensity. This increased emission is expected as the cooling of the sample lowers the likelihood of excited state distortion, resulting in fewer non-radiative pathways for excited state relaxation, and thus, more emission intensity. These compounds do not exhibit a significant change in emission vibrational fine structure upon cooling. This red shift accompanied with no structural change of the emission has been observed previously with similar $[Cu(P\hat{}P)(N\hat{}N)]^{+}$ compounds.[18]

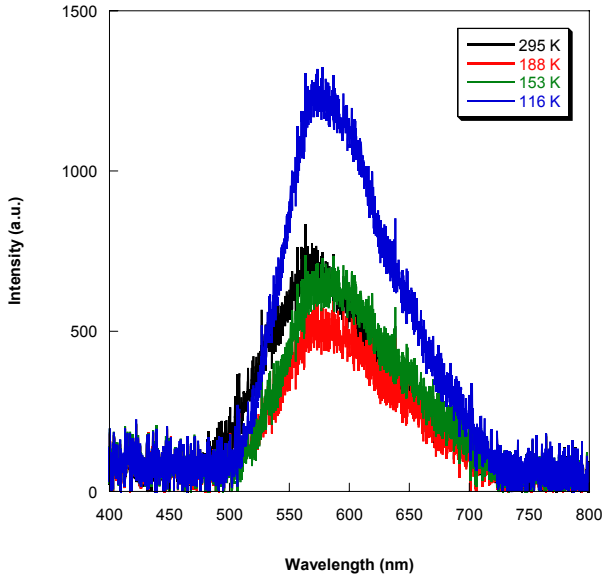

Figure 28. Selected spectra from the low temperature emission study of **1c**. Each spectrum illustrates the change in the spectra with decreasing temperature. The first spectrum is shown, followed by one illustrating the decrease in emission, then the red shift of the emission, and finally the increased emission intensity of the sample at the coldest temperature.

Conclusions

A series of $[Cu(P^P)(N^N)]^+$ compounds has been synthesized and characterized for use in optical oxygen sensing materials. The sensing ability of the complexes appears to be strongly counterion dependent: BF_4^- compounds tend to show irreproducible results, $pfpb^-$ compounds do not sense oxygen (due in part to a lack of void space in the crystalline materials), and $tfpb^-$ compounds sense oxygen with the best sensitivity and stability. This study did not find that the more rigid P^P ligand xantphos was necessary to the production of a sensitive and stable material as previously postulated. The 2,9-dimethyl substituents, while they improve the photophysical properties, were also unnecessary for the sensing materials studied here.

In order to observe significant decomposition of the emission intensity of **1c**, the sample must be illuminated under an oxygen environment. The degradation of the material is also faster when illuminated with 365 nm LED light or when the 405 nm LED is operated at a higher voltage. It was also determined that the photodecomposition product does not emit or sense oxygen as the emission intensity and absorbance of **1c** does not change with irradiation. However, the effects of degradation can be mitigated through stirring of the sample surface.

Based on these observations we propose the degradation of the material occurs only at the surface. As the light penetration depth decreases, so does the relative proportion of decomposition material. When stirred, fresh material that was previously at the bottom of the sample is moved to the surface. Thus the sensing behavior is improved. By using the material for short periods of time and stirring the sample after each use, it appears that **1c** is a viable solid-state oxygen sensor.

References

1. Amao, Y.; Asai, K.; Okura, I. *J. Porphyrins Phthalocyanines* **2000**, *4*, 292.

2. Amao, Y.; Miyashita, T.; Okura, I. *J. Fluorine Chem.* **2001**, *107*, 101.

3. Demas, J. N.; DeGraff, B. A.; Coleman, P. B. *Anal. Chem.* **1999**, *71*, 793A.

4. Demas, J. N.; Harris, E. W.; McBride, R. P. *J. Am. Chem. Soc.* **1977**, *99*, 3547.

5. DeRosa, M. C.; Hodgson, D. J.; Enright, G. D.; Dawson, B.; Evans, C. E. B.; Crutchley, R. J. *J. Am. Chem. Soc.* **2004**, *126*, 7619.

6. Douglas, P.; Eaton, K. *Sens. Actuators, B* **2002**, *B82*, 200.

7. Li, Z. *Spectrochimica Acta Part A* **2011**, *81*, 475.

8. Miller, M. T.; Karpishin, T. B. *Sens. Actuators, B* **1999**, *61*, 222.

9. Mills, A. *Platinum Met. Rev.* **1997**, *41*, 115.

10. Papkovsky, D. B.; Ponomarev, G. V.; Trettnak, W.; O'Leary, P. *Anal. Chem.* **1995**, *67*, 4112.

11. Zhang, H.; Sun, Y.; Ye, K.; Zhang, P.; Wang, Y. *J. Mater. Chem.* **2005**, *15*, 3181.

12. Burney, J. Doctoral Thesis, University of Minnesota, 2007.

13. McGee, K. A.; Mann, K. R. *J. Am. Chem. Soc.* **2009**, *131*, 1896.

14. McGee, K. A.; Marquardt, B. J.; Mann, K. R. *Inorg. Chem.* **2008**, *47*, 9143.

15. McGee, K. A.; Veltkamp, D. J.; Marquardt, B. J.; Mann, K. R. *J. Am. Chem. Soc.* **2007**, *129*, 15092.

16. Smith, C. S.; Branham, C. W.; Marquardt, B. J.; Mann, K. R. *J. Am. Chem. Soc.* **2010**, *132*, 14079.

17. Smith, C. S.; Mann, K. R. *Chem. Mater.* **2009**, *21*, 5042.

18. Smith, C. S.; Mann, K. R. *J. Am. Chem. Soc.* **2012**, *134*, 8786.

19. Cuttell, D. G.; Kuang, S.-M.; Fanwick, P. E.; McMillin, D. R.; Walton, R. A. *J. Am. Chem. Soc.* **2002**, *124*, 6.

20. Everly, R. M.; Ziessel, R.; Suffert, J.; McMillin, D. R. *Inorg. Chem.* **1991**, *30*, 559.

21. Palmer, C. E. A.; McMillin, D. R. *Inorg. Chem.* **1987**, *26*, 3837.

22. Rader, R. A.; McMillin, D. R.; Buckner, M. T.; Matthews, T. G.; Casadonte, D. J.; Lengel, R. K.; Whittaker, S. B.; Darmon, L. M.; Lytle, F. E. *J. Am. Chem. Soc.* **1981**, *103*, 5906.

23. Borisov, S. M.; Zenkl, G.; Klimant, I. *ACS Applied Materials & Interfaces* **2010**, *2*, 366.

24. Collier, B. B.; Singh, S.; McShane, M. *Analyst* **2011**, *136*, 962.

25. Exstrom, C. L.; Britton, D.; Mann, K. R.; Hill, M. G.; Miskowski, V. M.; Schaefer, W. P.; Gray, H. B.; Lamanna, W. M. *Inorg. Chem.* **1996**, *35*, 549.

26. Dietrich-Buchecker, C.; Sauvage, J. P.; Kern, J. M. *J. Am. Chem. Soc.* **1989**, *111*, 7791.

27. Cuttell, D. G.; Kuang, S.-M.; Fanwick, P. E.; McMillin, D. R.; Walton, R. A. *Journal of the American Chemical Society* **2001**, *124*, 6.

28. Bruker, **2008**, *APEX II*, Madison, Wisconsin, USA.

29. Blessing, R. H. *Acta Cryst. A* **1995**, *A51*, 33.

30. Sheldrick, G. M., **2008**, *SADABS*, University of Gottingen, Germany.

31. Sheldrick, G. M. *Acta Cryst. A* **2008**, *A64*, 112.

32. Bruno, I. J.; Cole, J. C.; Edgington, P. R.; Kessler, M.; Macrae, C. F.; McCabe, P.; Pearson, J.; Taylor, R. *Acta Cryst. B* **2002**, *B58*, 389.

33. Spek, A. L., **2005**, *PLATON, A Multipurpose Crystallographic Tool*, Utrecht University, Utrecht, The Netherlands.

34. Spek, A. L. *Acta Cryst. D* **2009**, *D65*, 148.

35. Wrighton, M. S.; Ginley, D. S.; Morse, D. L. *J. Phys. Chem.* **1974**, *78*, 2229.

36. Avian Technologies, W. R., P.O. Box 822, Wilmington, OH 45177, USA; http://www.aviantechnologies.com/faq.html.

37. Kuang, S.-M.; Cuttell, D. G.; McMillin, D. R.; Fanwick, P. E.; Walton, R. A. *Inorg. Chem.* **2002**, *41*, 3313.

Chapter Four

Similarities in the Crystal Structures and Oxygen Sensing Abilities of Two Analogous Ru(II) and Zn(II) Complexes

Overview

The structure of zinc(II) *tris*-4,7-diphenylphenanthroline (bath) with the fluorinated anion *tetrakis*-(pentafluorophenyl)borate ($pfpb^-$) has been determined along with that of $[Ru(bath)_3](pfpb)_2$. The crystalline forms of these complexes pack in an identical manner with significant amounts of void space in the form of pseudochannels. These pseudochannels allow oxygen to diffuse within the lattice with preliminary response times less than 3 seconds. The fast response time and large amount of void space within these these crystalline materials contribute to each complex having high Stern-Volmer quenching constants. The zinc complex shows particular promise for use as an oxygen sensor as it is stable to photochemical degradation and is inexpensive to produce.

Introduction

The applications for oxygen sensing materials range from monitoring oxygen in biological systems to reaction vessels.[1-10] Research into the development of an ideal oxygen sensor focuses on several properties. These properties include: selectivity and sensitivity toward oxygen, long term stability, a linear response toward oxygen, and that the sensing material can be easily and cost effectively manufactured.

$[Ru(bpy_)_3]^{2+}$ (bpy = 2,2'-bipyridine) complexes suspended in sol gels, polymer matrices, and adsorbed onto zeolites have been extensively studied for use in dissolved oxygen sensors.[3,6-8,11-14] The oxygen sensing measurements obtained from such materials are often complicated by emission from multiple sites, decomposition, and curved Stern-Volmer response plots. Recent work from our group has focused on applying the

principles of the Ru(II) polypyridine complexes to oxygen sensing by using solid state materials with both 1,10-phenanthroline (phen) and bpy ligands.[15-17] Solid state oxygen sensors are of interest to the field since the use of a solid state crystalline material would eliminate the need for any support material, simplifying the response and data interpretation of the sensor.

We have found a relationship exists between the amount of void space within the crystalline lattice of these $[Ru(phen)_3]^{2+}$ and $[Ru(bpy)_3]^{2+}$ complexes and the sensing ability of the material.[17] The higher the percentage of void space within the crystal, the higher the fraction of emission quenched. Consequently, the sensitivity of the material is higher based on the larger Stern-Volmer quenching constant (K_{SV}). One compound [Ru(4,7-dimethyl-1,10-phenanthroline)$_3$](tfpb)$_2$ (where tfpb$^-$ = *tetrakis*-[*bis*-3,5-trifluoromethyl(phenylborate)]) sensed oxygen well and crystallizes with large amounts of void space.[17] However, we believed we could create more void space and increase the K_{SV} with larger substituents at the 4 and 7 positions of the phen ligand.

It is our thought that phenyl substituents should increase the amount of space within the crystalline lattice, much like the addition of methyl substituents in the same position on phen increased the amount of void space over the unsubstituted phen. The target complex, $[Ru(bath)_3]^{2+}$ (bath = 4,7-diphenyl-1,10-phenanthroline), has been embedded into support matrices and found to sense oxygen by others.[2,6,11,18-21] Given the desirable photophysical properties of $[Ru(phen)_3]^{2+}$ and $[Ru(bath)_3]^{2+}$ compounds, we decided to generate $[Ru(bath)_3](pfpb)_2$, where pfpb$^-$ is *tetrakis*-(pentafluorophenyl)borate, and explore the sensing ability of the compound in its solid state. The fluorinated anion should increase the solubility of oxygen and result in a more sensitive material.

Additionally, the phenyl substituents of the phen ligand have the ability to interact with the aromatic rings borate counterion, which could dictate the packing interactions in the solid state. The elimination of the support material should eliminate the observed decrease in emission intensity upon device fabrication previously observed while also simplifying data interpretation as only one emissive site should be present.[11,18]

In addition to generating a sensitive solid state sensor, it is also desired to create an inexpensive alternative to the ruthenium based sensors. Knowing that molecules with similar shapes tend to pack in similar ways, we expect that the less expensive compound $[Zn(bath)_3](pfpb)_2$ will pack in a similar fashion as $[Ru(bath)_3](pfpb)_2$.[15] If the zinc(II) materials contain void space and their emission is quenchable by oxygen, the relationship between void space and sensing should hold true. The result is a sensing device based on an earth abundant metal center.

However, the photophysical properties of the two compounds should not be identical as the emission from ruthenium(II) complexes is based on the charge transfer event from the metal center to the ligand.[20,22-24] The resulting emission is intense, less structured, and shifted significantly from the emission of the free ligand.[24] The emission process in ruthenium complexes is the result of phosphorescence, accounting for the long lifetimes observed for these compounds.[2,3,24] Zinc(II) complexes are d^{10} and any emission from the complex is most likely a ligand π to π^* transition.[22-28] Changes in the ligand significantly affect the emission from the complex, making ligand choice important.[25,29,30] Compounds based on zinc(II) tend to fluoresce, a process with a shorter lifetime than processes based on phosphorescence.[24,31,32] The emission from the complex

should therefore be similar in peak shape and be minimally shifted when compared to emission from the ligand.[33]

Despite the possible limitations posed by the high energy emission and potentially short emission lifetime, zinc(II) compounds have been used in sensing materials. Emissive zinc compounds have been used to sense pesticides, nerve gases, and hydrogen sulfide.[34-37] There are also examples of turn-on fluorescence zinc sensors and zinc compounds used in OLEDs (organic light emitting devices), demonstrating that zinc compounds can be emissive.[29,38-44] Based on the use of zinc compounds in optical sensing devices, $[Zn(bath)_3](pfpb)_2$ is a promising candidate for solid state optical oxygen sensing devices.

Both the zinc(II) and ruthenium(II) complexes were synthesized, crystallized, and tested for use as viable solid state oxygen sensors. While the type of emission and the specific sensing mechanism were found to differ, the complexes made with zinc(II) could provide a cost effective alternative to those made with ruthenium(II).

Experimental

General Considerations for Synthesis. The chloride salt $[Ru(bath)_3]Cl_2$ was purchased from Alfa Aesar. $ZnCl_2$, $ZnSO_4$ and $NaPF_6$ were purchased from Aldrich, 4,7-diphenyl-1,10-phenanthroline from Fluka, and Kpfpb from Boulder Scientific Company. Na(tfpb) was available from a prior study.[45] All were used as received. All other reagents and solvents were used without further purification. ^1H NMR spectra were recorded on Varian Unity or Inova 300 MHz instruments and ^{19}F NMR spectra were recorded on a Varian Unity 300 MHz instrument. Chemical shifts are reported in units of ppm with an

external reference to the residual proton resonance in deuterated acetonitrile for the ^{1}H spectra and the internal $CFCl_3$ reference for the ^{19}F NMR spectra. High resolution mass spectrometry was carried out on a Bruker BioTOF II mass spectrometer.

$[Ru(bath)_3](pfpb)_2$ (1)

$[Ru(bath)_3]Cl_2$ (0.1260 g, (0.1078 mmol) and 0.1590 g (0.2215 mmol) of Kpfpb were dissolved in 10 mL of acetonitrile dried using an MBraun solvent purification system. The solution was precipitated with distilled water, and sticky precipitate was resulted. Methanol (2 mL) was added to the material and the vial was sonicated, resulting in the formation of an orange powdered precipitate. The orange precipitate was collected via gravity filtration. This crude material was then purified by dissolving the crude material in CH_2Cl_2 and chromatigraphing the material down a short alumina column. The solvent was then evaporated yielding 0.1619 g (0.06521 mmol, 61 %) of a red-orange crystalline material. ^{1}H NMR (CD_3CN): δ 8.28 (d, 6 H, J = 5.4 Hz), 8.22 (s, 6 H), 7.65 (d, 6 H, J = 5.7 Hz), 7.62 (m, 30 H) ^{19}F NMR (CD_3CN): δ -134.36 (m, 16 H), -164.40 (m, 8 H), -168.84 (m, 16 H).

$[Zn(bath)_3](pfpb)_2$ (2)

4,7-diphenyl-1,10-phenanthroline (0.468 g, 1.41 mmol) was added to 100 mL of acetonitrile. To this mixture, CH_2Cl_2 was added dropwise and the solution heated until the ligand was completely dissolved. The solution was cooled to room temperature and 0.0547 g (0.401 mmol) of $ZnCl_2$ was added and the solution was allowed to stir at room temperature for 2 hours. An acetonitrile solution of Kpfpb (0.606 g, 0.844 mmol) was

added to the reaction and again it was allowed to stir. Distilled water was added to the solution resulting in precipitation of a white solid (0.821 g, 85 % yield). The solid was isolated by vacuum filtration and dried under vacuum. ^{1}H NMR (CD_3CN): δ 8.47 (d, 6 H, *J* = 5.1 Hz), 8.17 (s, 6 H), 7.81 (d, 6 H, *J* = 5.1 Hz), 7.62 (m, 30 H) ^{19}F NMR (CD_3CN): δ -134.36 (m, 16 H), -164.40 (m, 8 H), -168.85 (m, 16 H). HRESIMS (M^{2+}): *m/z* calcd for $ZnC_{72}N_6H_{48}$ 530.16; found 531.7355

The following compounds were synthesized for spectroscopic comparison to 2. Synthesis and *preliminary* NMR data are presented.

$[Zn(phen)_3](PF_6)_2$ (3a)

To 2 mL of distilled H_2O was added 0.0191 g (0.140 mmol) of $ZnCl_2$ and was allowed to stir until the $ZnCl_2$ was dissolved. Phen (0.0854 g, 0.431 mmol) was added to the stirring solution. After 2 hours, $NaPF_6$ (0.0508 g, 0.302 mmol) was added and a milky white precipitate was immediately formed. The resulting solid was collected via vacuum filtration and washed with distilled H2O and diethylether. The solid was dried under vacuum yielding 0.0890 g of **3a** (71 % yield). ^{1}H NMR (CD_3CN): δ 8.76 (d, 6 H, *J* = 8.4 Hz), 8.22 (m, 12 H), 7.78 (q, 6 H, *J* = 5.1, 8.4 Hz) ^{19}F NMR (CD_3CN): δ -74.93, -77.43.

[Zn(phen)$_3$](tfpb)$_2$ (3b)

[Zn(phen)$_3$]SO$_4$ was synthesized through the addition of phen to a solution of ZnSO$_4$. The isolated sulfate salt (0.0200g, 0.0285 mmol) was then dissolved in 5 mL of methanol and the solution was warmed. Na(tfpb) (0.0490 g, 0.0553 mmol) was dissolved in 1 mL in a separate vial. The two methanol solutions were combined resulting and distilled H$_2$O added to precipitate a white solid. The solid was collected via vacuum filtration and dried under vacuum. **3b** was collected in an 76 % yield (0.0506 g). ^{1}H NMR (CD$_3$CN): δ 8.76 (dd, 6 H, *J* = 1.5, 8.4 Hz), 8.22 (m, 12 H), 7.78 (dd, 6 H, *J* = 4.8, 8.1 Hz), 7.67 (m, 24 H) ^{19}F NMR (CD$_3$CN): δ -63.87.

[Zn(dimethyl)$_3$](tfpb)$_2$ (4)

To 5 mL of methanol was added 4,7-dimethyl-1,10-phenanthroline (0.0409 g, 0.1963 mmol). A 5 mL methanol solution of ZnCl$_2$ (0.0082 g, 0.060 mmol) was then added and the resulting solution allowed to stir. After 2 hours, 0.1208 g (0.1363 mmol) of Na(tfpb) was added. A white solid was precipitated from the solution through the addition of distilled H$_2$O. The solid was collected via vacuum filtration, washed with distilled H$_2$O, and dried under vacuum. 0.0.819 g of **4** were collected (56 % yield). ^{1}H NMR (CD$_3$CN): δ 8.36 (s, 6 H), 8.01 (d, 6 H, *J* = 4.8 Hz), 7.68 (m, 24 H), 7.59 (d, 6 H, *J* = 4.8 Hz), 2.87 (s, 18 H) ^{19}F NMR (CD$_3$CN): δ -63.85.

$[Zn(dpbpy)_3](pfpb)_2$ (5)

The dpbpy ligand (0.0515 g, 0.167 mmol) was dissolved in 5 mL of CH_2Cl_2 and the solution stirred. To this was added a 1 mL CH_2Cl_2 solution of $ZnCl_2$ (0.0070 g, 0.051 mmol) at which point the solution became slightly yellow in color. Kpfpb (0.0750 g, 0.104 mmol) was dissolved in 1 mL of acetonitrile and this solution was added to the CH_2Cl_2 solution. Attempts were made to precipitate the solution with both diethylether and H_2O. The solvent was then reduced to half its original volume at which point an off-white solid began precipitating. The solid was collected via vacuum filtration and dried under vacuum resulting in 0.0348 g (29 % yield) of **5**. ^1H NMR (CD_3CN): δ 8.95 (m), 8.12 (m), 7.95 (m), 7.86 (m), 7.61 (m) ^{19}F NMR (CD_3CN): δ -134.33, -164.34, -168.86.

X-ray Crystallography

All data for the structure determinations of $[Ru(bath)_3](pfpb)_2 \cdot 2\ CH_3CN$ (**1**), $[Zn(bath)_3](pfpb)_2 \cdot 1.5\ CH_2Cl_2$ (**2a**), and $[Zn(bath)_3](pfpb)_2 \cdot 3\ CH_3CN$ (**2b**) were collected at the X-ray Crystallographic Laboratory (Department of Chemistry, University of Minnesota). Crystals were grown by the slow evaporation of saturated acetonitrile solutions or a mixture of a dichloromethane and methanol. Single crystals were attached to glass fibers and mounted on a Bruker SMART Platform CCD for data collection at 173 K (**1** and **2a**) or 123 K (**2b**) using graphite monochromated MoKα radiation (λ = 0.71073 Å).[46] An initial set of cell constants was calculated from reflections harvested from three sets of 20 frames oriented such that orthogonal wedges of reciprocal space were surveyed. Final cell constants were calculated from a minimum set of 3602

strong reflections from the actual data collection. Data were collected to the extent of at least 1.5 hemispheres at a resolution of 0.80 Å (**1** and **2a**) or 0.77 Å (**2b**) using φ-scans. Three major sections of frames were collected with 0.30 º steps in ω at 3 different ϕ settings and a detector position of -28 º in 2θ. For all structures, the intensity data were corrected for absorption and decay using SADABS v2.10.[47,48] Space groups were determined based on systematic absences and intensity statistics. The structures were determined using a direct-methods solution. Several full-matrix least-squares/difference Fourier cycles were performed to locate remaining non-hydrogen atoms. All calculations were performed using the SHELXTL-V6.12 suite of programs on Pentium computers.[46,49] Additional crystallographic information can be found in Table 1. Packing analysis parameters were measured using PLATON/VOID with pictorial representations of the solvent channels done with edited *.res files in Mercury.[50-52]

The detection of solvent accessible voids by PLATON/VOID is done in the following way: The unit cell is filled with the atoms from the structural model and each specific atom is assigned its respective van der Waals radius. A grid search generates a list of grid points with a minimum distance of 1.2 Å from the nearest van der Waals surface. This list of grid points is then used to produce a new list of grid points that makes up the solvent accessible areas. For the sets of grid points, the center of gravity and volume of the void are calculated. The overall solvent accessible volume is calculated along with the volume and center of gravity of individual 'voids'.

Table 1. Crystallographic Data and Refinement Parameters.

Compound	**1**	**2a**	**2b**
empirical formula	$C_{120}H_{48}B_2F_{40}N_6Ru$	$C_{121}H_{50}B_2Cl_2F_{40}N_9Zn$	$C_{126}H_{57}B_2F_{40}N_9Zn$
crystal color, morphology	orange, prism	colorless, plate	pink, block
crystal system	Triclinic	Triclinic	Triclinic
space group	$P\bar{1}$	$P\bar{1}$	$P\bar{1}$
crystallization solvent	acetonitrile	dichloromethane/methanol	acetonitrile
a, Å	16.753(2)	16.804(3)	16.918(2)
b, Å	18.356(3)	18.332(3)	18.294(2)
c, Å	18.592(3)	18.413(3)	18.622(3)
α, deg	86.698(2)	87.494(4)	87.306(2)
β, deg	78.312(2)	78.913(3)	79.963(2)
γ, deg	73.826(2)	73.943(3)	74.641(2)
volume (V), Å^3	5377.1(13)	5349.2(17)	5472.6(12)
Z	2	2	2
formula weight, g mol^{-1}	2456.33	2505.56	2543.80
density (calculated), g cm^{-3}	1.517	1.556	1.544
temperature, K	173(2)	173(2)	123(2)
absorption coefficient (μ), mm^{-1}	0.269	0.405	0.351
F(000)	2448	2504	2552
θ range, deg	1.16 to 26.37	1.13 to 25.00	1.44 to 27.57
index ranges	$-20 \le h \le 20$	$-19 \le h \le 19$	$-21 \le h \le 21$
	$-22 \le k \le 22$	$-21 \le k \le 19$	$-23 \le k \le 23$
	$-23 \le l \le 23$	$-21 \le l \le 21$	$-24 \le l \le 23$
reflections collected	51470	31122	65096
independent reflections	21708 [R_{int} = 0.0550]	18183 [R_{int} = 0.0822]	24690 [R_{int} = 0.0406]
weighting factors,[a] *a, b*	0.0836, 0.0000	0.0811, 14.9604	0.0548, 2.6205
max, min transmission	0.9357, 0.9357	0.9880, 0.8232	0.9493, 0.8442
data/restraints/parameters	21708/0/1529	18183/31/1610	24690/12/1617
R_1, wR_2 [$I > 2\sigma(I)$]	0.0651, 0.1564	0.0952, 0.1996	0.0435, 0.1059
R_1, wR_2 (all data)	0.1238, 0.1700	0.2045, 0.2402	0.0729, 0.1216
GOF	1.030	1.063	1.029
largest diff. peak, hole eÅ^{-3}	0.820, -0.750	0.788, -0.606	0.662, -0.451

[a] $w = [\sigma^2(F_o^2) + (aP)^2 + (bP)]^{-1}$, where $P = (F_o^2 + 2F_c^2)/3$.

Oxygen Sensing Instrumentation

The crystalline samples for oxygen sensing were prepared by placing a small amount of crushed crystals into a depression in a ¼'' diameter aluminum rod. The prepared sample was then placed into a swage cross-tube fitting apparatus designed to allow gas to flow over the sample and for front face illumination. A schematic diagram is shown in Figure 1. A 405 nm for measurements made of **1** or 350 nm LED for measurements made of **2** was filtered through an interference filter and used as the excitation source. Light was brought to the sample by the center fiber of a "six around one" bifurcated fiber optic probe. The emission was collected through the six fiber channel and sent to an Ocean Optics USB-2000 spectrometer. The spectrometer, mass flow controllers, temperature, and pressure monitors were interfaced to a computer to allow control of the unattended data acquisition via a custom LabVIEW program.[15-17,53,54]

The emission data collected were analyzed with a spreadsheet written in Microsoft Excel. Data from three cycles of spectra obtained at approximately 0.0, 0.10, 0.21, 0.25, 0.40, 0.50, 0.65, 0.80, 0.90 and 1.0 mole fraction of oxygen in nitrogen were used for the Stern-Volmer plots. The acquisitions were performed at room temperature or 21.8 ± 1 °C. Exact gas mole fractions were calculated by referencing the feedback voltage of the mass flow controllers to a calibration previously performed.[53] The emission intensity was integrated across the entire peak and divided by the integrated LED intensity for each spectrum to give I_0 (intensity under N_2) and I (intensity at a given O_2 mixture). I_0/I was plotted versus oxygen mole fraction in nitrogen to yield a Stern-Volmer plot. A linear regression model was used to calculate the slope or K_{SV} parameter.

It should be noted that the K_{SV}'s reported here are expressed in units of mole fraction and have not been corrected for the atmospheric pressure in Minneapolis, MN of 0.97 atm. In order to compare these K_{SV} numbers to those reported previously, the K_{SV} in mole fraction needs to be corrected by dividing the current value by 0.97 atm to give the K_{SV} in units of atm^{-1}.

Pressure Jump Experiment

A microcrystalline sample of $[Zn(bath)_3](pfpb)_2$ was deposited onto a brass rod and affixed with acetonitrile. The rod was then placed into a pressure tight version of the swage cross cell used for oxygen sensing studies, complete with fiber optic probe. A 365 nm LED was used as the excitation source. The cell was pressurized with air to approximately 48 psi and after allowing the pressure to equilibrate, and an electronic valve was actuated to release the pressure in the cell back to atmospheric pressure (14.3 psi). This process took approximately 2 milliseconds. Emission data were obtained for the pressurized sample as a function of time every 20 ms using the Ocean Optics software before and following the actuation of the electronic valve to release the pressure. Emission intensity data obtained by this method show a very fast initial change followed by a characteristic long tail due to the diffusional nature of the sample equilibration. The integrated emission response at 48 psi was subtracted from all the data points and then the resulting data were normalized so that the integrated emission at infinity (P = 14.3 psi) was 1.

Lifetime Measurements

Lifetime measurements of sensing compounds are made using the same method reported previously.[17,53] A brief summary of the apparatus is given.

A similar swage cross-tube fitting apparatus used for the sensing measurements was used for lifetime measurements. The sample, light, and gas ports were oriented in the same fashion. The atmosphere within the cell is controlled with mass flow controller valves and a computer program. The sample is illuminated by light from a pulsed LED which is sent to the sample through one leg of the fiber optic probe. Emitted light is filtered and then returns through the other leg of the fiber optic probe to a Hamamatzu R928 PMT run at 1250 V using the last 5 dynodes. The signal from the PMT is amplified and read by an oscilloscope that has been triggered by a logic pulse produced by the LED. At least 30 transients are averaged, with each consisting of the average of at least 20 traces using a custom LabVIEW program. Further fitting is done with Solver in Excel. The slopes of the resulting plots of ln(emission intensity) vs. t are used to calculate the lifetime of the sample.[17] For those lifetimes that were found to be biexponential the resulting plot of ln(emission intensity) vs. t were fit to a biexponential of the form shown in Equation 1.

$$I = a_1 \exp(-k_1 t) + a_2 \exp(-k_2 t) + a_3 \qquad \textbf{(1)}$$

where I is equal to the light intensity at some time t. The values of a_1, a_2 are related to the fractional contribution of that process to the overall lifetime. The sum of these two values must equal 1. The term a_3 is a correction constant. The rate constants for the individual processes are given by k_1 and k_2. The biexponential lifetimes components are obtained by dividing 1 by either k_1 or k_2.

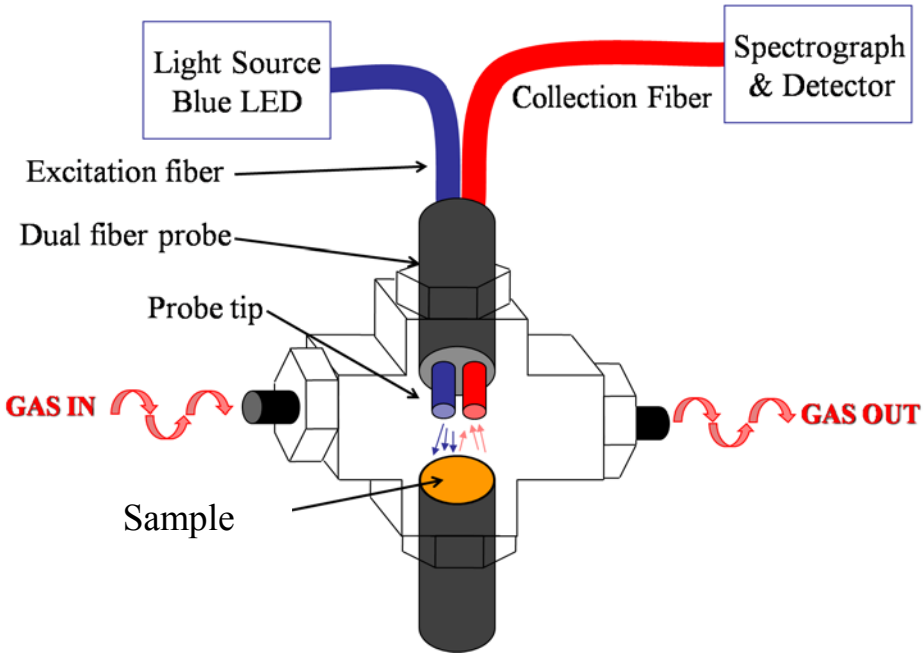

Figure 1. A schematic diagram of the sample holder used for all sensing and lifetime measurements.

Results and Discussion

X-ray Crystallography

The complex $[Ru(bath)_3](pfpb)_2$, (**1**), is shown in Figure 2 and crystallizes in the space group $P\bar{1}$ with approximately 2 molecules of disordered acetonitrile per asymmetric unit. The electron density from these solvent molecules was removed with the program PLATON/SQUEEZE to improve the structural refinement.[50] Solvent accessible space of 510.8 $Å^3$ was found per unit cell containing 93 electrons. This electron count correlates well with the structure having 4 acetonitrile molecules per unit cell as expected based on a Z = 2 and the two molecules of solvent initially observed in the asymmetric unit.

A phenyl ring of one of the 4,7-diphenyl-1,10-phenanthroline ligands was disordered over two positions with occupancies of 51.9 and 48.1 %. This disordered ring also lies close to the solvent channel in layer 1 to be described shortly. As previously stated, four molecules of acetonitrile were removed from the structure before any further calculations or packing analysis were performed.

The packing of the structure consists of two distinct layers. Voids exist within both of these layers, but take different morphologies. Layer 1 contains only anions and runs perpendicular to the crystallographic *a* axis (Figure 3). This layer contains a large amount of void space among the anions that closely resembles connected channels that run parallel to the crystallographic *b* axis. The disruption of the channels may be due in part to the disordered phenyl ring present in layer 2 which sits above and below layer 1. Layer 2 consists of both cations and anions (Figure 4). This second layer also has regions of void space, but the amount of void space in this layer is considerably smaller than that

within the anion layer. Within layer 2 the void space takes the form of isolated pockets that do not appear to be connected to the channels in layer 1. Alternating layers can be seen in Figure 5. The total amount of void space when disordered solvent is removed is 583.4 $Å^3$ or 10.8 % of the unit cell volume. This calculation was also performed with the disordered phenyl ring present in the most probable location based on the disorder statistics.

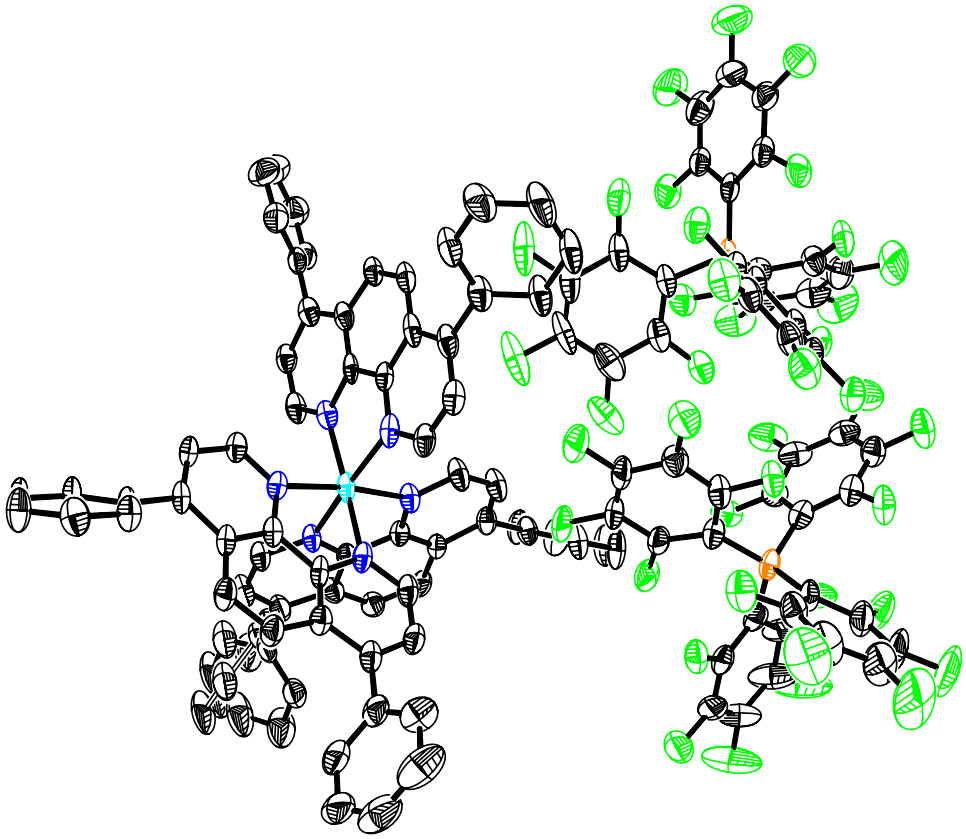

Figure 2. Thermal ellipsoid diagram of **1** with probability surfaces drawn at 50 % probability. Hydrogen atoms and solvent have been removed for clarity. The disordered phenyl ring is shown as hollow bonds in the bottom left.

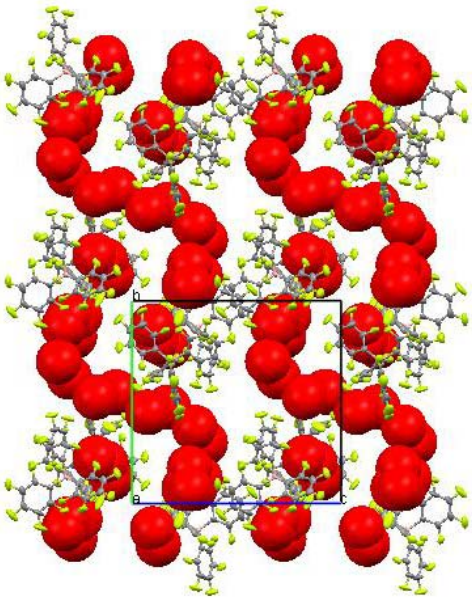

Figure 3. Layer 1 as viewed down the *a* axis. Regions of void space are represented by red spheres and appear as a disconnected channel snaking through the crystal. The breaks in the channel can clearly be seen.

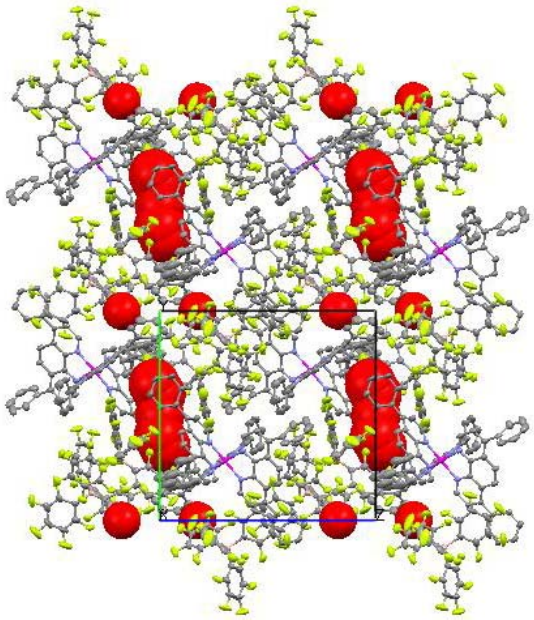

Figure 4. Layer 2 as viewed down the *a* axis. Regions of void space are represented by red spheres and appear as isolated pockets that do not connect to the voids of layer 1.

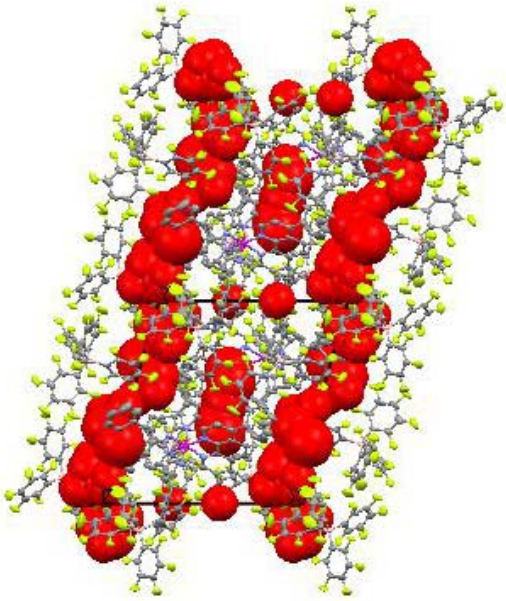

Figure 5. The alternating orientation of layers 1 and 2 is shown as viewed *c* axis. Layer 1 appears to be a channel running on both sides of layer 2, which contains void pockets.

Crystals of **2a** were grown from dichloromethane and the structure is shown in Figure 6. The structure of $[Zn(bath)_3](pfpb)_2 \cdot CH_2Cl_2$ was solved in space group $P\bar{1}$ and had similar unit cell parameters to the structure of **1**. This structure does not contain the phenyl-substituent disorder found in **1**. However, positional disorder of one of the perfluorophenyl rings of the anion was modeled with occupancies of 73 % and 27 %. Two half occupied dichloromethane molecules per asymmetric unit were placed and modeled over their corresponding inversion centers. These solvent molecules were then removed with the PLATON/SQUEEZE program.[50] Solvent accessible void space of 574.8 $Å^3$ was found per unit cell containing 131 electrons, corresponding to approximately 3 molecules of dichloromethane.

After the solvent was removed, PLATON/VOID was conducted on the data. This calculation found 563.8 $Å^3$ of void space accounting for 10.3 % of the unit cell volume. Visual examination of the void space diagrams reveals striking similarities to the packing motif observed in **1**. While it was expected that the two structures should pack in similar ways given their similar shapes, it was surprising to see that even when grown from a different solvents, the structures are, for all practical purposes, identical. Layer 1 can be seen in Figure 7 and again is a layer of anions with a snaking void space pseudochannel passing through. The disorder of the anion causes slight discrepancies in the void space when compared to the structure of **1**, but these are negligible. In fact, this disorder in the anion may help to complete the channel as fewer breaks can be seen in the void space diagram when viewed down the *a* axis. Layer 2 is again located above and below layer 1 and consists of both cations and anions. Layer 2 contains void space in the form of isolated pockets (Figure 8). The arrangement of the two layers with respect to one

another can be seen in Figure 9. When viewed along the *c* axis, the disruptions in the layer 1 channels are more obvious in the structure of **2a** than in **1**.

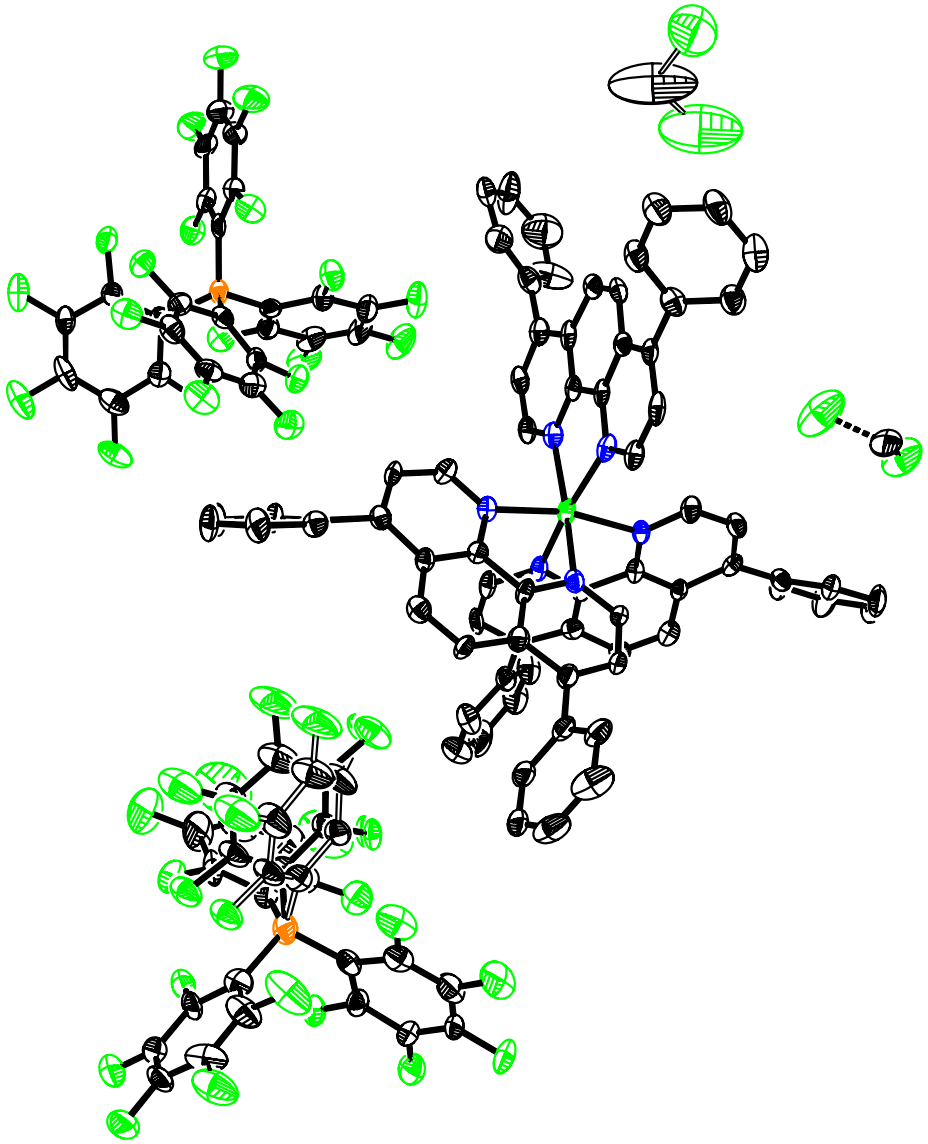

Figure 6. Thermal ellipsoid drawing of **2a** with probability surfaces drawn at 50 % probability. Partially occupied solvent molecules and anion disorder are shown. Hydrogen atoms have been removed for clarity. The disordered perfluorophenyl ring of the anion is shown as hollow bonds in the bottom left of the figure.

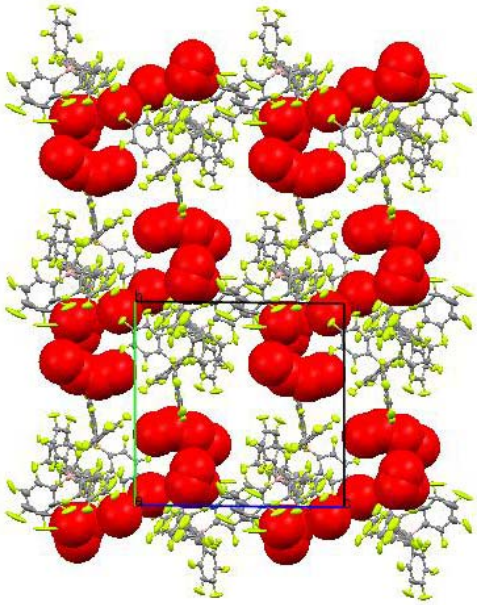

Figure 7. Layer 1 as viewed down the *a* axis. Regions of void space are represented by red spheres and appear as a disconnected channel snaking through the crystal. The breaks in the channel can clearly be seen.

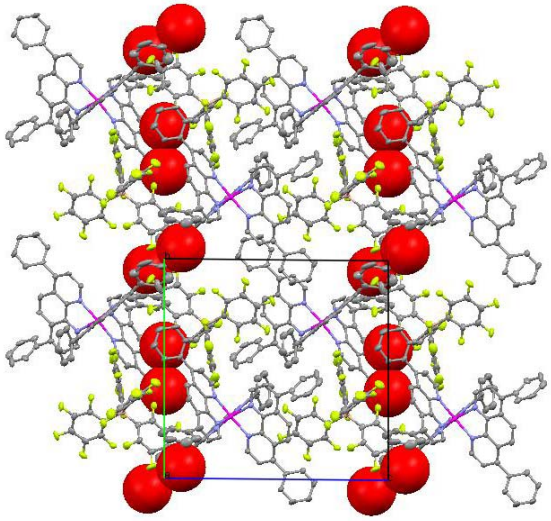

Figure 8. Layer 2 as viewed down the *a* axis. Regions of void space are represented by red spheres and appear as isolated pockets that do not connect to the voids of layer 1.

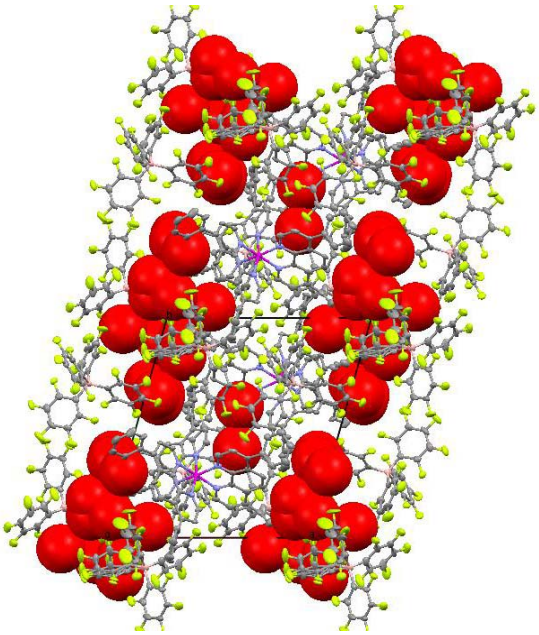

Figure 9. The alternating orientation of layers 1 and 2 is shown as viewed *c* axis. Layer 1 appears to be the channel running on both sides of layer 2, which contains void pockets.

Crystals of **2b** were grown from acetonitrile and the structure is shown in Figure 10. The structure of $[Zn(bath)_3](pfpb)_2 \cdot 3\ CH_3CN$ was solved in space group $P\bar{1}$ and had similar unit cell parameters to both **1** and **2a**. This structure was collected at a lower temperature than those previously discussed, but this lower temperature does not appear to have a significant impact on the unit cell or other parameters. Three acetonitrile molecules per asymmetric unit were placed and one is disordered over two positions. The model refines to have occupancies of 67 % and 33 % for this disordered solvent molecule. The acetonitrile molecules were then removed with the PLATON/SQUEEZE program.[50] Solvent accessible void space of 701.5 $Å^3$ was found per unit cell and contained 133 electrons corresponding to approximately six acetonitrile molecules as is expected based on a Z = 2 and the original placement of three acetonitrile molecules. This zinc structure does not exhibit any additional disorder.

PLATON/VOID was then conducted and 684.7 $Å^3$ of void space, corresponding to 12.8 % of the unit cell volume, was found. Examination of the packing diagrams reveals that the packing motif of **2b** is strikingly similar to **1** and **2a**, as was expected. However, the structure of **2b** contains 2 % more void space than the structure of **2a**. Perhaps the linear nature of the co-crystallized acetonitrile molecules requires the metal complex to pack in a way that necessitates more space. When compared to the structure of **1**, three molecules of acetonitrile could be placed in **2b** where only two could be placed in **1**. This additional solvent molecule is most likely the cause of the increased void space in **2b** compared to **1**.

Layer 1 can be seen in Figure 11 and once again consists of anions with a snaking void space pseudochannel. Due to the larger amount of void space present in this

structure, the appearance of the void space is much different. However, when looking at the diagram, two channels can be seen running parallel to the *b* axis. One has been denoted with arrows in the figure. The void still snakes through the layer in the same manner as it does in **2a**, but is much more spread out. As a result, the voids appear more isolated than previous structures.

The second layer, layer 2, is present above and below layer 1 and consists of both cations and anions. The voids in this layer are isolated pockets like in structures **1** and **2a** as shown in Figure 12. The arrangement of the two layers with respect to one another can be seen in Figure 13. When viewed down the *c* axis the two layers appear to take a configuration more like that of **2a**, meaning layer 1 appears to consist of isolated pockets instead of a channel. The void space within the two layers does not connect as the voids are contained within their specific layer.

When all three structures are compared side by side, the similarities between them are obvious. When looking at layer 1, all three contain the snaking void space parallel to the *b* axis (Figure 14). Each structure contains slight nuances in the exact shape of the voids, but this is due to the various disorder found in each of the structures. Figure 15 shows the similarities between layer 2 among the three structures. Again, small isolated pockets of void space are observed in each structure. The similar shape of **1** and **2** allows the structures of **1**, **2a**, and **2b** to be nearly identical. When predicting the oxygen sensing ability of these compounds, we expect that each of these materials will sense with large K_{SV}'s due to the large amount of void space. Any differences in the sensing mechanism or sensitivity must be due to the photophysical changes related to the change of the metal center and not to the ability of oxygen to diffuse through the crystal lattice.

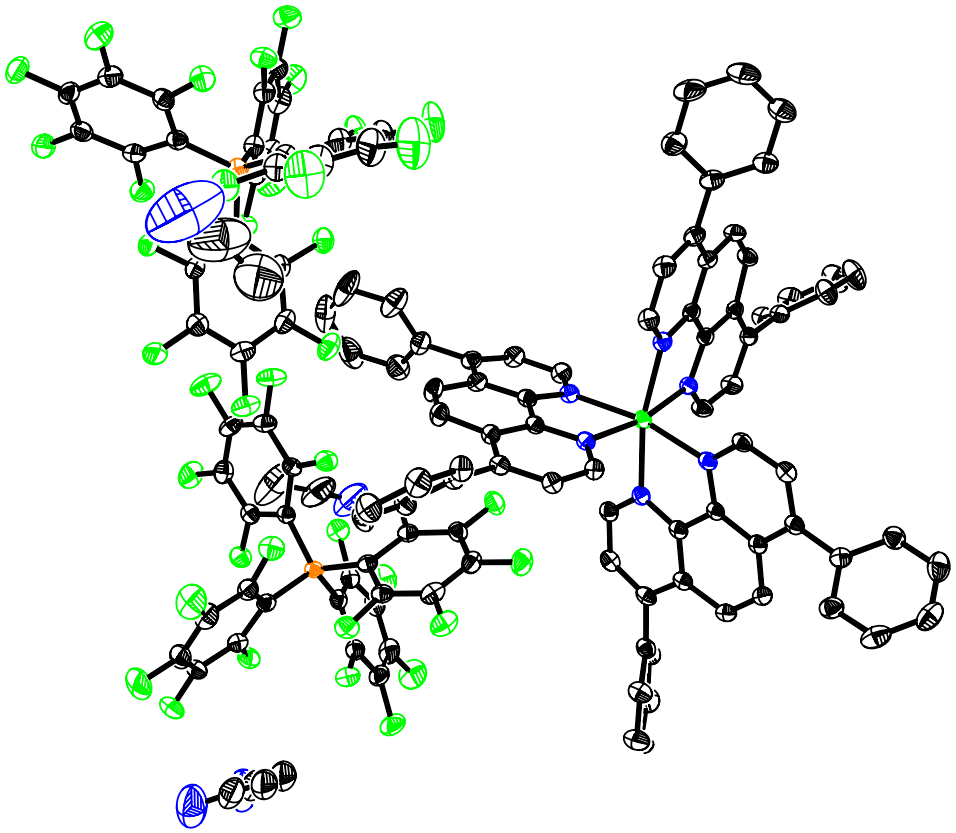

Figure 10. Thermal ellipsoid drawing of **2b** with probability surfaces drawn at 50 % probability. Solvent molecules are shown and hydrogen atoms have been removed for clarity.

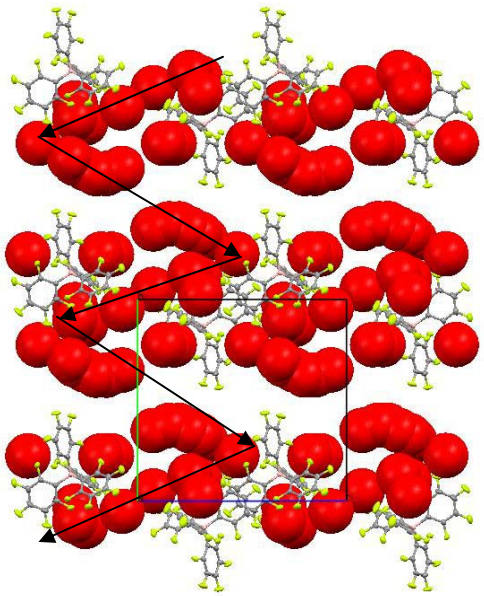

Figure 11. Layer 1 as viewed down the *a* axis. Regions of void space are represented by red spheres and appear as a disconnected channel snaking through the crystal. The breaks in the channel can clearly be seen. Arrows denote the flow of the channel on the left side of the diagram

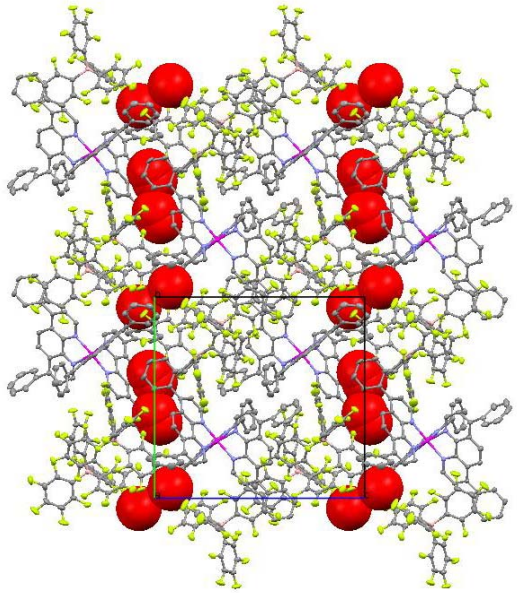

Figure 12. Layer 2 as viewed down the *a* axis. Regions of void space are represented by red spheres and appear as isolated pockets that do not connect to the voids of layer 1.

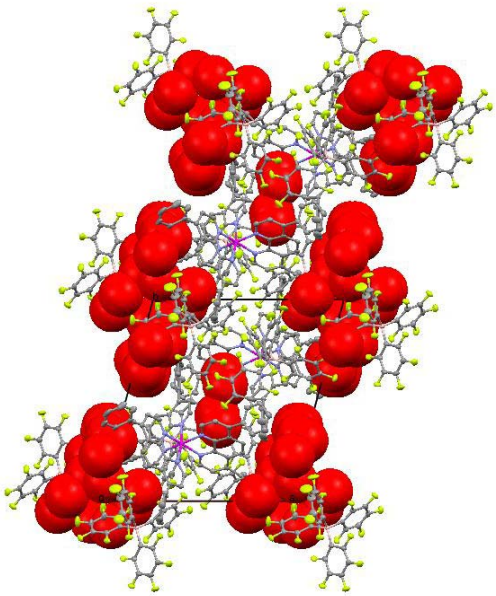

Figure 13. The alternating orientation of layers 1 and 2 is shown as viewed *c* axis. Layer 1 appears more disconnected in this structure than it has previously. Layer 2 is in the middle of the figure and contains only small void pockets.

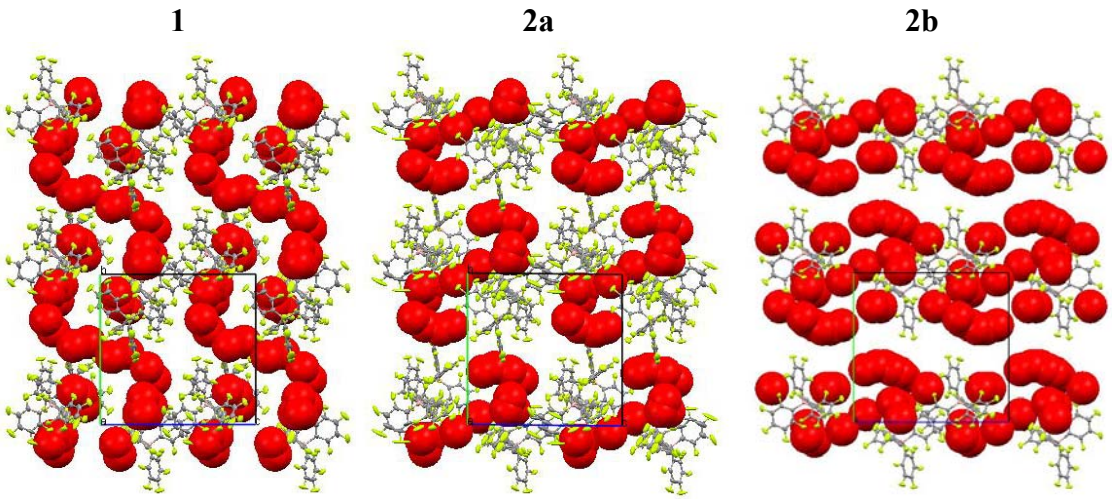

Figure 14. Layer 1 of all three structures is shown side by side for comparison.

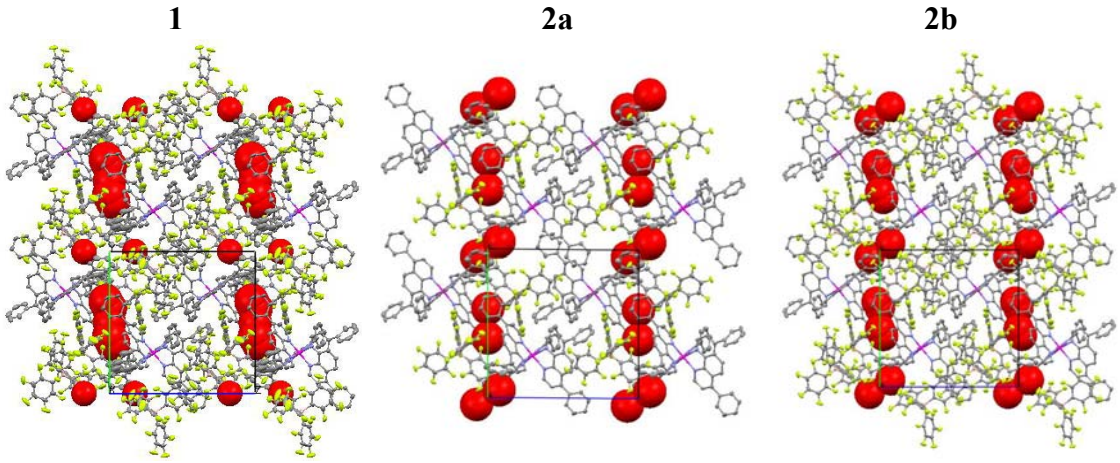

Figure 15. Layer 2 of all three structures is shown side by side for comparison.

*Photophysical Characterization of **1***

The emission of **1** was collected using material recrystallized from acetonitrile (Figure 16). The K_{SV} data give an initial K_{SV} of 25.57 that decreases slightly to 22.7 over the course of the 6 hour data collection (Figure 17). The resulting Stern-Volmer plots are linear, but both the emission intensity under nitrogen and sensitivity of the sample degrades under LED illumination. In order to determine if a loss of solvent could account for the change in sensitivity, a second data collection was performed using the sample previously tested. If solvent is being lost, the K_{SV} parameter should begin to stabilize. However, the K_{SV} again decreased from the initial value of 24.6 to 21.9 over 6 hours. The plots remain linear, but the emission intensity under nitrogen and sensitivity continue to decrease, suggesting solvent loss is not the cause of the instability. It is more likely that the compound is degrading with time.

Such a large K_{SV} was predicted based on the previously determined relationship between fraction of void space within the crystal lattice and the fraction of emission quenched under air.[17] Fraction of emission quenched is defined in Equation 2.

$$\frac{(I_0 - I)}{I_0} \qquad \textbf{(2)}$$

As this ruthenium compound has the largest amount of void space, it should also quench a larger fraction of the emission under air, resulting in a large K_{SV}. This relationship is illustrated in Figure 18.

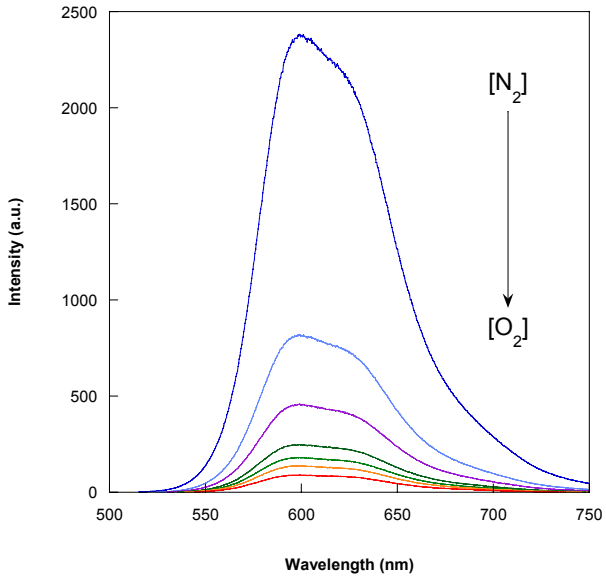

Figure 16. Emission profile of **1** collected using a 405 nm LED excitation source. Spectra under select concentrations of oxygen are shown. This sensing behavior is reversible upon returning the sample environment to pure nitrogen.

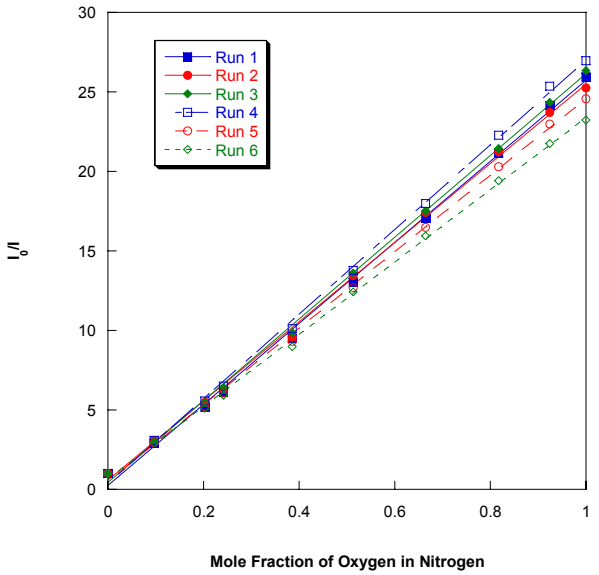

Figure 17. Stern-Volmer plots generated for the first run of a recrystallized sample of **1** using a 405 nm LED excitation source.

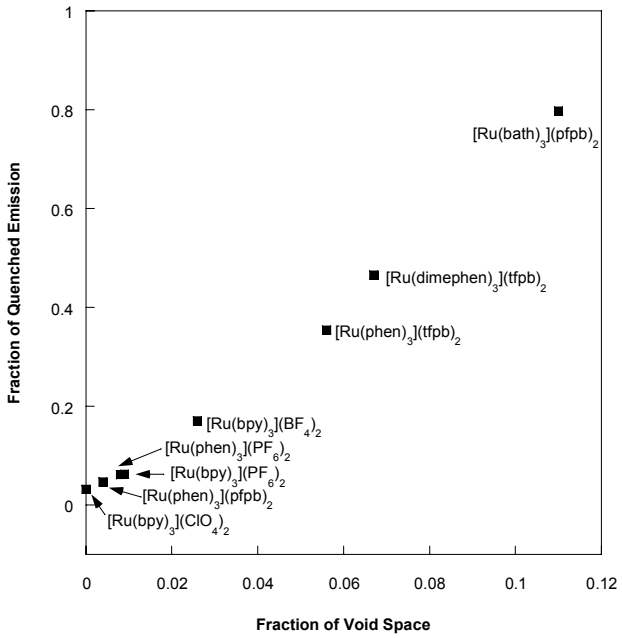

Figure 18. When the data from this study is combined with that from previous study, the relationship between fraction of emission quenched under air versus fraction of void space within the crystalline lattice is still valid.[17]

The lifetime of the recrystallized material was determined and found to be biexponential. The weighted average lifetime for **1** is 4.67(5) μs under nitrogen, 0.96(3) μs under air, and 0.31(2) μs under oxygen. The K_{SV} calculated from the lifetime data is 13.7. This calculated K_{SV} value is lower than that determined from the emission data of 25.57. As a result, the quenching mechanism for **1** must involve both dynamic and static quenching.

During the course of the lifetime determination, the lifetime under nitrogen was found to decrease slightly with exposure to the LED light source. An additional study was then performed to see if the decrease in the lifetime could be mitigated through stirring the sample on the surface. When stirred, the surface of the sample is refreshed and any damaged or degraded material is mixed back into the bulk of the sample and fresh material is moved to the surface. Before the sample was refreshed, the weighted lifetime was 4.11(2) μs under nitrogen. The sample was stirred and the weighted lifetime returned to a value of 4.5(3) μs. This process was repeated and a weighted lifetime of 4.67(5) μs was obtained. The results of this study indicate that the degradation observed during the lifetime study can be reversed through surface refreshing.

*Photophysical Characterization of **2***

The emission profile of the free ligand was collected under nitrogen using both a 405 nm LED and 350 nm LED excitation source (Figure 19). The emission of the free ligand is weak, but the peak shape of the emission does change with the excitation source. The emission is more structured when the higher energy 350 nm LED is used for excitation.

When determining which LED source was appropriate to use as the excitation source for **2**, an interesting phenomenon was observed. When a 405 nm LED was used as the excitation source, the spectra of **2** contained two broad peaks centered at 491 nm and 570 nm. This emission is weak and not sensitive to changes in oxygen concentration (Figure 20). When the excitation source was changed to a 350 nm LED, the emission becomes more structured, intense, and is blue shifted, centered at approximately 411 nm (Figure 21). One intense peak can be seen at 391 nm that contains shoulders at approximately 411 nm and 481 nm. The emission is similar to the emission of the free ligand in both energy and shape. This transition is sensitive to changes in oxygen concentration. This emission is most likely due to the π to π^* transition of the bath ligand. A comparison of the two emission profiles is shown in Figure 22. The differences in the structure and intensity of the emission are clearly seen.

The same shift in emission when the excitation source is changed from 350 nm to 405 nm is seen with $[Zn(phen)_3](tfpb)_2$ and $[Zn(dimephen)_3](tfpb)_2$ where dimephen = 4,7-dimethyl-1,10-phenanthroline. The spectra of the three zinc compounds and the free bath ligand all have the same relative emission peak shape when the same excitation source is used (Figures 23 and 24). However, with $[Zn(phen)_3](tfpb)_2$, the opposite sensing behavior to that of **2** is observed as the lower energy state is oxygen sensitive and the higher energy state is not.

Attempts to elucidate the structure of the emission bands of **2** at lower temperatures were made at both liquid nitrogen and liquid helium temperatures using a 405 nm and 375 nm LED. However, the emission intensity of the complex at these temperatures was not large enough to obtain resolvable emission profiles. The lower

wavelength LEDs were not used due to concerns regarding burning out these expensive LEDs at the larger operating voltages required for this experiment.

In order to explore the effect of the ligand on the emission of the resulting zinc(II) compound, $[Zn(dpbpy)_3](pfpb)_2$ (dpbpy = 4,4'-diphenyl-2,2'-bipyridine) was synthesized and the reaction powder excited with the 350 nm LED. The emission of the bipyridine compound is located at a similar energy to the emission of the phen based compound, but the emission peak shape has become less structured (Figure 25). The change in emission can only be due to the change in the ligand set. The high energy of the emission for both compounds again suggest that the emission is from the ligand based π to π^* transition.

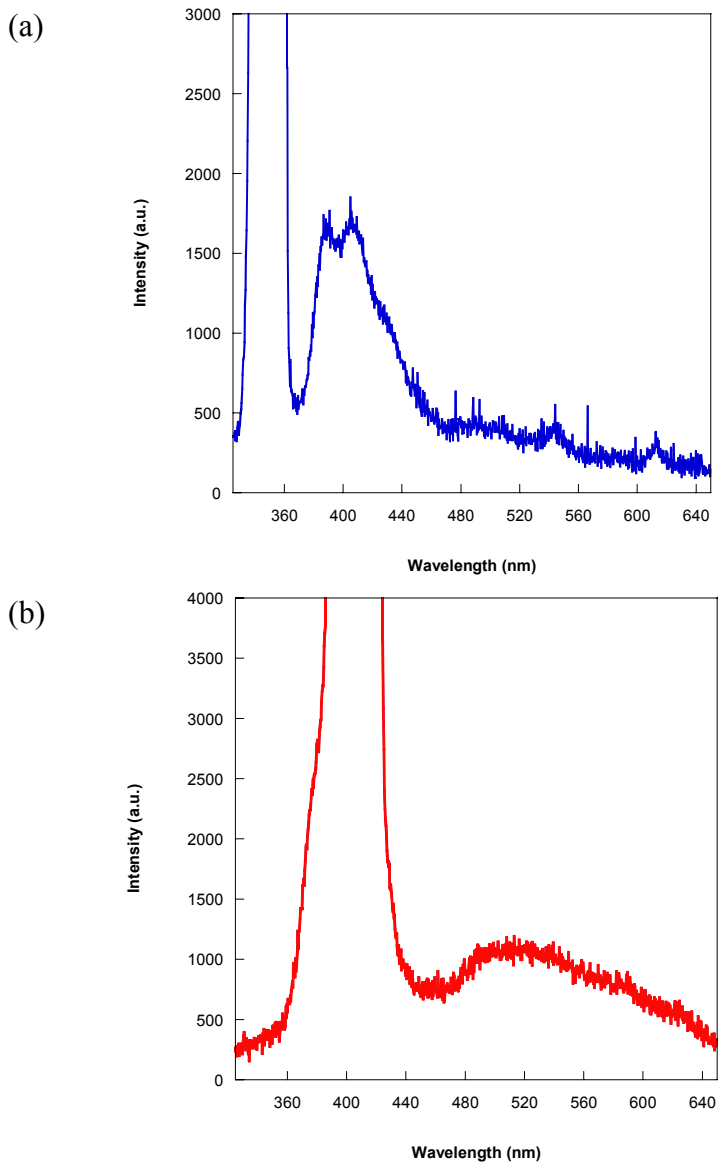

Figure 19. The emission profile of the free bath ligand when a 350 nm LED (a) and a 405 nm LED (b) excitation source is used.

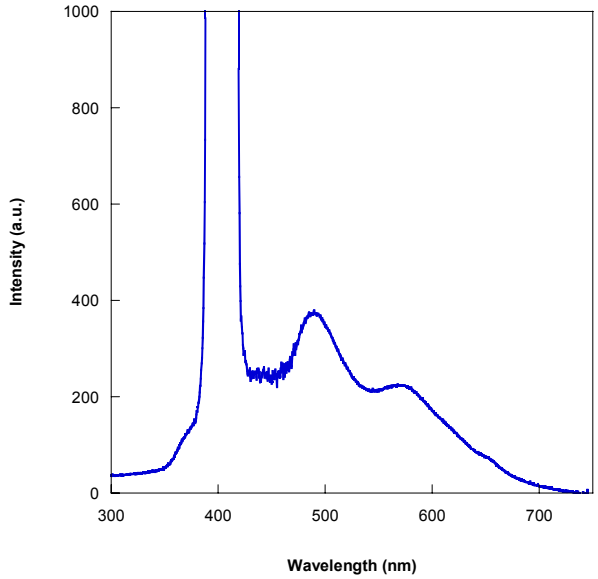

Figure 20. Emission profile of **2** using a 405 nm LED excitation source. The LED is off scale indicating the emission from the complex is weak.

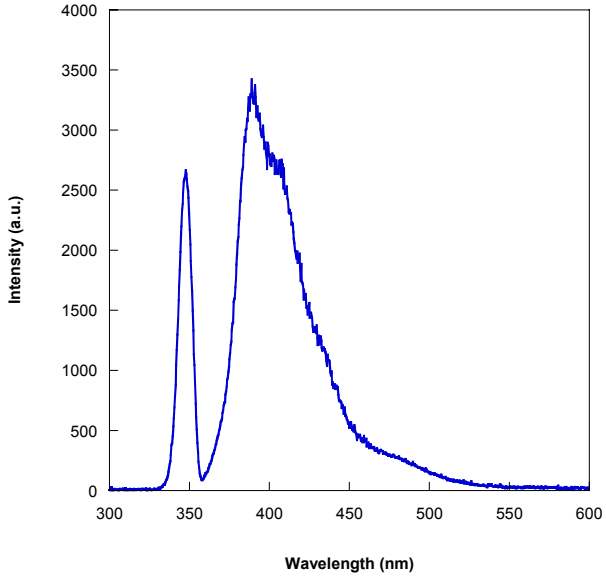

Figure 21. Emission profile of **2** using a 350 nm LED excitation source. The emission from the complex using this excitation source is more intense than that observed using the 405 nm LED.

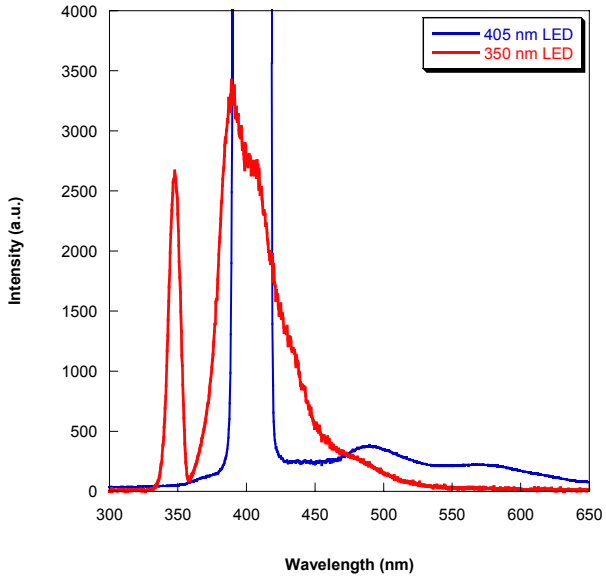

Figure 22. Overlaid plot of the emission from **2** using the 405 nm LED (blue) and 350 nm LED (red).

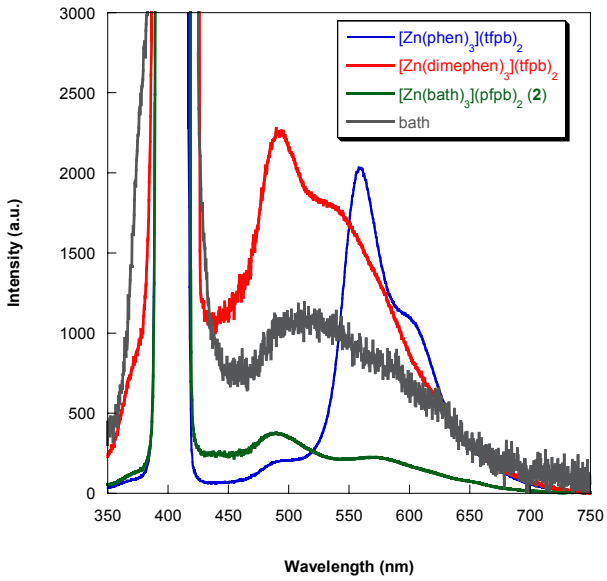

Figure 23. The emission spectra of various Zn(II) complexes and bath taken under nitrogen with a 405 nm LED excitation source. The intensity of the bath spectrum was multiplied by 200 to bring it on scale with the other complexes.

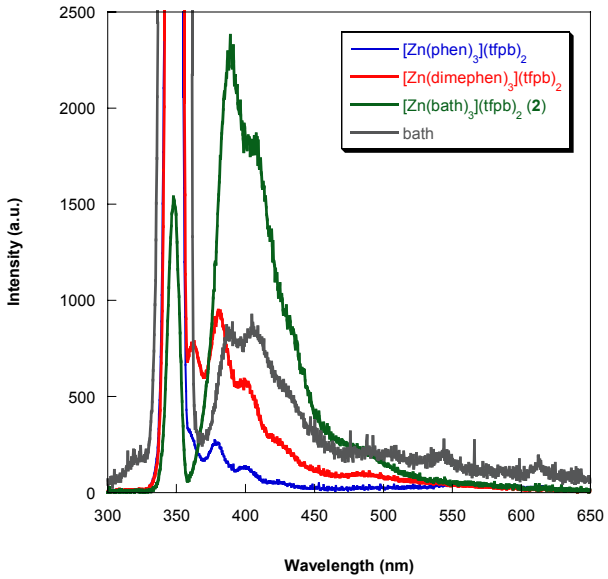

Figure 24. The emission spectra of various Zn(II) complexes and bath taken under nitrogen with a 350 nm LED. The intensity values of the original bath spectrum were multiplied by 50 to bring them on scale with the compounds.

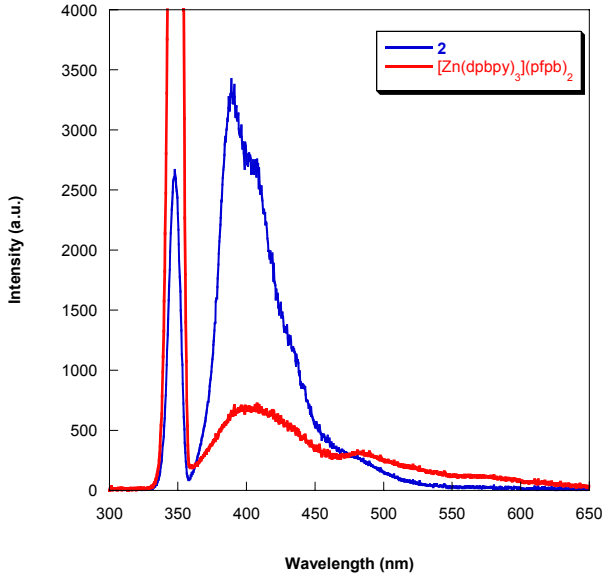

Figure 25. The emission profile of **2** (blue) and Zn(dpbpy-bpy)$_3$](pfpb)$_2$ (red) for comparison.

Several samples of **2a** were tested for oxygen sensitivity using a 350 nm LED as the excitation source. The Stern-Volmer constants ranged from 2.3(5) to 5.9(2). Those samples with lower K_{SV}'s exhibited slightly curved Stern-Volmer plots (Figure 26). The data were further analyzed using a two-site model to determine if multiple components could account for this curvature. This model has been previously described and will briefly be described herein.[15] Curved Stern-Volmer plots can be fit to a two-site model according to Equation 3 where I_0 is the integrated emission intensity with no quencher present, I is the integrated emission intensity with a given concentration of oxygen present, f is the fractional contribution to the unquenched emission where $f_1 + f_2 = 1$. The different Stern-Volmer quenching constants are given as K_{SV1} and K_{SV2} and $[O_2]$ is the concentration of oxygen under which I was determined.

$$\frac{I_0}{I} = \frac{1}{\frac{f_1}{1+K_{SV1}[O_2]} + \frac{f_2}{1+K_{SV2}[O_2]}} \qquad \textbf{(3)}$$

The data collected during the sensing experiments was fit to this two-site model using Microsoft Excel to give the resulting K_{SV1}, K_{SV2}, f_1, and f_2 parameters. The analysis indicated two K_{SV}'s can be used to describe the data and are equal to 4.26(7) and 0.03(4) with the larger constant accounting for 91 % of the data. Based on the inconsistent sensing and need for two components to explain the data, crystals of **2** grown from dichloromethane do not appear viable options for oxygen sensing devices and were consequently not studied further.

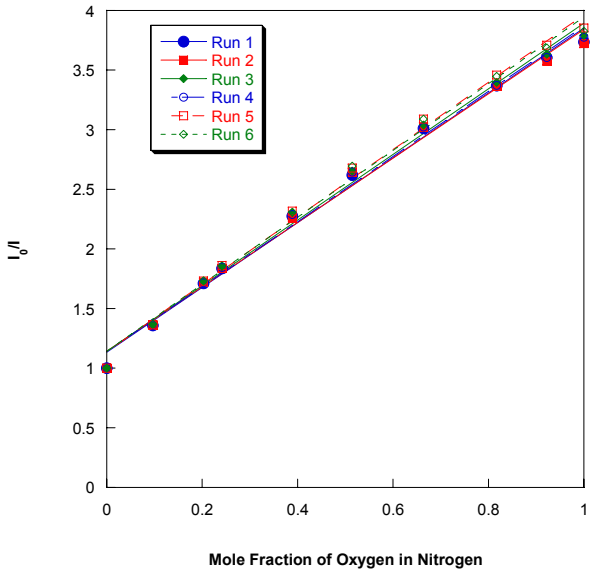

Figure 26. Stern-Volmer plot for **2a** is shown. The data was fit to a linear regression model, but clearly the data is curved. The data was fit with a two-site model to more accurately represent the sensing behavior of the material.

Several different studies were conducted using crystals of **2b** which were harvested from the mother liquor after various amounts of time. This study was performed to determine if the amount of time between when the crystals form and when the samples are prepared affects sensing ability of the material. The first sample was prepared immediately after crystallization, meaning crystals were collected from the mother liquor, was tested first. The sample was prepared by crushing the crystals into the depression of the aluminum rod. The emission profile can be seen in Figure 27. During the first phase of testing, a steady increase of the K_{SV} was observed over approximately 25 hours. This increase in the K_{SV} parameter is due to the proposed loss of the acetonitrile solvent molecules found in the crystal lattice. After the solvent loss, the sample gives an average K_{SV} of 8.5(2). For the remainder of the experiment, the K_{SV} is remains stable, exhibiting only 0.22 % change in sensitivity over a period of 115 hours. These two distinct processes can be seen in Figure 28.

When compared to two platinum based polymeric materials, **2b** shows greater stability as its K_{SV} changes 0.04 % per day where sensing materials made from platinum tetrakis-(pentafluorophenyl)porphyrin embedded into polystyrene change 9.2 % per day and 0.5 % per day when embedded into polytrifluoroethylmethacrylate.[55] The stability of **2b** is a significant improvement over these polymer supported oxygen sensing materials.

A second sample was prepared after the crystals were immersed in the mother liquor for approximately 2 months. These crushed crystals had a K_{SV} of 6.2(2), again after an initial period of increasing sensitivity. A third sample was prepared several months after the mother liquor had evaporated. This sample of **2b** also exhibited the same initial growth of the K_{SV} followed by a period of stabilization.

A final study was performed with crystals harvested after complete evaporation of the mother liquor. The K_{SV} parameters were 3.53(9) and 4.7(1) for two separate samples, much lower than the value observed for the materials allowed to sit in the mother liquor for two months.

The comparison of these studies where the time in the mother liquor varied suggest that crystals harvested from the mother liquor are more sensitive to changes in oxygen concentration than those allowed to dry out over a period of time. One possible explanation is that nature tends to favor crystalline lattices that are packed efficiently. As the crystals sit for an extended period of time in the acetonitrile, the lattice could be constantly changing. The lattice of the crystals is shifting in an attempt to generate smaller and smaller amounts of void space. If less void space is present in the crystalline material, the sensing ability of the compound should also decrease. When fresh crystals are tested, the solvent is quickly removed by the gas flow and the lattice does not have the opportunity to rearrange, leaving the void space intact. As a result, the crystals should be used immediately after crystallization from acetonitrile to obtain the best sensitivity.

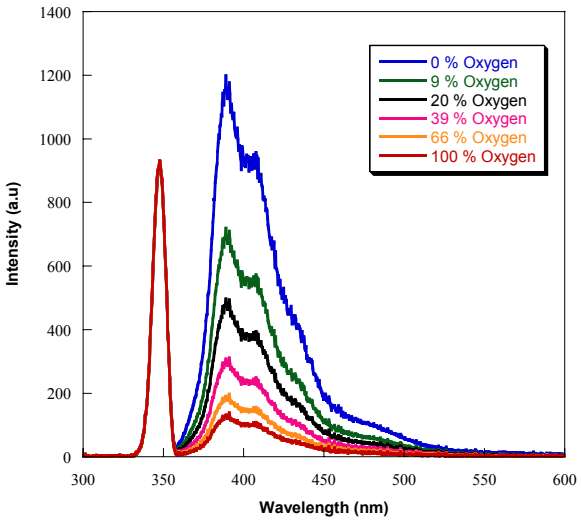

Figure 27. Emission profile of crushed acetonitrile crystals of **2b** under different concentrations of oxygen. The LED peak is also shown centered at approximately 350 nm.

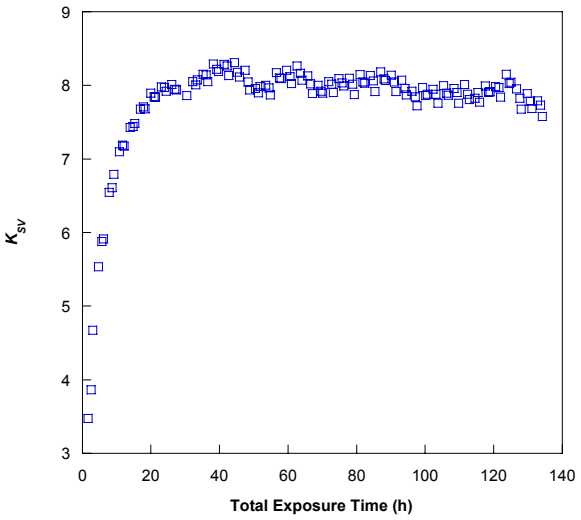

Figure 28. A long term study of a sample of **2b** crystals taken directly from the mother liquor. The Stern-Volmer constant initially increases then stabilizes to approximately 8.5.

A sample of solid precipitated from the acetonitrile reaction mixture with water was tested without further crystallization with the idea that using this material could lessen the number of steps in the process of obtaining a reliable sensor. However, the sensitivity of the reaction material was dependent on the batch from which the material was obtained. Samples of reaction material from two different syntheses had K_{SV} parameters ranging from 6.91(7) to 7.55(7) indicating that the crystallization step cannot be skipped in order to obtain reliable sensing behavior. A representative data collection is shown in Figure 29.

Previously, our group has had success with casting films of a sensing material onto the top of the rods used in the swage cross-tube apparatus. When films of **2** are cast with acetonitrile directly onto the aluminum rod, the spectral results are not similar to those obtained for acetonitrile crystals. Samples cast from acetonitrile exhibit a different emission peak shape, are red shifted from that of **2b**, and are not sensitive to oxygen. This change in emission profile and sensing ability is most likely due to the fluxional nature of the zinc metal center. When quickly redissolved, it is hypothesized that the bath ligands come off of the metal center, resulting in a different zinc(II) complex and free ligand. This hypothesis is supported by the similar shape of the film's emission to the emission of the free ligand (Figure 30).

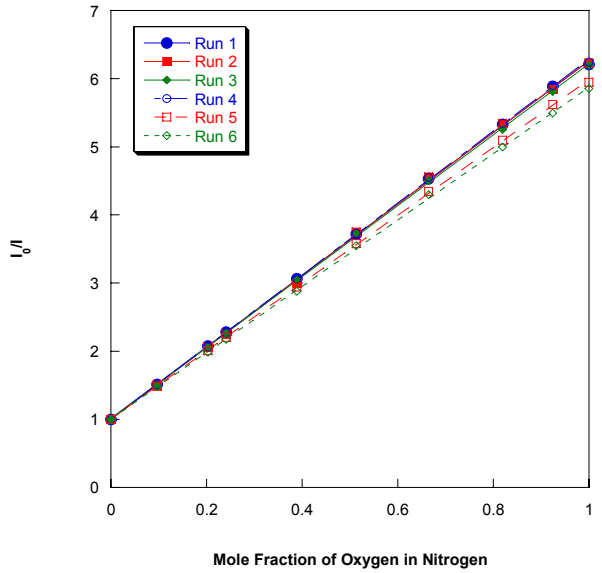

Figure 29. Stern-Volmer plot obtained for a sample of reaction powder of **2** precipitated from acetonitrile with water.

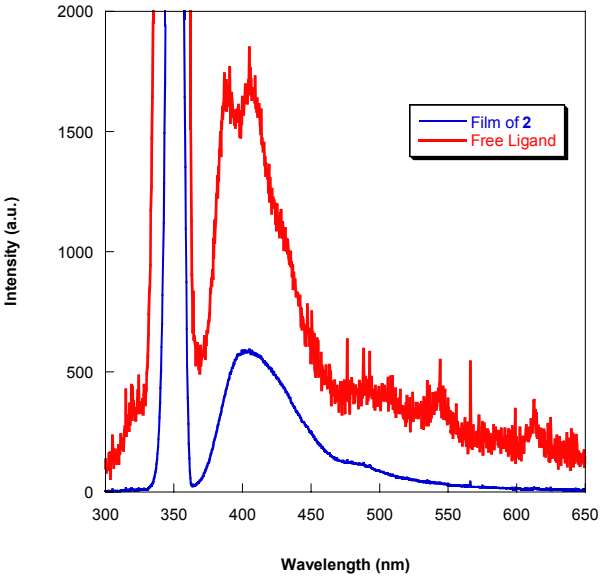

Figure 30. Emission profile of a film of **2** (blue) overlaid with the spectrum of free ligand (red). The spectrum of the free ligand was increased by a factor of 100 to bring it on scale with that of the film of **2**.

The relationship between fraction of void space within the crystalline lattice and the fraction of quenched emission under air for the family of $[Zn(phen)_3]^{2+}$ compounds is similar to that for the analogous family of ruthenium compounds. While not as many structures have been obtained, the overall trend is still apparent (Figure 31).

Lifetime measurements for **2b** were attempted. However, the lifetime of the complex was too close to the detection limit of our instrumentation (approximately 7 nanoseconds) and could not be accurately obtained.

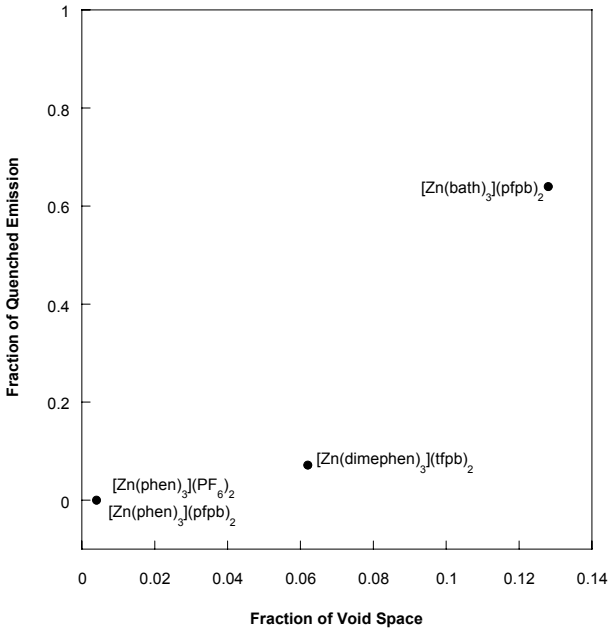

Figure 31. The Zn(II) complexes appear to follow a similar trend as the Ru complexes with regards to the amount of void space present in the crystal lattice and the sensitivity of the compound.

Pressure Jump Results

To determine the response time of the sample, a pressure jump experiment was performed. Because this experiment used a film of the **2** cast onto the top of a rod, and it has been shown that this alters the photophysical characteristics of the material, caution should be used when generalizing this data. Correlation between this data and the sensing ability of **2b** should be done carefully. The film of **2** shows 95 % return in 2.2(1) seconds with 50 % return occurring after 0.44(8) seconds. Representative data are shown below in Figure 32.

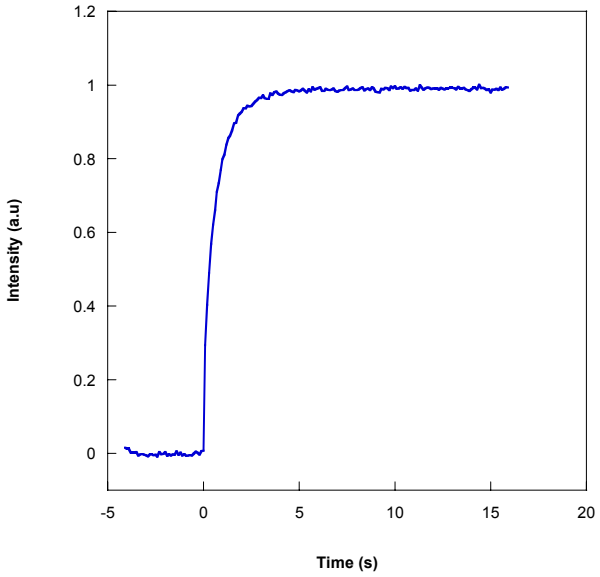

Figure 32. Representative plots of the response curves for a film of **2**. Excitation was performed with a 365 nm LED.

Comparison of the Sensing Mechanisms

There are three characteristics that can be used to compare a sensing material: lifetime, concentration of oxygen within the material, and the mobility of oxygen through the material. When only dynamic quenching is present in the material, the K_{SV} obtained from emission intensity and lifetime data is identical. When the K_{SV} obtained from lifetime data is smaller than the K_{SV} obtained from intensity data, static quenching must also be present in the material. For the ruthenium complex, a mixture of dynamic and static quenching is present in the material since the K_{SV} determined with lifetime measurements is lower than that obtained from emission intensity data. The static quenching is the result of the oxygen molecules being in close proximity to the excited state ruthenium complex which does not require the ruthenium to have a long lifetime. The dynamic quenching event occurs as a result of the long lifetime of the complex, as a given oxygen molecule now has the time to move through the material to reach an excited state ruthenium complex.

When we try to determine the quenching mechanism for the zinc compound we must again take into account the three components. We know that the ability of oxygen to move through the material must be the same as that for the ruthenium complex since their structures are nearly identical. If we also assume that the amount of oxygen within the material is the same, then the only characteristic that can contribute to the difference in sensing ability is the lifetime. The lifetime for the zinc complex is shorter than we are able to measure at this time (less than 6 ns), leading us to believe that static quenching is a viable route to explain the sensing behavior of the compound. Lifetime measurements can only provide direct information about dynamic quenching. Since the lifetime of the

zinc complex is extremely short, we can assume that no dynamic quenching is present in the compound. The oxygen simply does not have the time to move through the void space channels to reach an excited state zinc complex. As a result, the emission of an excited state can only be quenched by an oxygen molecule in close proximity.

The difference in the sensing mechanism between the two complexes is most likely the main reason why the sensitivity of the ruthenium complexes is approximately 3 times greater than that of the zinc complex. The ruthenium complex is able to undergo dynamic quenching due to its longer lifetime, making the material a better oxygen sensor. However, the ability of this zinc compound to sense oxygen with a K_{SV} greater than 5 and the stable nature of the sensing ability of **2b** make the compound in this form a promising oxygen sensor. A change in the ligand set would prove advantageous here as the ligand could be designed to shift the resulting emission into the red, eliminating the need for a high energy LED. If the lifetime was also increased, the sensing ability may improve due to the increased probability of involving a dynamic quenching mechanism.

Conclusions

We have shown that solid state samples of $[Ru(bath)_3](pfpb)_2$ and $[Zn(bath)_3](pfpb)_2$ crystallize with similar amounts and morphologies of void space. As a result, oxygen can move through the lattice more easily to quench excited state emission. The previously determined relationship between fraction of void space and fraction of emission quenched was further supported through the analysis of the ruthenium and zinc structures.

Problems arose with determining the lifetime of the zinc compound as it was too close to the detection limit of our instrumentation. The short lifetime suggests that the event responsible for emission quenching is likely a static quenching process. The ruthenium compound possesses a long lifetime, but this lifetime is less sensitive to oxygen than the emission intensity. As a result, the quenching event is attributed to both dynamic and static quenching processes.

While the ruthenium complex is more sensitive toward changes in oxygen concentration, it suffers from emission intensity degradation as observed during the lifetime determination. This degradation was mitigated through surface refreshing, but the need to consistently refresh the sample surface may limit the practical applications for devices made from this material. The zinc compound is an example of a viable, earth abundant alternative. The K_{SV} of approximately 8 coupled with the long term stability of the material increases the number of applications where this material could be used.

References

1. Collier, B. B.; Singh, S.; McShane, M. *Analyst* **2011**, *136*, 962.

2. Demas, J. N.; DeGraff, B. A. *J. Chem. Educ.* **1997**, *74*, 690.

3. Demas, J. N.; DeGraff, B. A.; Coleman, P. B. *Anal. Chem.* **1999**, *71*, 793A.

4. DeRosa, M. C.; Hodgson, D. J.; Enright, G. D.; Dawson, B.; Evans, C. E. B.; Crutchley, R. J. *J. Am. Chem. Soc.* **2004**, *126*, 7619.

5. Gouterman, M. *J. Chem. Educ.* **1997**, *74*, 697.

6. Mills, A. *Platinum Met. Rev.* **1997**, *41*, 115.

7. Mills, A. *Chem. Soc. Rev.* **2005**, *34*, 1003.

8. Trettnak, W.; Gruber, W.; Reininger, F.; Klimant, I. *Sens. Actuators, B* **1995**, *B29*, 219.

9. Yan, H.; Lu, J. *Sens. Actuators* **1989**, *19*, 33.

10. Wang, X.-d.; Chen, X.; Xie, Z.-x.; Wang, X.-r. *Angew. Chem. Int. Edit.* **2008**, *47*.

11. Choi, M. M. F.; Xiao, D. *Anal. Chim. Acta* **2000**, *403*, 57.

12. McFarland, S. A.; Lee, F. S.; Cheng, K. A. W. Y.; Cozens, F. L.; Schepp, N. P. *J. Am. Chem. Soc.* **2005**, *127*, 7065.

13. Meier, B.; Werner, T.; Klimant, I.; Wolfbeis, O. S. *Sens. Actuators, B* **1995**, *29*, 240.

14. Mulazzani, Q. G.; Sun, H.; Hoffman, M. Z.; Ford, W. E.; Rodgers, M. A. J. *J. Phys. Chem.* **1994**, *98*, 1145.

15. McGee, K. A.; Mann, K. R. *J. Am. Chem. Soc.* **2009**, *131*, 1896.

16. McGee, K. A.; Marquardt, B. J.; Mann, K. R. *Inorg. Chem.* **2008**, *47*, 9143.

17. McGee, K. A.; Veltkamp, D. J.; Marquardt, B. J.; Mann, K. R. *J. Am. Chem. Soc.* **2007**, *129*, 15092.

18. Zaharieva, J.; Milanova, M.; Todorovsky, D. *J. Optoelectron. Adv. Mater.* **2011**, *13*, 727.

19. Kim, H. J.; Jeong, Y. C.; Rhee, J. I. *Talanta* **2008**, *76*, 1070.

20. Campagna, S.; Puntoriero, F.; Nastasi, F.; Bergamini, G.; Balzani, V. *Top. Curr. Chem.* **2007**, *280*, 117.

21. Estella, J.; Wencel, D.; Moore, J. P.; Sourdaine, M.; McDonagh, C. *Anal. Chim. Acta*, *666*, 83.

22. Barbieri, A.; Accorsi, G.; Armaroli, N. *Chem. Commun.* **2008**, 2185.

23. Zheng, K.; Liu, X.; Deng, H.; Chao, H.; Yun, F.; Ji, L. *J. Mol. Struct.: THEOCHEM* **2003**, *626*, 295.

24. Accorsi, G.; Listorti, A.; Yoosaf, K.; Armaroli, N. *Chem. Soc. Rev.* **2009**, *38*, 1690.

25. Li, X.; Zhu, D.; Gao, W.; Zhang, Y.; Mu, Y. *J. Chem. Res.* **2006**, 371.

26. Liu, Q.-D.; Wang, R.; Wang, S. *Dalton Trans.* **2004**, 2073.

27. Senoue, M.; Iwaki, T.; Seki, K.; Yagi, M. *J. Photochem. Photobiol., A* **1996**, *101*, 257.

28. Kimachi, S.; Ikeda, S.; Miki, H.; Azumi, T.; Crosby, G. A. *Coord. Chem. Rev.* **1994**, *132*, 43.

29. Mikata, Y.; Yamashita, A.; Kawamura, A.; Konno, H.; Miyamoto, Y.; Tamotsu, S. *Dalton Trans.* **2009**, 3800.

30. Xu, H.; Xu, Z.-F.; Yue, Z.-Y.; Yan, P.-F.; Wang, B.; Jia, L.-W.; Li, G.-M.; Sun, W.-B.; Zhang, J.-W. *J. Phys. Chem. C* **2008**, *112*, 15517.

31. Consiglio, G.; Failla, S.; Oliveri, I. P.; Purrello, R.; Di, B. S. *Dalton Trans.* **2009**, 10426.

32. Benniston, A. C.; Harriman, A.; Lawrie, D. J.; Mayeux, A. *Phys. Chem. Chem. Phys,* **2004**, *6*, 51.

33. Rabold, G. P.; Piette, L. H. *Spectrosc. Lett.* **1968**, *1*, 225.

34. Galardon, E.; Tomas, A.; Roussel, P.; Artaud, I. *Dalton Trans.* **2009**, 9126.

35. Mahato, P.; Ghosh, A.; Mishra, S. K.; Shrivastav, A.; Mishra, S.; Das, A. *Chem. Commun. (Cambridge, U. K.)* **2010**, *46*, 9134.

36. Galardon, E.; Tomas, A.; Roussel, P.; Artaud, I. *Dalton Trans.* **2009**, 9126.

37. Wild, A.; Winter, A.; Hager, M. D.; Schubert, U. S. *Chem. Commun.* **2012**, *48*, 964.

38. Mameli, M.; Aragoni, M. C.; Arca, M.; Atzori, M.; Bencini, A.; Bazzicalupi, C.; Blake, A. J.; Caltagirone, C.; Devillanova, F. A.; Garau, A.; Hursthouse, M. B.; Isaia, F.; Lippolis, V.; Valtancoli, B. *Inorg. Chem. (Washington, DC, U. S.)* **2009**, *48*, 9236.

39. Yeh, A.; Chen, T.-R. *Mater. Lett.* **2005**, *59*, 2911.

40. Mikata, Y.; Wakamatsu, M.; Kawamura, A.; Yamanaka, N.; Yano, S.; Odani, A.; Morihiro, K.; Tamotsu, S. *Inorg. Chem.* **2006**, *45*, 9262.

41. Tan, R.; Wang, Z.-B.; Li, Y.; Kozera, D. J.; Lu, Z.-H.; Song, D. *Inorg. Chem.*, *51*, 7039.

42. Zhou, X.; Jin, X.; Li, D.; Wu, X. *Chem. Commun.* **2011**, *47*, 3921.

43. Liang, L. J.; Zhao, X. J.; Huang, C. Z. *Analyst* **2012**, *137*, 953.

44. Ma, Z.; Cao, Y.; Li, Q.; Guedes da Silva, M. F. t. C.; FraÃºsto da Silva, J. o. J. R.; Pombeiro, A. J. L. *J. Inorg. Biochem.* **2010**, *104*, 704.

45. Exstrom, C. L.; Britton, D.; Mann, K. R.; Hill, M. G.; Miskowski, V. M.; Schaefer, W. P.; Gray, H. B.; Lamanna, W. M. *Inorg. Chem.* **1996**, *35*, 549.

46. Bruker, **2003**, *SMART and SAINT*, Madison, Wisconsin, USA.

47. Blessing, R. H. *Acta Cryst. A* **1995**, *A51*, 33.

48. Sheldrick, G. M., **2008**, *SADABS*, University of Gottingen, Germany.

49. Sheldrick, G. M. *Acta Cryst. A* **2008**, *A64*, 112.

50. Spek, A. L., **2005**, *PLATON, A Multipurpose Crystallographic Tool*, Utrecht University, Utrecht, The Netherlands.

51. Spek, A. L. *Acta Cryst. D* **2009**, *D65*, 148.

52. Bruno, I. J.; Cole, J. C.; Edgington, P. R.; Kessler, M.; Macrae, C. F.; McCabe, P.; Pearson, J.; Taylor, R. *Acta Cryst. B* **2002**, *B58*, 389.

53. Smith, C. S.; Branham, C. W.; Marquardt, B. J.; Mann, K. R. *J. Am. Chem. Soc.* **2010**, *132*, 14079.

54. Smith, C. S.; Mann, K. R. *Chem. Mater.* **2009**, *21*, 5042.

55. Amao, Y.; Miyashita, T.; Okura, I. *J. Fluorine Chem.* **2001**, *107*, 101.

Chapter Five

Tricationic Ir(III) Terpyridine Complexes for the Detection of Oxygen

Reproduced in part with permission of the International Union of Crystallography from Acta Crystallographica C, **2010**, *C66*, m62.

Overview

In order to obtain a tricationic species, the synthesis of a family of Ir(III) *bis*-terpyridine complexes was attempted. Several complications arose during the synthesis of these materials including mixtures of products and low yields. After the compound was obtained, sensing experiments were performed and results indicate this family of compounds are poor oxygen sensors and unstable to LED illumination. However, four crystal structures of iridium tol-terpyridine complexes were obtained, increasing the number of known iridium terpyridine single crystal X-ray diffraction structures by more than 50 %. The first structure containing trichlorido(4'-(*p*-tolyl)-2,2':6',2''-terpyridine) iridium(III) as a dimethyl sulfoxide solvate is presented, along with a higher symmetry setting of the previously reported *bis*[(4'-(*p*-tolyl)-2,2':6',2''-terpyridine)]iridium(III) tris(hexafluorophosphate) acetonitrile disolvate and the unreported structures of the acetone and methanol solvates.[1] In our hands, no *bis*-terpy or *bis*-terpy* derivative has been isolated in appreciable amounts at this time.

Introduction

Iridium(III) complexes have been investigated for their use in several optical applications due to their desirable luminescent properties, including long excited state lifetimes and high quantum yields.[2-6] Applications in organic light emitting diodes (OLEDs) and light-emitting electrochemical cells (LECs) have received the most attention due to the increased efficiency of such devices caused by the singlet and triplet excited state mixing of iridium.[2,7-12] Tridentate ligands like terpyridine (terpy) have been used in many metal complexes. Terpy derivatives of ruthenium tend to have short lived

metal to ligand charge transfer (MLCT) states making them weak emitters, but when these ligands are bound to iridium, intense phosphorescence is observed. The lifetimes of these iridium complexes are on the order of microseconds, again due to the strong mixing of the singlet and triplet excited states of iridium.[13,14] *Bis*-terpy iridium complexes have already been used to model photochemical processes.[15-19] Based on these models and solution based luminescence measurements, the solid-state crystalline forms of such complexes may also exhibit several favorable luminescence characteristics.

For solid-state oxygen sensing applications, the solid-state forms of these compounds need to contain enough void space in the form of channels to allow oxygen to diffuse through the material and reach the excited state metal complex. The tricationic nature of these *bis*-terpy compounds would necessitate three counterions that could affect the crystalline packing. The use of three bulky tfpb$^-$ (where tfpb$^-$ = *tetrakis*[*bis*-3,5-trifluoromethyl(phenylborate)]) anions could facilitate inefficient packing within the crystal lattice to allow better oxygen diffusion throughout the material. Additionally, the fluorinated methyl groups will assist in increasing the solubility of oxygen within the material as carbon-fluorine bonds are oxophilic.[20-22] Making these structural changes should increase the likelihood of obtaining a large K_{SV} value resulting in an efficient luminescent and sensitive compound.

In order to investigate the solid state photophysical properties of these compounds, they first must be synthesized in good yield. Several syntheses of iridium(III) *bis*-terpy complexes have been reported with preparations ranging from stirring neat reactants at high temperatures for several hours to heating the reactants in a few milliliters of ethylene glycol for minutes.[14,19,23-28] These techniques often result in

reported yields of 25-45 % due in part to the inert nature of the iridium(III) core. A variety of synthetic techniques may be needed in order to obtain the amount of material desired. However, only a small amount of compound would be necessary to initially explore the solid-state photophysical and oxygen sensing properties.[14,19,23-28]

A family of *bis*-terpy Ir(III) compounds (Figure 1) was targeted. Several synthetic methods were employed and crystal structures obtained. At the start of this project, only 7 crystal structures were known of an iridium complex involving at least one terpyridine. Even if these compounds are not efficient oxygen sensors, a significant contribution to the crystallographic database will be made.

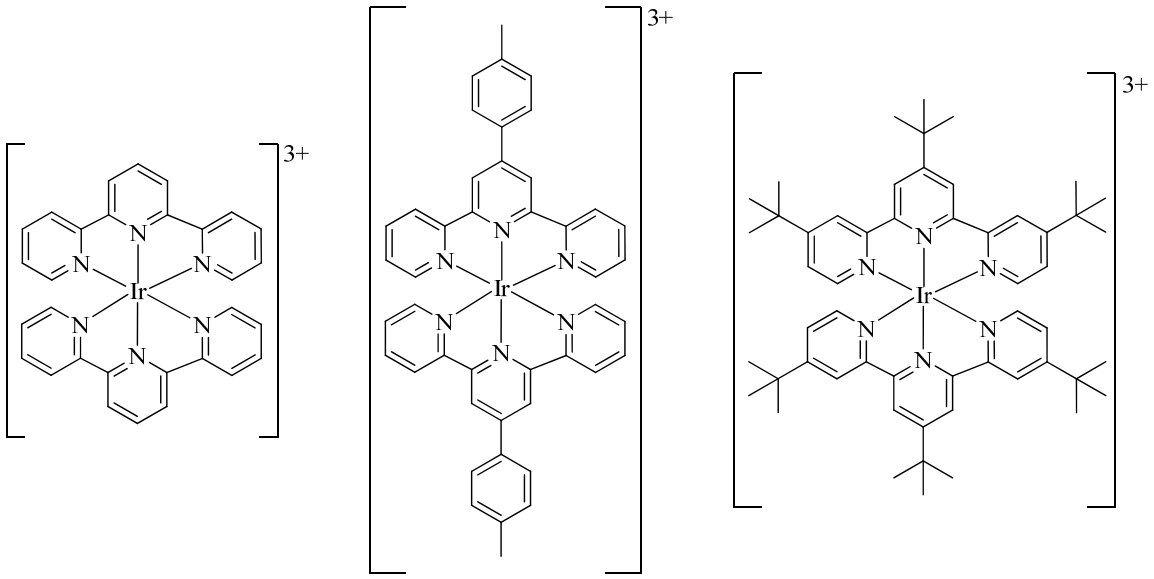

Figure 1. Terpy based synthetic targets from left to right: $Ir(terpy)_2^{3+}$, $Ir(tol\text{-}terpy)_2^{3+}$, $Ir(terpy\text{-}*)_2^{3+}$ (terpy-* = 4,4′,4″-tri-*tert*-butyl-2,2′:6′,2″terpyridine). Each cation was synthesized as a PF_6^- salt and metathesized to a $tfpb^-$ salt where possible.

Experimental

Note: Several attempts were made to synthesize the *bis*-terpy complexes and are described in detail in the Results and Discussion section. Below is the synthesis of the mono-tol-terpy derivative along with the syntheses that successfully resulted in the isolation of $[Ir(tol\text{-}terpy)_2]^{3+}$ compounds.

General Considerations for Synthesis. $IrCl_3 \bullet 3\ H_2O$ was purchased from Colonial Metals. The terpy derivatives 2,2′:6′,2″terpyridine (terpy) and 4′-tolyl-2,2′:6′,2″-terpyridine (tol-terpy) were purchased from Aldrich Chemical Co. along with sodium hexafluorophosphate ($NaPF_6$) and ammonium hexafluorophosphate (NH_4PF_6). All materials were used as received. Sodium *tetrakis*[*bis*-3,5-trifluoromethyl(phenylborate)] (Na(tfpb)) and 4,4′,4″-tri-*tert*-butyl-2,2′:6′,2″-terpyridine (terpy-*) were available from previous studies.[29] The solvents (acetonitrile, dichloromethane, diethyl ether, methanol, propylene carbonate, dimethylsulfoxide (DMSO), and ethylene glycol) were obtained from commercial sources and used without further purification.

A 300 MHz Varian Unity NMR spectrometer was utilized to obtain ^1H and ^{19}F NMR spectra. Chemical shifts are reported in units of ppm using an external reference to the residual proton resonance in deuterated dimethylsulfoxide, methanol, or acetonitrile for ^1H NMR spectra and the internal $CFCl_3$ reference for the ^{19}F NMR.

Ir(tol-terpy)Cl_3 (1)

To 15 mL of ethylene glycol was added 0.1509 g (0.4282 mmol) of $IrCl_3 \bullet 3\ H_2O$ and 0.1638 g (0.5065 mmol) of tol-terpy. This solution was refluxed in the dark and under nitrogen for 23 minutes. After cooling to room temperature, the resulting red precipitate was collected via vacuum filtration. The precipitate was washed with ethanol, water, and diethylether to yield 0.1860 g (66 % yield) of a brick red solid. ^{1}H NMR (DMSO-d_6): δ 9.20 (m, 2 H), 9.08 (m, 2 H), 8.90 (m, 2 H), 8.29 (m, 2 H), 8.12 (m, 2 H), 7.97 (m, 2 H), 7.49 (m, 2 H). It should be noted that the low solubility of this compound made the collection of a ^{1}H NMR spectrum difficult. As a result, all peaks were broad but still shifted from the peaks of free ligand. The tolyl-CH_3 peak is hidden under the DMSO-d_6 reference peak, but this problem could not be avoided as DMSO was the only deuterated solvent in which the compound was soluble. These solubility issues have been previously reported.[25] X-ray quality crystals of this material (**1a**) were grown through the cooling of a saturated DMSO solution.

[Ir(tol-terpy)$_2$](PF_6)$_3$ (2)

Route 1: This synthesis follows a reported synthetic procedure.[25] To 10 mL of ethylene glyocol was added 0.1011 g (0.1625 mmol) of **1** and 0.0577 g (0.178 mmol) of tol-terpy. The solution was then refluxed under nitrogen for 21 hours. The reaction was then heated to 180 °C for 22 hours. After the solution was allowed to cool to room temperature, a solution of 0.0945 g (0.563 mmol) of $NaPF_6$ and 12 mL of distilled H_2O was added to the reaction mixture. The resulting material was precipitated with the addition of 10 mL of distilled H_2O and collected via filtration. The green solid was

washed with ether and a mass of 0.1541 g of crude product was collected. An attempt to purify this material by column chromatography was made. A column of neutral alumina was prepared and loaded with dichloromethane. The crude material was loaded on the column and eluted with a 10:1 mixture of dichloromethane and acetone. Several orange and red-orange fractions were collected and redissolved in acetonitrile as their initial color matched that reported for the intended compound. A single crystal formed in one of the red-orange fraction vials and was used for the structure determination of $[Ir(tol\text{-}terpy)_2](PF_6)_3 \bullet 2\ CH_3CN$ (**2a**). No NMR analysis of the pure compound was performed as this was the only fraction containing appreciable amounts of the pure material. The other orange and red fractions still contained complex mixtures of products.

Route 2: This synthesis follows a second, more recently reported, synthetic procedure.[30] To 12 mL of ethylene glycol, which had been purged with argon for half an hour, was added 0.0510 g (0.145 mmol) of $IrCl_3 \bullet 3\ H_2O$ and 0.0945 g (0.292= mmol) of tol-terpy. The reaction was headed to 100 °C and allowed to stir for 2.5 hours. After this time, the temperature was elevated to 195 °C and the reaction continued at this temperature for 1.5 additional hours. The yellow-brown solution was allowed to cool to room temperature. The reaction mixture was poured into 5 mL of a saturated, aqueous solution of NH_4PF_6. The resulting yellow precipitate was collected via vacuum filtration. In order to purify the material, it was redissolved in acetonitrile and precipitated with diethylether. A total mass of 0.0680 g (37 % yield) of a bright yellow solid was collected. ^1H NMR (CD_3OD): δ 9.40 (s, 4 H), 9.03 (d, 4 H, J = 7.5 Hz),

8.33 (t, 4 H, J = 8.1 Hz), 8.24 (d, 4 H, J = 8.4 Hz), 7.95 (d, 4 H, J = 5.4 Hz), 7.61 (m, 8 H), 2.58 (s, 6 H) ^{19}F NMR (CD_3OD): δ -73.97, -76.48 Two sets of X-ray quality crystals of this material were grown from acetone (**2b**) and methanol (**2c**).

[Ir(tol-terpy)$_2$](tfpb)$_3$ (3)

To 12 mL of ethylene glycol, which had been purged with argon for half an hour, was added 0.0499 g (0.142 mmol) of $IrCl_3$ • 3 H_2O and 0.0949 g (0.294 mmol) of tol-terpy. The reaction was heated to 100 °C and allowed to stir for 2.5 hours. After this time, the temperature was elevated to 195 °C and the reaction continued at this temperature for 1.5 additional hours. At this time, the yellow-brown solution was allowed to cool to room temperature. The reaction mixture was poured into 5 mL of an aqueous solution containing 0.500 g (0.564 mmol) of Na(tfpb). Approximately 1 mL of methanol was added to the aqueous solution of Na(tfpb) to aide the solubility of the fluorinated anion. The resulting sticky, brown yellow precipitate was collected via vacuum filtration and washed with copious amounts of water. A total mass of 0.0825 g (17 % yield) of a bright yellow solid was collected. ^{1}H NMR (CD_3CN): δ 9.06 (s, 4 H), 8.70 (d, 4 H, J = 8.1 Hz), 8.23 (t, 4 H, J = 9.0 Hz), 7.67 (m, 40 H), 7.48 (m, 8 H), 2.57 (s, 6 H) ^{19}F NMR (CD_3CN): δ -63.85 Several attempts to grow crystals of this material were made, but all attempts produced amorphous materials not suitable for x-ray crystallography.

X-ray Crystallography

Crystals of Ir(tol-tpy)Cl_3 • DMSO (**1a**) were grown from a hot solution of DMSO and data were collected at the APS synchrotron sector 15-ID-C at Argonne National Laboratory, due to the extremely small size of at least one of the crystal dimensions. All data for the structure determinations of [Ir(tol-terpy$_2$]$(PF_6)_3$ • 2 CH_3CN (**2a**), [Ir(tol-terpy$_2$]$(PF_6)_3$ • 2 $(CH_3)_2CO$ (**2b**), [Ir(tol-terpy$_2$]$(PF_6)_3$ • CH_3OH (**2c**) were collected at the X-ray Crystallographic Laboratory (Department of Chemistry, University of Minnesota). Crystals of **2** were grown by the slow evaporation of saturated acetonitrile, acetone, or methanol solutions. Single crystals were attached to glass fibers and mounted on a Bruker SMART or APEX II Platform CCD for data collection at 173 K using graphite monochromated MoKα radiation (λ = 0.71073 Å).[31,32] An initial set of cell constants was calculated from reflections harvested from three sets of at least 12 frames oriented such that orthogonal wedges of reciprocal space were surveyed. Final cell constants were calculated from a minimum set of 2000 strong reflections from the actual data collection. Data were collected to the extent of at least 1.5 hemispheres at a resolution of at least 0.84 Å using φ-scans. Three major sections of frames were collected with at least 0.30 º steps in ω at 3 different ϕ settings and a detector position of -28 º in 2θ. For all structures, the intensity data were corrected for absorption and decay using SADABS v2.10 and space groups determined based on systematic absences and intensity statistics. [33,34] The structures were determined using a direct-methods solution. Several full-matrix least-squares/difference Fourier cycles were performed to locate remaining non-hydrogen atoms. All calculations were performed using the SHELXTL-V6.12 suite of programs on Pentium computers.[35] Additional crystallographic

information can be found in Table 1. Packing analysis parameters were measured using PLATON/VOID with pictorial representations of the solvent channels done with edited *.res files in Mercury.[36-38]

The detection of solvent accessible voids by PLATON/VOID is done in the following way: The unit cell is filled with the atoms from the structural model and each specific atom is assigned its respective van der Waals radius. A grid search generates a list of grid points with a minimum distance of 1.2 Å from the nearest van der Waals surface. This list of grid points is then used to produce a new list of grid points that makes up the solvent accessible areas. For the sets of grid points, the center of gravity and volume of the void are calculated. The overall solvent accessible volume is calculated along with the volume and center of gravity of individual 'voids'.

Table 1. Crystallographic Data and Refinement Parameters.

Compound	**1a**	**2a**
empirical formula	C_{24} H_{32} Cl_3 Ir N_3 O S	C_{48} H_{40} F_{18} Ir N_8 P_3
crystal color, morphology	yellow, needle	red, block
crystal system	Monoclinic	Monoclinic
space group	$P2_1/c$	*C2/c*
crystallization solvent	DMSO	Acetonitrile
a, Å	10.377(2)	14.6977(14)
b, Å	23.166(5)	16.3737(16)
c, Å	10.370(2)	21.420(2)
α, deg	90	90
β, deg	93.22(3)	105.639(2)
γ, deg	90	90
Volume (*V*), Å^3	2488.9(9)	4964.0(8)
Z	4	4
formula weight, g mol^{-1}	700.06	1355.99
density (calculated), g cm^{-3}	1.868	1.814
temperature, K	100(2)	173(2)
absorption coefficient (μ), mm^{-1}	3.079	2.900
F(000)	1360	2672
θ range, deg	1.53 to 17.17	1.96 to 26.37
index ranges	$-14 \le h \le 14$	$-18 \le h \le 18$
	$-33 \le k \le 33$	$-13 \le k \le 20$
	$-12 \le l \le 14$	$-26 \le l \le 26$
reflections collected	68215	13655
independent reflections	7484 [R_{int} = 0.0453]	4995 [R_{int} = 0.0458]
weighting factors,[a] *a, b*	0.0375, 14.1866	0.0837, 2.2984
max, min transmission	0.9848, 0.7908	0.7223, 0.5309
data/restraints/parameters	7484/61/346	4995/0/355
R_1, wR_2 [$I > 2\sigma(I)$]	0.0366, 0.0902	0.0508, 0.1289
R_1, wR_2 (all data)	0.0477, 0.1006	0.0782, 0.1455
GOF	1.106	1.108
largest diff. peak, hole eÅ^{-3}	3.317, -2.399	1.689, -1.217

[a] $w = [\sigma^2(F_o^2) + (aP)^2 + (bP)]^{-1}$, where $P = (F_o^2 + 2F_c^2)/3$.

Table 1 Continued. Crystallographic Data and Refinement Parameters.

Compound	**2b**	**2c**
empirical formula	$C_{50}\,H_{46}\,F_{18}\,Ir\,N_6\,O_2\,P_3$	$C_{45}\,H_{38}\,F_{18}\,Ir\,N_6\,O\,P_3$
crystal color, morphology	red, plate	orange, prism
crystal system	Monoclinic	Triclinic
space group	*C2/c*	$P\,\bar{1}$
crystallization solvent	Acetone	Methanol
a, Å	15.5763(17)	11.3119(6)
b, Å	16.3216(18)	14.3045(7)
c, Å	20.956(2)	15.4383(8)
α, deg	90	98.5060(10)
β, deg	101.407(2)	106.8740(10)
γ, deg	90	95.3260(10)
Volume (*V*), Å^3	5222.3(10)	2339.8(2)
Z	4	2
formula weight, g mol^{-1}	1390.04	1305.92
density (calculated), g cm^{-3}	1.768	1.854
temperature, K	173(2)	173(2)
absorption coefficient (μ), mm^{-1}	2.761	3.073
F(000)	2752	1284
θ range, deg	1.83 to 27.51	1.45 to 26.37
index ranges	$-17 \le h \le 19$	$-14 \le h \le 14$
	$-17 \le k \le 21$	$-17 \le k \le 17$
	$-26 \le l \le 27$	$-19 \le l \le 19$
reflections collected	17590	25195
independent reflections	5938 [R_{int} = 0.0412]	9499 [R_{int} = 0.0263]
weighting factors,[a] *a, b*	0.0381, 7.8537	0.0418, 3.3542
max, min transmission	0.7154, 0.3390	0.8615, 0.6557
data/restraints/parameters	5938/0/366	9499/63/728
R_1, wR_2 [$I > 2\sigma(I)$]	0.0345, 0.0721	0.0290, 0.0725
R_1, wR_2 (all data)	0.0464, 0.0764	0.0331, 0.0782
GOF	1.006	1.061
largest diff. peak, hole eÅ^{-3}	1.320, -1.317	1.324, -1.166

[a] $w = [\,\sigma^2(F_o^2) + (aP)^2 + (bP)]^{-1}$, where $P = (F_o^2 + 2F_c^2)/3$.

Oxygen Sensing Measurements

Preliminary oxygen sensing measurements were collected using samples prepared by placing a small amount of crushed crystals or reaction powder into a depression in a ¼'' diameter aluminum or brass rod. The prepared sample was then placed into a swage cross-tube fitting apparatus designed to allow gas to flow over the sample and for front face illumination (Figure 2). A 405 nm LED filtered through an interference filter was used as the excitation source and light was brought to the sample by the center fiber of a "six around one" bifurcated fiber optic probe. The emission was collected through the six fiber channel and sent to an Ocean Optics USB-2000 spectrometer. Nitrogen and oxygen gas were brought to the swage cross from gas cylinders and the flow was controlled through manipulation of manual valves. Individual spectra were manually collected through the Ocean Optics interface and analyzed with Microsoft Excel.

The samples tested for further oxygen sensing were prepared similarly by placing a small amount of reaction powder or crushed crystals into a depression in a ¼'' diameter aluminum or brass rod. The prepared sample was then placed into a swage cross-tube fitting apparatus designed to allow gas to flow over the sample and for front face illumination (Figure 2). A 405 nm LED filtered through an interference filter was used as the excitation source and light was brought to the sample by the center fiber of a "six around one" bifurcated fiber optic probe. The emission was collected through the six fiber channel and sent to an Ocean Optics USB-2000 spectrometer. The spectrometer, mass flow controllers, temperature, and pressure monitors were interfaced to a custom LabVIEW program to allow control of the unattended data acquisition.[22,39-41]

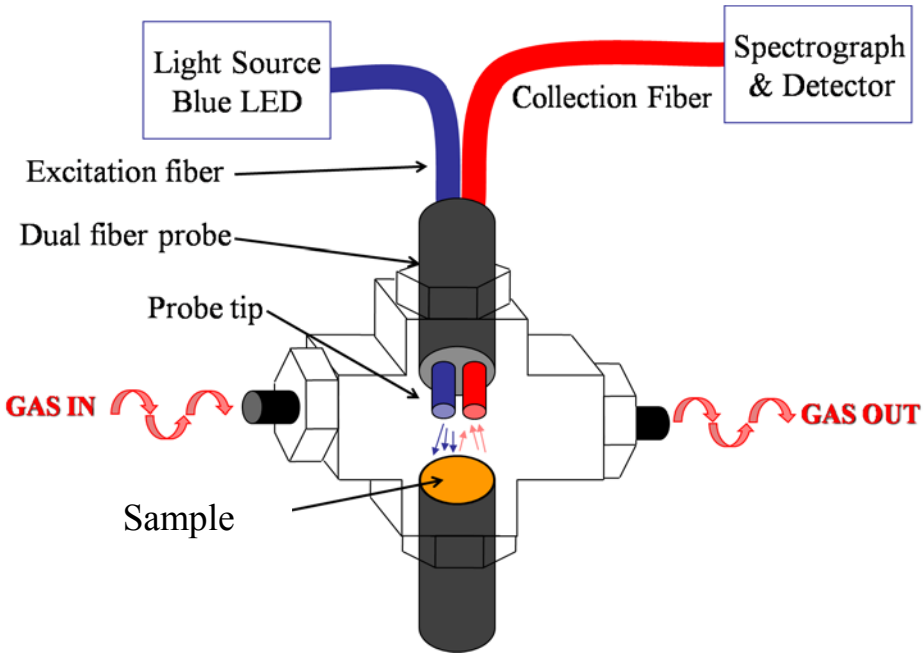

Figure 2. Diagram of the swage cross-tube fitting apparatus used for sensing measurements.

The emission data collected were analyzed with a spreadsheet written in Microsoft Excel. Data from six cycles of spectra obtained at approximately 0.0, 0.10, 0.21, 0.25, 0.40, 0.50, 0.65, 0.80, 0.90 and 1.0 mole fraction of oxygen in nitrogen were used for the Stern-Volmer plots. The acquisitions were performed at room temperature, approximately 21.8 ± 1 °C. Exact gas mole fractions were calculated by referencing the feedback voltage of the mass flow controllers to a calibration previously performed.[40] The emission intensity was integrated across the entire peak and divided by the integrated LED or LED double intensity for each spectrum to give I_0 (intensity under N_2) and I (intensity at a given O_2 mixture). I_0/I was plotted versus oxygen mole fraction in nitrogen to yield a Stern-Volmer plot. A linear regression model was used to calculate the slope or K_{SV} parameter.

It should be noted that the K_{SV}*'s* reported here are expressed in units of mole fraction and have not been corrected for the atmospheric pressure in Minneapolis, MN of 0.97 atm. In order to compare these K_{SV} numbers to those reported previously, the K_{SV} in mole fraction needs to be corrected by dividing the current value by 0.97 atm to give the K_{SV} in units of atm^{-1}.

A separate data collection was performed on the crystalline sample of **2b** where the sample was exposed to two cycles of gas concentrations to obtain spectra at approximately 0.0, 0.10, 0.21, 0.25, 0.40, 0.50, 0.65, 0.80, 0.90 and 1.0 mole fraction of oxygen in nitrogen and these were used to generate a Stern-Volmer plot. Then, for 8 hours the sample was exposed to nitrogen gas under constant illumination from a 405 nm LED and a spectrum was collected every ten minutes. Next, the sample was exposed to oxygen gas in a similar manner. Finally, the two cycles of gas concentrations were

repeated to obtain a final Stern-Volmer plot. The emission intensity of the sample under the long exposures to nitrogen and oxygen were analyzed for signs of decomposition.

Results and Discussion

Synthesis of mono-tolyl-terpy Derivative

Ir(tol-terpy)Cl_3 was synthesized and isolated following the prep from Collin and coworkers.[25] The reaction was done under nitrogen in a small amount of ethylene glycol with one equivalent of iridium trichloride and tol-terpy. After heating for 23 minutes, the red reaction mixture contained a red solid that was isolated and washed, resulting in a 66% crude yield, and the product was confirmed by ^{1}H NMR spectroscopy. Single crystals were grown from hot DMSO and X-ray data were collected at the ChemMatCARS microcrystallography beamline at APS sector 15-ID-C at Argonne National Laboratory. This structure is shown in Figure 3 and was reported in Acta Crystallographica C in 2010.[42]

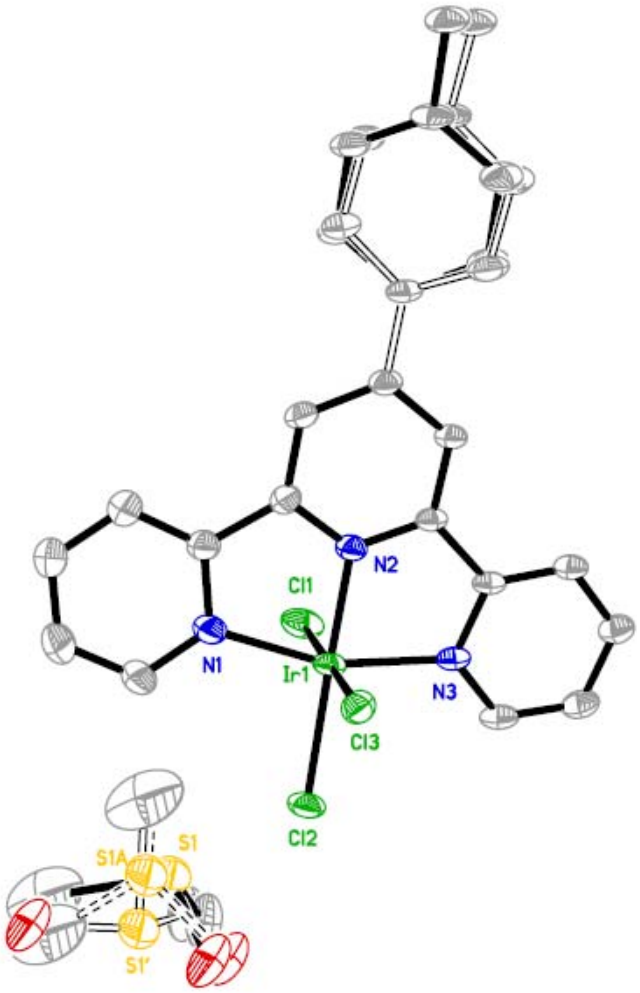

Figure 3. Thermal ellipsoid plot with 50% probability surfaces of **1a**. Disorder modeling of both the tolyl portion of the tol-terpy ligand and the DMSO are shown. Hydrogen atoms have been removed for clarity.

Synthesis of bis-tolyl-terpy Derivatives

A series of reactions were conducted in an attempt to isolate the *bis*-tol-terpy derivative and are summarized in Table 2. Most procedures for obtaining the *bis*-tol-terpy product proceed through a stepwise route.[15-19,23,25,28] In general, these stepwise procedures do not involve the isolation of the trichloride intermediate, but instead assume that it has been formed *in situ* and additional equivalents of ligand are added after a short reflux. Hypothesizing that reactions could be made more efficient by initially starting with two equivalents of ligand, reactions were attempted in ethylene glycol with two equivalents of ligand per equivalent of iridium trichloride.

As can be seen from the table, reactions conducted with traditional reflux techniques tend to result in complicated mixtures. Attempts to resolve this problem by varying and degassing solvent were unsuccessful in generating an iridium *bis*-tol-terpy complex. Reactions resulted in complicated ^{1}H NMR spectra suggest that cyclometallation of the tol-terpy ligand is occurring. Multiple components could not be separated by either alumina or silica chromatography, further complicating the isolation of any *bis*-tol-terpy complex that may be present in small yield. The *bis*-tol-terpy complex does not appear to be readily obtained through reactions of two equivalents of ligand in refluxing ethylene glycol as cyclometallation likely occurs before complexation of the second, or possibly first, tol-terpy ligand to iridium. Hypothesizing that the Ir(tol-terpy)Cl_3 complex was not being formed *in situ*, reactions were conducted with the previously isolated Ir(tol-terpy)Cl_3 species and one equivalent of ligand, again without successful isolation of [Ir(tol-terpy)$_2$]Cl_3.

Table 2. Selected Reactions Conducted in Attempts to Isolate *bis*-tol-terpy Complex.

Iridium Source	Terpy Source	Solvent	Reaction Method	Description of Reaction	^{1}H NMR Observations	Additional Comments
$IrCl_3$	tol-terpy	Ethanol (12 mL)	Reflux (8 hours)†	Red-brown marbled solid collected by filtration. Portions of solid emit red others blue-white.	Two components present. Peaks are shifted relative to the NMR of pure tol-terpy.	ESI-MS suggests protonated ligand.
$IrCl_3$	tol-terpy	Ethylene Glycol (0.5 mL)	Microwave (5 minutes)‡	Became red sol'n after 1 minute. Red-orange precipitate formed.	Crude reaction NMR mostly ligand.	Reaction elixir emits yellow.
Above reaction reheated			Microwave (45 minutes)	Red sol'n color persisted. Dirty yellow-orange solid collected, similar in color to color of pure ligand.	Isolated solid mostly ligand, "impurity" peaks match Collin reports.	TLC indicated an additional complex formed, but cannot be cleanly separated by chromatography.
$IrCl_3$	tol-terpy (1 eq)	Ethylene Glycol (15 mL)	Microwave (20 minutes)	Blood red sol'n formed after 15 seconds, red precipitate develops.	Two components present, one symmetric. May correspond to a terpy compound, but does not match reports by Collin.	Reaction elixir emits red.
Ir(tol-terpy)Cl_3	tol-terpy (1 eq)	Ethylene Glycol (2.5 mL)	Reflux (1 hour)	Red emissive solid collected.	Multiple peaks, possible cyclometalated product.	Reaction elixir emits yellow. Two components cannot be separated using TLC.
Ir(tol-terpy)Cl_3	tol-terpy (1 eq)	Ethylene Glycol (10 mL)	Reflux (24 hours)	Reaction green after 1 hour. Color persists with no formation of precipitate.	Multiple peaks (approximately 35), two components.	Solution emits yellow. No reaction of filtrate observed with ascorbic acid or hydrogen peroxide. No clear separation of crude mixture by TLC. After conversion to PF_6 salt, isolated orange solid and yellow solid by chromatography, both are unsymmetric products.

Two equivalents of terpy source used except where indicated.
All reflux reactions done under inert atmosphere unless indicated.
† Reflux refers to traditional water condenser based reflux techniques.
‡ Microwave indicates reaction was heated in a standard microwave using a dry ice condenser under air.

Table 2 Continued. Selected Reactions Conducted in Attempts to Isolate *bis* -tol-terpy Complex.

Iridium Source	Terpy Source	Solvent	Reaction Method	Description of Reaction	^{1}H NMR Observations	Additional Comments
Ir(tol-terpy)Cl_3	tol-terpy (1 eq)	Ethylene Glycol (15 mL, degassed)	Reflux (16 hours)†	After 15 minutes, reaction is yellow-green.	No change from reaction using non-degassed solvent.	Reaction elixir slowly turns brown while capped.
Ir(tol-terpy)Cl_3	tol-terpy (1 eq)	Ethylene Glycol (15 mL)	Reflux (24 hours, air)	Reaction turns red after several hours. Green color not observed.	Two symmetric products, neither of which is ligand or desired product. NMR inconsistent with previous reaction under inert atmosphere.	Reaction elixir slowly turns brown while capped.
$IrCl_3$	terpy	2-Methoxyethanol (5 mL)	Reflux (96 hours)	Monitored by NMR. Orange reaction mixture, collected orange solid.	4 hour NMR mostly monoterpy product. Continued heating complicates spectra.	Product isolated is dark red sticky solid that emits orange.
$IrCl_3$	terpy	2-Methoxyethanol (15 mL)	Microwave (10 min)‡ and Reflux (3 days)	After microwaving, reaction appeared to contain unreacted $IrCl_3$, transferred to reflux setup to continue heating. Orange-red solid collected	Appears to be monoterpy product as peaks correspond to those reported by Collin.	Collected 4.6% yield of monoterpy product.
$IrCl_3$	terpy-*	Ethylene Glycol (2 mL)	Reflux (5 hours)	Orange solid collected from a blood red solution.	Mostly starting ligand and small amount of another material.	Reaction elixir emits yellow. Melting point of isolated solid matches literature value for terpy-*. Components could not be separated with TLC.

Two equivalents of terpy source used except where indicated.
All reflux reactions done under inert atmosphere unless indicated.
† Reflux refers to traditional water condenser based reflux techniques.
‡ Microwave indicates reaction was heated in a standard microwave using a dry ice condenser under air.

In order to monitor the reaction for ligand cyclometallation, the reaction was performed at a lower temperature over a longer period of time with 2-methoxyethanol as the solvent. If cyclometallation was occurring, the symmetry of the molecule would be broken, resulting in a much more complicated ^{1}H NMR. After 4 hours, the reaction appeared to have formed a small amount of Ir(tol-terpy)Cl_3 due to the presence of 7 peaks in the ^{1}H NMR spectrum. Upon further heating, the reaction did not appear to generate more of this Ir(tol-terpy)Cl_3 product but instead produced an unsymmetric material and a ^{1}H NMR spectrum with more than 15 peaks. Again, it is hypothesized that this unsymmetric material is an iridium complex with at least one cyclometallated tol-terpy, breaking the symmetry and complicating the ^{1}H NMR interpretation. No appreciable quantity of solid was isolated from this reaction as portions of the reaction were removed for NMR analysis. Observation suggests that comparable yields of the various products were produced in the 2-methoxyethanol reactions in comparison to the reactions conducted in ethylene glycol. These results along with those from ethylene glycol reactions suggest that a delicate balance between reaction time and reflux temperature exists when trying to form *bis*-tol-terpy complexes. Ethylene glycol allows for short reaction times at high temperatures, but the viscosity of the solvent makes product isolation difficult. Longer reaction times are required when 2-methoxyethanol is used, but it appears that more solid could be cleanly isolated.

In order to quickly study potential synthetic methods, microwave synthesis techniques were investigated. Application of this technique to the synthesis of *bis*-tol-terpy complexes may prove advantageous seeing as the current routes require minimal amounts of solvent and high reflux temperatures. Ideally, the synthesis of the *bis*-tol-

terpy complex using microwave techniques could be achieved without isolating the neutral intermediate.

During the course of the reactions conducted in the microwave, color change of the reaction elixirs was observed after only a few seconds. When a precipitate could be isolated, it was not the desired *bis*-tolyl-terpy compound. Once again, ^{1}H NMR spectra indicated the formation of multi component mixtures, most likely containing cyclometallated products. Extending the reaction time in the microwave significantly increases the possibility of cyclometallation due to the rapid reflux that is achieved with ethylene glycol. Lower boiling solvents were investigated, but are not practical for this technique as they reflux more quickly, bumping the reaction mixture into the dry ice condenser. One reaction conducted in the microwave did generate Ir(terpy)Cl_3, but did so in only 4.6 % yield from a reaction intending to form the *bis*-terpy product. This result indicates that even in a large excess of ligand, it is extremely difficult to attach a single terpy ligand to iridium in good yield. While microwave techniques significantly shortened the total reaction time, the rapid, high temperature heating is again of concern.

Ethylene glycol is a difficult solvent to work with due not only to its high boiling point, viscosity, and solubility properties but also its ability to be oxidized during long reactions.[15] Consequently, propylene carbonate was investigated as a possible alternative to ethylene glycol. This solvent is much higher boiling and has several other advantages over ethylene glycol. Propylene carbonate is miscible with both water and diethyl ether allowing isolation of solids via nonspontaneous precipitation and would be ideal for use in microwave syntheses since it would not reflux during the time of the experiment, greatly simplifying the apparatus used for the microwave synthesis.

Several small test microwave reactions were done in vials and after a promising initial color change was observed, reactions were monitored by no-d ^{1}H NMR (no-deuterium proton nuclear magnetic resonance). This technique allowed the reaction to be performed and monitored in a non-deuterated and therefore less expensive solvent. Samples prepared for this technique must be much more concentrated than those used for typical ^{1}H NMR experiments. Thus, a highly concentrated sample of Ir(tol-terpy)Cl_3 and one equivalent of tol-terpy was prepared in an NMR tube using propylene carbonate as the solvent. At this saturated concentration, the starting materials were not completely soluble and a large amount of solid was observed in the bottom of the NMR tube. After heating the tube for several hours, no change was observed by ^{1}H NMR and it is hypothesized that large amount of unsolvated reactants did not allow the reaction to progress. Less concentrated vial reactions were then prepared, but again no change in reactivity was observed. While propylene carbonate does provide significant advantages over ethylene glycol, the inability of the solvent to completely dissolve reactants reduces its practicality for this synthetic application.

Overcoming cyclometallation appears to be the challenge to obtaining *bis*-tol-terpy complexes in high yields as long reaction times and high temperatures are favorable conditions for the production of these undesired complexes. To prevent cyclometallation, terpy-* (4,4′,4″-tri-*tert*-butyl-2,2′:6′,2″terpyridine) was used as the presence of the *tert*-butyl groups on the pyridine rings blocks the desired cyclometallating site. From the reaction of 2 equivalents of terpy-* in ethylene glycol, an orange solid was collected from a dark red solution and determined to be mostly ligand by ^{1}H NMR. The melting point of this orange solid was taken and the product decomposed at a temperature corresponding

to the literature melting point value for terpy-* (214 °C). The results of the synthesis with this ligand indicate that cyclometallation is not the only obstacle to obtaining these *bis*-terpy complexes in appreciable yield.

A few years after the initial struggles with the synthesis of these materials, a paper was published in which a simpler experimental technique was reported.[30] This technique was a modification of that reported by Collin et al. and resulted in greater than 50 % yields. In this paper, the reaction began with all reactants in a minimal amount of ethylene glycol. From here, the reaction was purged with nitrogen and heated to 100 °C. After a relatively short time period of two and a half hours, the temperature of the reaction was increased to just below the boiling point of ethylene glycol and allowed to react for an additional hour. After this time, the reaction is cooled and the intended compound was precipitated and collected. This reaction was performed with complicated 4'-substituted terpy derivatives in the paper, but was successful here with the tol-terpy derivative. This reaction was performed multiple times with yields of greater than 30 % for the PF_6^- salt. The reaction was carried out and the $tfpb^-$ salt obtained through the addition of a Na(tfpb) solution instead of the $NaPF_6$.

The only challenge occurred when trying to obtain *bis*-terpyridine. Following the stepwise procedure above, an unsymmetric product was observed in the ^1H NMR spectrum. Mass spectrometry was performed on this material and suggested that one of the outer pyridine rings had flipped over, resulting in a cyclometallated C^N^N binding mode of the terpy. The compound was also a dication, indicating that the second terpyridine ligand was bound in the intended N^N^N mode which breaks any symmetry in the molecule. The materials obtained through the literature procedure each involved a

terpy with a substitution at the 4' position of the central pyridine. It is known that substitution at this position enhances the electronic properties of the ligand and perhaps this change in the electronics hinders the cyclometallation of the outer pyridine rings.[25]

X-ray Crystallography

To our knowledge, only seven structures of terpyridine iridium(III) complexes were present in the Cambridge Structural Database (CSD, Version 5.30 of May 2009) before the publication of our Acta Crystallographica C paper in 2010.[42,43] The lack of both mono- and *bis*-terpyridine-based iridium(III) structures may be due in part to the inertness of the metal center coupled with the difficulty of making tricationic iridium(III) species in considerable yield.[25,44] The structures of the trichlorido[4'-(*p*-tolyl)-2,2':6',2''-terpyridine]iridium(III) dimethyl sulfoxide solvate, (**1a**), and three different solvates of bis[4'-(*p*-tolyl)-2,2':6',2''-terpyridine]iridium(III) *tris*(hexafluoridophosphate) were analyzed (**2a-c**).

The structure of **1a** is shown in Figure 3. The DMSO solvent molecule is disordered over three positions, one of which is an inversion center. The tolyl group at the 4'-position of the terpyridine ligand is positionally disordered over two positions with occupancies of 0.64(4) and 0.37(4). The plane formed by the Ir metal center and the atoms of the three chelating rings (N1/C1–C5, N2/C6–C10 and N3/C11–C15) of the tol-terpy ligand is planar, with an r.m.s. deviation of 0.0673 Å. This plane is twisted by 89.84(5) ° relative to the plane formed by the Ir atom and the three Cl ligands, which has an r.m.s. deviation of 0.0054 Å. Due to the bite angle of the tol-terpy ligand, the bond distance from Ir1 to the central N2 atom is 1.947(4) Å , which is significantly shorter than

those for the two outer atoms, N1 and N3 of 2.037(5) and 2.041(4) Å, respectively. The chloride ligand (Cl2) trans to the central N atom of the tol-terpy ligand exhibits the longest bond distance of the three chlorides [Ir1—Cl2 = 2.3856(13) Å]. All of the Ir—N and Ir—Cl bond distances in **1a** fall within the expected ranges based on a CSD search.

In the structure of **1a**, the DMSO molecule was modeled over three positions whose site-occupation factors were restrained to sum to 1.00 (actual occupation factors of the three orientations = 0.500(3), 0.328(3) and 0.173(2)). Similarity restraints were applied to the chemically equivalent bond lengths and angles across the three orientations, while the distances between the S and O atoms and between the S and C atoms were restrained to 1.678(5) and 1.862(5) Å, respectively. The atomic displacement parameters of the corresponding atom in each of the three orientations were constrained to be identical. The tolyl substituent was also disordered over two orientations, with C16 serving as the anchor atom. The atomic displacement parameters of corresponding atoms in the two orientations were also constrained to be identical, while similarity restraints were applied to the chemically equivalent bond lengths and angles.

The data for structure **2a**, or $[Ir(tol\text{-}terpy)_2](PF_6)_3 \bullet 2\ CH_3CN$, were collected initially to aid in the identification of the products from a reaction between $Ir(tol\text{-}terpy)Cl_3$ and tol-terpy. While the data collection temperature for **2a** was lower, at 173 K, the initial unit-cell parameters and cell volume were similar to a room-temperature structure reported by Yoshikawa et al. for the same compound (CSD refcode YIDGAU).[1] The previously reported structure was solved in space group *Cc*. However, closer examination of the bond distances within this structure led us to believe that the structure had been solved in the incorrect space group.

A comparison of the chemically equivalent bond distances between the two independent tol-terpy ligands in structure YIDGAU revealed many bond distances that were more than five standard deviations apart. This result was surprising considering the inherent D_{2d} symmetry of the molecule. Marsh reports that the space group *Cc* is often misassigned when a twofold axis has been overlooked.[45] It appears that many structures in *Cc* are often revised to be *C2/c* after this missing symmetry element is found.[45,46] Furthermore, this space group change leads to more reasonable bond lengths and angles within the structure. The ADDSYM routine in PLATON was conducted on the YIDGAU *.cif and conclusively found missing symmetry in the structure.[37] The addition of inversion and twofold symmetry to the structure leads to a solution in space group *C2/c*. Solving the structure of **2a** in the centrosymmetric space group *C2/c* gave bond lengths and angles comparable to those reported for a *bis*(2,2':6',2"-terpyridine)iridium(III) structure (CSD refcode FOHQAU), leading us to believe that *C2/c* is indeed the correct space group setting for **2a**.[25]

In **2a**, one P atom (P1) is in a general position, while the second (P2) lies on a twofold axis. The Ir atom also lies on this twofold axis, making half of the cation unique. One acetonitrile solvent molecule is located on a general position as well (Figure 4). Bond distances from the N atoms to the Ir atom are 2.052(6) (N1), 1.966(6) (N2) and 2.047(6) Å (N3), following the similar long–short–long pattern found in the mono-tol-terpy derivative **1a** and are within the expected range for Ir—N bond distances. The Ir atom and the atoms of the three chelating rings of the tol-terpy ligand are planar, with an r.m.s. deviation from the plane of 0.0457 Å. PLATON CALC VOID was then used to determine the amount and location of void space within the crystal.[36] When the co-

crystallized solvent was removed, 660.1 $Å^3$ of void space were found accounting for 13.2 % of the total volume of the crystal. The void space is shown in Figures 5-7 and takes the form of pockets, not the more desired channel form.

The solvate $[Ir(tol\text{-}terpy)_2](PF_6)_3 \bullet 2\ (CH_3)_2CO$ (**2b**) also crystallizes in the space group *C2/c* (Figure 8). The iridium atom (Ir1) and P2, F8 and F10 of one PF_6^- molecule lie on the twofold axis located at (½ y ¾), making half of the respective molecules unique. There is no disorder in the structure. Bond distances from the N atoms to the Ir atom are 2.058(3) (N1), 1.973(3) (N2) and 2.053(3) Å (N3). All bond distances and angles are within the normal ranges with the Ir-N distances following the long-short-long pattern observed in both **1a** and **2a** mentioned above. The Ir atom and the atoms of the three chelating rings of the tol-terpy ligand are planar, with an r.m.s. deviation from the plane of 0.0450 Å. The molecules of solvation were removed from the structure and PLATON/CALC VOID was performed.[36] There are 889.4 $Å^3$ of void space accounting for 17.3 % of the total volume of the crystal as seen in Figures 9-11. In this structure, the void space does take the form of channels that meander through the crystal along the *b* and *c* axes (Figure 12).

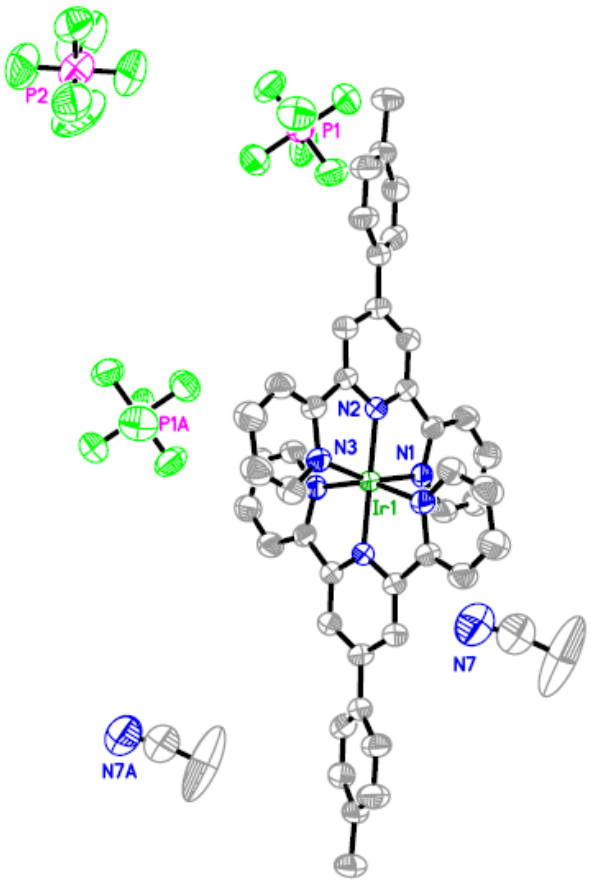

Figure 4. Structure diagram of **2a** with thermal ellipsoids drawn as 50 % probability surfaces. Hydrogen atoms have been removed for clarity and only select heteroatoms have been labeled.

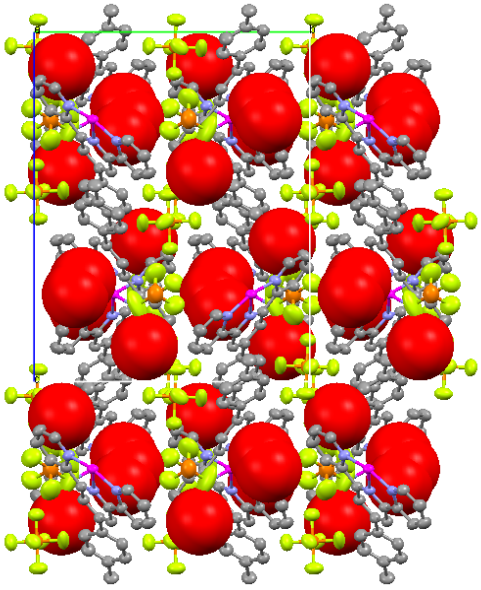

Figure 5. View of the void space within the structure of **2a** as viewed down the *a* axis. Solvent has been removed and void space is represented as red spheres. Hydrogen atoms have been removed for clarity.

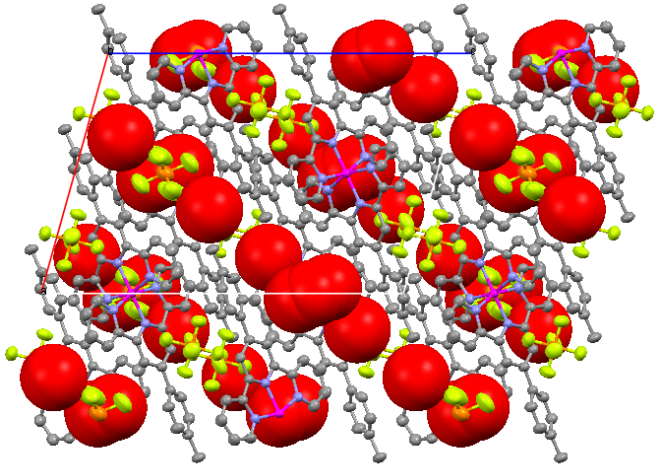

Figure 6. View of the void space within the structure of **2a** as viewed down the *b* axis. Solvent has been removed and void space is represented as red spheres. Hydrogen atoms have been removed for clarity.

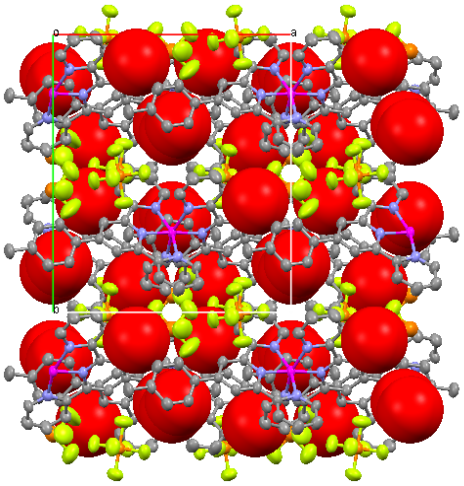

Figure 7. View of the void space within the structure of **2a** as viewed down the *c* axis. Solvent has been removed and void space is represented as red spheres. Hydrogen atoms have been removed for clarity.

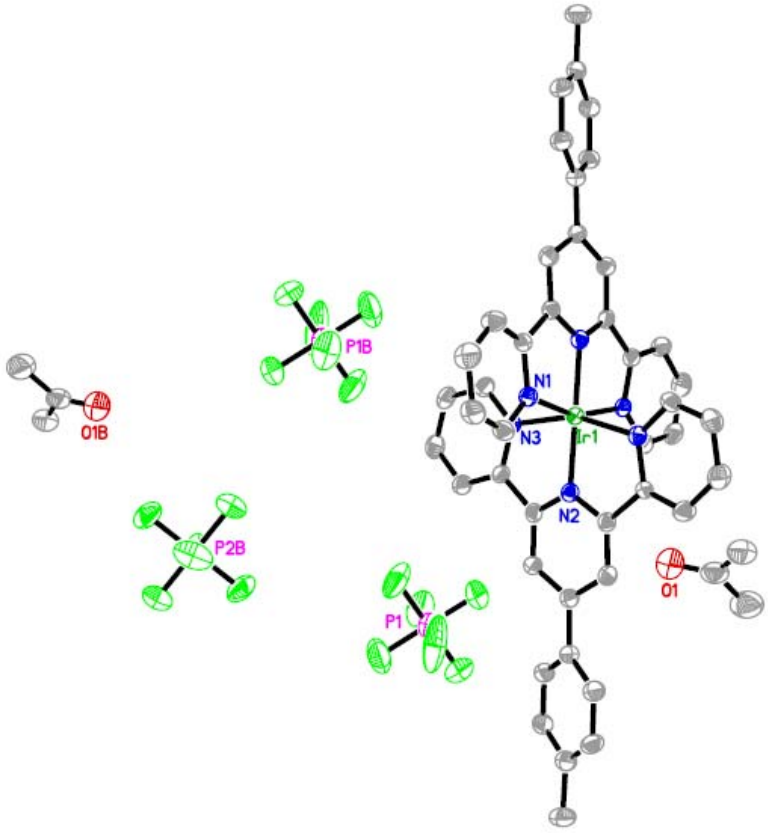

Figure 8. The structure of **2b** is shown with thermal ellipsoids drawn as 50 % probability surfaces. Select heteroatoms have been labeled. Hydrogen atoms have been removed for clarity.

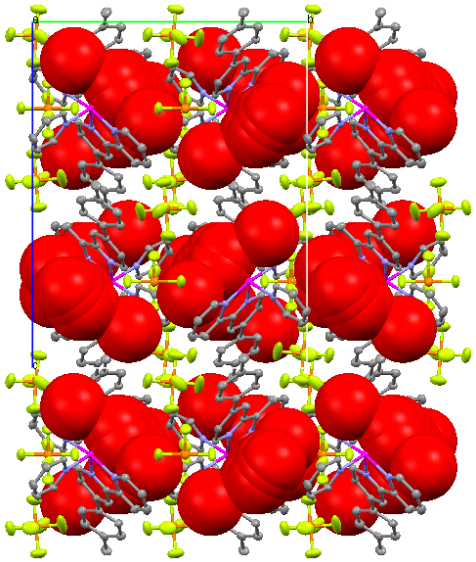

Figure 9. View of the void space within the structure of **2b** as viewed down the *a* axis. Solvent has been removed and void space is represented as red spheres. Hydrogen atoms have been removed for clarity.

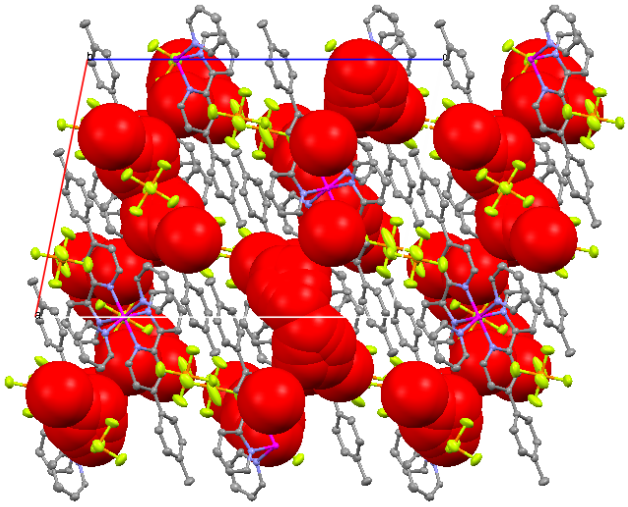

Figure 10. View of the void space within the structure of **2b** as viewed down the *b* axis. Solvent has been removed and void space is represented as red spheres. Hydrogen atoms have been removed for clarity.

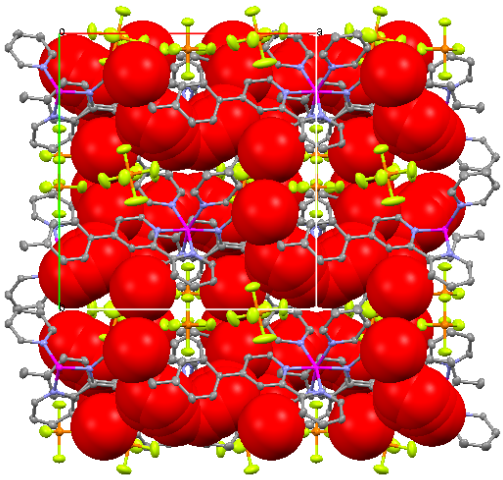

Figure 11. View of the void space within the structure of **2b** as viewed down the *c* axis. Solvent has been removed and void space is represented as red spheres. Hydrogen atoms have been removed for clarity.

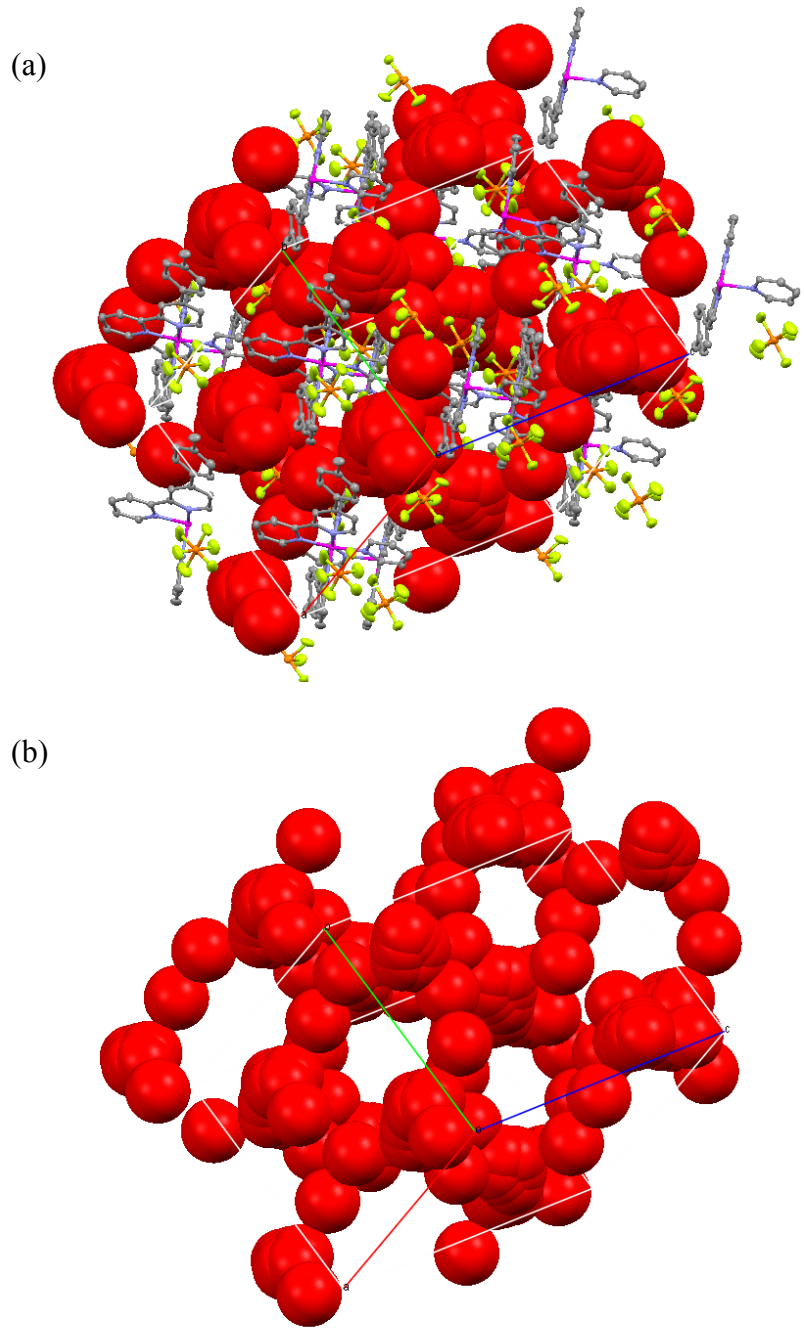

Figure 12. Alternate views of the channels present in the structure of **2b**. The top view (a) includes the molecules and the bottom view (b) displays only the void space channels.

The solvate $[Ir(tol\text{-}terpy)_2](PF_6)_3 \bullet CH_3OH$, (**2c**) crystallizes in the space group $P\bar{1}$ unlike the other solvates (Figure 13). In this structure, P3 and P4 lie on inversion centers making half of the corresponding PF_6^- molecule unique. Bond distances from the N atoms to the Ir atom are 2.052(3) (N1), 1.970(3) (N2), 2.058(3) (N3), 2.048(3) (N4), 1.972(3) (N5) and 2.057(3) Å (N6). All bond distances and angles are within normal ranges and the Ir-N bond distances again follow the long-short-long pattern as expected. The Ir atom and the atoms of the three chelating rings of the tol-terpy ligand are planar, with an r.m.s. deviation from the plane of 0.0749 Å for the tol-terpy containing N1 and 0.0388 Å for the tol-terpy containing N4. The two tol-terpy ligands are twisted 92.8 ° from one another.

The PF_6^- counterions of this structure are disordered. The PF_6^- containing P1 as the central atom is positionally disordered and modeled over two positions. These positions have occupancy factors of 81 % and 19 %, respectively. The bond distances within this PF_6^- were restrained to 1.573(1) Å to allow the model to converge. The PF_6^- containing P2 as the central atom is rotationally disordered and modeled over two positions which have occupancy factors of 89 % and 11 %. The final PF_6^- containing P4 as the central atom is disordered over the inversion center where P4 is located. The disorder is modeled over this inversion center and the occupancy was let to refine so that the occupancies of the two parts are 49.8 and 50.2.

Attempts to refine the position of the methanol alcohol proton were unsuccessful as this proton is surprisingly not involved in hydrogen bonding. Refinement of the position caused the proton to rotate about the O-CH_3 bond indefinitely, requiring this methanol molecule to be squeezed from the structure to achieve convergence.

PLATON/SQUEEZE was performed on the structure and found 25 electrons per unit cell corresponding to approximately 1.33 molecules of methanol. PLATON/CALC VOID was then performed on the squeezed structure.[36] A void space of 116.5 $Å^3$ was found accounting for 4.98 % of the total volume. However, the void space is in the form of pockets, not channels (Figures 14-16).

While the $tfpb^-$ salt was synthesized, it was very difficult to obtain X-ray quality crystals of the material. The three bulky, fluorinated counterions were desired as it was through that they would generate void space within the lattice. Upon further study, it appears that this large number of bulky counterions perhaps causes the material to have too much unsupported void space, collapsing the lattice, resulting in amorphous materials.

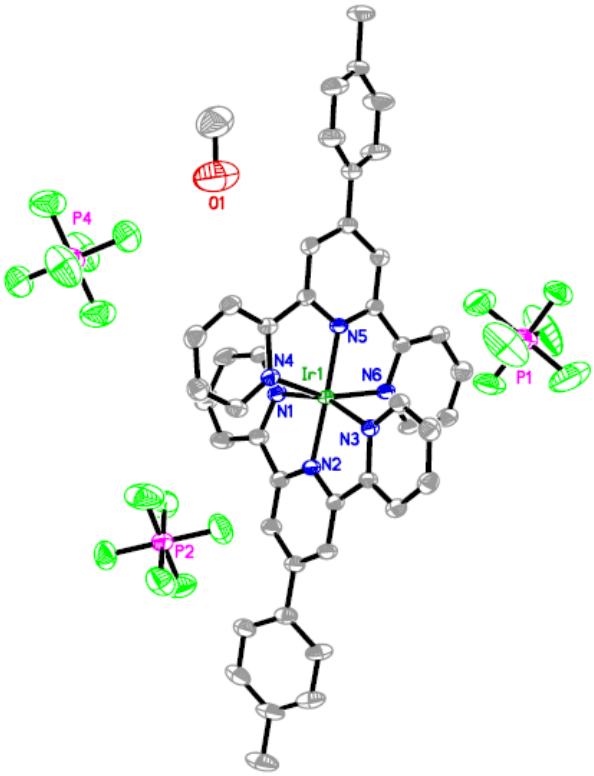

Figure 13. The structure of **2c** is shown with thermal ellipsoids are drawn as 50 % probability surfaces. All hydrogen atoms and disorder of the anions have been removed for clarity.

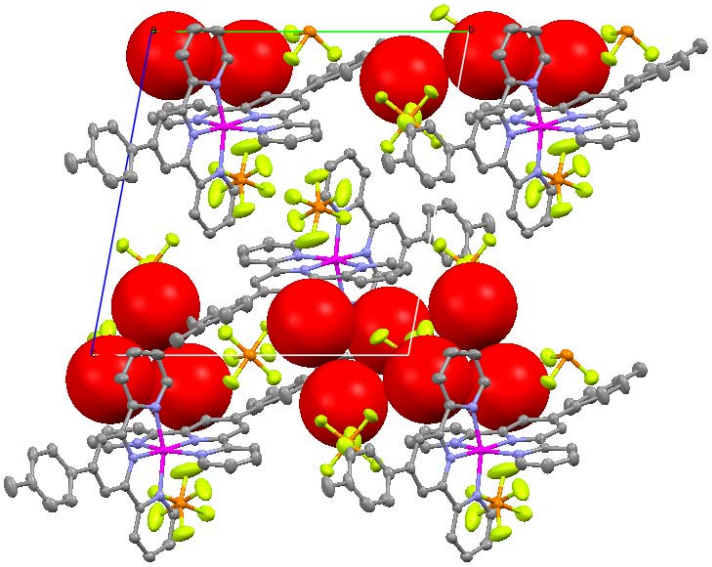

Figure 14. View of the void space within the structure of **2c** as viewed down the *a* axis. Solvent has been removed and void space is represented as red spheres. Hydrogen atoms have been removed for clarity.

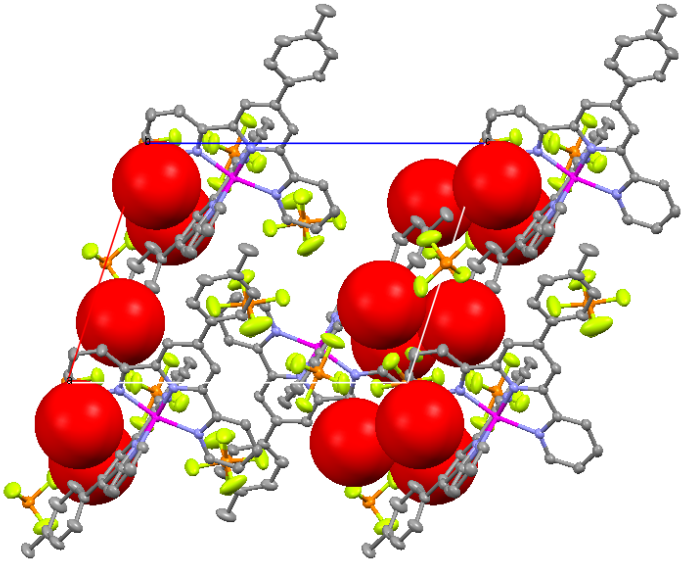

Figure 15. View of the void space within the structure of **2c** as viewed down the *b* axis. Solvent has been removed and void space is represented as red spheres. Hydrogen atoms have been removed for clarity.

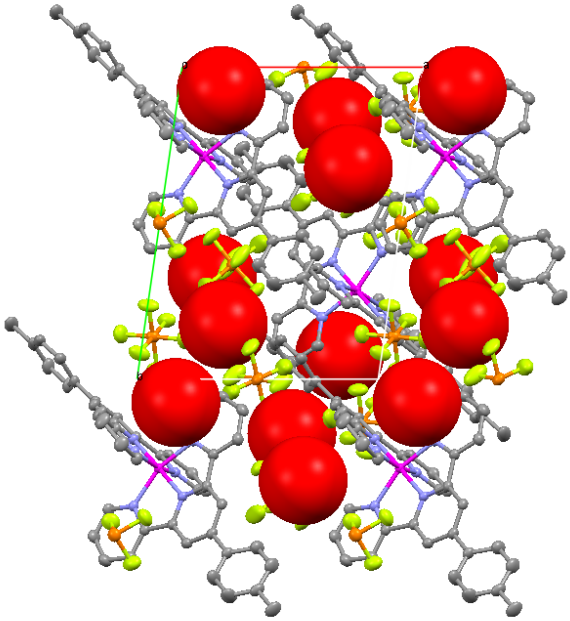

Figure 16. View of the void space within the structure of **2c** as viewed down the *c* axis. Solvent has been removed and void space is represented as red spheres. Hydrogen atoms have been removed for clarity.

Oxygen Sensing

Each form of **2** was tested for sensitivity toward oxygen. The reaction powder precipitated from warm acetonitrile with diethylether was preliminarily tested. This material did not emit well and was therefore referenced to second order diffraction caused by the grating (the LED double). The emission spectra, shown in Figure 17, reveal a broad emission with two features. The maximum wavelength of emission is located at 571 nm and the second peak is located at 531 nm. The two point Stern-Volmer data collected reveals the material does not sense as the K_{SV} is close to zero at approximately 0.06.

When the crystals of **2a** were tested, the emission of the material did not improve. The emission spectra can be seen in Figure 18 and can be describe as a having a maximum wavelength of emission at 531 nm and two shoulders centered at 571 and 596 nm. The two point Stern-Volmer data collected on the preliminary sensing set up indicated the K_{SV} for this material is 0.06.

Crystals of **2b** were tested on the automatic setup for both sensing and stability. The K_{SV} was determined before the stability study and found to be 0.07. The weak sample emission was found to decrease by almost 50 % under LED illumination when the sample is under a nitrogen atmosphere. The emission peak is the most intense at 596 nm and again the shape of the peak is slightly different from that of the other forms (Figure 19).

Crystals of **2c** were tested with a 10 point Stern-Volmer data collection. Again, the compound did not emit well. The emission peak exhibits a different structure with

the maximum wavelength of emission located at 551 nm and a shoulder slightly apparent at 596 nm (Figure 20). The K_{SV} for this material is again 0.06.

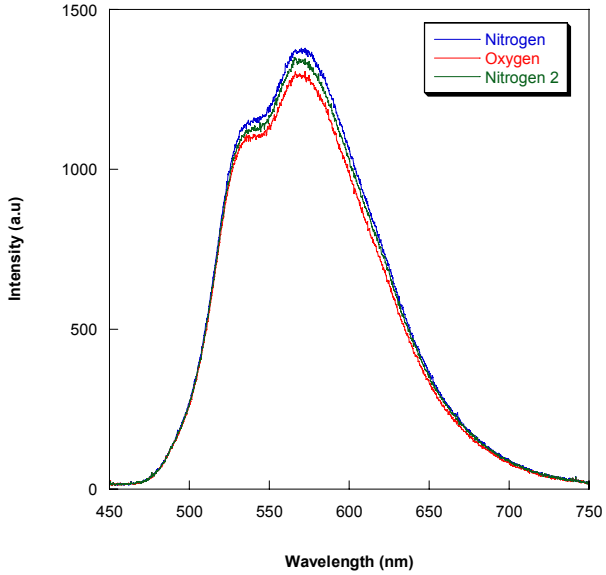

Figure 17. Emission profile and sensing behavior of reaction powder of **2**.

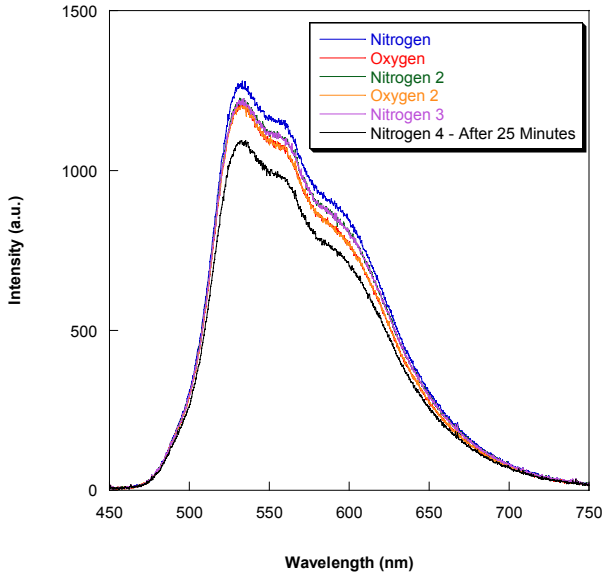

Figure 18. Emission profile and sensing behavior of **2a**. The compound shows little sensitivity toward oxygen and the intensity of the emission decreases under the LED as evidenced by the decrease in emission intensity with time.

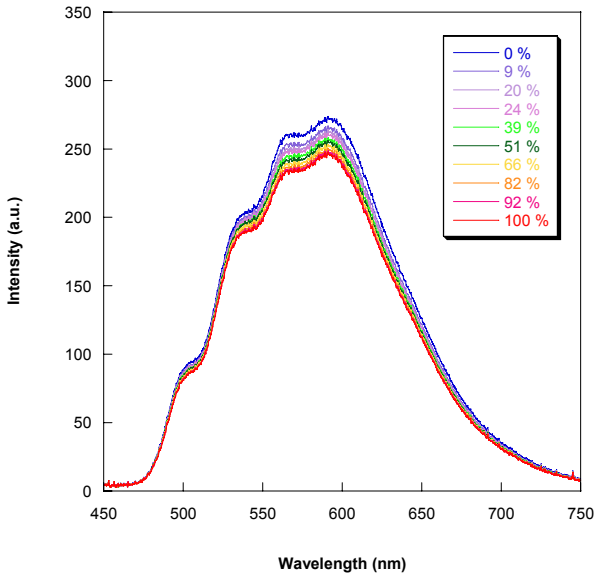

Figure 19. Emission profile and sensing behavior of **2b**. The emission does decrease with increasing concentration of oxygen, but not significantly.

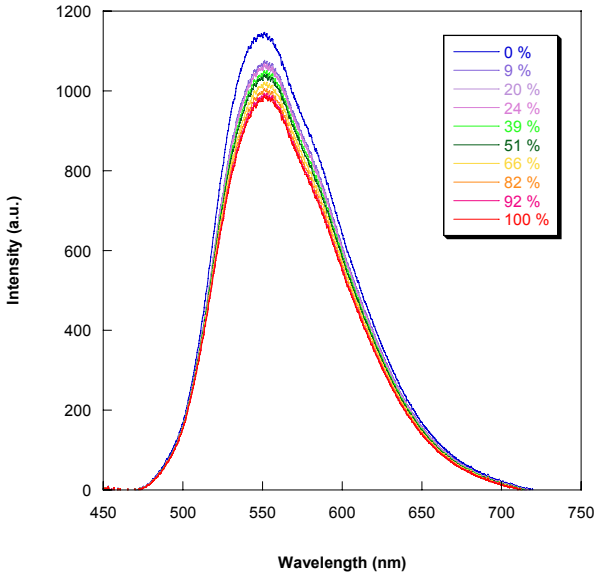

Figure 20. Emission profile and sensing behavior of **2c**, again sensing is minimal.

When the emission from each of these materials is compared (Figure 21), it becomes evident that a change in the polarity of the recrystallization solvent results in a change in the emission profile of the material. When the compound is crystallized from the polar solvent methanol, the emission spectrum is broad with a slight shoulder apparent on the lower energy side of the peak. When a slightly less polar mixture of acetonitrile and either water or ether is used, the emission spectra have three peaks, again on the lower energy side of the peak. Finally, when acetone is used, the least polar of the solvents explored here, four peaks are apparent in the emission spectra with the fourth peak appearing on the higher energy side of the emission peak. The crystallization solvent does not appear to affect the sensing ability of the compound, even though the void space within the structure is greatly affected.

The reaction powder of **3** was tested on the automatic setup for oxygen sensitivity. The compound was again weakly emissive with a slightly more promising K_{SV} of 0.3(3) (Figure 22). However, the emission of this compound appeared to degrade over the course of the sensing study.

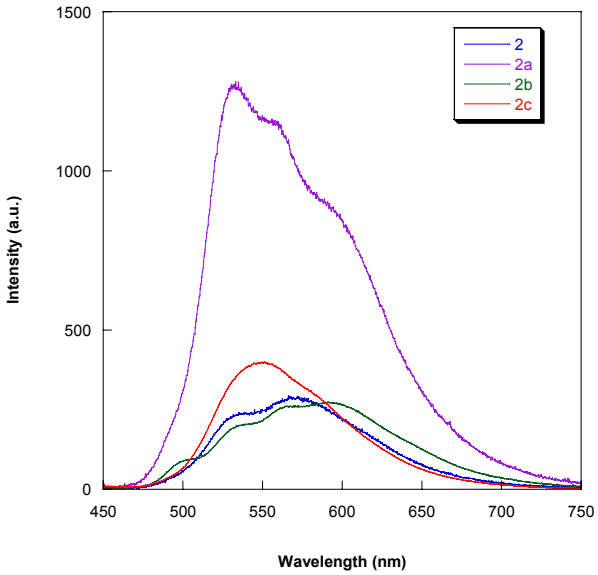

Figure 21. The emission spectra of all $[Ir(tol\text{-}terpy)_2](PF_6)_3$ samples obtained under nitrogen. There appears to be a trend in the emission peak shape with changing crystallization solvent.

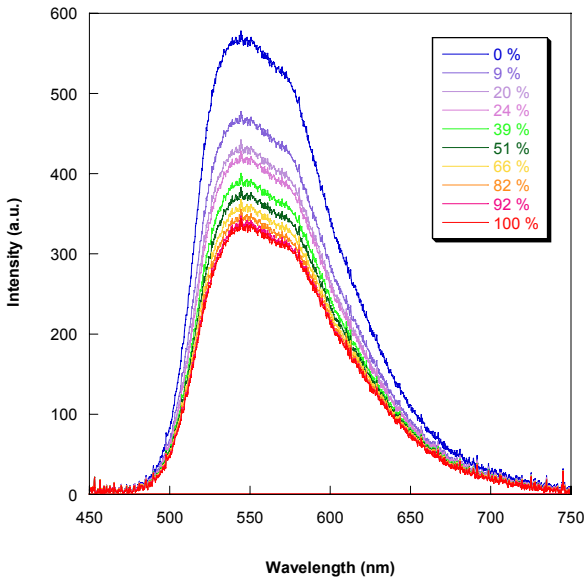

Figure 22. Emission profile and sensing behavior of a reaction powder sample of **3**.

Conclusions

Overall, the synthesis of these materials has proven to be more challenging than expected. There does appear to be one synthetic method which allows the synthesis of *bis*-terpy Ir(III) complexes when the terpy ligand is substituted at the 4' position. Several materials were tested for sensitivity toward oxygen, but unfortunately these materials do not sense oxygen reliably. There does appear to be a change in the emission spectra with crystallization solvent as those materials crystallized from lower polarity solvents exhibit more features in their emission spectra. Modification of the counterion to the bulkier $tfpb^-$ anion was attempted to generate more void space and increase the sensitivity of the material to oxygen. This counterion led to materials that were greasy, amorphous, and not sensitive to oxygen.

However, the single crystal X-ray crystallography structures obtained during this research will contribute significantly to the structural database. When all of the structures reported herein are published, the number of structures known Ir(III) *bis*-terpy complexes will increase by more than 50%.

References

1. Yoshikawa, N.; Yamabe, S.; Kanehisa, N.; Kai, Y.; Takashima, H.; Tsukahara, K. *Eur. J. Inorg. Chem.* **2007**, 1911.

2. McGee, K. A.; Mann, K. R. *Inorg. Chem.* **2007**, *46*, 7800.

3. DeRosa, M. C.; Hodgson, D. J.; Enright, G. D.; Dawson, B.; Evans, C. E. B.; Crutchley, R. J. *J. Am. Chem. Soc.* **2004**, *126*, 7619.

4. Gao, R.; Ho, D. G.; Hernandez, B.; Selke, M.; Murphy, D.; Djurovich, P. I.; Thompson, M. E. *J. Am. Chem. Soc.* **2002**, *124*, 14828.

5. Tamayo, A. B.; Alleyne, B. D.; Djurovich, P. I.; Lamansky, S.; Tsyba, I.; Ho, N. N.; Bau, R.; Thompson, M. E. *J. Am. Chem. Soc.* **2003**, *125*, 7377.

6. Neve, F.; Crispini, A.; Campagna, S.; Serroni, S. *Inorg. Chem.* **1999**, *38*, 2250.

7. Chin, C. S.; Eum, M.-S.; Kim, S. y.; Kim, C.; Kang, S. K. *Eur. J. Inorg. Chem.* **2007**, 372.

8. Chou, P.-T.; Chi, Y. *Chem.--Eur. J.* **2007**, *13*, 380.

9. Lamansky, S.; Djurovich, P.; Murphy, D.; Abdel-Razzaq, F.; Lee, H.-E.; Adachi, C.; Burrows, P. E.; Forrest, S. R.; Thompson, M. E. *J. Am. Chem. Soc.* **2001**, *123*, 4304.

10. Okada, S.; Okinaka, K.; Iwawaki, H.; Furugori, M.; Hashimoto, M.; Mukaide, T.; Kamatani, J.; Igawa, S.; Tsuboyama, A.; Takiguchi, T.; Ueno, K. *Dalton Trans.* **2005**, 1583.

11. Ragni, R.; Plummer, E. A.; Brunner, K.; Hofstraat, J. W.; Babudri, F.; Farinola, G. M.; Naso, F.; De Cola, L. *J. Mater. Chem.* **2006**, *16*, 1161.

12. Su, H.-C.; Chen, H.-F.; Fang, F.-C.; Liu, C.-C.; Wu, C.-C.; Wong, K.-T.; Liu, Y.-H.; Peng, S.-M. *J. Am. Chem. Soc.* **2008**, *130*, 3413.

13. Yoshikawa, N.; Matsumura-Inoue, T.; Kanehisa, N.; Kai, Y.; Takashima, H.; Tsukahara, K. *Anal. Sci.* **2004**, *20*, 1639.

14. Yoshikawa, N.; Matsumura-Inoue, T. *Anal. Sci.* **2003**, *19*, 761.

15. Flamigni, L.; Collin, J.-P.; Sauvage, J.-P. *Acc. Chem. Res.* **2008**, *41*, 857.

16. Williams, J. A. G.; Wilkinson Andrew, J.; Whittle Victoria, L. *Dalton Trans.* **2008**, 2081.

17. Baranoff, E.; Dixon, I. M.; Collin, J.-P.; Sauvage, J.-P.; Ventura, B.; Flamigni, L. *Inorg. Chem.* **2004**, *43*, 3057.

18. Flamigni, L.; Baranoff, E.; Collin, J.-P.; Sauvage, J.-P. *Chem.--Eur. J.* **2006**, *12*, 6592.

19. Flamigni, L.; Ventura, B.; Barigelletti, F.; Baranoff, E.; Collin, J.-P.; Sauvage, J.-P. *Eur. J. Inorg. Chem.* **2005**, 1312.

20. Dias, A. M. A.; Bonifacio, R. P.; Marrucho, I. M.; Padua, A. A. H.; Costa Gomes, M. F. *Phys. Chem. Chem. Phys,* **2003**, *5*, 543.

21. McGee, K. A.; Marquardt, B. J.; Mann, K. R. *Inorg. Chem.* **2008**, *47*, 9143.

22. McGee, K. A.; Veltkamp, D. J.; Marquardt, B. J.; Mann, K. R. *J. Am. Chem. Soc.* **2007**, *129*, 15092.

23. Baranoff, E.; Collin, J.-P.; Flamigni, L.; Sauvage, J.-P. *Chem. Soc. Rev.* **2004**, *33*, 147.

24. Burger, K.; Wagner, F. E.; Vertes, A.; Bencze, E.; Mink, J.; Labadi, I.; Nemes-Vetessy, Z. *J. Phys. Chem. Solids* **2001**, *62*, 2059.

25. Collin, J.-P.; Dixon, I. M.; Sauvage, J.-P.; Williams, J. A. G.; Barigelletti, F.; Flamigni, L. *J. Am. Chem. Soc.* **1999**, *121*, 5009.

26. Flamigni, L.; Barbieri, A.; Sabatini, C.; Ventura, B.; Barigelletti, F. In *Photochemistry and Photophysics of Coordination Compounds II* 2007, p 143.

27. Goodall, W.; Williams, J. A. G. *Dalton* **2000**, 2893.

28. Licini, M.; Williams, J. A. G. *Chem. Commun.* **1999**, 1943.

29. Exstrom, C. L.; Britton, D.; Mann, K. R.; Hill, M. G.; Miskowski, V. M.; Schaefer, W. P.; Gray, H. B.; Lamanna, W. M. *Inorg. Chem.* **1996**, *35*, 549.

30. Natrajan, L. S.; Toulmin, A.; Chew, A.; Magennis, S. W. *Dalton Trans.* **2010**, *39*, 10837.

31. Bruker, **2003**, *SMART and SAINT*, Madison, Wisconsin, USA.

32. Bruker, **2008**, *APEX II*, Madison, Wisconsin, USA.

33. Sheldrick, G. M., **2008**, *SADABS*, University of Gottingen, Germany.

34. Blessing, R. H. *Acta Cryst. A* **1995**, *A51*, 33.

35. Sheldrick, G. M. *Acta Cryst. A* **2008**, *A64*, 112.

36. Spek, A. L., **2005**, *PLATON, A Multipurpose Crystallographic Tool*, Utrecht University, Utrecht, The Netherlands.

37. Spek, A. L. *Acta Cryst. D* **2009**, *D65*, 148.

38. Bruno, I. J.; Cole, J. C.; Edgington, P. R.; Kessler, M.; Macrae, C. F.; McCabe, P.; Pearson, J.; Taylor, R. *Acta Cryst. B* **2002**, *B58*, 389.

39. McGee, K. A.; Mann, K. R. *J. Am. Chem. Soc.* **2009**, *131*, 1896.

40. Smith, C. S.; Branham, C. W.; Marquardt, B. J.; Mann, K. R. *J. Am. Chem. Soc.* **2010**, *132*, 14079.

41. Smith, C. S.; Mann, K. R. *Chem. Mater.* **2009**, *21*, 5042.

42. Hinkle, L. M.; Young, V. G., Jr.; Mann, K. R. *Acta Cryst. C* **2010**, *C66*, m62.

43. Allen, F. H.; Motherwell, W. D. S. *Acta Cryst. B* **2002**, *B58*, 407.

44. Cusanelli, A.; Frey, U.; Richens, D. T.; Merbach, A. E. *J. Am. Chem. Soc.* **1996**, *118*, 5265.

45. Marsh, R. E. *Acta Cryst. B* **1997**, *B53*, 317.

46. Herbstein, F. H.; Marsh, R. E. *Acta Cryst. B* **1998**, *B54*, 677.

Bibliography

Chapter 1

1. Chestnut, L. G.; Mills, D. M. *J. Environ. Manage.* **2005**, *77*, 252.
2. Grubert, J. P. *J. Environ. Eng. Sci.* **2003**, *2*, 99.
3. Mills, A. *Platinum Met. Rev.* **1997**, *41*, 115.
4. Choi, M. M. F.; Xiao, D. *Anal. Chim. Acta* **2000**, *403*, 57.
5. Clark, L. C., Jr.; Wold, R.; Granger, D.; Taylor, Z. *J. Appl. Physiol.* **1953**, *6*, 189.
6. Severinghaus, J. W.; Astrup, P. B. *J. Clin. Monit.* **1986**, *2*, 174.
7. Severinghaus, J. W.; Astrup, P. B. *J. Clin. Monit.* **1986**, *2*, 125.
8. Trettnak, W.; Gruber, W.; Reininger, F.; Klimant, I. *Sens. Actuators, B* **1995**, *B29*, 219.
9. Skoog, D. A. W., Donald M.; Holler, F. John; Crouch, Stanley R. *Fundamentals of Analytical Chemistry*; 8th ed.; Brooks/Cole-Thompson Learning: Belmont, CA, 2004.
10. Yan, H.; Lu, J. *Sens. Actuators* **1989**, *19*, 33.
11. Preidel, W.; Rao, J. R.; Mund, K.; Schunck, O.; David, E. *Sens. Actuators, B* **1995**, *B28*, 71.
12. Mortimer, A. G.; Reed, G. P. *Sens. Actuators, B* **1995**, *B24*, 328.
13. Turro, N. J. *Modern Molecular Photochemistry*; University Science Books: Sausalito, CA, 1991.
14. Demas, J. N.; Harris, E. W.; McBride, R. P. *J. Am. Chem. Soc.* **1977**, *99*, 3547.
15. Douglas, P.; Eaton, K. *Sens. Actuators, B* **2002**, *B82*, 200.
16. Mills, A. *Chem. Soc. Rev.* **2005**, *34*, 1003.
17. Demas, J. N.; DeGraff, B. A.; Coleman, P. B. *Anal. Chem.* **1999**, *71*, 793A.
18. McFarland, S. A.; Lee, F. S.; Cheng, K. A. W. Y.; Cozens, F. L.; Schepp, N. P. *J. Am. Chem. Soc.* **2005**, *127*, 7065.
19. Ramasamy, S. M.; Hurtubise, R. J. *Talanta* **1998**, *47*, 971.

20. Miessler, G. L.; Tarr, D. A. *Inorganic Chemistry*; 3rd ed.; Pearson Prentice Hall: Upper Saddle River, New Jersey, 2004.

21. DiMarco, G.; Lanza, M. *Sens. Actuators, B* **2000**, *B63*, 42.

22. Amao, Y.; Asai, K.; Okura, I. *J. Porphyrins Phthalocyanines* **2000**, *4*, 292.

23. Gillanders, R. N.; Tedford, M. C.; Crilly, P. J.; Bailey, R. T. *Anal. Chim. Acta* **2004**, *502*, 1.

24. Papkovsky, D. B.; Ponomarev, G. V.; Trettnak, W.; O'Leary, P. *Anal. Chem.* **1995**, *67*, 4112.

25. Atwater, B. W. *Journal of Fluorescence* **1992**, *2*, 237.

26. Meier, B.; Werner, T.; Klimant, I.; Wolfbeis, O. S. *Sens. Actuators, B* **1995**, *29*, 240.

27. McGee, K. A.; Mann, K. R. *J. Am. Chem. Soc.* **2009**, *131*, 1896.

28. McGee, K. A.; Marquardt, B. J.; Mann, K. R. *Inorg. Chem.* **2008**, *47*, 9143.

29. Smith, C. S.; Branham, C. W.; Marquardt, B. J.; Mann, K. R. *J. Am. Chem. Soc.* **2010**, *132*, 14079.

30. Smith, C. S.; Mann, K. R. *Chem. Mater.* **2009**, *21*, 5042.

31. Smith, C. S.; Mann, K. R. *J. Am. Chem. Soc.* **2012**, *134*, 8786.

32. McGee, K. A.; Veltkamp, D. J.; Marquardt, B. J.; Mann, K. R. *J. Am. Chem. Soc.* **2007**, *129*, 15092.

33. Demas, J. N.; DeGraff, B. A. *J. Chem. Educ.* **1997**, *74*, 690.

34. Barbieri, A.; Accorsi, G.; Armaroli, N. *Chem. Commun.* **2008**, 2185.

35. Walesa-Chorab, M.; Stefankiewicz, A. R.; Ciesielski, D.; Hnatejko, Z.; Kubicki, M.; Klak, J.; Korabik, M. J.; Patroniak, V. *Polyhedron* **2011**, *30*, 730.

36. Ma, Z.; Cao, Y.; Li, Q.; Guedes da Silva, M. F. C.; Frausto da Silva, J. J. R.; Pombeiro, A. J. L. *J. Inorg. Biochem.* **2010**, *104*, 704.

37. Righetto, S.; Rondena, S.; Locatelli, D.; Roberto, D.; Tessore, F.; Ugo, R.; Quici, S.; Roma, S.; Korystov, D.; Srdanov, V. I. *J. Mater. Chem* **2006**, *16*, 1439.

38. Mikata, Y.; Yamashita, A.; Kawamura, A.; Konno, H.; Miyamoto, Y.; Tamotsu, S. *Dalton Trans.* **2009**, 3800.

39. Li, X.; Zhu, D.; Gao, W.; Zhang, Y.; Mu, Y. *J. Chem. Res.* **2006**, 371.

40. Liu, Q.-D.; Wang, R.; Wang, S. *Dalton Trans.* **2004**, 2073.

41. Chen, S.-C.; Yu, R.-M.; Zhao, Z.-G.; Chen, S.-M.; Zhang, Q.-S.; Wu, X.-Y.; Wang, F.; Lu, C.-Z. *Cryst. Growth Des.* **2010**, *10*, 1155.

42. Gomes, C. S. B.; Gomes, P. T.; Duarte, M. T.; Di Paolo, R. E.; MacÌ§anita, A. n. L.; Calhorda, M. J. *Inorg. Chem.* **2009**, *48*, 11176.

43. Kuo, K.-L.; Huang, C.-C.; Lin, Y.-C. *Dalton Trans.* **2008**, 3889.

44. Zhou, X.; Jin, X.; Li, D.; Wu, X. *Chem. Commun.* **2011**, *47*, 3921.

45. Liang, L. J.; Zhao, X. J.; Huang, C. Z. *Analyst* **2012**, *137*, 953.

46. Wild, A.; Winter, A.; Hager, M. D.; Schubert, U. S. *Chem. Commun.* **2012**, *48*, 964.

47. Winter, A.; Friebe, C.; Chiper, M.; Schubert, U. S.; Presselt, M.; Dietzek, B.; Schmitt, M.; Popp, J. *Chem. Phys. Chem.* **2009**, *10*, 787.

48. Galardon, E.; Tomas, A.; Roussel, P.; Artaud, I. *Dalton Trans.* **2009**, 9126.

49. Priimov, G. U.; Moore, P.; Helm, L.; Merbach, A. E. *Inorg. Reac. Mech.* **2001**, *3*, 1.

50. Benniston, A. C.; Harriman, A.; Lawrie, D. J.; Mayeux, A. *Phys. Chem. Chem. Phys,* **2004**, *6*, 51.

51. Cuttell, D. G.; Kuang, S.-M.; Fanwick, P. E.; McMillin, D. R.; Walton, R. A. *J. Am. Chem. Soc.* **2002**, *124*, 6.

52. Miller, M. T.; Karpishin, T. B. *Sens. Actuators, B* **1999**, *61*, 222.

53. Shi, L.; Li, B. *Eur. J. Inorg. Chem.* **2009**, *2009*, 2294.

54. Shi, L.; Li, B.; Yue, S.; Fan, D. *Sens. Actuators, B* **2009**, *137*, 386.

55. Zhang, Q.; Zhou, Q.; Cheng, Y.; Wang, L.; Ma, D.; Jing, X.; Wang, F. *Adv. Mater.* **2004**, *16*, 432.

56. Everly, R. M.; Ziessel, R.; Suffert, J.; McMillin, D. R. *Inorg. Chem.* **1991**, *30*, 559.

57. Cuttell, D. G.; Kuang, S.-M.; Fanwick, P. E.; McMillin, D. R.; Walton, R. A. *J. Am. Chem. Soc.* **2001**, *124*, 6.

58. Palmer, C. E. A.; McMillin, D. R. *Inorg. Chem.* **1987**, *26*, 3837.

59. Ichinaga, A. K.; Kirchhoff, J. R.; McMillin, D. R.; Dietrich-Buchecker, C. O.; Marnot, P. A.; Sauvage, J. P. *Inorg. Chem.* **1987**, *26*, 4290.

60. Rader, R. A.; McMillin, D. R.; Buckner, M. T.; Matthews, T. G.; Casadonte, D. J.; Lengel, R. K.; Whittaker, S. B.; Darmon, L. M.; Lytle, F. E. *J. Am. Chem. Soc.* **1981**, *103*, 5906.

61. McMillin, D. R.; McNett, K. M. *Chem. Rev.* **1998**, *98*, 1201.

62. Cunningham, C. T.; Moore, J. J.; Cunningham, K. L. H.; Fanwick, P. E.; McMillin, D. R. *Inorg. Chem.* **2000**, *39*, 3638.

63. McGee, K. A.; Mann, K. R. *Inorg. Chem.* **2007**, *46*, 7800.

64. DeRosa, M. C.; Hodgson, D. J.; Enright, G. D.; Dawson, B.; Evans, C. E. B.; Crutchley, R. J. *J. Am. Chem. Soc.* **2004**, *126*, 7619.

65. Gao, R.; Ho, D. G.; Hernandez, B.; Selke, M.; Murphy, D.; Djurovich, P. I.; Thompson, M. E. *J. Am. Chem. Soc.* **2002**, *124*, 14828.

66. Tamayo, A. B.; Alleyne, B. D.; Djurovich, P. I.; Lamansky, S.; Tsyba, I.; Ho, N. N.; Bau, R.; Thompson, M. E. *J. Am. Chem. Soc.* **2003**, *125*, 7377.

67. Neve, F.; Crispini, A.; Campagna, S.; Serroni, S. *Inorg. Chem.* **1999**, *38*, 2250.

68. Chin, C. S.; Eum, M.-S.; Kim, S. y.; Kim, C.; Kang, S. K. *Eur. J. Inorg. Chem.* **2007**, 372.

69. Chou, P.-T.; Chi, Y. *Chem.--Eur. J.* **2007**, *13*, 380.

70. Lamansky, S.; Djurovich, P.; Murphy, D.; Abdel-Razzaq, F.; Lee, H.-E.; Adachi, C.; Burrows, P. E.; Forrest, S. R.; Thompson, M. E. *J. Am. Chem. Soc.* **2001**, *123*, 4304.

71. Okada, S.; Okinaka, K.; Iwawaki, H.; Furugori, M.; Hashimoto, M.; Mukaide, T.; Kamatani, J.; Igawa, S.; Tsuboyama, A.; Takiguchi, T.; Ueno, K. *Dalton Trans.* **2005**, 1583.

72. Ragni, R.; Plummer, E. A.; Brunner, K.; Hofstraat, J. W.; Babudri, F.; Farinola, G. M.; Naso, F.; De Cola, L. *J. Mater. Chem.* **2006**, *16*, 1161.

73. Su, H.-C.; Chen, H.-F.; Fang, F.-C.; Liu, C.-C.; Wu, C.-C.; Wong, K.-T.; Liu, Y.-H.; Peng, S.-M. *J. Am. Chem. Soc.* **2008**, *130*, 3413.

74. Ayala, N. P.; Flynn, C. M., Jr.; Sacksteder, L.; Demas, J. N.; DeGraff, B. A. *J. Am. Chem. Soc.* **1990**, *112*, 3837.

75. Baranoff, E.; Dixon, I. M.; Collin, J.-P.; Sauvage, J.-P.; Ventura, B.; Flamigni, L. *Inorg. Chem.* **2004**, *43*, 3057.

76. Bolink, H. J.; Coronado, E.; Costa, R. D.; Lardies, N.; Orti, E. *Inorg. Chem.* **2008**, *47*, 9149.

77. Flamigni, L.; Collin, J.-P.; Sauvage, J.-P. *Acc. Chem. Res.* **2008**, *41*, 857.

78. Flamigni, L.; Ventura, B.; Barigelletti, F.; Baranoff, E.; Collin, J.-P.; Sauvage, J.-P. *Eur. J. Inorg. Chem.* **2005**, 1312.

79. Goodall, W.; Williams, J. A. G. *Dalton* **2000**, 2893.

80. Licini, M.; Williams, J. A. G. *Chem. Commun.* **1999**, 1943.

81. Natrajan, L. S.; Toulmin, A.; Chew, A.; Magennis, S. W. *Dalton Trans.* **2010**, *39*, 10837.

82. Williams, J. A. G.; Wilkinson Andrew, J.; Whittle Victoria, L. *Dalton Trans.* **2008**, 2081.

83. Yoshikawa, N.; Matsumura-Inoue, T.; Kanehisa, N.; Kai, Y.; Takashima, H.; Tsukahara, K. *Anal. Sci.* **2004**, *20*, 1639.

84. Yoshikawa, N.; Yamabe, S.; Kanehisa, N.; Kai, Y.; Takashima, H.; Tsukahara, K. *Eur. J. Inorg. Chem.* **2007**, 1911.

85. Yoshikawa, N.; Matsumura-Inoue, T. *Anal. Sci.* **2003**, *19*, 761.

Chapter 2

1. Matthey, J., *Platinum Today*, http://www.platinum.matthey.com/pgm-prices/ (accessed June 2012).

2. Media, B., *Daily Metal Prices & Market News*, www.metalmarkets.org.uk, (accessed June 2012).

3. Liang, L. J.; Zhao, X. J.; Huang, C. Z. *Analyst* **2012**, *137*, 953.

4. Walesa-Chorab, M.; Stefankiewicz, A. R.; Ciesielski, D.; Hnatejko, Z.; Kubicki, M.; Klak, J.; Korabik, M. J.; Patroniak, V. *Polyhedron* **2011**, *30*, 730.

5. Wild, A.; Winter, A.; Hager, M. D.; Schubert, U. S. *Chem. Commun.* **2012**, *48*, 964.

6. Zhou, X.; Jin, X.; Li, D.; Wu, X. *Chem. Commun.* **2011**, *47*, 3921.

7. Hwang, S.-H.; Wang, P.; Moorefield, C. N.; Jung, J.-C.; Kim, J.-Y.; Lee, S.-W.; Newkome, G. R. *Macromol. Rapid Comm.* **2006**, *27*, 1809.

8. Ma, Z.; Cao, Y.; Li, Q.; Guedes da Silva, M. F. t. C.; FraÃºsto da Silva, J. o. J. R.; Pombeiro, A. J. L. *J. Inorg. Biochem.* **2010**, *104*, 704.

9. Righetto, S.; Rondena, S.; Locatelli, D.; Roberto, D.; Tessore, F.; Ugo, R.; Quici, S.; Roma, S.; Korystov, D.; Srdanov, V. I. *J. Mater. Chem* **2006**, *16*, 1439.

10. Winter, A.; Friebe, C.; Chiper, M.; Schubert, U. S.; Presselt, M.; Dietzek, B.; Schmitt, M.; Popp, J. *Chem. Phys. Chem.* **2009**, *10*, 787.

11. Barbieri, A.; Accorsi, G.; Armaroli, N. *Chem. Commun.* **2008**, 2185.

12. Winter, A.; Friebe, C.; Hager, M. D.; Schubert, U. S. *Macromol. Rapid Comm.* **2008**, *29*, 1679.

13. Zhao, Q.-L.; Li, G.-P. *Acta Cryst. E* **2009**, *65*, m693.

14. Bruker, **2008**, *APEX II*, Madison, Wisconsin, USA.

15. Blessing, R. H. *Acta Cryst. A* **1995**, *A51*, 33.

16. Sheldrick, G. M., **2008**, *SADABS*, University of Gottingen, Germany.

17. Bruker, **2003**, *SMART and SAINT*, Madison, Wisconsin, USA.

18. Sheldrick, G. M. *Acta Cryst. A* **2008**, *A64*, 112.

19. Spek, A. L., **2005**, *PLATON, A Multipurpose Crystallographic Tool*, Utrecht University, Utrecht, The Netherlands.

20. Bruno, I. J.; Cole, J. C.; Edgington, P. R.; Kessler, M.; Macrae, C. F.; McCabe, P.; Pearson, J.; Taylor, R. *Acta Cryst. B* **2002**, *B58*, 389.

21. McGee, K. A.; Mann, K. R. *J. Am. Chem. Soc.* **2009**, *131*, 1896.

22. McGee, K. A.; Veltkamp, D. J.; Marquardt, B. J.; Mann, K. R. *J. Am. Chem. Soc.* **2007**, *129*, 15092.

23. Smith, C. S.; Branham, C. W.; Marquardt, B. J.; Mann, K. R. *J. Am. Chem. Soc.* **2010**, *132*, 14079.

24. Smith, C. S.; Mann, K. R. *Chem. Mater.* **2009**, *21*, 5042.

25. Benniston, A. C.; Harriman, A.; Lawrie, D. J.; Mayeux, A. *Phys. Chem. Chem. Phys,* **2004**, *6*, 51.

26. Cotton, F. A.; Wilkinson, G. S.; Murillo, C. A.; Bochmann, M. *Advanced Inorganic Chemistry*; 6th ed.; Interscience Publishers: New York, 1972.

Chapter 3

1. Amao, Y.; Asai, K.; Okura, I. *J. Porphyrins Phthalocyanines* **2000**, *4*, 292.

2. Amao, Y.; Miyashita, T.; Okura, I. *J. Fluorine Chem.* **2001**, *107*, 101.

3. Demas, J. N.; DeGraff, B. A.; Coleman, P. B. *Anal. Chem.* **1999**, *71*, 793A.

4. Demas, J. N.; Harris, E. W.; McBride, R. P. *J. Am. Chem. Soc.* **1977**, *99*, 3547.

5. DeRosa, M. C.; Hodgson, D. J.; Enright, G. D.; Dawson, B.; Evans, C. E. B.; Crutchley, R. J. *J. Am. Chem. Soc.* **2004**, *126*, 7619.

6. Douglas, P.; Eaton, K. *Sens. Actuators, B* **2002**, *B82*, 200.

7. Li, Z. *Spectrochimica Acta Part A* **2011**, *81*, 475.

8. Miller, M. T.; Karpishin, T. B. *Sens. Actuators, B* **1999**, *61*, 222.

9. Mills, A. *Platinum Met. Rev.* **1997**, *41*, 115.

10. Papkovsky, D. B.; Ponomarev, G. V.; Trettnak, W.; O'Leary, P. *Anal. Chem.* **1995**, *67*, 4112.

11. Zhang, H.; Sun, Y.; Ye, K.; Zhang, P.; Wang, Y. *J. Mater. Chem.* **2005**, *15*, 3181.

12. Burney, J. Doctoral Thesis, University of Minnesota, 2007.

13. McGee, K. A.; Mann, K. R. *J. Am. Chem. Soc.* **2009**, *131*, 1896.

14. McGee, K. A.; Marquardt, B. J.; Mann, K. R. *Inorg. Chem.* **2008**, *47*, 9143.

15. McGee, K. A.; Veltkamp, D. J.; Marquardt, B. J.; Mann, K. R. *J. Am. Chem. Soc.* **2007**, *129*, 15092.

16. Smith, C. S.; Branham, C. W.; Marquardt, B. J.; Mann, K. R. *J. Am. Chem. Soc.* **2010**, *132*, 14079.

17. Smith, C. S.; Mann, K. R. *Chem. Mater.* **2009**, *21*, 5042.

18. Smith, C. S.; Mann, K. R. *J. Am. Chem. Soc.* **2012**, *134*, 8786.

19. Cuttell, D. G.; Kuang, S.-M.; Fanwick, P. E.; McMillin, D. R.; Walton, R. A. *J. Am. Chem. Soc.* **2002**, *124*, 6.

20. Everly, R. M.; Ziessel, R.; Suffert, J.; McMillin, D. R. *Inorg. Chem.* **1991**, *30*, 559.

21. Palmer, C. E. A.; McMillin, D. R. *Inorg. Chem.* **1987**, *26*, 3837.

22. Rader, R. A.; McMillin, D. R.; Buckner, M. T.; Matthews, T. G.; Casadonte, D. J.; Lengel, R. K.; Whittaker, S. B.; Darmon, L. M.; Lytle, F. E. *J. Am. Chem. Soc.* **1981**, *103*, 5906.

23. Borisov, S. M.; Zenkl, G.; Klimant, I. *ACS Applied Materials & Interfaces* **2010**, *2*, 366.

24. Collier, B. B.; Singh, S.; McShane, M. *Analyst* **2011**, *136*, 962.

25. Exstrom, C. L.; Britton, D.; Mann, K. R.; Hill, M. G.; Miskowski, V. M.; Schaefer, W. P.; Gray, H. B.; Lamanna, W. M. *Inorg. Chem.* **1996**, *35*, 549.

26. Dietrich-Buchecker, C.; Sauvage, J. P.; Kern, J. M. *J. Am. Chem. Soc.* **1989**, *111*, 7791.

27. Cuttell, D. G.; Kuang, S.-M.; Fanwick, P. E.; McMillin, D. R.; Walton, R. A. *Journal of the American Chemical Society* **2001**, *124*, 6.

28. Bruker, **2008**, *APEX II*, Madison, Wisconsin, USA.

29. Blessing, R. H. *Acta Cryst. A* **1995**, *A51*, 33.

30. Sheldrick, G. M., **2008**, *SADABS*, University of Gottingen, Germany.

31. Sheldrick, G. M. *Acta Cryst. A* **2008**, *A64*, 112.

32. Bruno, I. J.; Cole, J. C.; Edgington, P. R.; Kessler, M.; Macrae, C. F.; McCabe, P.; Pearson, J.; Taylor, R. *Acta Cryst. B* **2002**, *B58*, 389.

33. Spek, A. L., **2005**, *PLATON, A Multipurpose Crystallographic Tool*, Utrecht University, Utrecht, The Netherlands.

34. Spek, A. L. *Acta Cryst. D* **2009**, *D65*, 148.

35. Wrighton, M. S.; Ginley, D. S.; Morse, D. L. *J. Phys. Chem.* **1974**, *78*, 2229.

36. Avian Technologies, W. R., P.O. Box 822, Wilmington, OH 45177, USA; http://www.aviantechnologies.com/faq.html.

37. Kuang, S.-M.; Cuttell, D. G.; McMillin, D. R.; Fanwick, P. E.; Walton, R. A. *Inorg. Chem.* **2002**, *41*, 3313.

Chapter 4

1. Collier, B. B.; Singh, S.; McShane, M. *Analyst* **2011**, *136*, 962.

2. Demas, J. N.; DeGraff, B. A. *J. Chem. Educ.* **1997**, *74*, 690.

3. Demas, J. N.; DeGraff, B. A.; Coleman, P. B. *Anal. Chem.* **1999**, *71*, 793A.

4. DeRosa, M. C.; Hodgson, D. J.; Enright, G. D.; Dawson, B.; Evans, C. E. B.; Crutchley, R. J. *J. Am. Chem. Soc.* **2004**, *126*, 7619.

5. Gouterman, M. *J. Chem. Educ.* **1997**, *74*, 697.

6. Mills, A. *Platinum Met. Rev.* **1997**, *41*, 115.

7. Mills, A. *Chem. Soc. Rev.* **2005**, *34*, 1003.

8. Trettnak, W.; Gruber, W.; Reininger, F.; Klimant, I. *Sens. Actuators, B* **1995**, *B29*, 219.

9. Yan, H.; Lu, J. *Sens. Actuators* **1989**, *19*, 33.

10. Wang, X.-d.; Chen, X.; Xie, Z.-x.; Wang, X.-r. *Angew. Chem. Int. Edit.* **2008**, *47*.

11. Choi, M. M. F.; Xiao, D. *Anal. Chim. Acta* **2000**, *403*, 57.

12. McFarland, S. A.; Lee, F. S.; Cheng, K. A. W. Y.; Cozens, F. L.; Schepp, N. P. *J. Am. Chem. Soc.* **2005**, *127*, 7065.

13. Meier, B.; Werner, T.; Klimant, I.; Wolfbeis, O. S. *Sens. Actuators, B* **1995**, *29*, 240.

14. Mulazzani, Q. G.; Sun, H.; Hoffman, M. Z.; Ford, W. E.; Rodgers, M. A. J. *J. Phys. Chem.* **1994**, *98*, 1145.

15. McGee, K. A.; Mann, K. R. *J. Am. Chem. Soc.* **2009**, *131*, 1896.

16. McGee, K. A.; Marquardt, B. J.; Mann, K. R. *Inorg. Chem.* **2008**, *47*, 9143.

17. McGee, K. A.; Veltkamp, D. J.; Marquardt, B. J.; Mann, K. R. *J. Am. Chem. Soc.* **2007**, *129*, 15092.

18. Zaharieva, J.; Milanova, M.; Todorovsky, D. *J. Optoelectron. Adv. Mater.* **2011**, *13*, 727.

19. Kim, H. J.; Jeong, Y. C.; Rhee, J. I. *Talanta* **2008**, *76*, 1070.

20. Campagna, S.; Puntoriero, F.; Nastasi, F.; Bergamini, G.; Balzani, V. *Top. Curr. Chem.* **2007**, *280*, 117.

21. Estella, J.; Wencel, D.; Moore, J. P.; Sourdaine, M.; McDonagh, C. *Anal. Chim. Acta*, *666*, 83.

22. Barbieri, A.; Accorsi, G.; Armaroli, N. *Chem. Commun.* **2008**, 2185.

23. Zheng, K.; Liu, X.; Deng, H.; Chao, H.; Yun, F.; Ji, L. *J. Mol. Struct.: THEOCHEM* **2003**, *626*, 295.

24. Accorsi, G.; Listorti, A.; Yoosaf, K.; Armaroli, N. *Chem. Soc. Rev.* **2009**, *38*, 1690.

25. Li, X.; Zhu, D.; Gao, W.; Zhang, Y.; Mu, Y. *J. Chem. Res.* **2006**, 371.

26. Liu, Q.-D.; Wang, R.; Wang, S. *Dalton Trans.* **2004**, 2073.

27. Senoue, M.; Iwaki, T.; Seki, K.; Yagi, M. *J. Photochem. Photobiol., A* **1996**, *101*, 257.

28. Kimachi, S.; Ikeda, S.; Miki, H.; Azumi, T.; Crosby, G. A. *Coord. Chem. Rev.* **1994**, *132*, 43.

29. Mikata, Y.; Yamashita, A.; Kawamura, A.; Konno, H.; Miyamoto, Y.; Tamotsu, S. *Dalton Trans.* **2009**, 3800.

30. Xu, H.; Xu, Z.-F.; Yue, Z.-Y.; Yan, P.-F.; Wang, B.; Jia, L.-W.; Li, G.-M.; Sun, W.-B.; Zhang, J.-W. *J. Phys. Chem. C* **2008**, *112*, 15517.

31. Consiglio, G.; Failla, S.; Oliveri, I. P.; Purrello, R.; Di, B. S. *Dalton Trans.* **2009**, 10426.

32. Benniston, A. C.; Harriman, A.; Lawrie, D. J.; Mayeux, A. *Phys. Chem. Chem. Phys,* **2004**, *6*, 51.

33. Rabold, G. P.; Piette, L. H. *Spectrosc. Lett.* **1968**, *1*, 225.

34. Galardon, E.; Tomas, A.; Roussel, P.; Artaud, I. *Dalton Trans.* **2009**, 9126.

35. Mahato, P.; Ghosh, A.; Mishra, S. K.; Shrivastav, A.; Mishra, S.; Das, A. *Chem. Commun. (Cambridge, U. K.)* **2010**, *46*, 9134.

36. Galardon, E.; Tomas, A.; Roussel, P.; Artaud, I. *Dalton Trans.* **2009**, 9126.

37. Wild, A.; Winter, A.; Hager, M. D.; Schubert, U. S. *Chem. Commun.* **2012**, *48*, 964.

38. Mameli, M.; Aragoni, M. C.; Arca, M.; Atzori, M.; Bencini, A.; Bazzicalupi, C.; Blake, A. J.; Caltagirone, C.; Devillanova, F. A.; Garau, A.; Hursthouse, M. B.; Isaia, F.; Lippolis, V.; Valtancoli, B. *Inorg. Chem. (Washington, DC, U. S.)* **2009**, *48*, 9236.

39. Yeh, A.; Chen, T.-R. *Mater. Lett.* **2005**, *59*, 2911.

40. Mikata, Y.; Wakamatsu, M.; Kawamura, A.; Yamanaka, N.; Yano, S.; Odani, A.; Morihiro, K.; Tamotsu, S. *Inorg. Chem.* **2006**, *45*, 9262.

41. Tan, R.; Wang, Z.-B.; Li, Y.; Kozera, D. J.; Lu, Z.-H.; Song, D. *Inorg. Chem.*, *51*, 7039.

42. Zhou, X.; Jin, X.; Li, D.; Wu, X. *Chem. Commun.* **2011**, *47*, 3921.

43. Liang, L. J.; Zhao, X. J.; Huang, C. Z. *Analyst* **2012**, *137*, 953.

44. Ma, Z.; Cao, Y.; Li, Q.; Guedes da Silva, M. F. t. C.; FraÃºsto da Silva, J. o. J. R.; Pombeiro, A. J. L. *J. Inorg. Biochem.* **2010**, *104*, 704.

45. Exstrom, C. L.; Britton, D.; Mann, K. R.; Hill, M. G.; Miskowski, V. M.; Schaefer, W. P.; Gray, H. B.; Lamanna, W. M. *Inorg. Chem.* **1996**, *35*, 549.

46. Bruker, **2003**, *SMART and SAINT*, Madison, Wisconsin, USA.

47. Blessing, R. H. *Acta Cryst. A* **1995**, *A51*, 33.

48. Sheldrick, G. M., **2008**, *SADABS*, University of Gottingen, Germany.

49. Sheldrick, G. M. *Acta Cryst. A* **2008**, *A64*, 112.

50. Spek, A. L., **2005**, *PLATON, A Multipurpose Crystallographic Tool*, Utrecht University, Utrecht, The Netherlands.

51. Spek, A. L. *Acta Cryst. D* **2009**, *D65*, 148.

52. Bruno, I. J.; Cole, J. C.; Edgington, P. R.; Kessler, M.; Macrae, C. F.; McCabe, P.; Pearson, J.; Taylor, R. *Acta Cryst. B* **2002**, *B58*, 389.

53. Smith, C. S.; Branham, C. W.; Marquardt, B. J.; Mann, K. R. *J. Am. Chem. Soc.* **2010**, *132*, 14079.

54. Smith, C. S.; Mann, K. R. *Chem. Mater.* **2009**, *21*, 5042.

55. Amao, Y.; Miyashita, T.; Okura, I. *J. Fluorine Chem.* **2001**, *107*, 101.

Chapter 5

1. Yoshikawa, N.; Yamabe, S.; Kanehisa, N.; Kai, Y.; Takashima, H.; Tsukahara, K. *Eur. J. Inorg. Chem.* **2007**, 1911.

2. McGee, K. A.; Mann, K. R. *Inorg. Chem.* **2007**, *46*, 7800.

3. DeRosa, M. C.; Hodgson, D. J.; Enright, G. D.; Dawson, B.; Evans, C. E. B.; Crutchley, R. J. *J. Am. Chem. Soc.* **2004**, *126*, 7619.

4. Gao, R.; Ho, D. G.; Hernandez, B.; Selke, M.; Murphy, D.; Djurovich, P. I.; Thompson, M. E. *J. Am. Chem. Soc.* **2002**, *124*, 14828.

5. Tamayo, A. B.; Alleyne, B. D.; Djurovich, P. I.; Lamansky, S.; Tsyba, I.; Ho, N. N.; Bau, R.; Thompson, M. E. *J. Am. Chem. Soc.* **2003**, *125*, 7377.

6. Neve, F.; Crispini, A.; Campagna, S.; Serroni, S. *Inorg. Chem.* **1999**, *38*, 2250.

7. Chin, C. S.; Eum, M.-S.; Kim, S. y.; Kim, C.; Kang, S. K. *Eur. J. Inorg. Chem.* **2007**, 372.

8. Chou, P.-T.; Chi, Y. *Chem.--Eur. J.* **2007**, *13*, 380.

9. Lamansky, S.; Djurovich, P.; Murphy, D.; Abdel-Razzaq, F.; Lee, H.-E.; Adachi, C.; Burrows, P. E.; Forrest, S. R.; Thompson, M. E. *J. Am. Chem. Soc.* **2001**, *123*, 4304.

10. Okada, S.; Okinaka, K.; Iwawaki, H.; Furugori, M.; Hashimoto, M.; Mukaide, T.; Kamatani, J.; Igawa, S.; Tsuboyama, A.; Takiguchi, T.; Ueno, K. *Dalton Trans.* **2005**, 1583.

11. Ragni, R.; Plummer, E. A.; Brunner, K.; Hofstraat, J. W.; Babudri, F.; Farinola, G. M.; Naso, F.; De Cola, L. *J. Mater. Chem.* **2006**, *16*, 1161.

12. Su, H.-C.; Chen, H.-F.; Fang, F.-C.; Liu, C.-C.; Wu, C.-C.; Wong, K.-T.; Liu, Y.-H.; Peng, S.-M. *J. Am. Chem. Soc.* **2008**, *130*, 3413.

13. Yoshikawa, N.; Matsumura-Inoue, T.; Kanehisa, N.; Kai, Y.; Takashima, H.; Tsukahara, K. *Anal. Sci.* **2004**, *20*, 1639.

14. Yoshikawa, N.; Matsumura-Inoue, T. *Anal. Sci.* **2003**, *19*, 761.

15. Flamigni, L.; Collin, J.-P.; Sauvage, J.-P. *Acc. Chem. Res.* **2008**, *41*, 857.

16. Williams, J. A. G.; Wilkinson Andrew, J.; Whittle Victoria, L. *Dalton Trans.* **2008**, 2081.

17. Baranoff, E.; Dixon, I. M.; Collin, J.-P.; Sauvage, J.-P.; Ventura, B.; Flamigni, L. *Inorg. Chem.* **2004**, *43*, 3057.

18. Flamigni, L.; Baranoff, E.; Collin, J.-P.; Sauvage, J.-P. *Chem.--Eur. J.* **2006**, *12*, 6592.

19. Flamigni, L.; Ventura, B.; Barigelletti, F.; Baranoff, E.; Collin, J.-P.; Sauvage, J.-P. *Eur. J. Inorg. Chem.* **2005**, 1312.

20. Dias, A. M. A.; Bonifacio, R. P.; Marrucho, I. M.; Padua, A. A. H.; Costa Gomes, M. F. *Phys. Chem. Chem. Phys,* **2003**, *5*, 543.

21. McGee, K. A.; Marquardt, B. J.; Mann, K. R. *Inorg. Chem.* **2008**, *47*, 9143.

22. McGee, K. A.; Veltkamp, D. J.; Marquardt, B. J.; Mann, K. R. *J. Am. Chem. Soc.* **2007**, *129*, 15092.

23. Baranoff, E.; Collin, J.-P.; Flamigni, L.; Sauvage, J.-P. *Chem. Soc. Rev.* **2004**, *33*, 147.

24. Burger, K.; Wagner, F. E.; Vertes, A.; Bencze, E.; Mink, J.; Labadi, I.; Nemes-Vetessy, Z. *J. Phys. Chem. Solids* **2001**, *62*, 2059.

25. Collin, J.-P.; Dixon, I. M.; Sauvage, J.-P.; Williams, J. A. G.; Barigelletti, F.; Flamigni, L. *J. Am. Chem. Soc.* **1999**, *121*, 5009.

26. Flamigni, L.; Barbieri, A.; Sabatini, C.; Ventura, B.; Barigelletti, F. In *Photochemistry and Photophysics of Coordination Compounds II* 2007, p 143.

27. Goodall, W.; Williams, J. A. G. *Dalton* **2000**, 2893.

28. Licini, M.; Williams, J. A. G. *Chem. Commun.* **1999**, 1943.

29. Exstrom, C. L.; Britton, D.; Mann, K. R.; Hill, M. G.; Miskowski, V. M.; Schaefer, W. P.; Gray, H. B.; Lamanna, W. M. *Inorg. Chem.* **1996**, *35*, 549.

30. Natrajan, L. S.; Toulmin, A.; Chew, A.; Magennis, S. W. *Dalton Trans.* **2010**, *39*, 10837.

31. Bruker, **2003**, *SMART and SAINT*, Madison, Wisconsin, USA.

32. Bruker, **2008**, *APEX II*, Madison, Wisconsin, USA.

33. Sheldrick, G. M., **2008**, *SADABS*, University of Gottingen, Germany.

34. Blessing, R. H. *Acta Cryst. A* **1995**, *A51*, 33.

35. Sheldrick, G. M. *Acta Cryst. A* **2008**, *A64*, 112.

36. Spek, A. L., **2005**, *PLATON, A Multipurpose Crystallographic Tool*, Utrecht University, Utrecht, The Netherlands.

37. Spek, A. L. *Acta Cryst. D* **2009**, *D65*, 148.

38. Bruno, I. J.; Cole, J. C.; Edgington, P. R.; Kessler, M.; Macrae, C. F.; McCabe, P.; Pearson, J.; Taylor, R. *Acta Cryst. B* **2002**, *B58*, 389.

39. McGee, K. A.; Mann, K. R. *J. Am. Chem. Soc.* **2009**, *131*, 1896.

40. Smith, C. S.; Branham, C. W.; Marquardt, B. J.; Mann, K. R. *J. Am. Chem. Soc.* **2010**, *132*, 14079.

41. Smith, C. S.; Mann, K. R. *Chem. Mater.* **2009**, *21*, 5042.

42. Hinkle, L. M.; Young, V. G., Jr.; Mann, K. R. *Acta Cryst. C* **2010**, *C66*, m62.

43. Allen, F. H.; Motherwell, W. D. S. *Acta Cryst. B* **2002**, *B58*, 407.

44. Cusanelli, A.; Frey, U.; Richens, D. T.; Merbach, A. E. *J. Am. Chem. Soc.* **1996**, *118*, 5265.

45. Marsh, R. E. *Acta Cryst. B* **1997**, *B53*, 317.

46. Herbstein, F. H.; Marsh, R. E. *Acta Cryst. B* **1998**, *B54*, 677.